FINAL REPORT

Integrity Management for Wrinklebends and Buckles

To

US Department of Transportation

December 2007

Final Report

to

Integrity Management for Wrinklebends and Buckles

Prepared for

US Department of Transportation PHMSA
Contract No. DTRS56-05-T-0003
Project No. G005189

by

X. K. Zhu, B. N. Leis, and E. B. Clark

December 2007

BATTELLE
505 King Avenue
Columbus, Ohio, 43201-2693

Neither Battelle, nor any person acting on their behalf:

Makes any warranty or representation, expressed or implied, with respect to the accuracy, completeness or usefulness of any information contained in this report or that the use of any information, apparatus, method, or process disclosed in this report may not infringe privately owned rights.

Assumes any liabilities with the respect to the use of, or for damages resulting from the use of any information, apparatus, method or process disclosed in this report.

REPORT DOCUMENTATION PAGE

Form Approved
OMB No. 0704-0188

1. REPORT DATE *(DD-MM-YYYY)*	**2. REPORT TYPE**	**3. DATES COVERED** *(From - To)*
28/12/2007	Final	08/12/2004 – 31/12/2007

4. TITLE AND SUBTITLE:
Integrity Management for Wrinklebends and Buckles

5a. CONTRACT NUMBER
DTRS56-05-T-0003

5b. GRANT NUMBER

5c. PROGRAM ELEMENT NUMBER

6. AUTHOR(S)
Xiankui Zhu B. N. Leis, and E. B. Clark

5d. PROJECT NUMBER
164

5e. TASK NUMBER

5f. WORK UNIT NUMBER
132

7. PERFORMING ORGANIZATION NAME(S) AND ADDRESS(ES) AND ADDRESS(ES)

Battelle
505 King Avenue
Columbus, OH 43201

8. PERFORMING ORGANIZATION REPORT NUMBER

G005189

9. SPONSORING / MONITORING AGENCY NAME(S) AND ADDRESS(ES)

10. SPONSOR/MONITOR'S ACRONYM(S)

11. SPONSOR/MONITOR'S REPORT NUMBER(S)

12. DISTRIBUTION / AVAILABILITY STATEMENT

13. SUPPLEMENTARY NOTES

14. ABSTRACT
This report reviewed the evolution of wrinkle-bending practices, and developed technology to help formulate and evaluate integrity management plans for vintage construction that includes these features. This technology has its roots in numerical analysis developed consistent with factors identified as first-order drivers for incidents involving wrinklebends. Appendices were presented that detailed support for such aspects. Factors unique to wrinklebend integrity involve the wrinkle geometry whose severity was characterized by H/L, the grade and geometry of the line pipe, the production of the wrinkle as hot-formed or cold-formed, the pipeline's operation, the possible presence of pitting or areal corrosion, and the constraint on the bend provided by the pipeline's fixity in the right-of-way. The role of these factors was assessed in terms of in-line inspection measurements or field digs to determine H/L, whereas information on the line pipe and its service should be available from file-data and SCADA or knowledge of demand and pipeline topography. The quality of the product stream, the condition of the pipeline coating, and control of cathodic protection were noted as potentially important factors driving ID and OD corrosion.

Criteria were developed to identify the few wrinkles that could be potentially problematic that might remain in service – that also are located in areas of high consequence including those operating in lines grandfathered to operation up to 80-percent of SMYS. The criteria developed should facilitate identifying wrinkles that merit removal or such consideration, or the use of an operating strategy to mange and avoid future problems. Validation was developed via close correspondence between predictions based on these criteria as compared to full-scale tests on wrinklebends as well as by comparisons of predictions to the response of an in-service rupture and the behavior of bends removed from service.

15. SUBJECT TERMS
wrinklebend, fatigue, corrosion, cracking, failure, criteria, integrity management, grade, line-pipe steel

16. SECURITY CLASSIFICATION OF:			**17. LIMITATION OF ABSTRACT**	**18. NUMBER OF PAGES**	**19a. NAME OF RESPONSIBLE PERSON**
Standard					**Brian Leis**
a. REPORT	**b. ABSTRACT**	**c. THIS PAGE**			**19b. TELEPHONE NUMBER** *(include area code)*
Final		iii			**614.424.4421**

Standard Form 298 (Rev. 8-98)
Prescribed by ANSI Std. Z39.18

This page intentionally blank.

Table of Contents

Page

List of Figures

Page

List of Tables

Page

Acknowledgments

This report presents work that leverages co-funding from the PRCI for their project PR-3-0113, which followed a smaller multiyear joint-industry project (JIP) begun in late 1990s. Useful discussions with Mr. R. J. Olson in regard to his work on modern cold-field practices completed in the early 90s for the PRCI as project PR-3-9214 is gratefully acknowledged as part of this JIP. Throughout this work as well as the JIP, useful discussions on field issues with Bill Amend then of Southern California Gas Company, Jerry Rau then of Panhandle Pipeline Company, and many others in the industry are also gratefully acknowledged. Finally, the cost-share support, technical discussions, and provision of many wrinklebends removed from service along with extensive data provided by Southern California Gas Company (Sempra) is gratefully acknowledged as is the technical insight, practical guidance, and personal interest of Rick Gailing of that company.

Executive Summary

This report reviewed the evolution of wrinkle-bending practices, and developed technology to help formulate and evaluate integrity management plans for vintage construction that includes these features. This technology has its roots in numerical analysis developed consistent with factors identified as first-order drivers for incidents involving wrinklebends. Appendices were presented that detailed support for such aspects. Factors unique to wrinklebend integrity involve the wrinkle geometry whose severity was characterized by *H/L*, the grade and geometry of the line pipe, the production of the wrinkle as hot-formed or cold-formed, the pipeline's operation, the possible presence of pitting or areal corrosion, and the constraint on the bend provided by the pipeline's fixity in the right-of-way. The role of these factors was assessed in terms of in-line inspection measurements or field digs to determine *H/L*, whereas information on the line pipe and its service should be available from file-data and SCADA or knowledge of demand and pipeline topography. The quality of the product stream, the condition of the pipeline coating, and control of cathodic protection were noted as potentially important factors driving ID and OD corrosion.

Criteria were developed to identify the few wrinkles that could be potentially problematic that might remain in service – that also are located in areas of high consequence. The criteria developed should facilitate identifying wrinkles that merit removal or such consideration, or the use of an operating strategy to mange and avoid future problems. Validation was developed via close correspondence between predictions based on these criteria as compared to full-scale tests on wrinklebends.

Conclusions drawn in the course of this work relate to the themes of each of the appendices, as well as the focus of the work – wrinklebend integrity assessment. The most significant conclusions include:

- wrinkle shape characterized by *H/L* has been successfully related to fatigue resistance and criteria developed meeting the objective of this project including the effects of grade, line pipe geometry, and service loading;
- consideration has been given to the effect of service at 72-percent of SMYS as well as to cases where the maximum stress could be as high as 80-percent of SMYS, as can occur for some grandfathered lines: depending on the wrinkle's severity and other conditions, operation at the higher stress reduced the service life by as much as a factor of two – all else being equal;
- pitting corrosion can significantly reduce the life of a wrinklebend, with life-reduction indicated possible up to a factor of about thirty;
- the criteria were validated through successful prediction of full-scale pressure cycling of wrinklebends – and through its successful prediction of the response of ripple-bends produced in modern bending machines reported independently;
- the criteria also were validated through successful prediction of a range of wrinklebend scenarios from an in-service guillotine rupture through several wrinkles whose severity covered severe through benign, and included the effects of corrosion based on bends removed from service for a variety of reasons;
- the validated criterion can be implemented using data available from field and in-line measurements to characterize *H/L*, supplemented by file data addressing pipeline design

and line pipe properties, wrinkle-bending practices, as well as its construction, operation, and maintenance – where data are uncertain, conservative fallbacks were provided;

- the criteria are simple to use and applicable on a case-specific basis if desired by the user in applications to single wrinkles – multiple wrinkles were independently found to be less severe than otherwise identical single wrinkles; and finally
- the criteria is generic in terms of pressure history – so it can be used for liquid as well as gas pipelines by reference to differences in service. Use of the criteria was illustrated in the discussion section, supported by a high-level flow chart to identify the key steps.

While the significance of ID and OD pitting and areal corrosion can be assessed based on the present work, and the present work has validated these criteria via full-scale testing and field results, the available data are limited so care should be taken when adapting these criteria to field scenarios. While this work established the role of constraint applied locally to the wrinkle, as well as globally to the bend as factors affecting wrinklebend integrity its significant influence on integrity in regard to areal corrosion was not anticipated. Because little data exist to validate this aspect, further work should be considered to better quantify the practical significance of corrosion, and to validate the results of this project. Current rehabilitation has created a supply of wrinkles that could support this assessment.

Background

The challenge of efficiently and safely operating the natural gas and hazardous liquid transmission system in the US has existed and evolved since pipelines were recognized as the best way to transport hydrocarbons between supply basins, processing plants, and markets. This project was one of four concurrent activities completed under a consolidated program designed to improve the integrity of the pipeline infrastructure in the U.S. This project targeted integrity assessment for wrinklebends, a construction feature used into the mid 50s – the period when much of the transmission pipeline infrastructure was built. The results support developing and validating integrity assessment for wrinklebends in response to Government requirements for Integrity Management Plans (IMPs) as stipulated in recent regulations[1,2]* and addressed in industry responses to those regulations[e.g., 3,4].

While developing the structure and requirements of a high-level IMP that resulted in the recent regulatory changes involved significant effort on the part of the Government, the real challenge lies in successfully implementing those requirements to ensure the system integrity sough by the regulatory changes. Auditors must be able to identify and concur that the requirements of the plan have been met. This is relatively easy for newer pipelines, as modern construction practices and materials are coupled with quality controls – and the effects of service and time have not yet become a factor. It is much more difficult for existing systems made with vintage steels and construction practices that have been in service for some time. Auditors must be able to track the efforts of the pipeline engineer throughout the IMP, and quantify and agree that the objectives of the plan have been met. Tools must exist or be developed to effectively implement the IMP and track the related process and continuous improvement in safety records. The present project is directed at such needs and actions specific to wrinklebends.

Many potential **threats** exist for wrinklebends, which develop because of pressure, pressure cycles, thermal exposure and cycling, and possible external and internal corrosion. The severity of these threats on the **condition** of the pipeline depends on how the wrinkle was made, the transported product quality, the right-of-way (RoW) and other factors. Consequently, the tools developed must address complex time dependent factors controlling corrosion or cracking, and facilitate determining a **re-inspection interval** when condition must be re-evaluated to ensure safety. Ideally, this process will include the ability to capture systemic changes that bring new threats into consideration, while being both simple and reliable in field applications.

* Numbers in superscript parenthesis refer to the list of references at the end of this report.

Introduction

Wrinklebends made with various wrinkle-bending practices were built into early transmission pipelines to change the direction or elevation of the line. Wrinkle-bending refers to processes used historically by the pipeline industry to identify bends made by intentionally creating local buckles in the line pipe to reduce the length of (foreshorten) the inside radius of what became a bend. The formation of buckles is strongly dependent on the locally unsupported length and thickness, as well as the presence of imperfections – variables central to buckling theory[5]. For this reason, pipe parameters like wall thickness, pipe diameter, and their ratio are significant in the formation of bends made via buckles that cause foreshortening. In many applications, the term buckle was used in reference to a significant change in shape due to instability associated with only a small increase in load[5]. In contrast to this situation, the buckles that formed the intrados of wrinklebends were localized, reflecting only a small change in shape. Engineers historically used terms like "cripple" or "wrinkle" to describe a such local instabilities[5], suggesting one possible origin for the term wrinklebend. References 6 through 16 detail wrinklebend practices from cold bends, through hot bends made via various "fire bending" methods[6]. Appendix A presents a much more comprehensive history of wrinkle-bending and presents related practices through the advent of early bending machines, which developed as early field bending practices evolved from the 30s through the 50s. A significant step occurred about 1942, when "smooth bending" machines were used first on the War Emergency pipelines. Broader use of smooth bending machines continued through the 1940's.

Because this shift to new technology occurred gradually, wrinklebends continued in use into the early 50s. At that time, wrinkle bending was still considered viable by some, whereas others raised concerns[e.g., 16]. This view that wrinklebend integrity ranged from viable to problematic likely reflected the fact that wrinklebend quality and uniformity varied considerably. Very likely this could be traced to several factors, such as the wide variety of wrinkle-bending methods apparently used. The inherent instability and minimal process control possible – particularly for hot bending – meant that the skill and experience of the pipeline contractor and/or operator was inherent in wrinkle uniformity. The historic literature noted above indicated some wrinklebends exhibited uniform wrinkle geometries spaced at regular intervals while others were essentially complex shaped buckles that significantly deformed the local pipe geometry. Other hot and cold bends produced by a wrinkle-bending process have nearly smooth intrados without any significant pipe deformation. Fortunately, by the mid 50s, track-mounted integral "vertical bending" machines[15] were in commercial service, which spelled the end to early uncontrolled wrinkle-bending practices.

Depending on the geographic conditions and routing, some transmission pipelines contain a few wrinklebends, while others through hilly terrain can contain thousands of wrinklebends, some of which lie in Class 3 or 4 locations or through terrain crossed by navigable waterways. Depending on location, an incident in a transmission pipeline could have a significant cost impact for the line's operator and can potentially cause negative repercussions throughout the pipeline industry. Wrinklebends used in early pipeline construction differ from the cold field bends used today in the techniques used to make the bend and methods used to control the process. Present day bends are made cold in hydraulic machines with the capability to control the displacement imposed with mandrels to preserve the shape of the pipeline's circular cross-section. In contrast, the making of a wrinklebend – whether formed either hot or cold – involved

forces or stored energy in the bending apparatus that once the wrinkle started to form complicated controlling its size.

Pipeline incident data indicate that only a few wrinklebends have failed in service. Appendix B presents details of some wrinklebend failures as the basis to understand factors important in their integrity management. Evaluation of such wrinklebends failures indicates they are due to the initiation and growth of cracks to a critical size. Such cracking traces to fatigue induced by pressure cycles, but equally local ground movement can be a factor, with thermal cycling, and corrosion on the inside diameter (ID) and the outside diameter (OD) also plausible[e.g., 17,18]. Fatigue crack initiation and subsequent growth is possible in pipelines that experience significant pressure cycles[e.g., 19], which is more likely and occurs sooner in pipelines with larger, more frequent pressure cycles, and severe wrinkles. Thermal cycling can be an issue where hilly countryside has the potential for local washout that exposes the pipeline to diurnal or longer thermal cycles. Wheel loading is another plausible source of cyclic stress that has contributed to wrinkle bend failure.

While occasional failures have occurred at wrinklebends, thousands of wrinklebends have been in problem-free service for 60 years or more. This is evident from Appendix C, which evaluates historical incident data for wrinklebends based on data reported in three databases gathered under Government purview since 1950s to the present[20-22]. The first dataset was assembled by the Federal Power Commission (FPC), while the second and third datasets were assembled under the auspices of the US Department of Transportation (DoT), in its Office of Pipeline Safety (OPS). As tabulated in Appendix C, the incident rate expressed per mile-year for January 1950 to June 1965 was $1x10^{-5}$, while for 1970 through mid 1984 the rate was 9.8×10^{-7}, and from mid 1984 to mid 2002 the rate was 1.4×10^{-6}. Such rates are less than incident rates for other pipeline threats[e.g., 22,23]. Initially the incident rate for wrinklebend failures was comparable to the rate for the construction-related threat category, for which the failure rate is the order of 10^{-5}. The analysis in Appendix C indicates that over 80-percent of the wrinklebend failures occurred within the first 50 years of service, at a rate that was roughly constant over that period. Beyond 50 years, the failure rate drops sharply, and is since asymptotically approaching zero, implying that the poorly formed wrinklebends failed quickly, with those remaining in service being largely benign.

ASME B 31.8S[4] presents one approach to manage the integrity of wrinklebends that can be considered historically benign under the premise that historically benign construction features remain benign and not a threat to pipeline integrity where the pipeline's service remains unchanged. An equally plausible although more extreme approach to address the risk posed by wrinklebends is to remove them. While appealing at first glance, this approach ignores the just noted fact that thousands of wrinkles remain benign in service. Such observations imply wrinkle removal at significant cost can be without benefit to public or environmental safety, which occurs when their removal does not affect risk reduction. More importantly, because stresses in a wrinklebend can be increased where local soil restraint to their flexing is altered, such actions might increase risk nearby wrinklebends that remain in service.

It follows that the most rational approach to manage the integrity of systems constructed using wrinklebends bases decisions on their serviceability in a given pipeline. With this approach, wrinklebends that pose a potential threat are identified and removed or reinforced, with action taken only where risk reduction motivates their removal.

As occurs for all threat assessment[4], serviceability is assessed in terms of factors specific to the threat and other case-specific factors such as the consequences of failure. Factors unique to wrinkles can involve wrinkle geometry, pipeline operation, the line pipe involved, with their evaluation involving file-data on grade and other line pipe issues, whereas SCADA data or knowledge of demand and pipeline topography underlie assessing the significance of pressure cycles. Factors unique to each wrinkle like location, size, and shape could be determined by in-line inspection (ILI) data coupled with file information. Such data are evaluated with a criterion that weighs the importance of the various factors facilitates identifying the few wrinkles that could be potentially problematic – that also are located in areas of high consequence. In turn, this facilitates simple identification of wrinkles that merit removal or consideration of an operating strategy to control future problems.

Given the cost trade-offs involved with widespread wrinklebend replacement or line looping as compared to selective replacement of a few potentially problematic wrinkles, there is clear value in a validated criterion that determines the serviceability of wrinklebends – while ensuring safety. There is a significant safety and environmental benefit in avoiding a failure or in line blow-down or draining as needed for widespread wrinklebend replacement. Likewise, there is value in avoiding the direct costs and indirect costs associated with a failure, and in avoiding the impact of the negative press and the potential of additional prescriptive regulations that often occur in the wake of a failure involving loss of life or significant environmental consequences.

It follows that a validated criterion that determines the safe serviceability of wrinklebends can be an essential tool in completing the required integrity management plan (IMP) for operators of systems with wrinklebends. This report develops such a criterion in terms of the pipe and wrinkle geometry, whether the bend was made cold or hot, the pipeline's field situation (type of bend, pipeline topography and stability, etc.), with consideration of the effects of possible corrosion. The criterion is formulated in a manner that addresses a wide range of potential field and service situations. This is done to avoid excessive conservatism that occurs for a one-size-fits-all formulation. Accordingly, criteria are developed specific to the pipe grade and other factors unique to typical pipeline service and operating conditions. Such is done for a range of steels, because the nucleation of fatigue cracks, which was found to be the first-order factor controlling the life of such wrinkles, can be highly dependent on the pipe steel. As wrinklebend serviceability can depend on aspects unique to its forming, such details are presented prior to formulating the criteria.

Report Organization

This report presents technology developed for integrity assessment of wrinklebends against the historical backdrop of pipe bending as practiced on transmission pipelines construction since the 1920s. As evident from Appendix A, Figure A11, the report addresses wrinklebends made from the 1920s through the early 1950s.

To facilitate continuity in the development of the integrity management tools and discussion of their implications for wrinklebend threat assessment and related rehabilitation, historical as well as technical details are relegated to appendices. As indicated above, Appendix A presents the history of technologies used to create bends, through the 1950s. Appendix B presents results of field observations and measurements, and their implications for factors driving local curvature and strain, and related definitions. It also presents failure analyses to help identify factors that need to be addressed by the management tools. Appendix C considers the in-service failure experience to provide perspective for the appropriate approach to manage integrity at wrinklebends. Appendix B taken together with Appendix C provides the basis to identify the structure of the integrity management criteria and to determine the extent to which wrinkles must be managed relative to other threats to pipeline safety. Comments on worldwide acceptance of features like wrinklebends in pipelines and piping systems are presented in Appendix D. The literature that characterizes the structural significance of and integrity implications for wrinkles is presented in Appendix E. These appendices set the basis for the numerical methods used to quantify wrinklebend severity as characterized in this report, from which the integrity management tools and practices are identified in the ensuing sections. Details that underlie mechanics theories, models, and related results can be found in Appendix F, while other details related to effective plastic hardening models and fatigue damage parameters can be found in Appendix G. As each appendix is presented as a self-standing document, readers interested in these details should consider the appendices first, and then continue here with the body of this report. Data useful to validate this mechanics analysis can be found in the literature cited in Appendices B and E, as well as in the co-funding companion report for this project[24], and its appendices.

Readers only interested in "integrity assessment" should continue here where analysis details and results needed to develop integrity criteria for wrinklebends are developed next. Readers interested in the history and analysis of factors that control failure at wrinklebends should consult Appendices A and B, respectively, before returning here to details that underlie the integrity criteria. Those interested in worldwide acceptance of features like wrinklebends should review Appendix C. Those interested only in the literature and details that address mechanics analyses and experiments, and related details should consider the remaining four appendices, beginning with Appendix D that addresses the literature.

After developing technology for wrinklebend integrity assessment, field aspects are discussed. The report closes with comments on field implementation and related issues, followed by a summary and conclusions.

Objective, Deliverable, and Scope

Results in Appendices B, C, and E and the companion report developed by the cost-share for this project[24] indicate that wrinkle shape and size are plausible metrics of wrinkle severity for failure controlled by mechanical loadings induced by pressure or thermal cycling, with the related stresses and strains modified by the presence of pitting or more general corrosion. The objective of this project was to understand the related structural and material issues and thereby develop criteria to assess severity of wrinklebends under service conditions. Validated criterion were sought to evaluate the integrity of wrinklebends, which could be used for case-specific analyses based on field and in-line measurements, and company file data on pipeline design and line pipe properties, and where available construction, operation, and maintenance records. The objectives were to be met in the context of typical operation as well as for situations involving operation at a maximum allowable operating pressure (MAOP) of up to 80 percent of the specified minimum yield stress (SMYS), which can occur for example in pipelines whose operation is grandfathered to conditions prior to the introduction of the federal regulations in the early 1970s.

As planned, this objective was to be met in terms of an integrity criterion that was simple to use and applicable on a case-specific basis if desired by the user. The metric for validation was close correspondence between results of the criterion applied to full-scale tests on wrinklebends. As one can infer that multiple wrinkles behaved differently than single wrinkles, this aspect was to be considered. Likewise, because some wrinkles were made cold, while others were made with heated pipe, this aspect also was to be considered, as was the effect of restraint to movement of the wrinkle due to the surrounding soil. Finally, this work has identified differences in the way wrinklebends are made, which can significantly alter the shape of the wrinkle in addition to its known effect on inherent fatigue resistance. These three aspects have not been evaluated. Accordingly, care should be taken to address them in any practical application of this work. Finally, because the co-funding derived from work for the PRCI whose membership includes operators of gas as well liquid pipelines, the scope considered pressure histories and line pipe geometries relevant to gas and liquid pipelines, with the focus remaining onshore applications.

The deliverable sought was an integrity criterion that meets the objective, which was both generic and simple to use, as well as being applicable on a case-specific basis if desired by the user. The metric for validation was close correspondence between results of the criterion applied to full-scale tests on wrinklebends data for which are independently reported[24]. It is anticipated that the criteria delivered will be implemented in reference to data available from field and/or in-line measurements[1] and the operator's records regarding the pipeline's design, construction, operation, and maintenance. Finally, note that this report discriminates between historical construction bending features referred to herein as wrinklebends – and "ripple-bends"[2] which has

---

[1] Certain types of geometry tools are consistent with "adequate geometry characterization", while others are not. Tools consistent with the capabilities needed to detect and characterize wrinklebends have recently become commercially available. Care must be taken to select the tool and identify the required output to ensure utility of the ILI data generated for integrity assessment. Tool requirements are discussed later.

[2] This term traces to Mr. Eugene (Gene) Smith formerly of Natural Gas Pipeline Company, who as chairman of the Line Pipe Supervisory Committee (currently the Materials Committee) of the Pipeline Research Committee

been identified with the longer pitch and smaller amplitude discontinuities that occasionally develop in modern machine-bent pipe. Although this discrimination is noted, the criterion developed could be applied to such features.

By contract, including reference to the cost-share companion project this project considered the scope presented in Table 1, with the results presented later providing coverage for each.

Table 1. Work scope for this project, including coverage by the cost-share project

Task	Deliverable / Milestone
CS1	develop field-usable wrinklebend criteria for 24" X52
CS2	extend criteria to cover diameters from 12 to 36 inches
CS3	extend criteria to cover grades from B to X60
CS4	develop operation-specific criteria
CS5	validate criteria via full-scale testing
1	develop data for localized corrosion effects on fatigue
2	evaluate effects of ID and OD corrosion effects on wrinkle shape
3	embed corrosion effects in severity assessment criteria
4	evaluate effects of local and global constraint
5	embed constraint effects in severity assessment criterion
6	quantify interaction between pressure, constraint, and wrinkle shape
7	quantify effects of hot vs cold formed wrinkles on wrinkle shape
8	quantify effects of hot forming on mechanical and fatigue properties
9	embed constraint and forming history effects in severity criterion
10	quantify differences between wrinkles and large-scale buckles
11	evaluate the significance of service at 80-percent of SMYS
12	complete final report

(PRC), (now the Pipeline Research Council International (PRCI)) suggested its use for this purpose during a much earlier study by the PRCI[25].

Approach

Meeting this project's objectives within the scope noted requires the ability to transform readily measurable features including wrinkle shape and size into parameters like stress and strain that control failure due to fatigue and the presence of corrosion. It also requires the ability to assess how differences in grade, line-pipe geometry, and wrinkle fabrication effect line pipe resistance to fatigue and corrosion, while accounting for differences in operation and maintenance.

Factors that control or characterize resistance to fatigue can be grouped in reference to whether one is interested in the onset of detectable cracking, the rate of its growth, or final fracture. Of these three, the last two require information about crack size, which is unlikely available. More importantly, the present objective involves integrity assessment, which is focused on decisions made to avoid failure that hopefully occur prior to the formation of cracks whose size s use of fracture mechanics. Consequently, this work requires factors that influence fatigue life up through the formation of detectable cracks, which can be used to relate wrinkle shape and size to fatigue crack initiation resistance. The same applies to concern for corrosion, as such failures develop via plastic collapse absent the effects of cracking until the onset of stable tearing.

Once focused on resistance absent concern for cracking, factors that control or characterize line-pipe resistance to fatigue and corrosion can be characterized in terms of stress and strain. In regard to fatigue, factors that control resistance can be grouped as traditional nominal stress-based schemes, and the more recent schemes that focus on conditions local to where failure occurs. In contrast, corrosion criteria involve plastic-collapse, which all involve a measure of the collapse stress and parameters that characterize the increased local stress due to the corrosion. For both corrosion and fatigue at even long life, failure involves at least localized microplastic response, in which cases stresses and strains are no longer linearly related. For this reason, in general schemes that focus on conditions local to where failure occurs must utilize both stress and strain local to the failure, or a measure of their effects. Appendix F presents details of the mechanics theories, models, and results in support of characterizing failure and resistance in terms of stresses and strains. Appendix G furthers these detailed considerations in terms of effective plastic hardening models and fatigue damage parameters, which are central to failure assessment in terms of multiaxial plastic collapse and fatigue.

Schemes that focus on conditions local to where failure occurs are much more complicated than those that represent this situation in terms of nominal stress and some form of stress-concentration factor like K_t or the intensification factor (SIF) approach used in some pressure-vessel codes. Such nominal-stress-based schemes can be effective when dealing with scenarios like machine-formed bellows, whose cross-section and shape are consistently repeated in their forming[e.g., see 26]. However, when dealing with wrinklebends each of which can be unique, schemes adaptable to the locally unique conditions are necessary, with those capable of dealing with nonlinear stress-strain response essential as indicated above. For this reason, a "local stress-strain approach", sometimes termed a "critical-location approach" has been adopted[27,28].

Local Stress-Strain Approach and Wrinklebend Curvature

The local stress-strain approach is illustrated in Figure 1, reproduced from Reference 29. Conceptually, the surface location on the wrinkle where the strains are highest is represented in this schematic by the root of a notch, denoted B in the figure – which corresponds to the crown of the wrinklebend. The through-wall bending gradient in the wrinklebend is represented by the

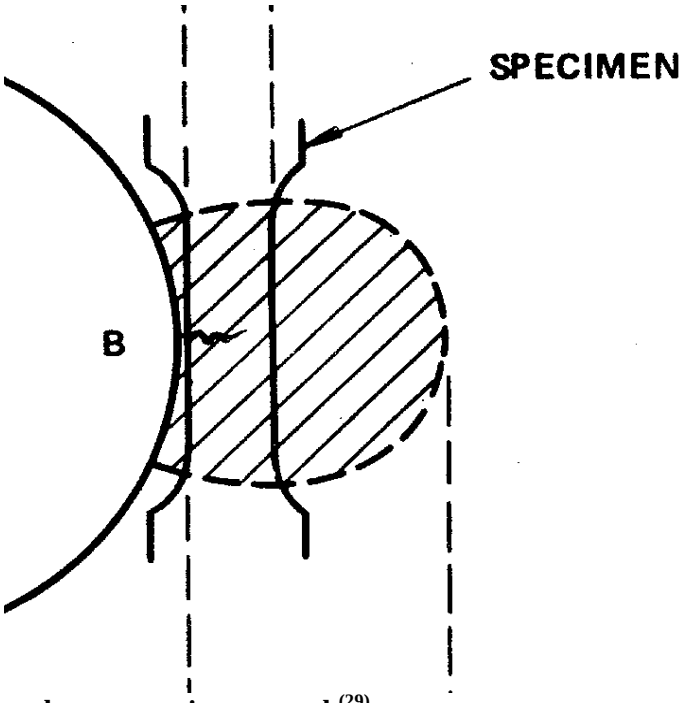

Figure 1. Schematic of the local stress-strain approach[29]

gradient at the notch, which decreases for its peak value at the notch to nominal levels remote to it. Cyclic stretching at the notch parallels cyclic flexing at the wrinklebend due to cyclic pressure or thermal effects. As indicated in the schematic, the properties and response at the notch-root or the surface of the wrinklebend can be represented by the behavior of a test specimen made of the same material subject to the same local conditions. Such specimens are used to generate the stress-strain response characterizing plastic collapse or fatigue resistance.

Numerical analogs constructed according to this approach have shown that when the same strain or damage history is imposed on statistically similar samples, statistically similar resistance develops for a variety of gradient fields, all else being equal[e.g., 30]. Likewise, numerical models formulated consistent with the deformation theory of plasticity and Mendleson's strain-equivalence principle[31] have shown that nominal loadings can be related to the strains and stresses at the critical location in a variety of structural components[32]. Numerical models built in analogy to these concepts were successfully used to predict the failure of wrinklebends as part of the cost-share project for this work[24]. Accordingly, this project builds on this foundation.

Curvature, ILI Geometry Resolution, and Wrinklebend Severity

Integrity analysis of wrinklebends using a "critical-location approach" requires local curvature to characterize wrinkle severity, which requires adequate resolution of this parameter for input to the severity assessment. As evident from Figure 2, the local curvature shows a characteristic dependence on the length, L, (pitch) of the wrinkle and its height, H, (amplitude), with the maximum curvature at the crown (the most peaked area) typically near the circumferential center of the wrinkle. Such trends also are evident in numerical simulations of buckles.

Profiles through the crown or elsewhere around the wrinkle along a line tracing the length of the pipe facilitate measuring wrinkle height and length. Wrinkle shapes tend to be similar, until the height of the wrinkle becomes large compared to the length and a kink begins to form in place of

smooth curvature at the crown. Figure 2a shows some traces along a line through the crown of several wrinkles made in 20-inch diameter line pipe with a 0.310-inch thick wall. The ratio of pipe radius, R, to wall thickness, t, for this pipe was $R/t = 32$, which is relatively low for some cross-country pipeline designs. Figure 2b shows similar trends drawn in progressing around a wrinkle away from the crown for another pipeline of similar R/t. It is evident that wrinklebends develop a wrinkle whose cross-section protrudes beyond the pipeline's profile, as opposed to dents that penetrate its profile. The profile of this protrusion is like a cycloid or sinusoid, the later being expected if the wrinkle process involves formation of a localized smooth buckle. While such analytical profiles are smooth and symmetric, wrinkles are not always symmetric about their crown, either along or around the pipeline. However, when the circumferential extent of the wrinkle becomes large instability can occur as the adjacent sides of the wrinkle collapse onto each along with collapse of the cross-section – leading to very large curvature and equally large strains at what was the crown of the wrinkle. Figure 3a illustrates this scenario.

Empirical evidence suggests that the onset of collapse occurs for wrinkles traversing more than ~95-percent of the circumference, with the numerical results suggesting this becomes evident for larger-diameter line pipe at values of $H/L > \sim 0.70$. As Figure 3a illustrates, with collapse the smooth gradual radii of curvature evident in Figures 2a and 2b gives way to peaked wrinkles whose shapes often are asymmetric. But, for lower values of the wrinkle-aspect-ratio H/L, the shapes of wrinkles are well behaved such that H/L can serve as a surrogate for curvature in the crown of the wrinklebend. For such scenarios, the requirement for high displacement resolution to measure local curvature can be replaced by the much less demanding resolution adequate the parameters H and L. It follows that the critical-location approach of Figure 1 can employ the wrinkle aspect ratio (H/L) as a surrogate for curvature provided that $H/L \leq 0.7$. Because larger aspect ratios tend to reflect collapsed wrinklebends whose structural integrity cannot be simply characterized, the use of H/L as a surrogate for curvature does not limit the practical utility of the criteria developed hereafter.

As elaborated in Appendix B, there are several possible was to define H/L, three of which are shown here in Figure 3b. Some of these definitions are instructive in an analytical setting but virtually impossible to evaluate from ILI of field measurements, whereas others are simple to measure in the field but potentially less instructive from an analytical perspective. Still other definitions are hybrids of the analytically instructive and the practical field-based definitions. Recognizing that the criteria developed will be implemented under field conditions, all results are transformed and presented in terms of easily measured field parameters. In reference to Figure 3b, the notation used here, H/L, is consistent with that in the figure. Accordingly, the height of the wrinkle, H, is measured from the crown to a line projected along the straight portion of the pipeline back toward the wrinkle. If the wrinkle includes reverse curvature back into the pipeline's cross-section, measuring the height to the bottom of this curvature is both convenient and also conservative. The length of the wrinkle is the axial distance over which the pipeline's circular cross-section is upset. When uncertain, this dimension should be underestimated leading to a conservative value of H/L. Wrinklebends that appear collapsed should be considered for near-term replacement (i.e., a scheduled but not immediate repair). Straight edges and carpenters profile gages are effective tools for field measurements, whereas the output of a high-resolution ILI deformation or geometry tool should suffice in quantifying H/L. It remains now to transform this severity metric into measures of plastic collapse and fatigue resistance, and address the effect of corrosion.

(a) traces along the crowns of five different wrinkles

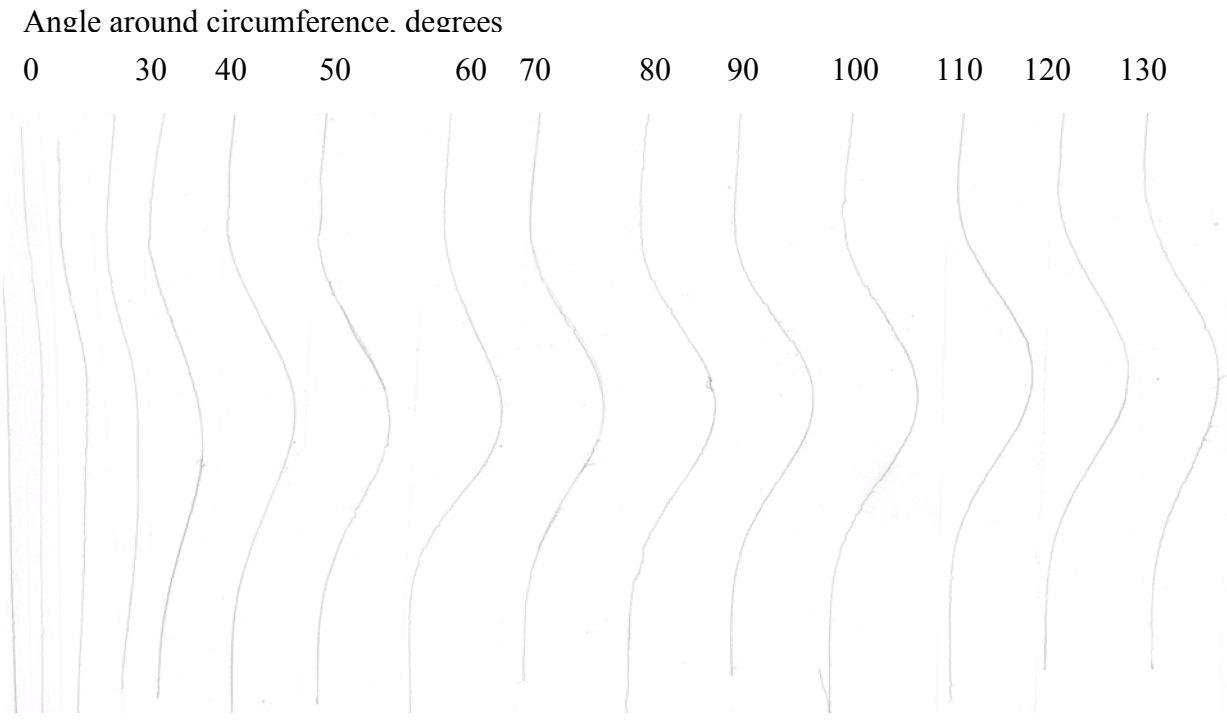

(b) typical traces around the wrinkle

Figure 2. Wrinkle shapes observed in vintage 20-inch x 0.310-inch X42 line pipe

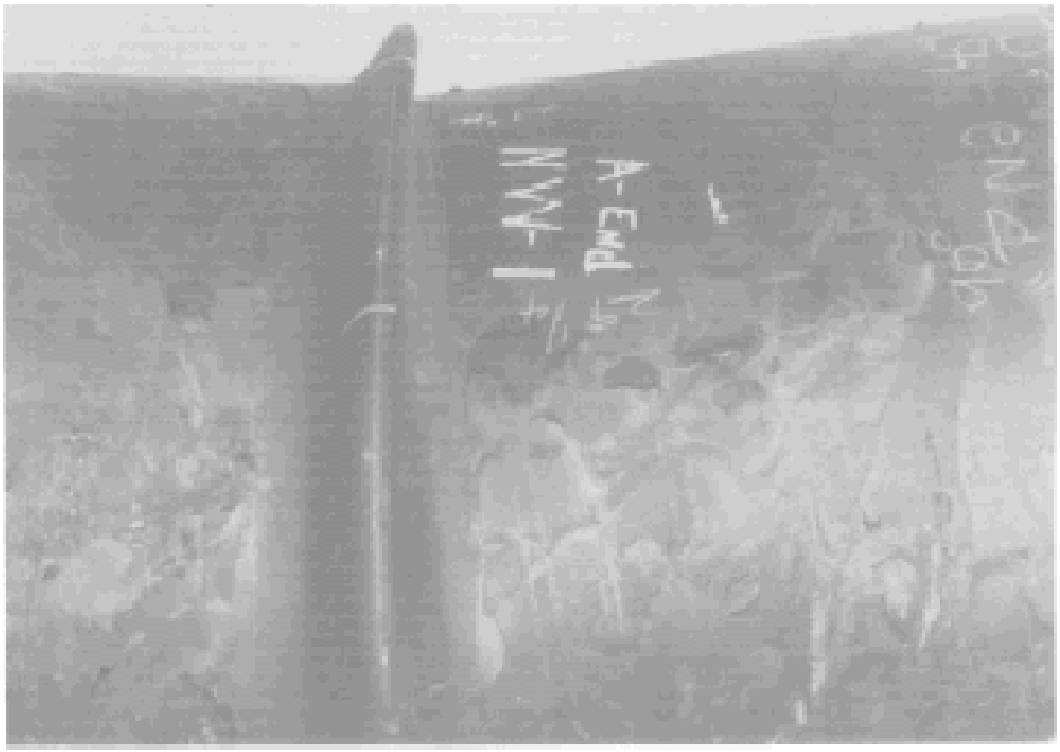

(a) view of a severe (collapsed) wrinklebend (shows ~top-half of the line pipe)

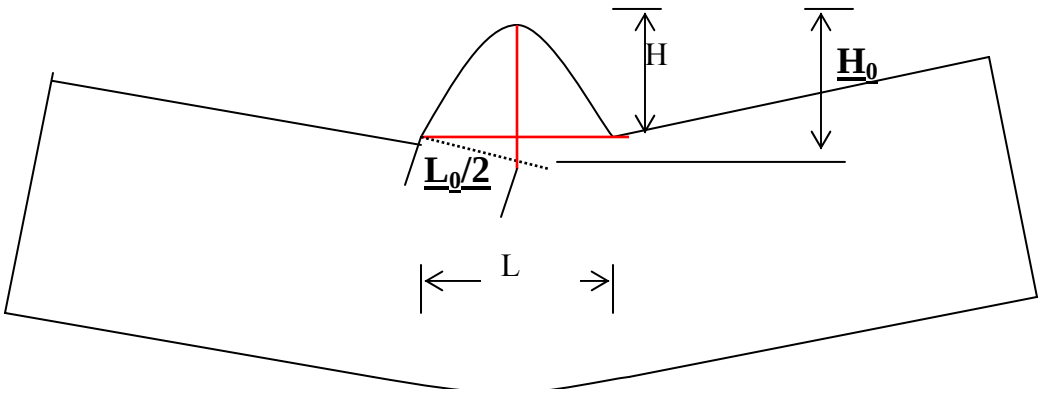

Three definitions considered:

***H/L* (generally adopted as it is easiest measured in the field)**

H_0/L_0

H/L_0

(b) nondimensional definition of severity

Figure 3. Aspects of wrinklebend severity

Transforming Wrinklebend Shape to Integrity-Related Metrics

Wrinklebends can fail because of cycling imposed in service or secondary loads that exceed the line pipe steel's resistance to the stresses and strains and accumulated damage over the service history. Integrity management is focused on decisions made to avoid failure that occur prior to the formation of critical cracking, which for thin-walled structures subject to cyclic and other secondary loading focuses on fatigue life up through the formation of detectable cracks. Where corrosion is present, its influence on the local stresses and strains must be addressed, as must its possible synergistic effect on fatigue resistance. Likewise, where the possibility for hot-formed wrinkles exists, related changes in the stresses and strains must be addressed as must the effects on fatigue resistance. The companion cost-share project successfully adopted a damage-parameter as the conceptual basis to characterize the coupled effects of stresses and strains on structural resistance to fatigue, which in turn could be related to wrinkle shape through curvature then to strain, then to stress and strain.

The damage parameter used in the companion cost-share project represented the collapse limit state under displacement control in terms of true stress and true strain developed at failure in the usual tensile test, denoted here as σ_f and ε_f, whereas the limit state for load control was represented in terms of the ultimate tensile stress (UTS) developed in that same test. Expressions such as the Ramberg-Osgood[33] power-hardening law given as:

$$\epsilon = \sigma/E + 1/K\ \sigma^{m} \qquad (1)$$

can be used to represent such parameters for purposes of analysis, where E = elastic modulus, and K and m are fitting constants. Appendix F elaborates related functional forms and details, whereas Appendix G considers hardening rules and their implications in forming hysteresis loops in cases where cycle-by-cycle deformation and fatigue analysis is implemented. Full-range stress-strain response needed to quantify the variables in Equation 1 have been developed and presented for GrB, X42, X46, X52 in the cost-share companion report[24].

The literature indicates some early vintage line-pipe steels (40s era) easily develop values of ε_f in excess of 0.50[e.g., see 34], while other line-pipe steels from subsequent construction are known to fail at ε_f as low as 0.04[e.g., see 35]. On this basis it is essential to have some idea of the properties of the line pipe for the wrinkle being evaluated – because a low of ε_f such as just noted could require a different approach to integrity management.

The damage parameter used in the companion cost-share project represented the fatigue limit state under displacement control, in a format that embeds the load control case, using an energy-based fatigue damage parameter[36], which has been validated for uniaxial mean stress as well as multiaxial local mean stress and strain conditions. Through this damage parameter, D, equivalent fatigue damage states for various different stress ratios are expressed in the form:

$$D = \sigma_m\ \Delta\epsilon^t + \Delta\sigma\ \Delta\epsilon^t, \qquad (2a)$$

where σ_m denotes the mean stress, $\Delta\sigma$ and $\Delta\epsilon^t$ respectively denote ranges of stress and total strain. For fully reversed or nearly fully reversed cycling, this $\sigma_m = 0$ such that $\Delta\sigma\ \Delta\epsilon$ when expressed in terms of amplitudes can be written:

$$D = \sigma_{max}\ \Delta\epsilon^t/2, \qquad (2b)$$

where σ_{max} denotes the maximum critical location stress and $\Delta\epsilon_t$ is as above. For the results to follow, strain is expressed as percent-strain. When multiaxial stresses and strain states are

involved, the quantities in this equation are replaced by their von Mises equivalent[e.g., see 31] values, which are evaluated after the vector component ranges are determined.

As outlined in Appendix G, this project evaluated other damage parameters for the present application in regard to the hardening rules used in their application to cyclic loadings at wrinklebends. The results in Appendix G indicate that the Smith-Watson-Topper[37] (SWT) damage parameter, whose form is identical to Equation 2a under fully reversed conditions – i.e., Equation 2b – performed slightly better in comparing damage-model predictions with full-scale testing of wrinklebends[24] than did Equation 2a. Consequently, this damage parameter is adopted for use hereafter.

Because the surface condition can affect significant differences in fatigue resistance, fatigue data tend to be developed using polished smooth specimens as the reference condition – with a reduction factor applied to that results to account for surface roughness. This practice was followed in the cost-share companion project, with such results developed and presented for GrB, X42, X46, X52, on through higher strength grades not relevant to vintage pipelines[24]. The fatigue life of polished specimens, N^p, can be expressed as a function of damage, D, developed in terms of Equation 2 as:

$$N^p = f\, D^{\,c}, \tag{3}$$

where the symbols "f" and "c" denote the set of empirical constants typically required to represent fatigue resistance in a piecewise power-law format reported in Reference 24. As outlined in that report, because the surface of pipelines is not highly polished but typically can be quite rough surface and include a layer of mill-scale life reduction factors were applied consistent with handbook results specifically focused on surface finish[38].

Handbook trends indicate that where plastic strain controls failure as occurs for lower-cycle fatigue, surface finish tends to be a secondary factor. This occurs because the plastic straining itself creates significant surface roughness as compared to the initially polished surface, which overrides roughness effects due to other sources. However, surface finish can have a first-order effect on fatigue resistance where elastic response tends to control the response. As outlined in Reference 24, plastic strain dominates elastic response at lives the order of 100 to 200 cycles to failure for the steels evaluated. Accordingly, surface finish can be anticipated to increasingly become a factor for cyclic loadings the order of many hundred cycles, becoming fully effective at and beyond the transition fatigue life. For the steels evaluated, this was ~5,000 to ~20,000 cycles, which involves lives the order of the number of cycles associated with some pipeline operations over the book-life of the pipeline. It follows that when typical fatigue resistance data are applied to analyses of pipelines, surface finish should be considered. Handbook data indicate that where elastic response dominates, a life-reduction factor of 0.1 appears to be conservative for many in-service scenarios, while a factor of 0.01 would certainly be conservative in general.

While surface finish is an important factor, surface residual stresses induced in steel and pipe making are not considered in reference to Equations 2 and 3 because the inelastic action in forming the wrinklebend overrides such history for cold-formed wrinkles, while the high temperatures associated with heating wipe it out for hot-formed wrinkles. Subsequent service establishes a unique stress-strain cycle, which has been addressed in the mechanics analysis that is presented here in Appendices F and G, which builds on Appendix F of Reference 24.

Results

According to the detailed analyses and results in Appendices F and G, a combined isotropic/kinematic hardening model was adopted as the plastic hardening model in all finite-element analyses (FEA) calculations reported in this section. As noted earlier, for the present applications the SWT damage parameter was selected as the damage measure for fatigue analysis. Detailed outcomes and results follow in sequence for each of the scenarios identified in the work scope presented as Table 1.

Develop Field-Usable Criteria as Function of Wrinklebend Shape

Following practices comparable to that detailed in Appendices F and G, and in Appendix F or Reference 24, FEA calculations were made using the combined hardening model in ABAQUS for three wrinkle shapes, *H/L* = ~0.15, *H/L* = ~0.30, and *H/L* = ~0.48, which reasonably span the characteristics of wrinklebends in long-term service. These analyses considered near worst-case cycling from 72 percent of SMYS down to 10 percent of SMYS as the reference service condition, with the pipeline taken at a diameter of 24 inches and a wall thickness of 0.283 inches made of X52 steel. The same analyses were done for cycling from 80 percent of SMYS down to 10 percent of SMYS in regard to scenarios involving, for example, wrinklebends operating in pipelines grandfathered to run as high as 80 percent.

Based on the FEA numerical stress and strain at the critical location of the wrinkle, i.e., the ID of the wrinkle crown, the SWT damage parameter was determined for the three wrinkle shapes. The set of three data points for the damage parameter determined from the FEA calculations can be very well curve-fitted by a linear equation:

$$\begin{aligned} D_f &= 0.692(H/L), \qquad \text{for } 72\% - 10\% \text{ SMYS} \\ D_f &= 0.827(H/L), \qquad \text{for } 80\% - 10\% \text{ SMYS} \end{aligned} \tag{4}$$

where H is the wrinkle height and L is the wrinkle wavelength.

From the material fatigue resistance curve in Equation A16 and the above Equation 4, the wrinkle size can be expressed as a function of the fatigue life or the pressure cycle to failure as follows:

$$\begin{aligned} H/L &= 394.51(2N_f)^{-1.02} + 3.03(2N_f)^{-0.28}, \quad \text{for } 72\% - 10\% \text{ SMYS} \\ H/L &= 330.11(2N_f)^{-1.02} + 2.54(2N_f)^{-0.28}, \quad \text{for } 80\% - 10\% \text{ SMYS} \end{aligned} \tag{5}$$

These equations can be used as the wrinklebend criterion to estimate the fatigue life for a given size of the wrinkle shape and maximum service stress. Evaluating these equations indicates that the service life of wrinklebends decreases rapidly as the wrinkle size increases. For example, for the wrinkle size of *H/L* = 0.1, the fatigue life is indicated by Equations 5 to be about 100,000 for cycling from 72 percent of SMYS down to 10 percent of SMYS, whereas the life is slightly shorter for cycling from 80 percent of SMYS down to 10 percent of SMYS. However, when a significant increase in the wrinkle severity reflected in its shape is considered, for example *H/L* = 0.5, the fatigue service life for cycling from 72 percent of SMYS down to 10 percent of SMYS drops considerably to about 1000 cycles. This slight decrease in life for cycling from a maximum stress of 72 percent of SMYS versus 80 percent of SMYS is expected because the initial pressure at the higher maximum stress gives rise to a higher stress ratio as compared to

cycling at a lower maximum pressure, which in turn leads to shorter life. Accordingly, wrinkles in pipelines grandfathered to operate at marginally higher pressure are somewhat more severe than in other pipelines – all else being equal. However, this increase in severity is marginal as compared to parameters such as wrinkle shape.

The wrinkle size versus fatigue life relationship in Equations 5 is a simple basis to estimate wrinklebend life, provided that the wrinkle shape is known from field measurements or ILI data. In such cases, this simple criterion can be used by field engineers to assess the integrity of the practical wrinklebends for the size and grade of line pipe considered and the service loading evaluated. The key question is: can this simple criterion be extended to other line pipe geometries (diameter, D, and thickness, t, for a range of D/t) and service loadings, without introducing great complexity? Beyond this useful generalization, how does grade influence the trends? These questions were asked and answered by work done to complete the next several tasks in Table 1.

Extend the Scope to Cover Diameters from 12 to 36 Inches

If the form of Equations 4 and 5 can be simply generalized in nondimensional terms to cover an extensive range of pipeline geometries, then the simple wrinklebend criterion developed in Task 1 will have great utility without complexity. This was done for pressure cycling involving a maximum stress of 72 percent of SMYS down to 10 percent of SMYS as well as for cycling from 80 percent of SMYS down to 10 percent of SMYS.

The possibility that a simple criterion would evolve from these analyses was evaluated by expanding the FEA database to include diameters from 12 to 36 inches, in different combinations of wall thicknesses and diameter. Detailed FEA calculations were completed for the same range of wrinklebend for diameters from 12 to 36 inches, for wall thickness from 0.14 to 0.5 inches. The pairs of diameter and thickness lead to the radius to thickness ratios *R/t* from 16 to 57, which reflects the typical range of line pipe geometries from heavier wall through quite light wall scenarios. The material considered for this set of parametric analyses was X42 in conjunction with the combined plastic hardening model. The analyses considered the same pressure-cyclic conditions discussed above in regard to X52 line-pipe steel – that is 72 to 10 percent of SMYS and 80 to 10 percent of SMYS.

Based on the FEA stress and strain at the critical location of wrinklebend, the SWT damage parameter is determined as shown in Figure 4, with the linearly fitted equations for cyclic pressure of 72 to 10 percent of SMYS as:

$$\begin{aligned} D_f &= 0.565(H/L), && R/t \geq 25 \\ D_f &= 0.405(H/L), && R/t = 21.2 \\ D_f &= 0.115(H/L), && R/t = 16 \end{aligned} \tag{6a}$$

and for 80 to 10 percent of SMYS as:

$$\begin{aligned} D_f &= 0.678(H/L), && R/t \geq 25 \\ D_f &= 0.486(H/L), && R/t = 21.2 \\ D_f &= 0.148(H/L), && R/t = 16 \end{aligned} \tag{6b}$$

The variation of the coefficients in Equations 6 with the *R/t* is plotted in Figures 5 for cyclic pressure of 72 to 10 percent and from 80 to 10 percent of SMYS. The coefficients have been curve-fitted for the two pressure cases with the results as included in this figure. Therefore, the form of Equation 6 can be simply generalized, with a general damage parameter including pipe geometry approximated for cyclic pressure of 72 to 10 percent of SMYS as:

$$\begin{aligned} D_f &= 0.565(H/L), && R/t \geq 25 \\ D_f &= 0.05(R/t - 13.5)(H/L), && 13.5 < R/t < 25 \end{aligned} \tag{7a}$$

and for 80 to 10 percent of SMYS as:

$$\begin{aligned} D_f &= 0.678(H/L), && R/t \geq 25 \\ D_f &= 0.06(R/t - 13.5)(H/L), && 13.5 < R/t < 25 \end{aligned} \tag{7b}$$

Using the material fatigue resistance curve in Equation A16, the relationship between the wrinkle size *H/L* and the fatigue life N_f can be expressed as follows:

for $R/t \geq 25$ and cyclic pressure of 72 to 10 percent of SMYS;

$$\frac{H}{L} = 483.19(2N_f)^{-1.02} + 3.72(2N_f)^{-0.28} \tag{8a}$$

whereas for $13.5 < R/t < 25$ and cyclic pressure of 72 to 10 percent of SMYS;

$$\left(0.05\frac{R}{t} - 0.675\right)\left(\frac{H}{L}\right) = 273(2N_f)^{-1.02} + 2.1(2N_f)^{-0.28} \tag{8b}$$

while for $R/t \geq 25$ and cyclic pressure of 80 to 10 percent of SMYS;

$$\frac{H}{L} = 402.65(2N_f)^{-1.02} + 3.10(2N_f)^{-0.28} \tag{9a}$$

but for $13.5 < R/t < 25$ and cyclic pressure of 80 to 10 percent of SMYS;

$$\left(0.06\frac{R}{t} - 0.81\right)\left(\frac{H}{L}\right) = 273(2N_f)^{-1.02} + 2.1(2N_f)^{-0.28} \tag{9b}$$

The influence of line pipe geometry on fatigue life can be illustrated for different line pipes from the equations above, considering for example line pipes with *R/t* = 16, 20. For these two line-pipe geometries the wrinklebend fatigue lives can be estimated from *H/L* as follows:

for cyclic pressure of 72 to 10 percent of SMYS;

$$\frac{H}{L} = 840(2N_f)^{-1.02} + 6.46(2N_f)^{-0.28}, \qquad \text{for } R/t = 20 \tag{10a}$$

$$\frac{H}{L} = 2184(2N_f)^{-1.02} + 16.8(2N_f)^{-0.28}, \qquad \text{for } R/t = 16 \tag{10b}$$

while for cyclic pressure of 80 to 10 percent of SMYS;

$$\frac{H}{L} = 700(2N_f)^{-1.02} + 5.38(2N_f)^{-0.28}, \qquad \text{for } R/t = 20 \tag{11a}$$

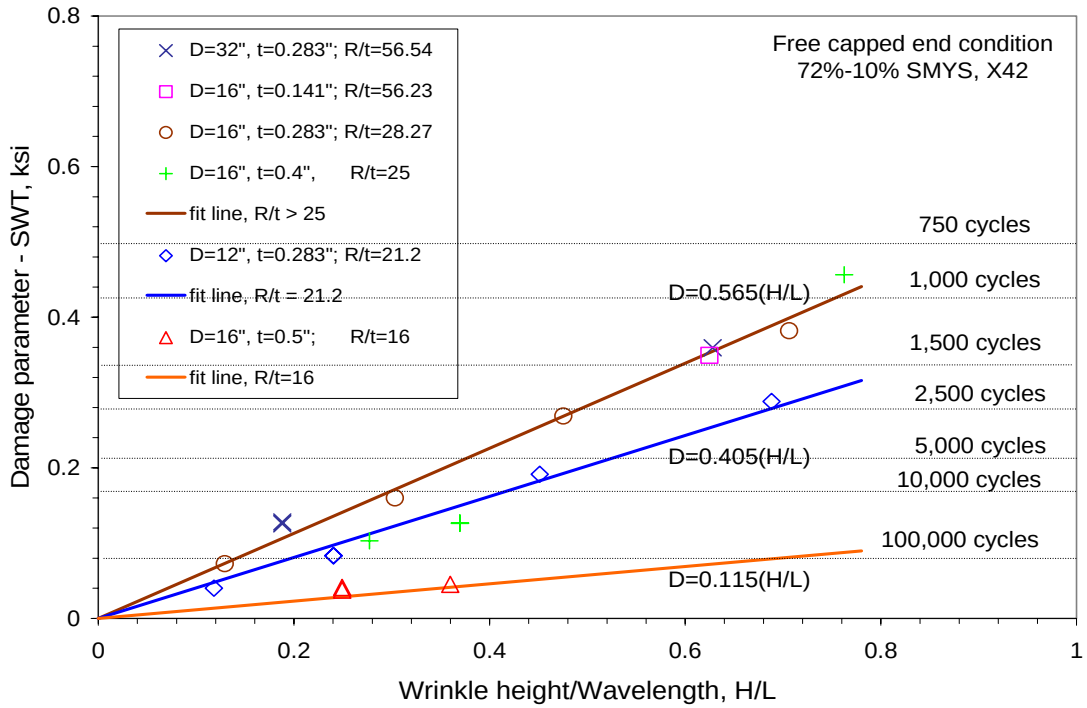

(a) 72%-10% SMYS

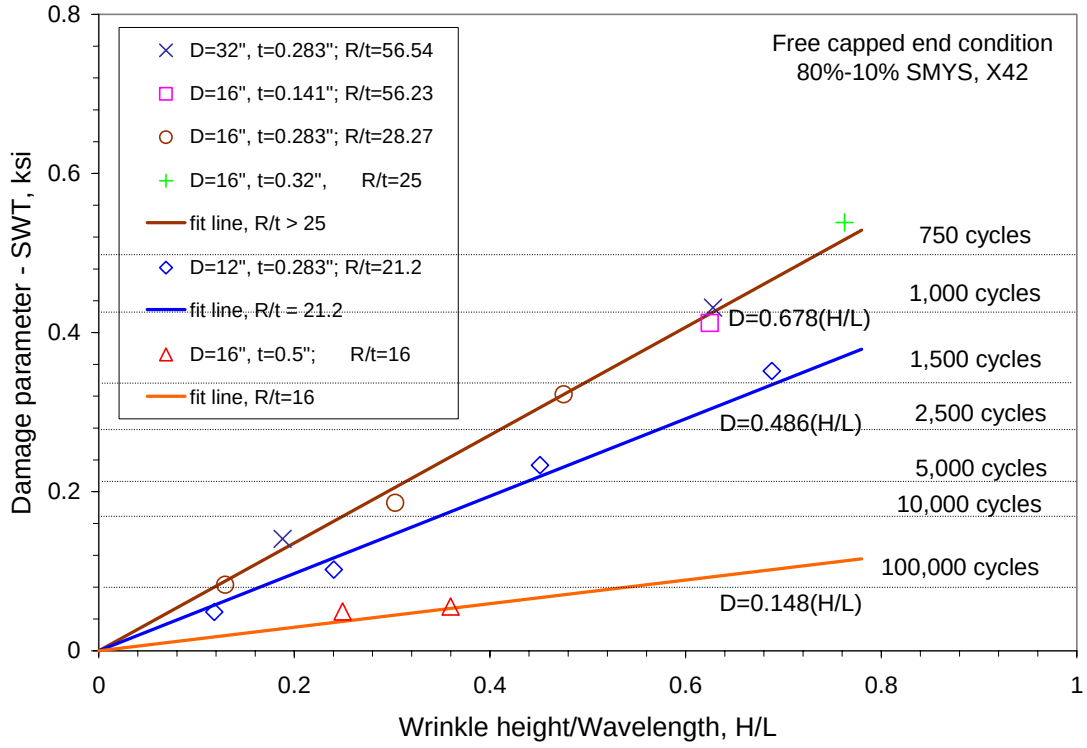

(b) 80%-10% SMYS

Figure 4. SWT damage parameter versus wrinkle size for different pipe sizes

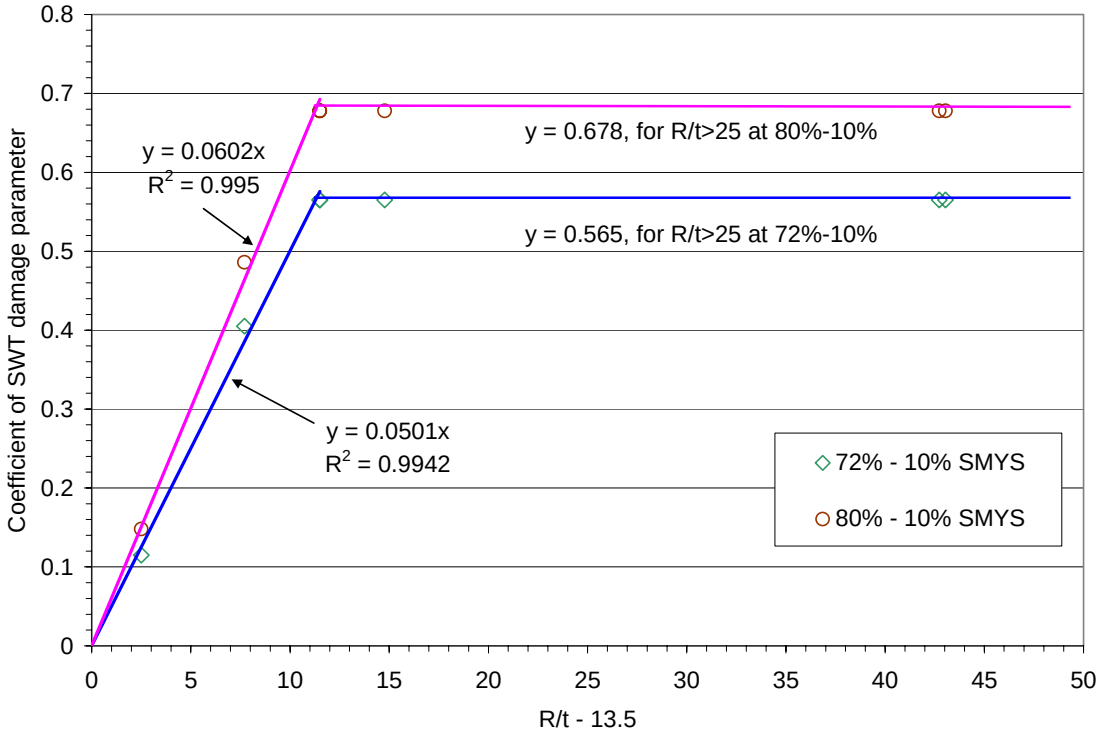

Figure 5. *R/t* effect on wrinklebend damage D1 for combined model

$$\frac{H}{L} = 1820\left(2N_f\right)^{-1.02} + 14.0\left(2N_f\right)^{-0.28}, \qquad \text{for } R/t = 16 \tag{11b}$$

From Equations 8, 9, and 10, the fatigue lives for a given wrinkle shape given by *H/L* have been determined for pipe sizes of *R/t* = 25, 20, and 16 with the results as presented in Figure 6 for pressure cycling from 72 to 10 percent and from 80 to 10 percent of SMYS. The trends in these figures clearly demonstrate that the line-pipe nondimensionl size characterized by *R/t* has significant effect on the wrinklebend life for *R/t* < 25. That is, as the stiffness of the cross-section increases as *R/t* falls below 25, the line-pipe's response to the formation of this wrinkle and its propagation around the circumference changes significantly. For less-stiff cross-sections that occur for line pipe whose geometries lead to *R/t* equal or larger than 25, the formation of the wrinkle and its propagation around the circumference is largely independent of geometry. For these less-stiff cross-sections, this integrity criterion is more or less identical. For *R/t* < 25, at a given value of *H/L* the wrinklebend fatigue life will be significantly increased as the cross-section stiffens. Conversely, the life reduces as the cross-section becomes more flexible through increased *R/t*.

In summary, this section has shown that for a similar wrinkle size, a wrinklebend with a larger pipe diameter and/or thinner wall thickness is likely to fail sooner than a wrinklebend with smaller pipe diameter and/or thicker wall thickness for otherwise similar service conditions. But, where the pipeline diameter is large enough or a wall thickness is thin enough, i.e. $R/t \geq 25$, the wrinklebend fatigue life becomes be independent of the line-pipe geometry.

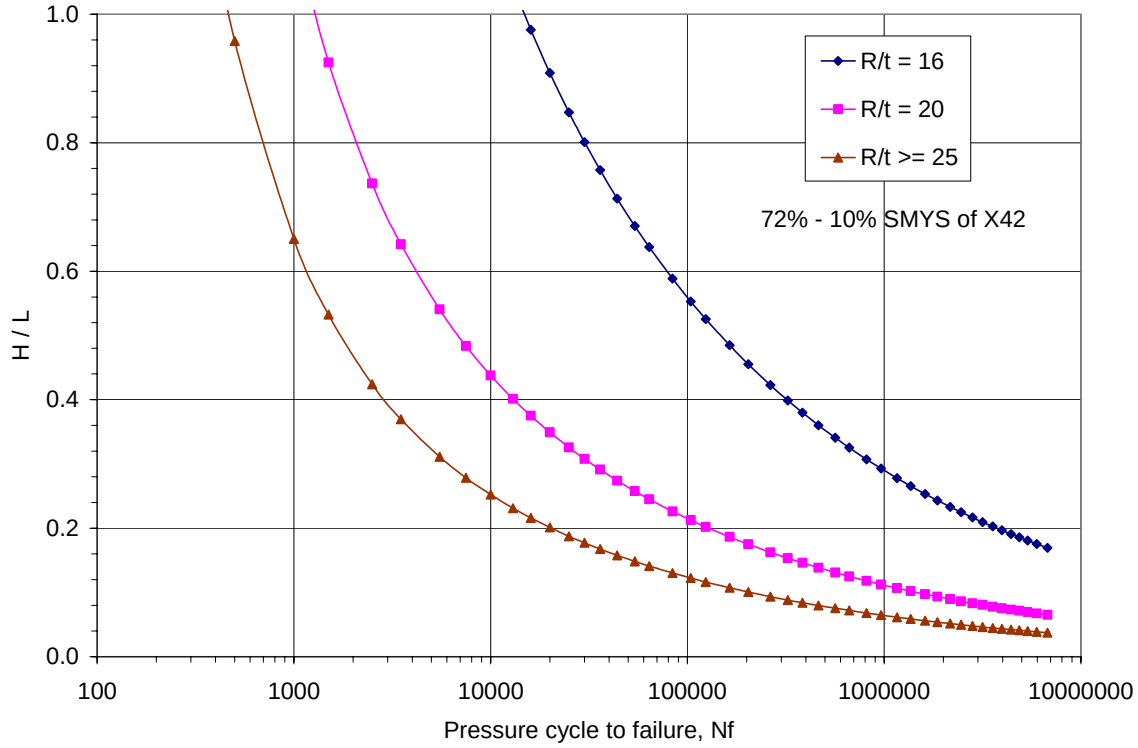

(a) cyclic pressure from 72 to 10 percent of SMYS

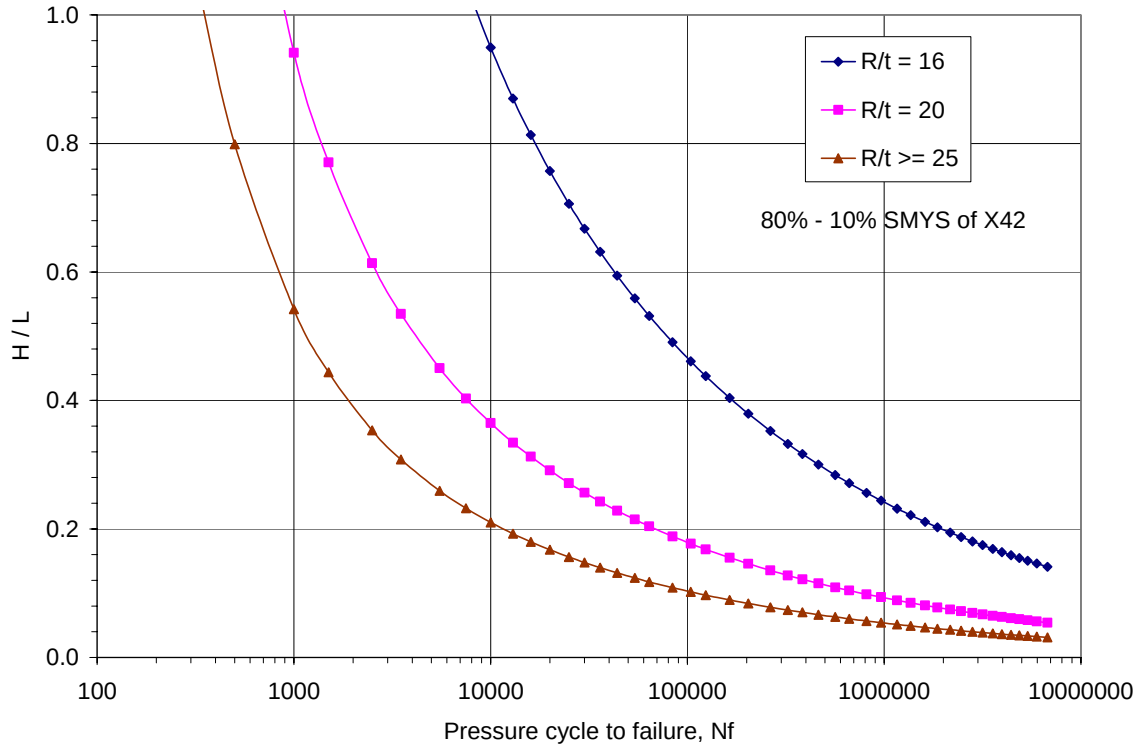

(b) cyclic pressure from 80 to 10 percent of SMYS

Figure 6. Effect of pipe geometry (*R/t*) on wrinklebend life

For the sake of comparison with the damage parameter adopted for the prior cost-share project, Figures 7 and 8 contrast the effect of the pipe geometry in terms of *R/t* on wrinklebend criteria in reference to the damage parameter of Equation 2, and the total energy form of this parameter, respectively, as detailed in Appendix G. Part a in these figures presents results for pressure cycling from 72 to 10 percent whereas part b presents results for cycling from 80 to 10 percent of SMYS. Because the SWT parameter used in Figure 4 affords the most consistent predictions as demonstrated in that appendix, all subsequent discussion of fatigue life is made here in terms of the SWT damage parameter.

Extend the Scope to Cover Grades from GrB to X60

As for the case of line-pipe geometry just discussed, if the form of Equation 4 can be simply generalized in nondimensional terms to cover the range of line-pipe grades of concern for wrinklebends, then the simple criterion developed in Task 1 will have great utility without added complexity. This possibility was evaluated by expanding the FEA database to include line-pipe steel grades from B to X60. Detailed FEA calculations were conducted for different wrinklebends in pipeline steel grades, GrB, X42, X52, and X60. These numerical analyses focused on 16-inch diameter line pipe with a wall thickness of 0.283 inch, realizing that the outcome could be generalized as just discussed across the range of pipe geometries. The applied loading is as has been used above, considering a cyclic pressure from 72 percent to 10 percent of SMYS and 80 percent to 10 percent of SMYS for each of the four steel grades noted.

Based on the FEA stress and strain at the critical location of wrinklebend, the SWT damage parameter was determined as shown in Figures 9a and 9b respectively for pressure cycling from 72 to 10 percent and from 80 to 10 percent of SMYS. These results can be linearly fitted by the following equations relating the damage parameter to wrinklebend geometry, which for cyclic pressure of 72 to 10 percent of SMYS gives:

$$\text{GrB:}\quad D_f = 0.348(H/L) \tag{12a}$$

$$\text{X42:}\quad D_f = 0.565(H/L) \tag{12b}$$

$$\text{X52:}\quad D_f = 0.692(H/L) \tag{12c}$$

$$\text{X60:}\quad D_f = 0.897(H/L) \tag{12d}$$

while for 80 to 10 percent of SMYS one obtains:

$$\text{GrB:}\quad D_f = 0.418(H/L) \tag{12e}$$

$$\text{X42:}\quad D_f = 0.678(H/L) \tag{12f}$$

$$\text{X52:}\quad D_f = 0.827(H/L) \tag{12g}$$

$$\text{X60:}\quad D_f = 1.075(H/L) \tag{12h}$$

Such results are presented for all cases in Figures 9a and 9b respectively for pressure cycling from 72 to 10 percent and from 80 to 10 percent of SMYS.

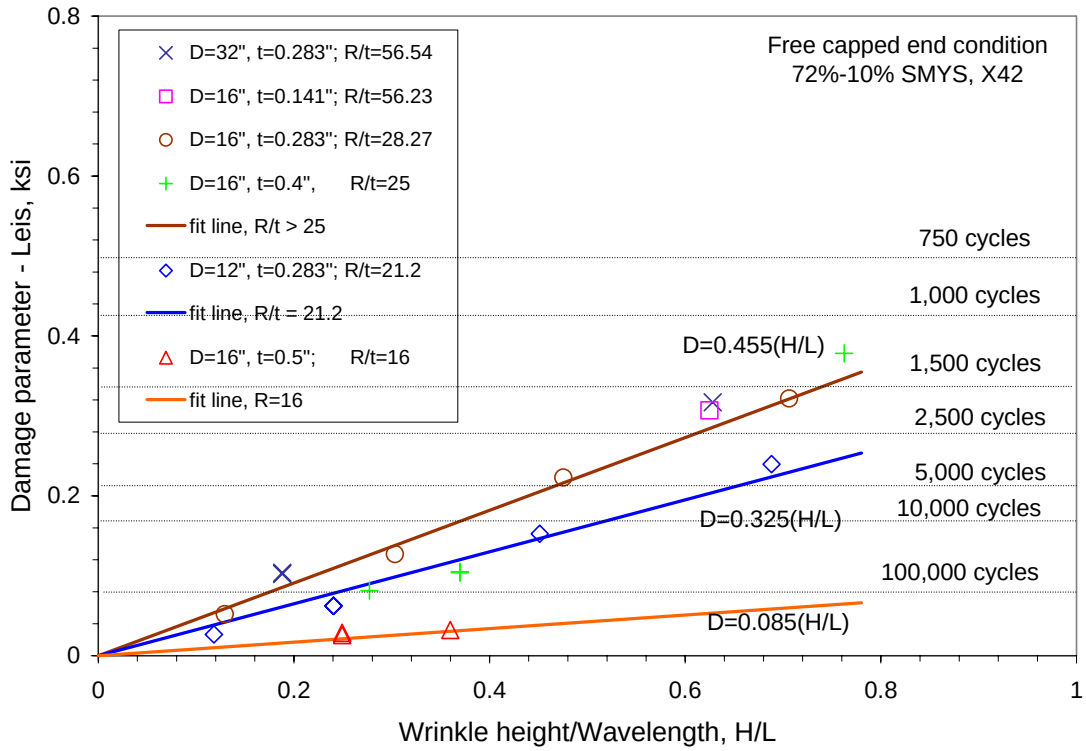

(a) cyclic pressure from 72 to 10 percent of SMYS

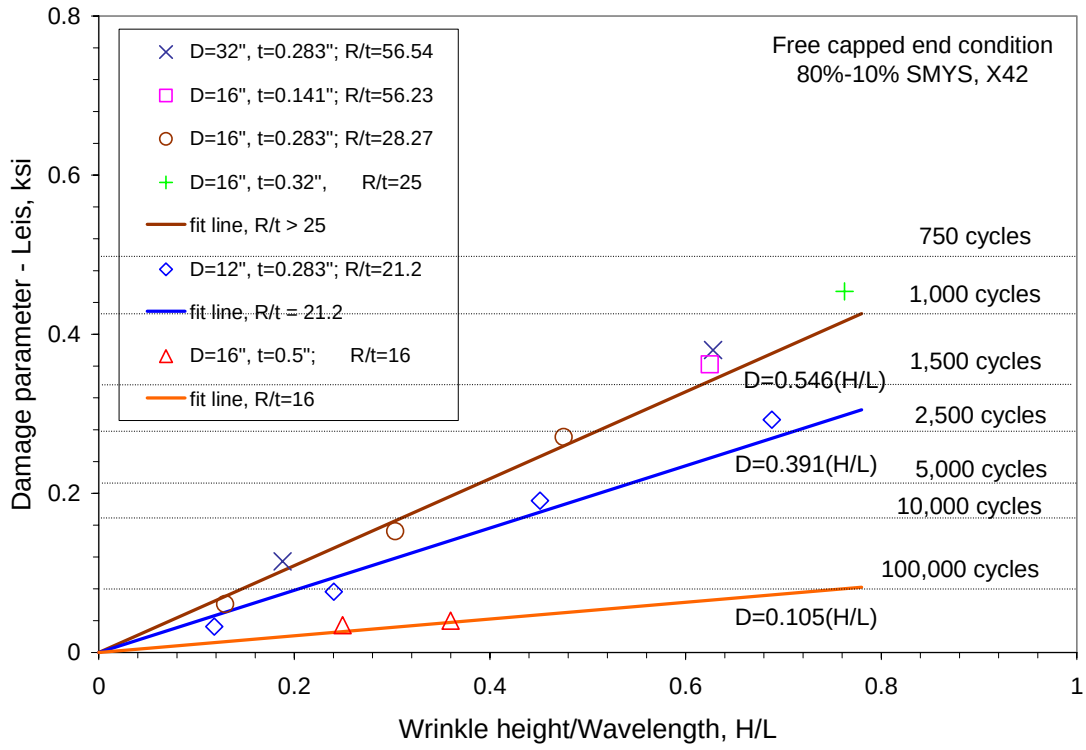

(b) cyclic pressure from 80 to 10 percent of SMYS

Figure 7. *R/t* effect on wrinklebend criteria for the SWT damage parameter

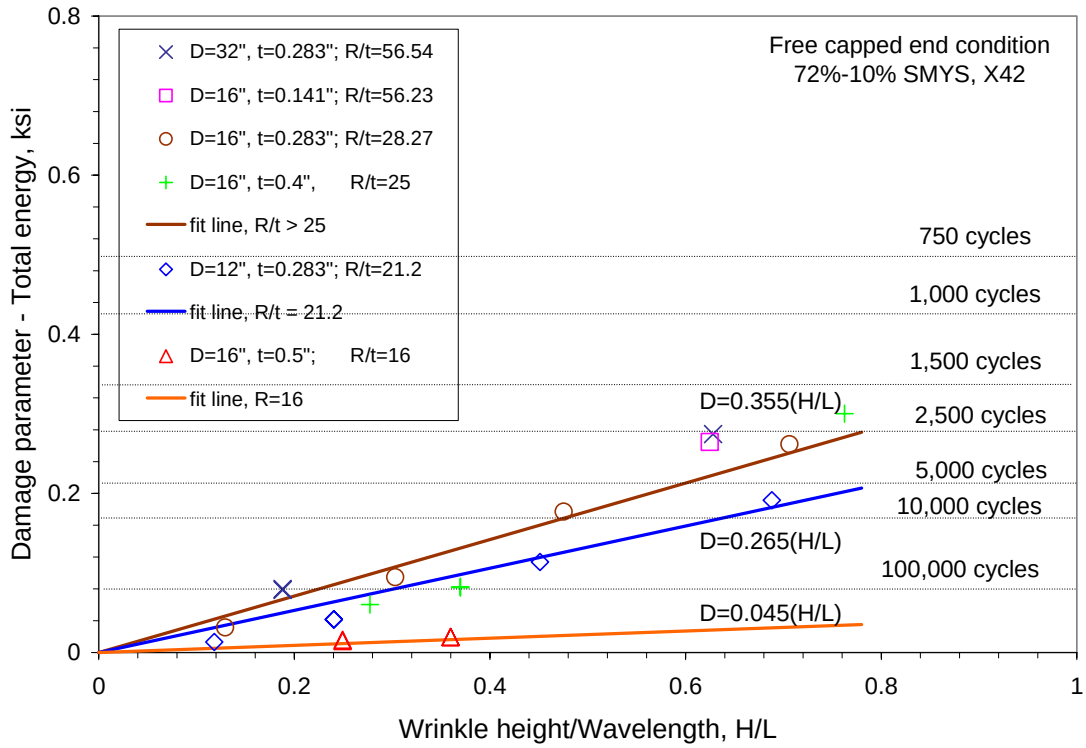

(a) cyclic pressure from 72 to 10 percent of SMYS

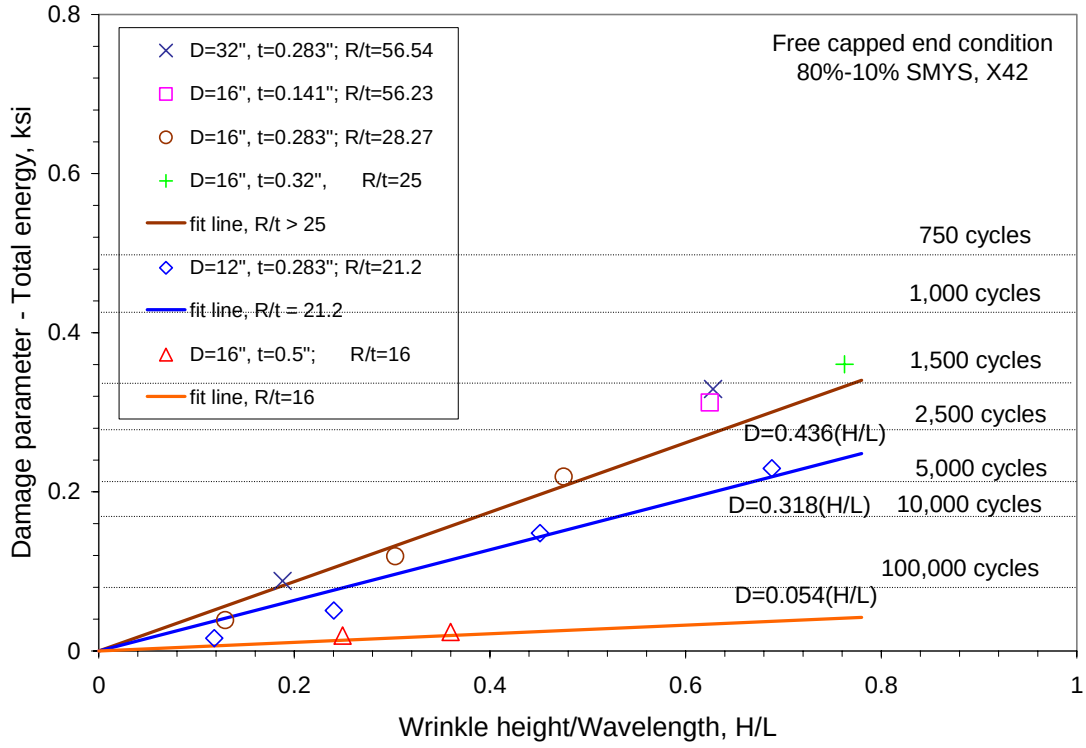

(b) cyclic pressure from 80 to 10 percent of SMYS

Figure 8. R/t effect on wrinklebend for total energy parameter used in Reference 24

As above, using the material fatigue resistance curve in Equation A16, the relationship between the wrinkle size *H/L* and the fatigue life N_f can be determined. Accordingly, the damage parameter can be eliminated leading to curves defining the wrinkle size versus fatigue life and relationships determined for cyclic pressure of 72 to 10 percent of SMYS as:

$$\text{GrB:}\quad \frac{H}{L} = 784.48\left(2N_f\right)^{-1.02} + 6.03\left(2N_f\right)^{-0.28} \tag{13a}$$

$$\text{X42:}\quad \frac{H}{L} = 483.19\left(2N_f\right)^{-1.02} + 3.72\left(2N_f\right)^{-0.28} \tag{13b}$$

$$\text{X52:}\quad \frac{H}{L} = 394.51\left(2N_f\right)^{-1.02} + 3.03\left(2N_f\right)^{-0.28} \tag{13c}$$

$$\text{X60:}\quad \frac{H}{L} = 304.35\left(2N_f\right)^{-1.02} + 2.34\left(2N_f\right)^{-0.28} \tag{13d}$$

while for 80 to 10 percent of SMYS one obtains:

$$\text{GrB:}\quad \frac{H}{L} = 653.11\left(2N_f\right)^{-1.02} + 5.02\left(2N_f\right)^{-0.28} \tag{13e}$$

$$\text{X42:}\quad \frac{H}{L} = 402.65\left(2N_f\right)^{-1.02} + 3.10\left(2N_f\right)^{-0.28} \tag{13f}$$

$$\text{X52:}\quad \frac{H}{L} = 330.11\left(2N_f\right)^{-1.02} + 2.54\left(2N_f\right)^{-0.28} \tag{13g}$$

$$\text{X60:}\quad \frac{H}{L} = 253.95\left(2N_f\right)^{-1.02} + 1.95\left(2N_f\right)^{-0.28} \tag{13h}$$

Based on these eight equations, the relationships between the wrinkle size *H/L* and pressure cycles to failure can be determined as shown in parts a and b of Figure 10 for pressure cycling from MAOP of either 72 or 80 percent of SMYS, respectively. These figures indicate that the pipeline grade has a significant effect on the fatigue resistance of a wrinklebend, all else being equal. For a specific wrinkle severity defined in terms of *H/L*, the fatigue service life increases with decreasing pipeline grade. For example, for a given wrinkle size of *H/L* = 0.2 and MAOP at 72 percent of SMYS, the number of cycles to failure ranges from about 5,500, 10,000, 20,000, 100,000 respectively for grades X60, X52, X42 and GrB. Thus, it is clear that for the same wrinkle severity the fatigue service life for a higher pipeline grade, such as X60, is much less than that for a lower grade steel, such as GrB. Thus, it can be said that in general wrinklebends made of lower grades of pipeline steel are more resistant to fatigue than are those made of higher-strength grades – all else being equal.

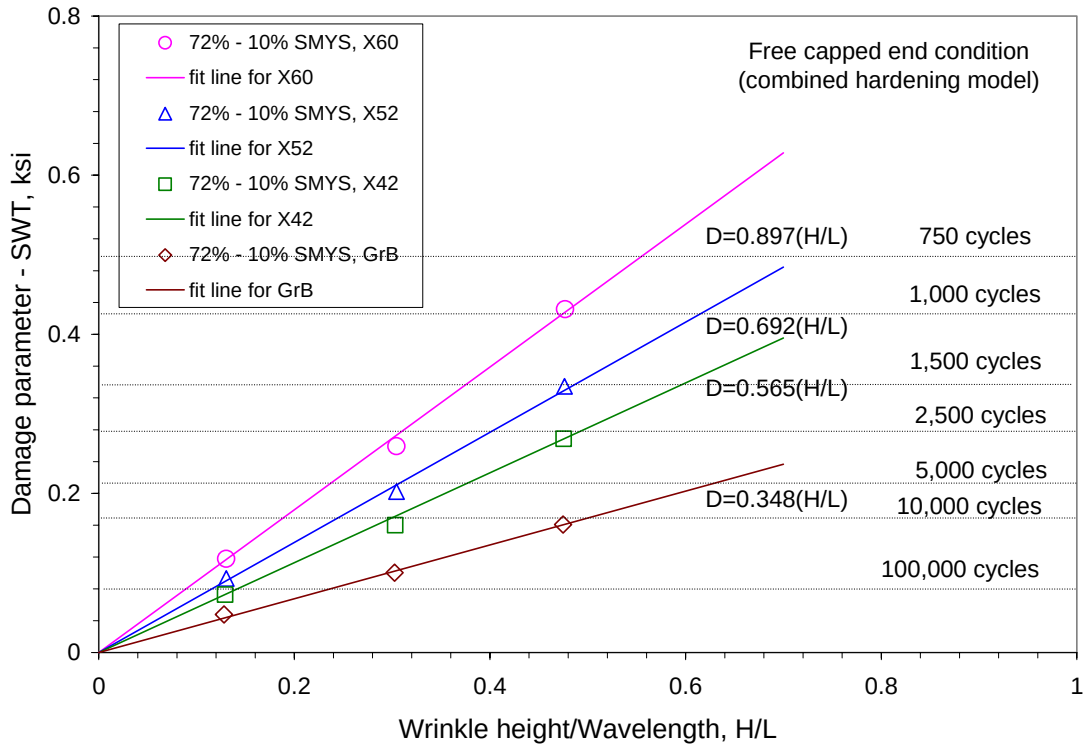

(a) cyclic pressure from 72 to 10 percent of SMYS

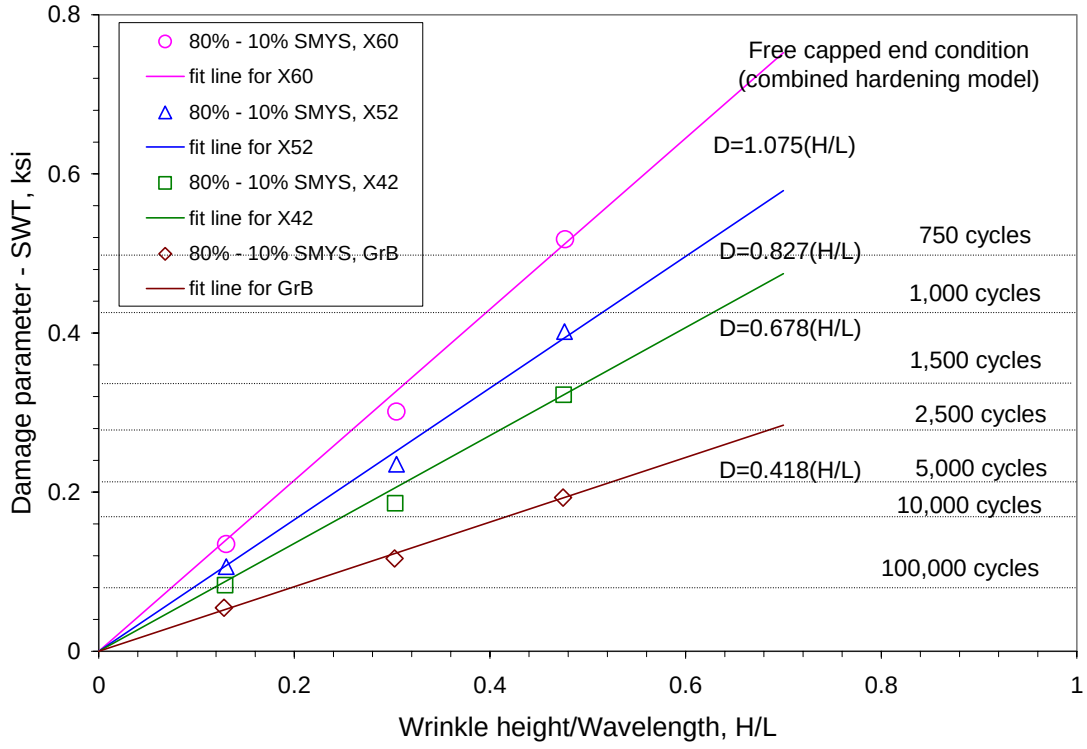

(b) cyclic pressure from 80 to 10 percent of SMYS

Figure 9. SWT damage parameter versus wrinkle size for GrB, X42, X52, and X60

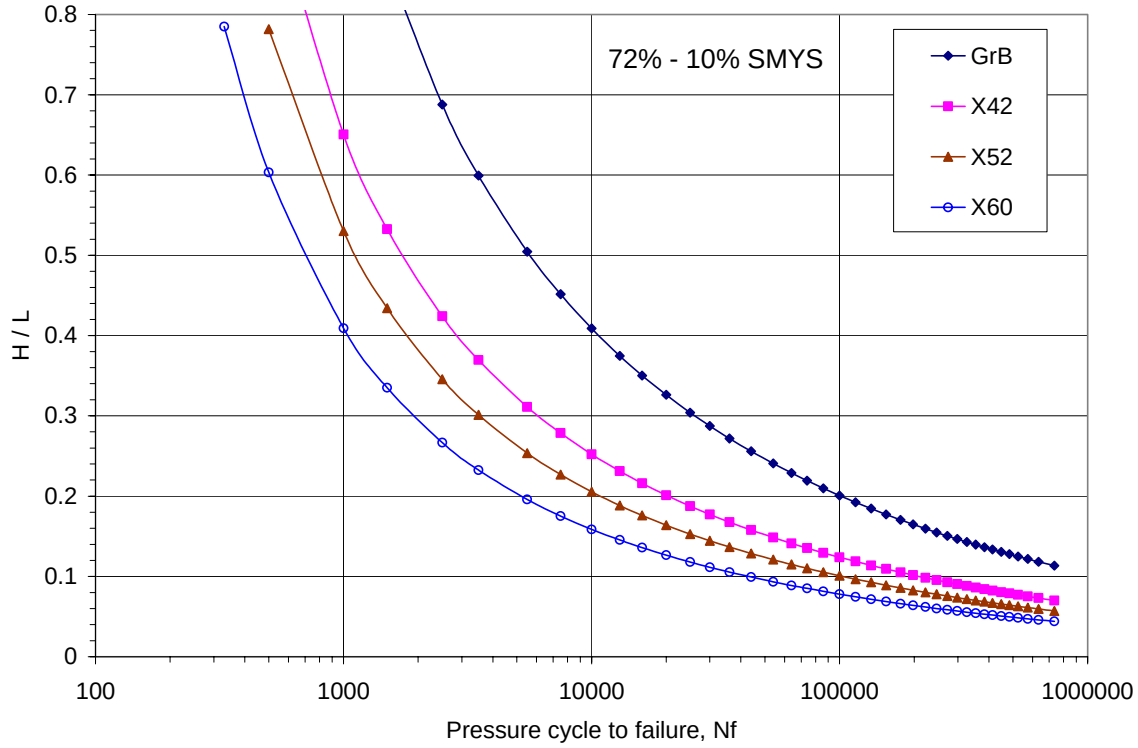

(a) cyclic pressure from 72 to 10 percent of SMYS

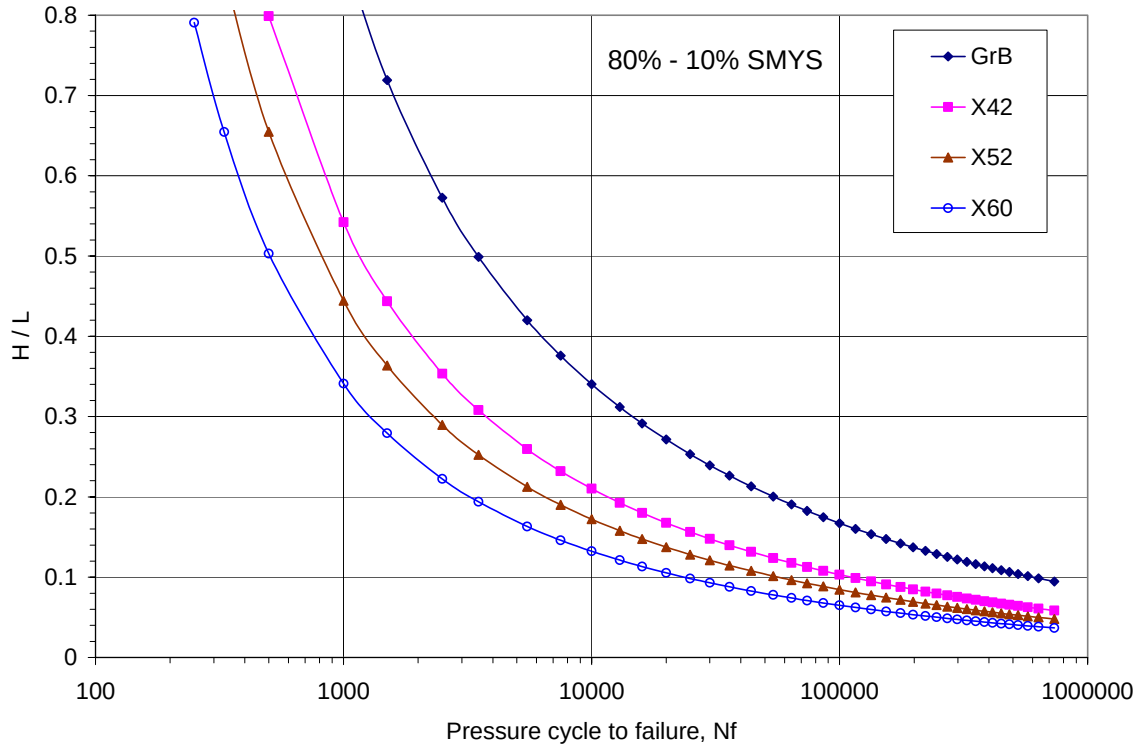

(b) cyclic pressure from 80 to 10 percent of SMYS

Figure 10 Pipeline steel grade effect on the wrinklebend criteria

In reference to Equation 12, the damage parameter can be approximated as a linear function of grade (equally the yield stress of steel), as illustrated in Figure 11 for pressure cycling from 72 to 10 percent as well as from 80 to 10 percent of SMYS. The fatigue damage parameter for different pipeline grades for pressure cycling from 72 percent to 10 percent SMYS can be approximately expressed as a function of the wrinkle size *H/L* and the yield stress σ_{YS} in the form:

$$D_f = (0.0184\sigma_{YS} - 0.3738)(H/L) \tag{14a}$$

for pressure cycling from 80 percent to 10 percent SMYS can be approximately expressed as a function of the wrinkle size *H/L* and the yield stress σ_{YS} in the form:

$$D_f = (0.022\sigma_{YS} - 0.4444)(H/L) \tag{14b}$$

Combined with the analysis for the effect of pipeline geometry, Equations 14 are appropriate for $R/t \geq 25$. Reference to the fatigue resistance curve in Equation A16, the relationship between the wrinkle size *H/L* and the fatigue life N_f for pressure cycling from 72 percent to 10 percent SMYS can be expressed as:

$$(0.0184\sigma_{YS} - 0.3738)\frac{H}{L} = 273(2N_f)^{-1.02} + 2.1(2N_f)^{-0.28} \tag{15a}$$

whereas for pressure cycling from 80 percent to 10 percent SMYS the fatigue life N_f can be expressed as:

$$(0.022\sigma_{YS} - 0.4444)\frac{H}{L} = 273(2N_f)^{-1.02} + 2.1(2N_f)^{-0.28} \tag{15b}$$

These equations are viable fatigue criterion for pipe geometries with $R/t \geq 25$ and near worst-case cyclic loading from MAOP at 72 or 80 percent of SMYS down to 10 percent of SMYS in Grades from B to X60 where the wrinklebend geometry is characterized as *H/L*. It follows that Equations 15 are broadly useful to assess the service life for a variety of pipeline grades, pipeline and wrinkle geometries. It remains to extend the utility of this criterion across a broad range of service conditions other than the near worst-case conditions considered to this point.

Extend the Scope to Address Specific Pipe Operating Conditions

Up to this point, the criterion for wrinklebend integrity has addressed only the effects of pressure cycling, and while now generalized in terms of line pipe properties for cycling from MAOP at 72 or 80 percent of SMYS across a range of line pipe geometry and grade, the criterion remains limited regarding service conditions. This section extends this criterion to applications involving pressure cycling other than pressure cycling between MAOP and 10 percent of SMYS. Because the form of this generalization depends on whether cycling occurs down from a fixed maximum, or up from a fixed minimum, this generalization is presented in turn for both scenarios.

Fixed Upper Pressure and Varied Lower Pressure

The effect of operating pressure on the wrinklebend integrity was evaluated by FEA considering a fixed upper bound pressure at either 72 percent or 80 percent of SMYS with the minimum pressure in the cycle ranging from a low of 10-percent of SMYS up to values approaching MAOP. These parametric analyses were developed for X42 line pipe steel, and as above used

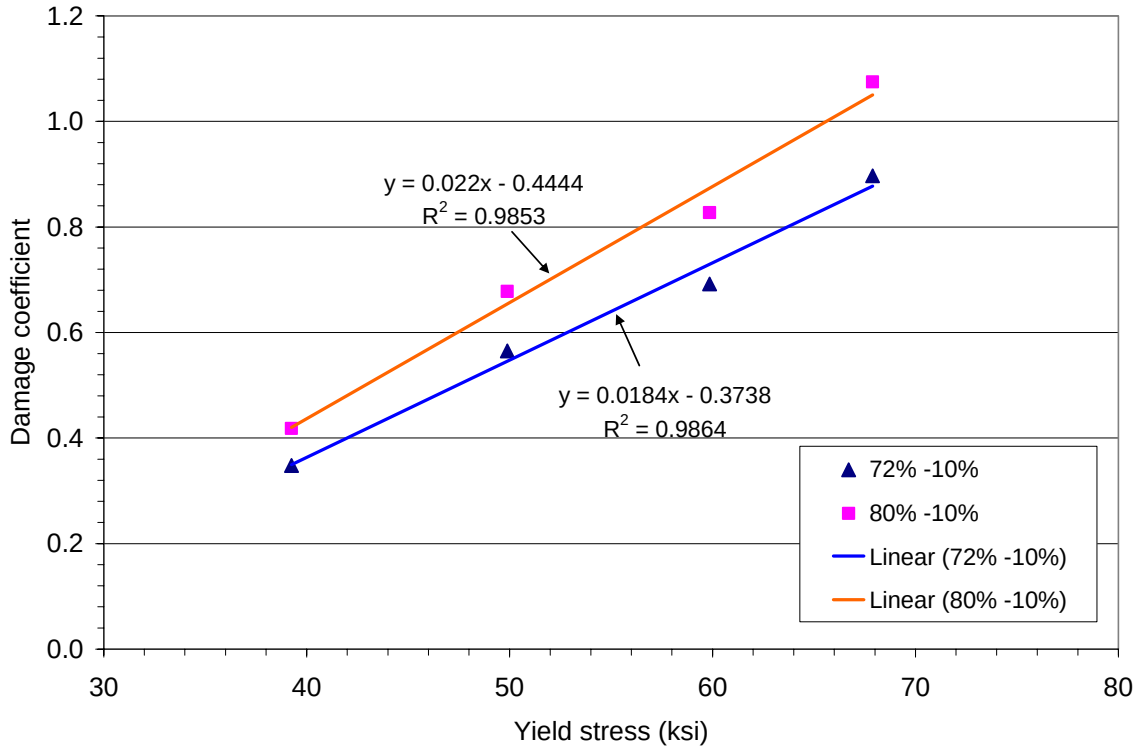

.

Figure 11. Damage coefficient versus yield stress of wrinklebend steel

the combined hardening model for reasons discussed in Appendix G. These simulations considered line pipe 16-inches in diameter with a wall thickness of 0.283 inch. The results for this set of line pipe geometry and grade will be subsequently generalized using the same approach discussed and illustrated in the previous sections.

Realizing that cycling from a maximum stress at either 80 or 72 percent of SMYS down to 10 percent of SMYS (a pressure ratio, R_p, equal to 0.125 or 0.139 respectively) was characterized above, it is necessary here to address the results for two additional cases, the results for which can be expressed as follows:

pressure cycling from MAOP at 72 percent down to 36 percent of SMYS ($R_p = 0.5$) leads to:

$$D_f = 0.305(H/L) \tag{16a}$$

$$\frac{H}{L} = 895.05(2N_f)^{-1.02} + 6.89(2N_f)^{-0.28} \tag{16b}$$

while for 72 to 57.6 percent of SMYS ($R_p = 0.8$) one obtains;

$$D_f = 0.115(H/L) \tag{17a}$$

$$\frac{H}{L} = 2373.91(2N_f)^{-1.02} + 18.26(2N_f)^{-0.28} \tag{17b}$$

For cycling from MAOP at 80 percent down to 40 percent of SMYS ($R_p = 0.5$) leads to:

$$D_f = 0.495(H/L) \tag{16c}$$

$$\frac{H}{L} = 551.52\left(2N_f\right)^{-1.02} + 4.24\left(2N_f\right)^{-0.28} \tag{16d}$$

while for 80 to 64 percent of SMYS ($R_p = 0.8$) one obtains;

$$D_f = 0.201\left(H/L\right) \tag{17c}$$

$$\frac{H}{L} = 1358.21\left(2N_f\right)^{-1.02} + 10.45\left(2N_f\right)^{-0.28} \tag{17d}$$

Figures 12a and 12b and Figures 13a and 13b, respectively, illustrate the effect of three operating pressures on wrinklebend damage and the service life for cycling from 72 or 80 percent of SMYS. These figures indicate that as the cyclic pressure ratio increases, the amount of fatigue damage decreases (i.e., the damage curves shift down) such that the service life increases (i.e., the service life curves shift up). This outcome is expected, because as the pressure (stress) ratio approaches to one, the cyclic loading conditions approach that for monotonic loading in which case the fatigue damage is zero. Conversely, when the cyclic pressure ratio decreases, the fatigue damage increases and the service life decreases.

The FEA results for other loading cases with the pressure (stress) ratios equal to 0.5 to 0.9 indicate that the damage parameter and the fatigue life can be approximated in the following general form for cycling from MAOP at 72 percent of SMYS:

$$D_f = \left(0.141R_p^{\,2} - 0.817R_p + 0.676\right)\left(H/L\right) \tag{18a}$$

$$\left(0.141R_p^{\,2} - 0.817R_p + 0.676\right)\frac{H}{L} = 273\left(2N_f\right)^{-1.02} + 2.1\left(2N_f\right)^{-0.28} \tag{18b}$$

where the value of the pressure ratio R_p ranges from zero to one. Likewise, the damage parameter and the fatigue life can be approximated in the following general form for cycling from MAOP at 80 percent of SMYS:

$$D_f = \left(-0.514R_p^{\,2} - 0.209R_p + 0.716\right)\left(H/L\right) \tag{18c}$$

$$\left(-0.514R_p^{\,2} - 0.209R_p + 0.716\right)\frac{H}{L} = 273\left(2N_f\right)^{-1.02} + 2.1\left(2N_f\right)^{-0.28} \quad . \tag{18d}$$

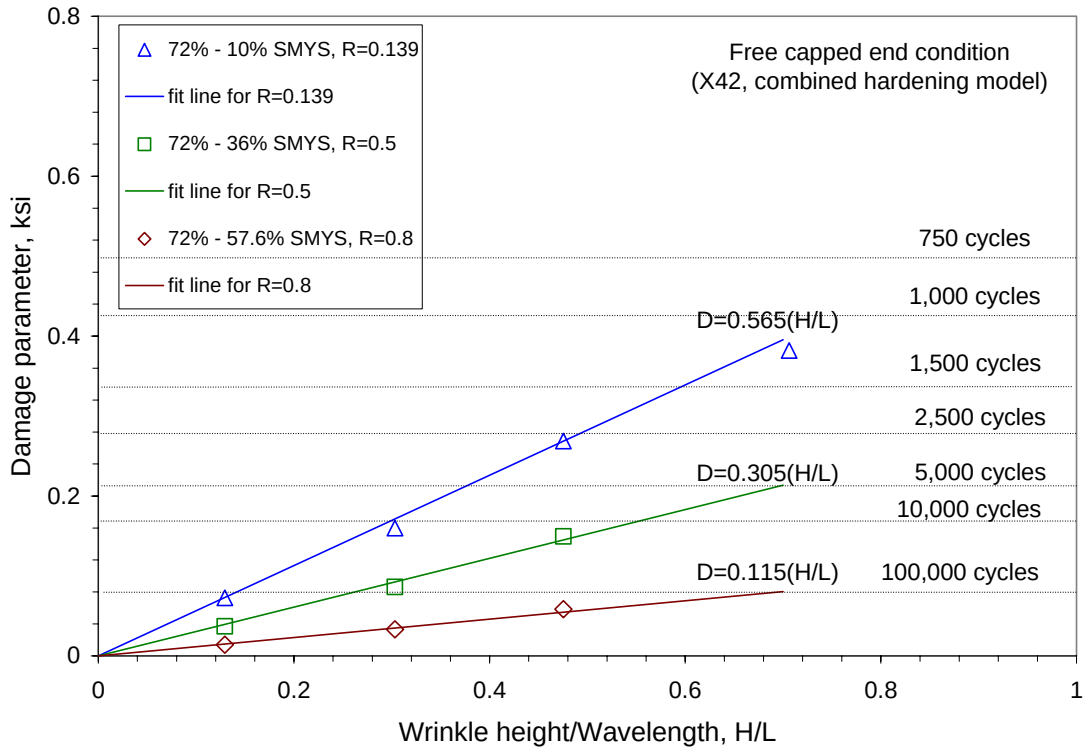

(a) cyclic pressure from 72 to 10 percent of SMYS

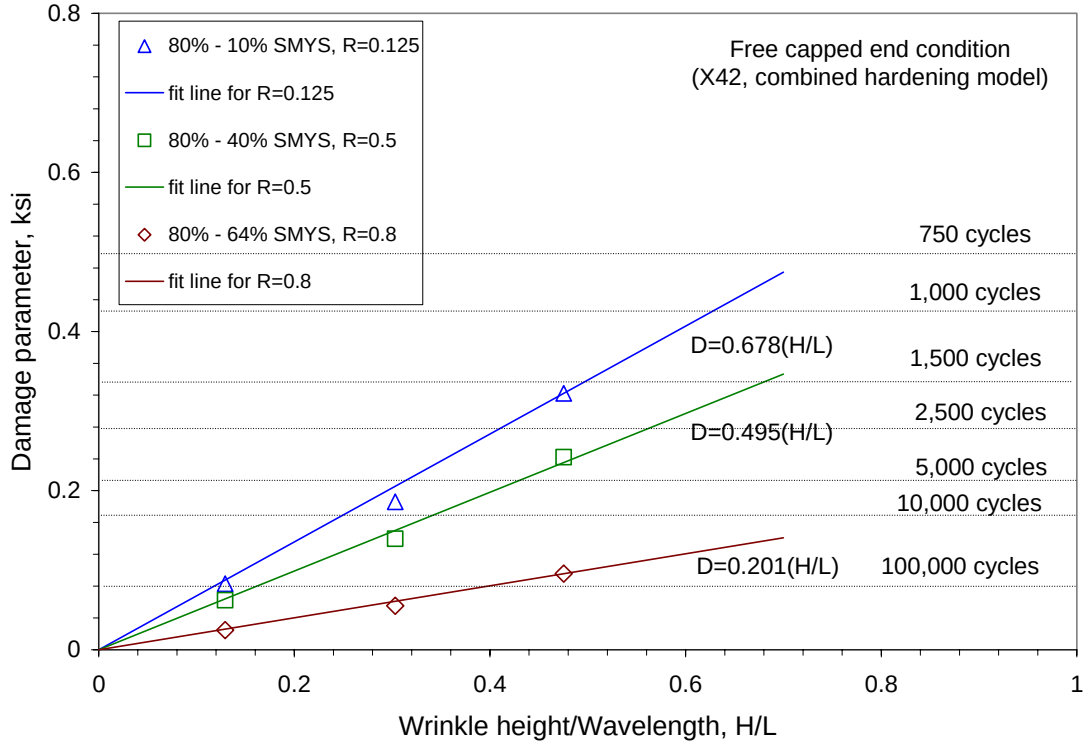

(b) cyclic pressure from 80 to 10 percent of SMYS

Figure 12. Effect of lower cyclic pressure on the damage parameter

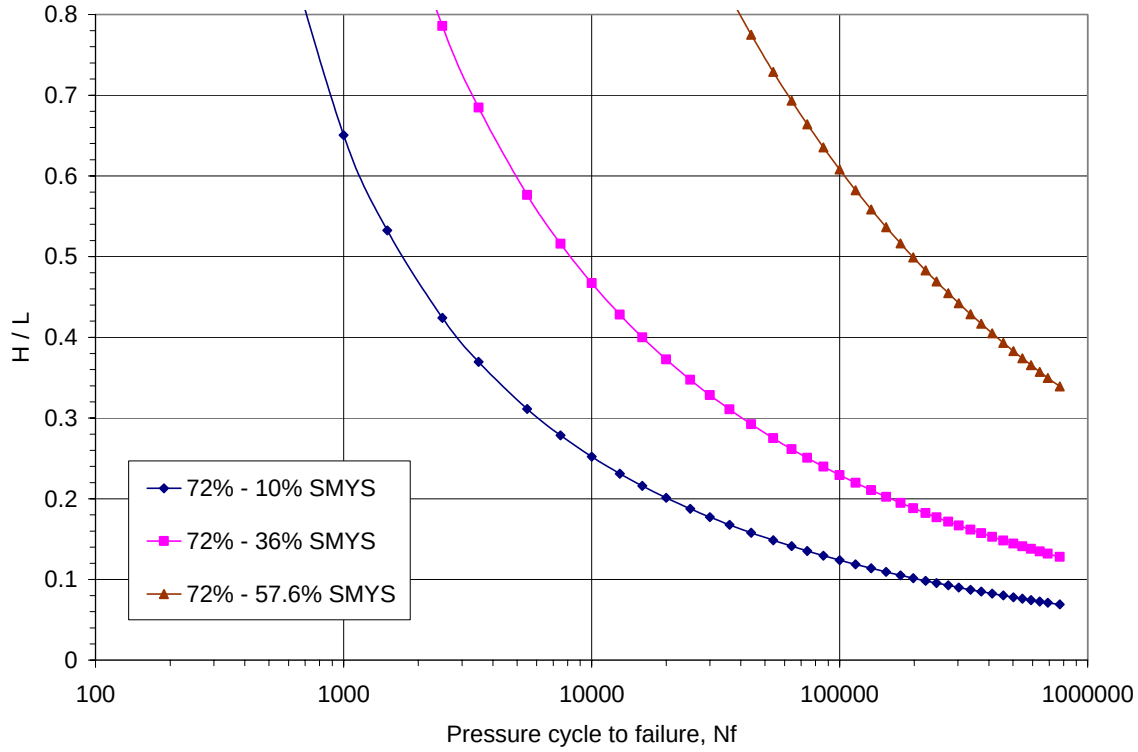

(a) cyclic pressure from 72 to 10 percent of SMYS

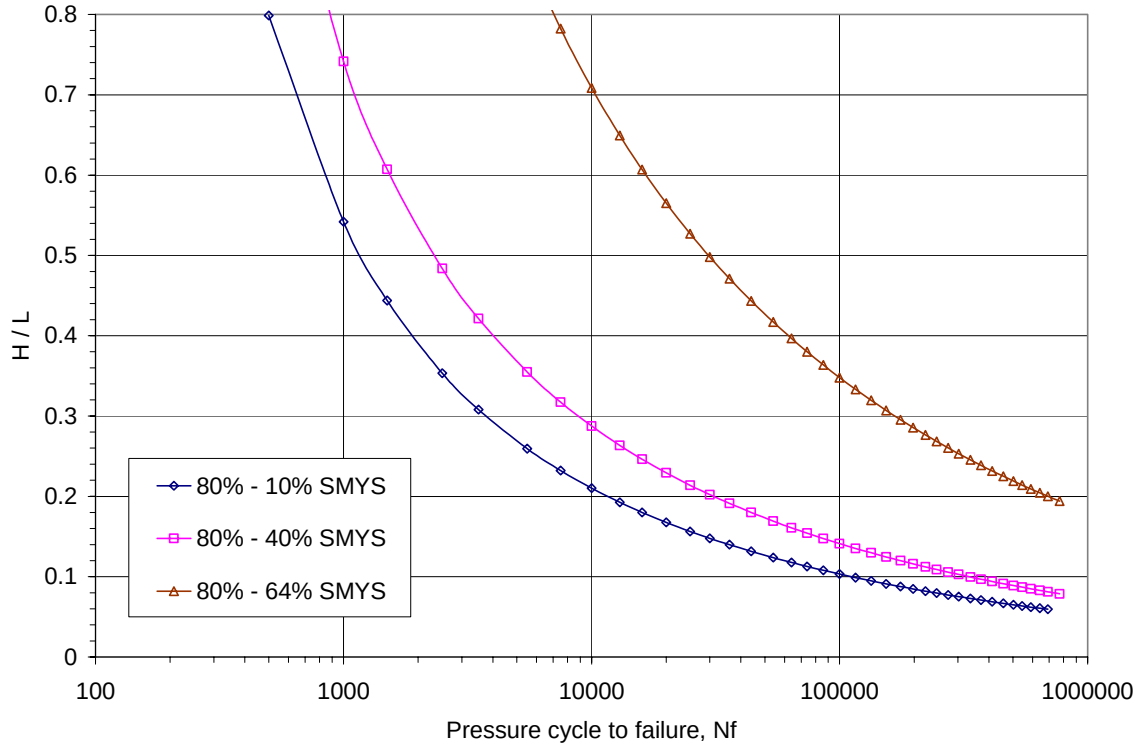

(b) cyclic pressure from 80 to 10 percent of SMYS

Figure 13. Effect of lower cyclic pressure on the service life

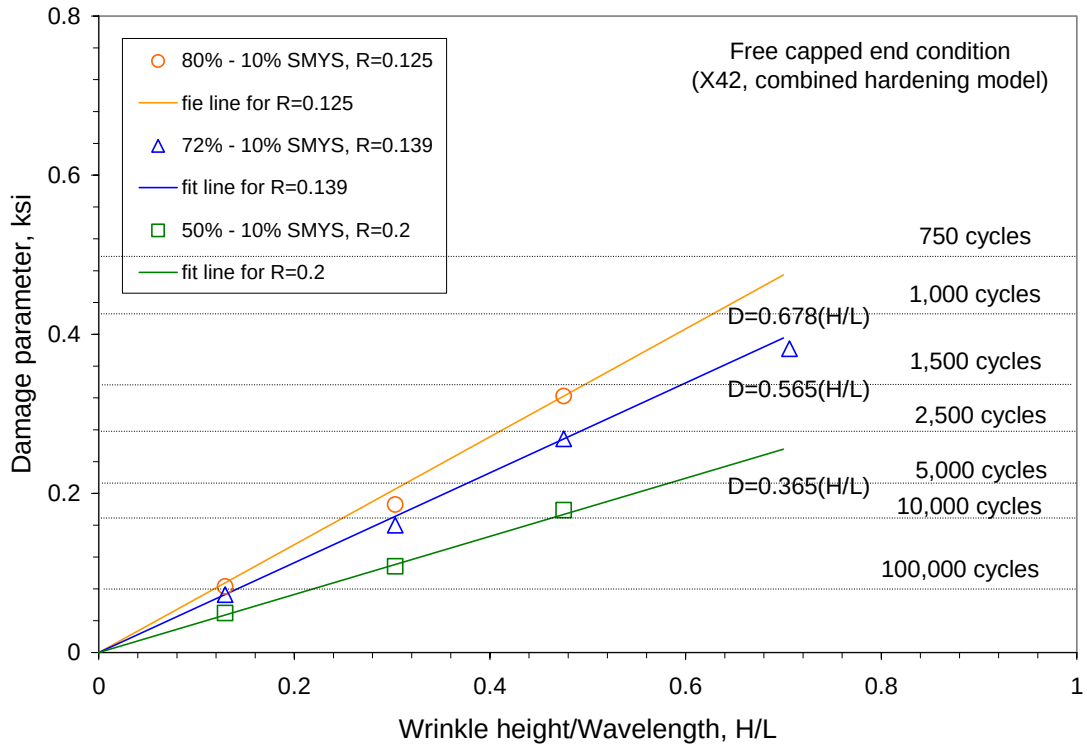

Figure 14. Effect of higher cyclic pressure on the damage parameter

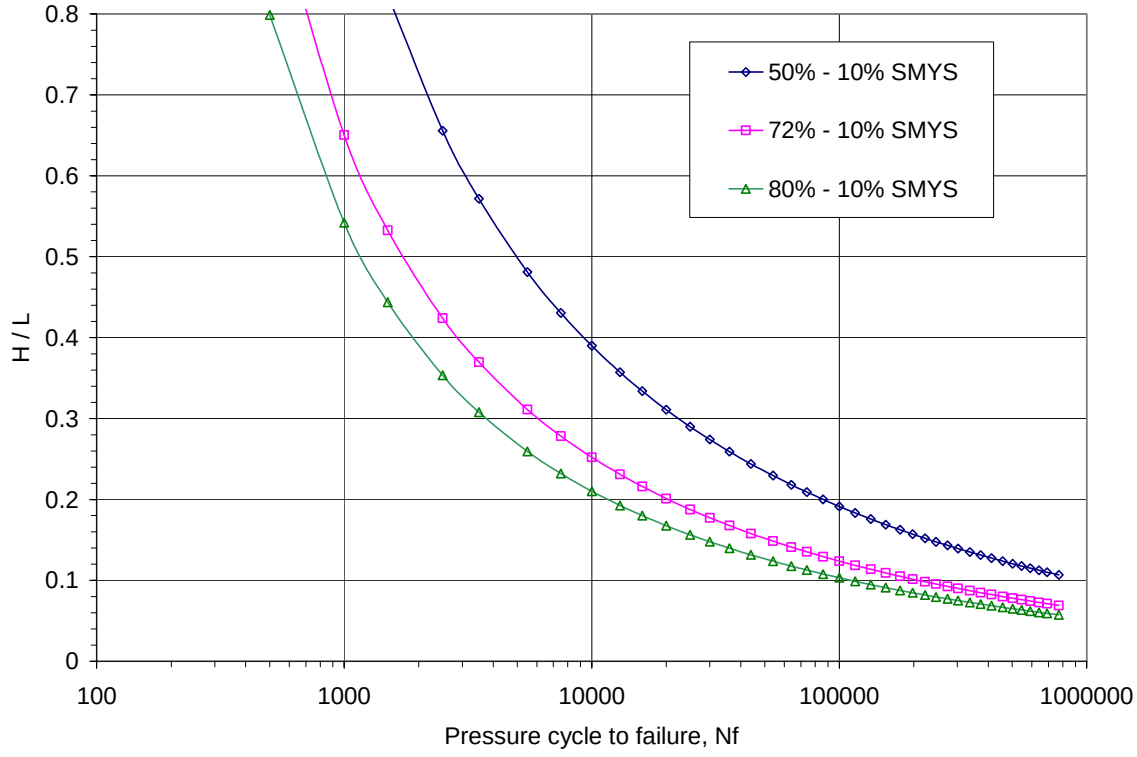

Figure 15. Effect of higher cyclic pressure on the service life

Fixed Lower Pressure and Varied Upper Pressure

An alternative view for pressure cycling considers the lower pressure as the reference condition with pressure cycling referenced to this level. While this is seldom the scenario at lease for pipelines operating at high demand, such situations have nevertheless been considered. As for the scenarios just considered, the effect of operating pressure can be evaluated by FEA similar to those for the section above. For the present section, results specific to a fixed lower pressure set at 10 percent of SMYS are presented.

As above, X42 line pipe with diameter of 16 inches and wall thickness of 0.283 inch was considered. Again, because cases involving 10 to 72 percent of SMYS (R_p = 0.139) and 10 to 80 percent of SMYS (R_p = 0.125) were considered above, it is useful here to simply illustrate one further case, which for present purposes reflects MAOP at 72 percent of SMYS that leads to damage and service life expressed respectively as:

$$D_f = 0.365(H/L) \tag{19a}$$

$$\frac{H}{L} = 747.95(2N_f)^{-1.02} + 5.75(2N_f)^{-0.28} \tag{19b}$$

for cycling from 50 to 10 percent of SMYS (R_p = 0.2).

Parts a and b of each of Figures 14 and 15 illustrate the effect of cyclic operating pressures on the wrinkle damage parameter and the fatigue service life, respectively, although in the context of cycling from a fixed higher pressure. These figures indicated that as the cyclic pressure ratio increases, the fatigue damage decreases (or the damage curves shift down) whereas the service life increases (or the service life curves shift up). Conversely, when the cyclic pressure ratio decreases, the fatigue damage increases and the service life decreases. While for other cyclic operating pressures referenced to a fixed lower limit similar FEA calculations could be done and the service life of wrinklebends determined as just noted, this scenario seldom occurs. Suffice it to note that the worst-case scenario for pipelines involves a pressure ratio equal to zero, i.e. the lower pressure remains zero during the cyclic pressure. For this application there is no difference between cycling down from a maximum or cycling up from a minimum, just as there is no difference for any fixed pressure ratio. In this context, Equations 18 can be used to address all such service scenarios provided the pressure ratio is correctly represented.

Validation of the Wrinklebend Criteria via Full-Scale Fatigue Testing

Prior to further generalization of the above developed wrinklebend integrity criteria it is appropriate to assess their practical viability via full-scale testing. This aspect was addressed in detail in Appendix G, such that this section simply summarizes the results specific to the use of the SWT damage parameter. Experimental details for this testing, including setup, the line pipe properties, and the results can be found in Appendix H of Reference 24.

From Appendix H of Reference 24, wrinklebends were introduced into 20-inch diameter line pipe with 0.250-inch thick wall. This testing evaluated wrinklebends made in modern GrB and X42 line pipe. All pipe was shipped with a fusion-bonded coating, which implies a lightly sandblasted surface, and the need to correct for surface roughness beginning at lives from ~5,000 to ~20,000 cycles. To limit the test time, as-bent wrinkle aspect ratios were selected to produce

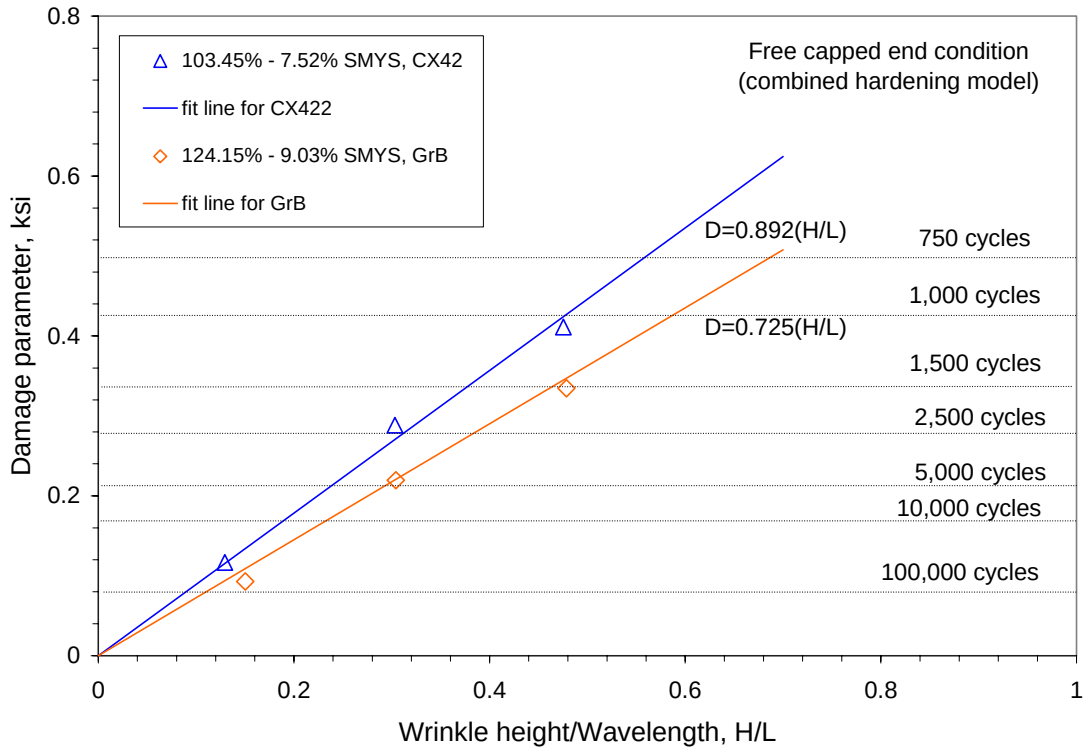

Figure 16. Damage parameter vs wrinkle shape for the full-scale testing

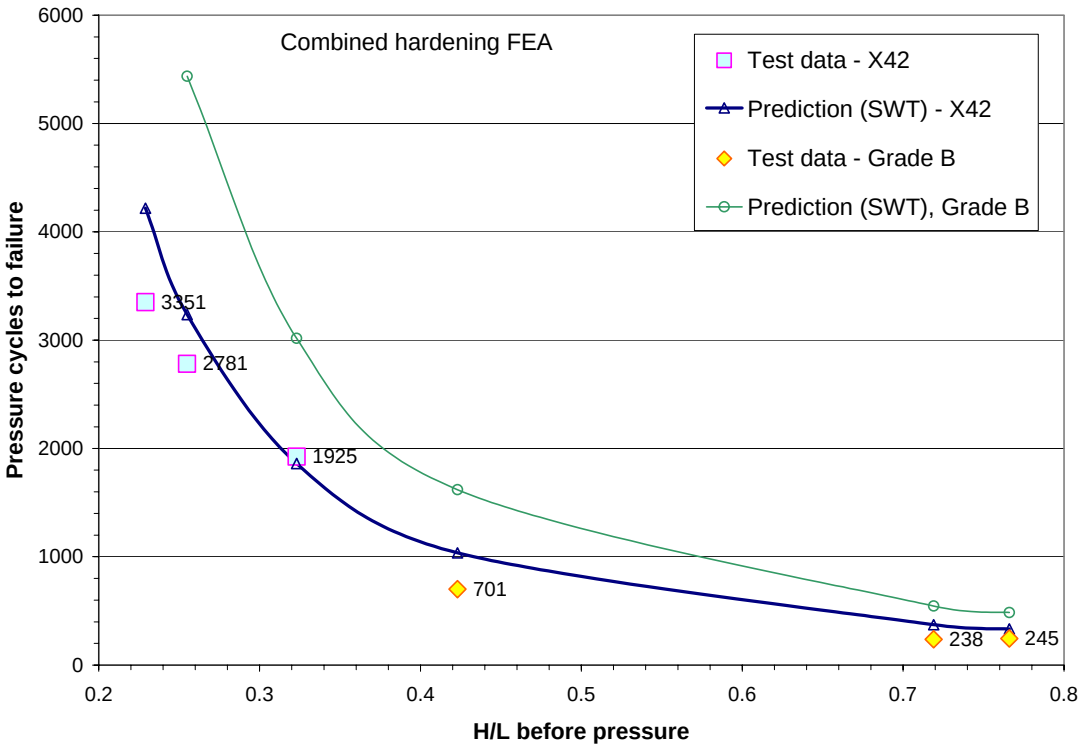

Figure 17. Pressure cycles to failure vs wrinkle shape for the full-scale testing

target lives between 500 and 5000 cycles under pressure cycling nominally from 1100 psi (7579 kPa) to 150 psi (1034 kPa), or R = 0.073, which was imposed under open-loop control. Actual as-bent wrinkle aspect ratios ranged from 0.229 to 0.766, which were close to the target sizes. Because the testing was done without restraint to the ends of the pipe, once pressurized these aspect ratios decreased significantly. Wrinkling was done in a bending machine under closely controlled conditions.

For the X42, the just-noted cyclic pressure corresponds to 103.5 to 7.5 percent of SMYS, while for the GrB this corresponds to 124.2 to 9 percent of SMYS. Figure 16 presents the damage parameter versus the wrinkle size for the nominal cyclic pressure, and compares this result with those for the results for cycling from 72 to 10 percent of SMYS specifically for X42. The expressions of the damage parameter and service life for these two cyclic pressures are:

For 103.5 to 7.5 percent SMYS (the X42 scenario at R_p=0.073),

$$D_f = 0.892\left(H/L\right) \tag{20a}$$

$$\frac{H}{L} = 306.05\left(2N_f\right)^{-1.02} + 2.35\left(2N_f\right)^{-0.28} \tag{20b}$$

For 124.2 to 9 percent of SMYS (the GrB scenario at R_p=0.073)

$$D_f = 0.725\left(H/L\right) \tag{21a}$$

$$\frac{H}{L} = 376.55\left(2N_f\right)^{-1.02} + 2.90\left(2N_f\right)^{-0.28} \tag{21b}$$

As is evident in Figure 16, the fatigue damage increases significantly when comparing cyclic loading from 72 to 10 percent of SMYS to the case involving cycling from 103.5 to 7.5 percent of SMYS, which is expected based on the results obtained in the previous sections. The cyclic loading for this testing at a pressure ratio of only 0.073 is less severe than that for near worst-case service ratio considered earlier at 0.139. For this experimental loading, the upper pressure is larger than the yield stress such that plastic strain are generated, which leads to related surface roughening that obviates the need for corrections for surface differences between polished specimens and a shot-blasted pipe surface.

Figure 17 presents the results of predicted fatigue life versus that observed in the testing. From this figure it is apparent that the wrinklebend criterion developed successfully predicts the service life for winklebends experiencing pressure cycling, as excellent agreement exists between the full-scale test results and the predictions for the X42 results, with good agreement for the GrB results. This validation indicates the effectiveness and viability of the wrinklebend integrity criteria developed, and supports the details embedded in the methodology, procedures, cyclic plastic hardening model, FEA calculations, and fatigue damage parameter.

Develop Data Characterizing the Effects of Localized Corrosion

As is well-known, notches such as pitting due to corrosion in structural components induce local stress concentration, whereas general areal loss alters the local stiffness and drives stress and strain redistribution. Because notches develop increased local stresses and strains, the value of the damage parameter is increased local to such features, consistent with the observation they act as sites for early crack nucleation. Thus, their presence reduces the service life associated with

fatigue. It follows that corrosion pits or areal metal-loss defects can reduce the fatigue resistance of pipeline steels – all else being equal. It also follows that the presence of pits or areal metal loss could be accounted for implicitly by using fatigue resistance data that empirically include pitting, like that developed in corrosion-fatigue testing in pitting environments[39]. Such results support the view that pits act as early nucleation sites, which reduce the total life to that of crack propagation – leading to order of magnitude or worse reductions in fatigue resistance depending on the total life and the role of other factors such as initial surface condition. An alternative approach continues the use of polished specimens to characterize fatigue resistance, but within the local stress-strain approach adopted to address wrinklebend curvature account for the presence of pits located on the tensile side of the crown of the wrinklebend. As the local stress field is relaxed by the presence of multiple pits, the worst-case in this context is a single pit.

Whereas the effects of larger-scale areal metal loss can be addressed by considering a locally reduced wall thickness on the damage parameter for a given wrinklebend size, the effect of pitting is to increase the local stresses beyond that characterized by wrinklebend size. Thus, it is necessary to develop the fatigue resistance when pitting is present and acts as a notch to reduce the fatigue life as compared to the smooth-specimen fatigue life used to date (Equation A16). In this context Dowling[40] observed, as many others have since the late 1960s, that for linear-elastic scenarios unnotched (typical smooth specimens) and notched specimens have the same fatigue life if the stress $\sigma = S$ in the smooth specimen is the same as the stress $\sigma = K_\sigma S$ at the notch in the notch specimen. In this discussion, σ denotes the local stress, and *S* denotes the global or nominal stress, while by definition $K_\sigma = 1$ for smooth specimens and $K_\sigma > 1$ for notched specimens. Considering the fatigue resistance curve for smooth specimens to have the general form:

$$\sigma_a^{smooth} = S_a^{smooth} = f(N_f) \tag{22}$$

and the local stress amplitude at notch given by definition as:

$$\sigma_a^{notch} = K_\sigma S_a^{notch}, \tag{23a}$$

then consistent with the above assertion:

$$\sigma_a^{notch} = \sigma_a^{smooth} \tag{23b}$$

Combining Equations 22 and 23b leads to:

$$S_a^{notch} = f(N_f)/K_\sigma, \tag{24}$$

which defines the S-N fatigue resistance curve for the notched specimens relative to that for smooth specimens. This construct is the analytical equivalent to testing notched or corrosion-pitted specimens. The form of Equation 24 has routinely been validated by such testing. It is apparent from Equation 24 that the S-N curve for the notched bars lies below that for smooth specimens in proportion to the so-called fatigue notch factor, here denoted as K_σ.

In analogy to scenarios where nonlinear stress-strain response occurs, as is the case for wrinklebends, this same approach is followed, specifically here to estimate the fatigue resistance where corrosion pitting is present. Developing this nonlinear analog requires the nonlinear equivalent of Equation 23a. By definition stress and strain concentration factors are defined respectively as:

$$K_\sigma = \frac{\sigma^{notch}}{S^{notch}} \quad \text{and} \quad K_\varepsilon = \frac{\varepsilon^{notch}}{E^{notch}} \tag{25a}$$

the geometric mean of which Neuber[41] analytically related to the theoretical elastic stress concentration factor K_t, such that:

$$K_t = \sqrt{K_\sigma K_\varepsilon} \tag{25b}$$

For the energy-based SWT damage parameter, this leads to:

$$D_{local} = \sigma_{\max}\varepsilon_{amp} = \left(K_\sigma S_{\max}\right)\left(K_\varepsilon E_{amp}\right) = K_t^2 D_{\text{nominal}} \tag{26}$$

where $D_{\text{nominal}} = S_{\max}E_{amp}$ is the nominal value of the SWT parameter in reference to the nominal maxima stress $S_{\max}$ and the nominal strain amplitude E_{amp}. From Equation 26 and the material fatigue curve in Equation A16, the nominal SWT-based fatigue resistance curve for pitting can be expressed as:

$$D_{\text{nominal}} = \left[273\left(2N_f\right)^{-1.02} + 2.1\left(2N_f\right)^{-0.28}\right] / K_t^2 \tag{27}$$

It remains to determine K_t for typical pitting, which is found to be $K_t = 1.635$ based on FEA for typical corrosion pit geometries. Figure 18 presents the fatigue resistance for pitting in line pipe steels developed on this basis in reference to the smooth specimen fatigue curve in Equation A16. It is apparent from this figure that the presence of corrosion pitting can significantly reduce the service life for a pipeline, with the less severe the related damage the

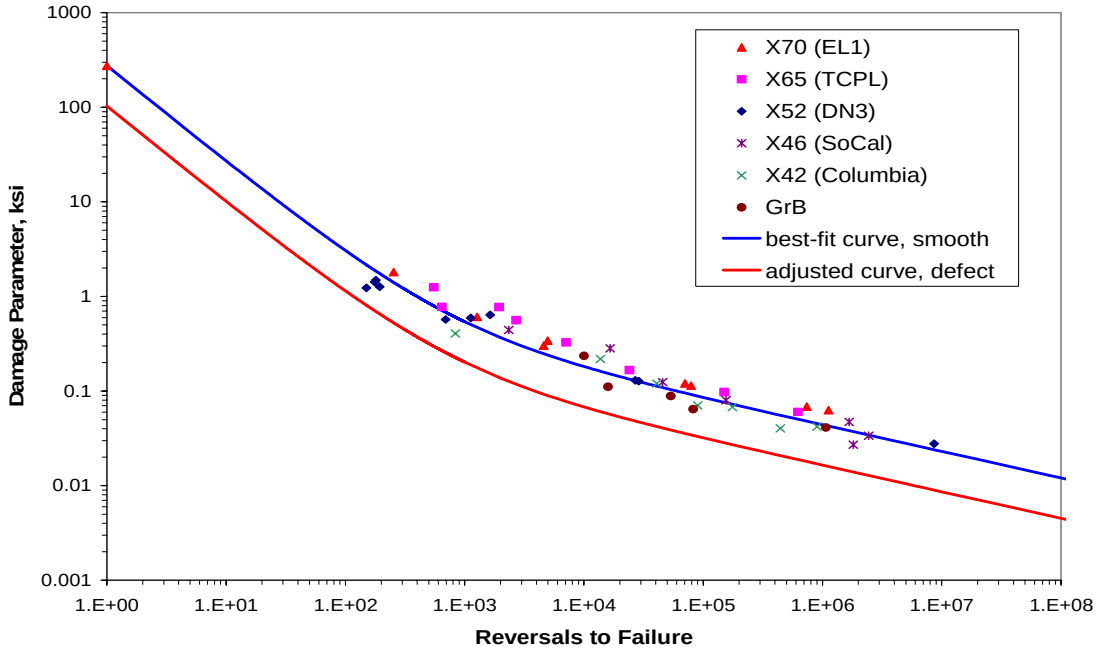

Figure 18. Localized corrosion effect on fatigue life for the pipeline steels

greater the life reduction in life because of the logarithmic scale. This is fully consistent with the earlier observations noted in regard to corrosion-fatigue data developed in pitting environments.

Note from Figure 18 that at long lives there is roughly a factor of 35 reduction in service life, just as noted earlier occurs in regard to typical corrosion-fatigue test data.

Parametric Evaluation of Corrosion Effects on Wrinklebend Life

Corrosion is possible on both the ID and OD of a wrinklebend, and can occur as pitting or as general metal loss (areal corrosion). Because the orientation of a wrinklebend depends on the plane that a change in direction was sought, and because the loadings can act to open or close the wrinkle, tension does not always occur on the ID or OD of the bend. From a fatigue perspective where fatigue interacts synergistically with corrosion, corrosion is worst if it forms on the tensile side of the wrinkle. Taken with the observation that tension can occur on either the OD or ID depending on the circumstances, the possible presence of corrosion should consider both cases. However, for thin-walled pipelines the results must be similar such that only the OD case is considered. As pitting corrosion in the crown of the wrinkle can be simply addressed in the context of Figure 18, the present section focuses on the effects of areal corrosion, with consideration of the scale of areal corrosion as it diminishes toward the scale of pitting.

Simulating the effects of corrosion defects on wrinklebend life is a significant challenge, which is no simpler when using FEA. As demonstrated in the cost-share project for this work, three dimensional (3D) conventional 20-node solid elements are inappropriate to use for wrinklebends due to the large displacement, the large rotation, and the significant computation costs. On the other hand, the 3D four-node shell elements are viable while forming the wrinklebend and during its loading, because the shell elements are best suited in simulating large deformations and large rotations in FEA. While shell elements can give reliable FEA results for reasonable computation costs, the regular shell element in ABAQUS is used for uniform states and only provides stress and strain values on the two shell element surfaces, which limit its utility to simulate defects formed on the wrinkle surfaces. For these reasons, a special technique using a composite shell model was built in ABAQUS and adopted to simulate the effects of OD corrosion defects that form long after the wrinklebend is formed.

Stress Predictions of Non-Uniform Pipe Walls using a Composite Shell Model

The role of areal metal loss was evaluated via FEA using a composite shell model in ABAQUS involving an end-capped pipe. As shown schematically in Figure 19, the pipe wall was assumed to comprise three materials with one part having two layers, and axial symmetry about the vertical plane through the wall at the end of this parallel segment. The pipe has an average diameter of 10 inches, with a total wall thickness of 0.2 inch comprising 0.2 inches for Material 1, with the thicknesses Materials 2 and 3 each being 0.1 inch. The half-length of the FEA pipe model was 20 inches, divided such that the length of each segment is 10 inches.

Figure 19. Schematic of the composite shell model for a pipe

The material properties of the composite pipe model were evaluated considering two groups of properties designed to simulate non-uniform thickness and ID or OD corrosion as follows:

Group 1. Material 3 is X42 which is the same as Material 1, whereas Material 2 is an assumed very weak material to simulate OD metal-loss due to the corrosion defect.

$$\text{Material 1: E=30,000 ksi, } \nu=0.3,\ \sigma_{ys} = 42\ \text{ksi},\ \sigma_{uts} = 60\ \text{ksi}$$

$$\text{Material 2: E=10 psi, } \nu=0.3,\ \sigma_{ys} = \sigma_{uts} = 4.2\ \text{psi}.$$

Group 2. Material 2 is X42 as the same as the Material 1, and Material 3 is an assumed very weak material to simulate ID metal-loss due to corrosion.

The response of this composite model can be interrogated analytically to serve as a benchmark for numerical analysis. For example, consider an internal pressure of 1225 psi, which leads to the following analytically determined stresses for Group 1:

In material 1: hoop stress = 30 ksi, axial stress = 15 ksi

In material 2: hoop stress = 0, axial stress = 0

In material 3: hoop stress = 60 ksi, axial stress = 30 ksi

This non-uniform-wall (corroded) pressure-loaded scenario also was evaluated as a pipe via FEA considering a composite shell model. Figure 20 shows the deformed non-uniform-wall pipe (with greatly magnified deformations) for properties representing Group 1. The FEA determined stresses for this scenario were:

- In material 1: hoop stress = 29.5 to 32.5 ksi, axial stress = 13 to 19 ksi
- In material 2: hoop stress = 0.18 to 0.30 ksi, axial stress = 0.07 to 0.09 ksi
- In material 3: hoop stress = 57.5 to 65 ksi, axial stress = 30 to 31.7 ksi

It follows that good agreement exists between the range of stresses found via FEA as compared

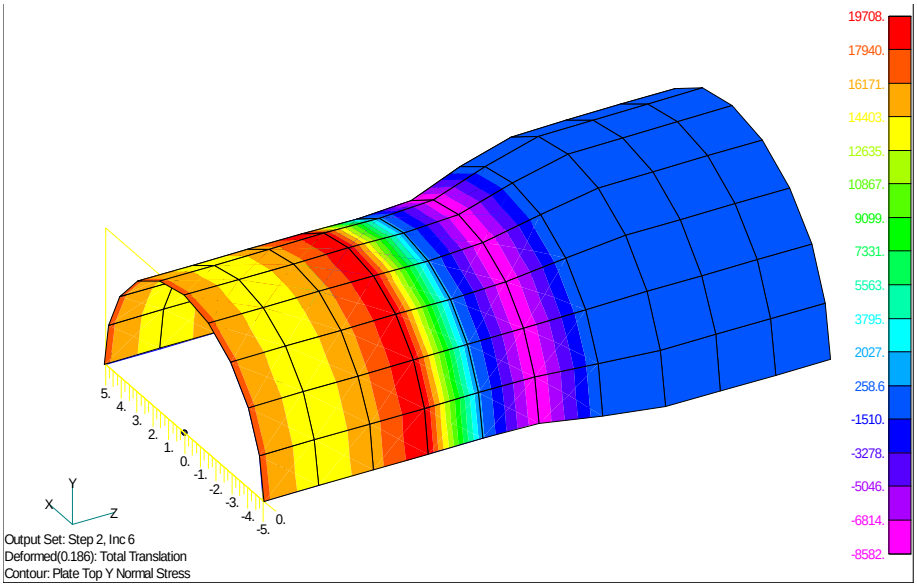

Figure 20. Highly magnified deformations in the "composite" shell model

to the analytically determined stresses. However, small differences develop in the vicinity of the properties transition where both axial and hoop stresses are affected by the abrupt interface between these properties through the wall thickness and the bending that develops local to this

interface. The two layer segment of the pipe where OD corrosion was simulated shows large local circumferential deformation. As expected, transferring this simulated metal loss to the ID (i.e., analysis for Group 2) leads to virtually identical results, confirming the above assertion such results were comparable. Similarity between the FEA results and the analytical results for this simple scenario indicates that a composite shell model can be used as the vehicle to simulate the effects of corrosion defects on wrinklebend structural response and service life.

Parametric evaluation of corrosion effects on wrinkle damage

The composite shell model demonstrated above was used to simulate corrosion defects under circumstances involving wrinklebends, for which the areal defect is represented by a locally "weak layer" with nominally no strength. The effect of the size of the defects is parametrically evaluated by varying the length and width – where for each case either the length is fixed and the width varied, or vice versa. Using this scheme, the effects of a broad range of corrosion defects can be simulated in comparison to the physical dimensions of typical wrinklebends.

The FEA considered a pipeline with diameter of 16 inches and wall thickness of 0.283 inch, which leads to $R/t = 28.3$. The length in the FEA model was 35 inches. Service cycling considered the near worst-case of 72 to 10 percent of SMYS for line pipe made of X42 steel. The wrinkle shape was taken as $H/L = 0.475$, such that the wrinkle height $H = 1.22$ inches, the half-wrinkle wavelength $L = 1.283$ inches, and the half-wrinkle arc length was ~1.77 inches. The corrosion depth d focused on cases where $d/t = 0.5$.

Two groups of the corrosion defect sizes were simulated in the FEA calculations:

- Group 1:the corrosion defect has a fixed length at 1.3 inches (~ 73 percent of wrinkle arch length), and varied defect width from 0.5 inches (3.65^o), 1.3 inches (10^o), 3.7 inches (27^o) to 6.9 inches (50^o).
- Group 2: the corrosion defect has a fixed width of 1.3 inches (10^o), and varied defect length from 0.5 inches, 1.3 inches, 2.6 inches, and 5.1 inches.

Using the composite shell approach, the corrosion defect is formed in the weak layer after the wrinklebend has been fully formed, which is the same scenario that occurs in the field for both areal metal loss and pitting. FEA simulations using the composite shell model within ABAQUS facilitate viable analyses of stress and strain at the crown of the wrinkles with a superimposed "critical location" representing a corrosion defect.

The FEA results show that the residual stress and the residual strain formed at a wrinkle area during the cold bending decrease for all corrosion defects considered in the two groups above after the corrosion defects are formed in the FEA simulations. This is reasonable because the corrosion presence reduces the local stiffness of the wrinklebend, although the global stiffness of the pipeline may remain unchanged. At the upper loading of 72 percent SMYS, the maximum tensile stress at the critical location of the corroded wrinklebend is nearly the same with slight increase as those for the defect-free wrinklebend under the same loading. However, in comparison to the defect-free wrinklebend, the compressive strains at the critical location of the corroded wrinklebend increase for both loadings of 72 percent and 10 percent SMYS due to the reduced stiffness at the local corrosion area. But the strain ranges either increase or decrease, depending on the corrosion defect size.

Figures 21a and 21b respectively illustrate the effect of the size of the corrosion defect on wrinklebend damage measured by the SWT fatigue damage parameter for *R/t* = 28 for pressure cycling from 72 to 10 percent and from 80 to 10 percent of SMYS. The results show that:

- the areal corrosion defect length does not increase the fatigue damage except for very short lengths, which in the limit approach the scale of pitting and/or circumferential grooves across the crown of the wrinkle of similar width – for such scenarios a portion of this increased local damage might trace to the effects of local bending that for the composite shell model can equal the simulated effects of the metal loss,
- the areal corrosion defect width does not increase the wrinklebend damage if the defect width is less than an arc of 22°, but gradually increases the wrinklebend damage when the defect width is large than an arc of 22°. Such situations are expected as they reflect the behavior of wrinkles in thinner-wall line pipe for which the reduced local stiffness results in increased curvature, all else being equal.

These trends imply that large areal corrosion should be evaluated considering the same diameter pipeline but using a reduced wall thickness comparable to the net thickness at the corrosion. In contrast, where pits are present, the results suggest analysis ignoring the pitting, followed by a reduction in the service life to the extent indicated in Figure 18. For cycling from a maximum stress of 72 percent of SMYS damage for the above-noted corrosion defect widths can be expressed as:

$$D_f = 0.565(H/L) \qquad \text{for defect width} < 22^o \tag{28a}$$

$$D_f = 0.598(H/L) \qquad \text{for defect width} = 27^o \tag{28b}$$

$$D_f = 0.771(H/L) \qquad \text{for defect width} = 50^o \tag{28c}$$

while for cycling from a maximum stress of 80 percent of SMYS damage for the above-noted corrosion defect widths can be expressed as:

$$D_f = 0.678(H/L) \qquad \text{for defect width} < 22^o \tag{28d}$$

$$D_f = 0.735(H/L) \qquad \text{for defect width} = 27^o \tag{28e}$$

$$D_f = 0.948(H/L) \qquad \text{for defect width} = 50^o \tag{28f}$$

For cycling from a maximum stress of 72 percent of SMYS these damage parameters can be generally written as:

$$D_f = \begin{cases} 0.565(H/L), & \theta \le 22^\circ \\ (0.0072\theta + 0.4065)(H/L), & \theta > 22^\circ \end{cases} \tag{29a}$$

where θ is the angle in degree corresponding to the corrosion defect width.

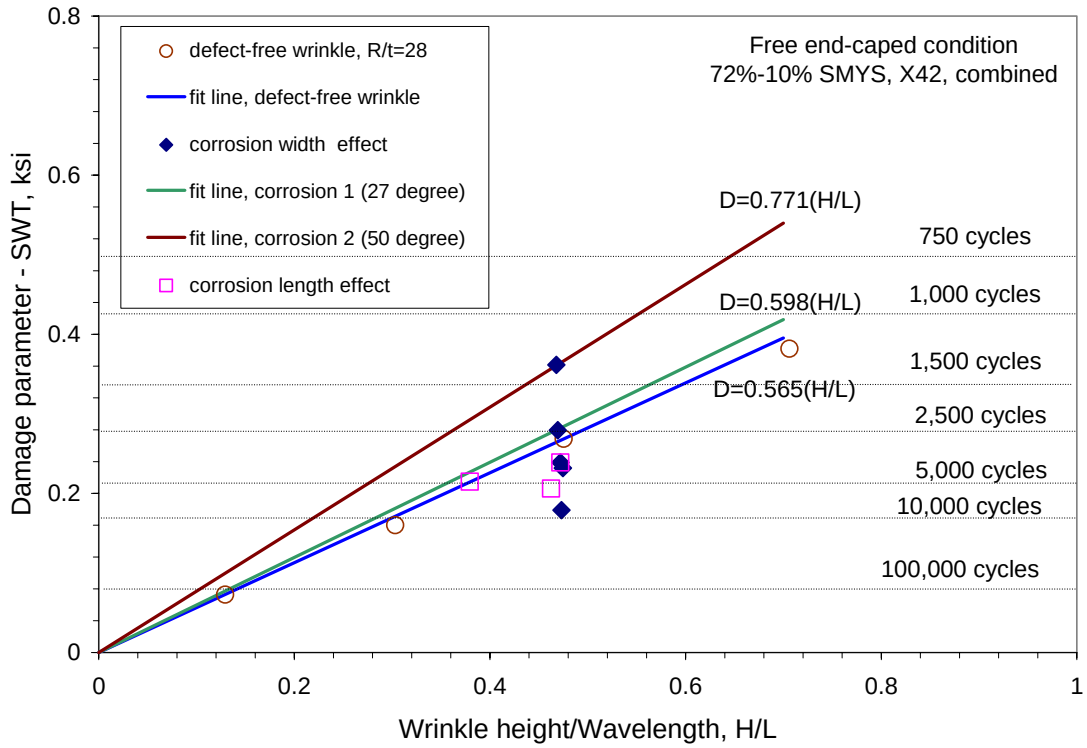

(a) cyclic pressure from 72 to 10 percent of SMYS

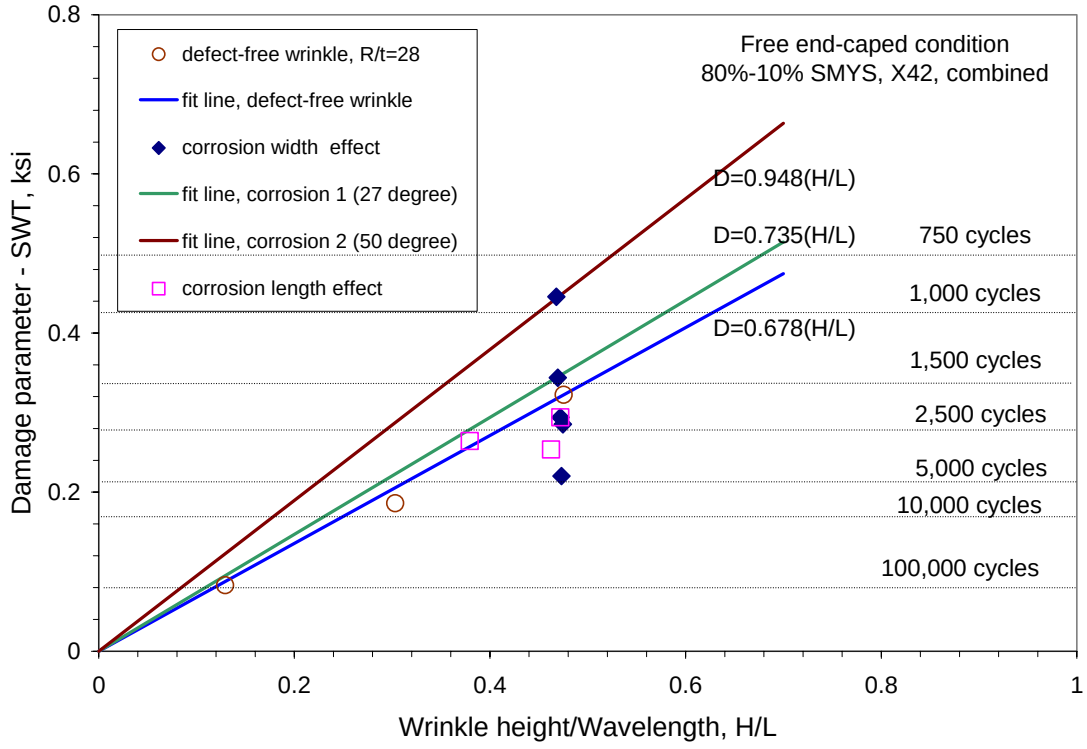

(b) cyclic pressure from 80 to 10 percent of SMYS

Figure 21. Corrosion size effect on the wrinklebend damage for pipeline with *R/t*=28

However, for cycling from a maximum stress of 80 percent of SMYS one obtains:

$$D_f = \begin{cases} 0.678(H/L), & \theta \le 22^\circ \\ (0.0093\theta + 0.4805)(H/L), & \theta > 22^\circ \end{cases} . \quad (29b)$$

The defect width angle in the equation above may have the upper bound value of 90^o.

The above results indicate that the corrosion width around the circumference of the wrinklebend is a first-order factor that increases the fatigue damage at a wrinklebend, while the corrosion length along the length of the pipeline located on the crown of the wrinklebend is a second-order parameter. This outcome is not a surprise, as the physical distances over which corrosion width can develop is large whereas the distance over which the length can develop is quite short.

Corrosion Effects on Wrinkle Damage for Smaller-Diameter Line Pipe

As was noted earlier, below $R/t = 25$ the damage parameter begins to show a dependence on geometry as the line-pipe's cross-section stiffens against wrinkle formation as thin-shell behavior is lost. For this reason it is appropriate to continue the FEA of corrosion effects for scenarios where the diameter decreases, or the wall thickness increases creating results where $R/t \le 25$.

Accordingly, FEA calculations were made using the composite shell model evaluating corrosion-defect size effects on wrinklebend damage for pipeline geometries with R/t less than 25. Recall that for such scenarios the fatigue damage decreased and the service live increased as R/t diminished. This section considers a smaller diameter X42 pipeline for which a diameter of 12 inches was evaluated with a wall thickness of 0.283 inch, which leads to $R/t = 21.2$. The FEA considered a model length of 35 inches.

The cyclic loading is as above, with cycling from 72 to 10 percent of SMYS. For this analysis a wrinkle shape with $H/L = 0.451$ was used, such that the wrinkle height $H = 1.123$ inches, the half-wrinkle wavelength $L = 1.244$ inches, and the half-wrinkle arc length is ~1.676 inches. The corrosion depth d again focused on $d/t = 0.5$.

As above, two groups of the corrosion defect sizes are simulated in the FEA calculations:

- Group 1: the corrosion defect has a fixed length at 1.3 inches (~ 77 percent of wrinkle arch length), and varied defect width from 0.5 inches (3.65^o), 1.3 inches (10^o), 3.7 inches (27^o) to 6.9 inches (50^o).
- Group 2: the corrosion defect has a fixed width of 1.3 inches (10^o), and varied defect length from 0.5 inches, 1.3 inches, 2.6 inches, and 5.1 inches.

Similar to the previous section, the composite shell model was used to form a corrosion defect through one weak layer after the wrinklebend was developed, which simulates the practical sequence of a corrosion defect forming at the wrinklebend after the pipeline enters service.

The FEA results again show that the residual stress and the residual strain formed at a wrinkle area during the cold bending decrease for all corrosion defects considered in the two groups after the corrosion defects are formed in the FEA simulations. This occurs because the corrosion defect reduces the local stiffness of the wrinklebend. Under loading at either 72 or 80 percent of SMYS, the maximum tensile stress at the critical location of the corroded wrinklebend has slightly increased compared to those for the defect-free wrinklebend under the same loading.

However, the compressive strains at the critical location of the corroded wrinklebend increase, which occurs because of the reduced stiffness local to the local corrosion. In contrast, the strain ranges are found to either increase or decrease, which outcome depends on the size of the corrosion.

Figures 22a and 22b respectively illustrate the effect of the size of the corrosion size on wrinklebend damage as measured by the SWT damage parameter for this case at $R/t = 21$ for pressure cycling from 72 to 10 percent and from 80 to 10 percent of SMYS. It is apparent that:

- the corrosion defect length does not increase the fatigue damage for the wrinklebend except for the very short lengths, just as occurred and was discussed above for higher values of *R/t*, and
- the corrosion defect width does not increases the wrinklebend damage if the defect width is less than 22^o, but gradually increase the wrinklebend damage if the defect width is larger than 22^o, which again is as occurred and was discussed above for higher values of *R/t*.

The damage parameters for these corrosion defect widths can be fitted for pressure cycling from 72 to 10 percent of SMYS for cases involving X42as:

$$D_f = 0.405(H/L) \qquad \text{for defect width} < 22^o \tag{30a}$$

$$D_f = 0.447(H/L) \qquad \text{for defect width} = 27^o \tag{30b}$$

$$D_f = 0.678(H/L) \qquad \text{for defect width} = 50^o \tag{30c}$$

while for pressure cycling from 80 to 10 percent of SMYS for cases involving X42as:

$$D_f = 0.486(H/L) \qquad \text{for defect width} < 22^o \tag{30d}$$

$$D_f = 0.551(H/L) \qquad \text{for defect width} = 27^o \tag{30e}$$

$$D_f = 0.834(H/L) \qquad \text{for defect width} = 50^o \tag{30f}$$

The damage parameter for such applications can be generally written for pressure cycling from 72 to 10 percent of SMYS for cases involving X42as:

$$D_f = \begin{cases} 0.405(H/L), & \theta \le 22^\circ \\ (0.0096\theta + 0.1936)(H/L), & \theta > 22^\circ \end{cases} \tag{31a}$$

where θ is the angle in degree corresponding to the corrosion defect width, whereas for pressure cycling from 80 to 10 percent of SMYS for cases involving X42 it has the form:

$$D_f = \begin{cases} 0.486(H/L), & \theta \le 22^\circ \\ (0.0121\theta + 0.2251)(H/L), & \theta > 22^\circ \end{cases} \tag{31b}$$

Comparing Equation 30 with Equation 28 shows that similar corrosion effects develop for these two pipeline geometries even though the damage is decreased for $R/t = 21.2$, which is consistent with the observations in Task 2. Other similar tendencies can be found for $R/t = 21$ and 28.

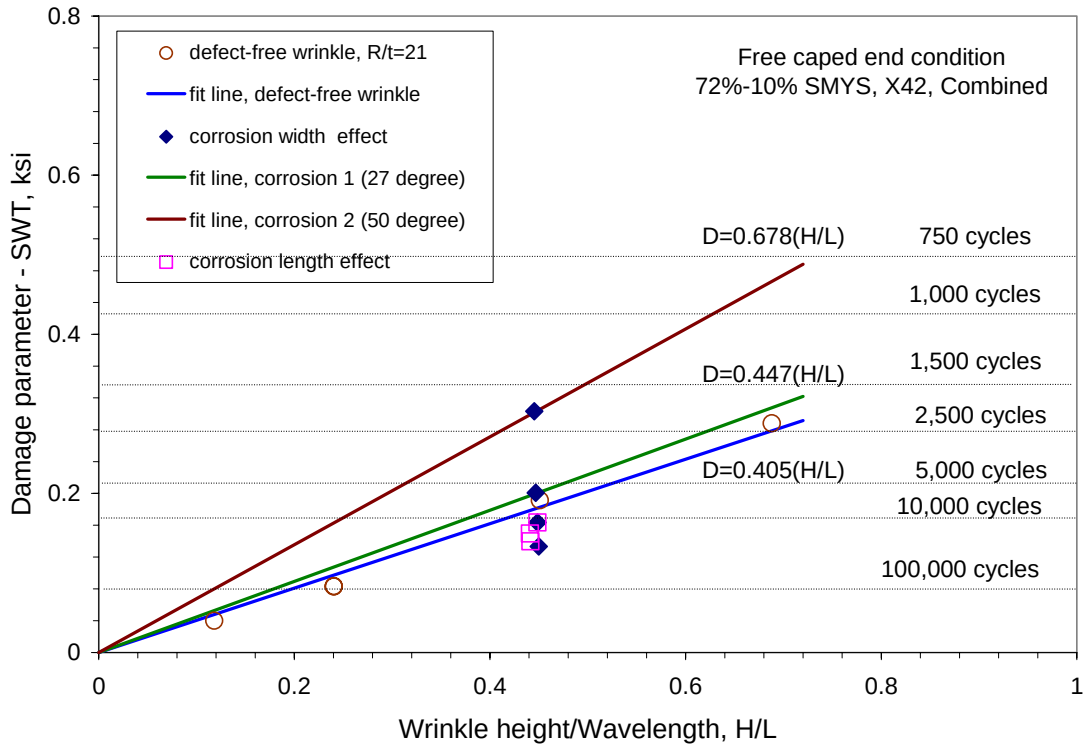

(a) cyclic pressure from 72 to 10 percent of SMYS

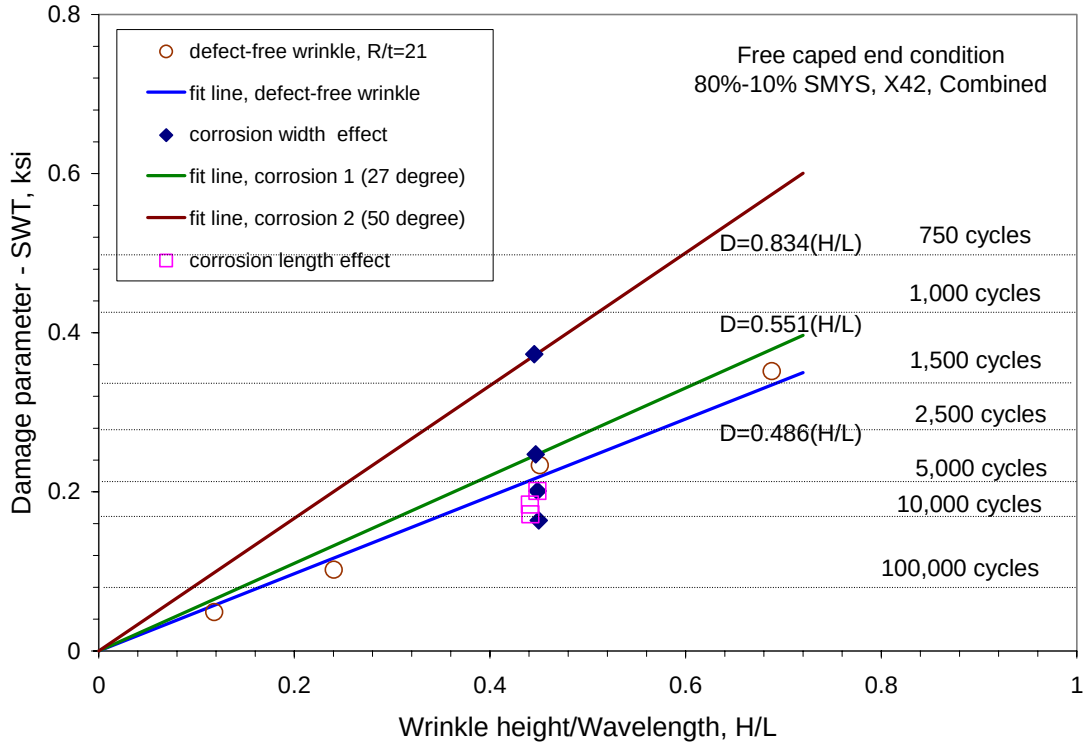

(b) cyclic pressure from 80 to 10 percent of SMYS

Figure 22. Corrosion size effect on the wrinklebend damage for pipeline with *R/t*=21

Trend Corrosion Results and Embed in the Severity Assessment Criteria

The results obtained in the prior two sections when coupled with the fatigue resistance curve in Equation A16 can be used to formulate wrinklebend integrity criteria that include consideration of corrosion effects.

For *R/t* = 28 and cycling from MAOP at 72 to 10 percent of SMYS, from Equations 29 and A16 one obtains:

$$\frac{H}{L} = 483.19\left(2N_f\right)^{-1.02} + 3.72\left(2N_f\right)^{-0.28}, \qquad \theta \le 22^{\circ} \tag{32a}$$

$$\left(0.0072\theta + 0.4065\right)\left(\frac{H}{L}\right) = 273\left(2N_f\right)^{-1.02} + 2.1\left(2N_f\right)^{-0.28}, \qquad \theta > 22^{\circ} \tag{32b}$$

For *R/t* = 28 and cycling from MAOP at 80 to 10 percent of SMYS, from Equations 29 and A16 one obtains:

$$\frac{H}{L} = 402.65\left(2N_f\right)^{-1.02} + 3.10\left(2N_f\right)^{-0.28}, \qquad \theta \le 22^{\circ} \tag{32c}$$

$$\left(0.0093\theta + 0.4805\right)\left(\frac{H}{L}\right) = 273\left(2N_f\right)^{-1.02} + 2.1\left(2N_f\right)^{-0.28}, \qquad \theta > 22^{\circ} \tag{32d}$$

Likewise for *R/t* = 21 and cycling from MAOP at 72 to 10 percent of SMYS, from Equations 31 and A16 one obtains:

$$\frac{H}{L} = 674.07\left(2N_f\right)^{-1.02} + 9.19\left(2N_f\right)^{-0.28}, \qquad \theta \le 22^{\circ} \tag{33a}$$

$$\left(0.0096\theta + 0.1936\right)\left(\frac{H}{L}\right) = 273\left(2N_f\right)^{-1.02} + 2.1\left(2N_f\right)^{-0.28}, \qquad \theta > 22^{\circ} \tag{33b}$$

Likewise for *R/t* = 21 and cycling from MAOP at 80 to 10 percent of SMYS, from Equations 31 and A16 one obtains:

$$\frac{H}{L} = 561.73\left(2N_f\right)^{-1.02} + 4.32\left(2N_f\right)^{-0.28}, \qquad \theta \le 22^{\circ} \tag{33c}$$

$$\left(0.0121\theta + 0.2251\right)\left(\frac{H}{L}\right) = 273\left(2N_f\right)^{-1.02} + 2.1\left(2N_f\right)^{-0.28}, \qquad \theta > 22^{\circ} \tag{33d}$$

Note that the criteria represented by Equations 32 and 33 are specific to cyclic loading as indicated and are for X42 pipeline steel. They will be generalized for other applications shortly.

Figures 23a and 23b show the predicted wrinklebend service life from Equation 32 for the pipeline geometric ratio *R/t* = 28 and the corroded wrinkle with a corrosion width of 22° or less, 30°, and 50°, respectively for pressure cycling from of MAOP at 72 to 10 percent of SMYS from 80 to 10 percent of SMYS for X42 line-pipe steel. Similarly, Figures 24a and 24b show the predicted wrinklebend service life from Equation 33 for the pipeline geometric ratio of *R/t* = 21 and the corroded wrinkle with a corrosion width of 22° or less, 30°, and 50°, respectively for

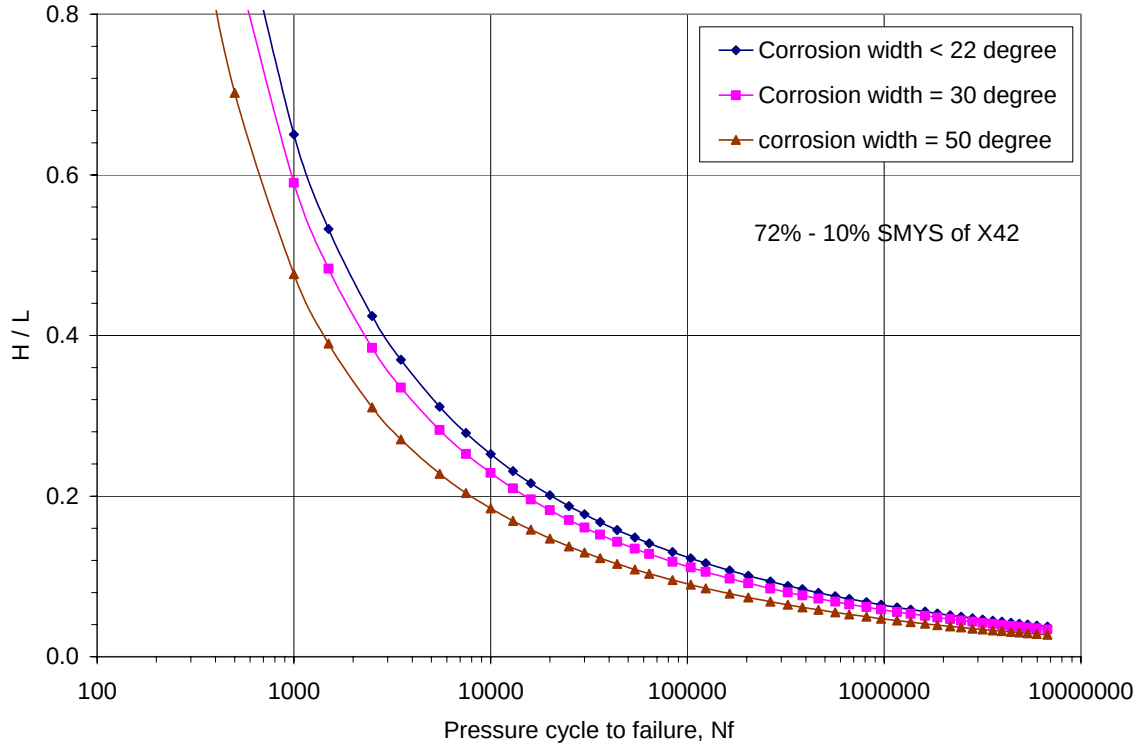

(a) cyclic pressure from 72 to 10 percent of SMYS

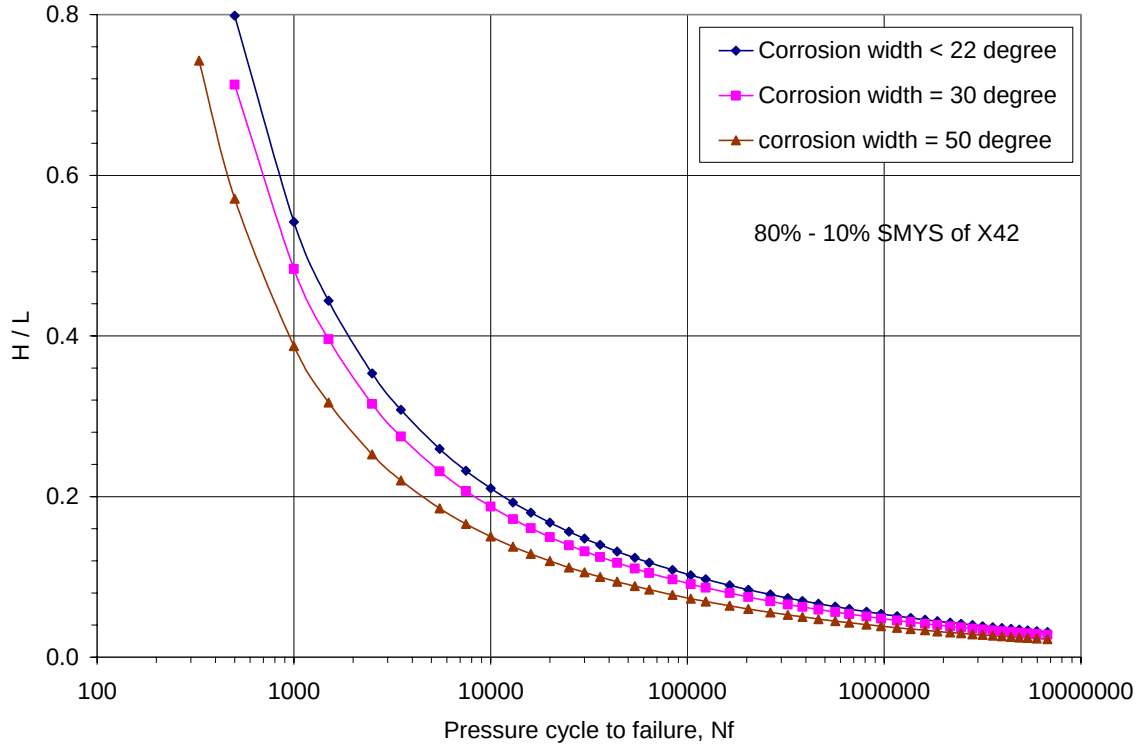

(b) cyclic pressure from 80 to 10 percent of SMYS

Figure 23. Wrinkle life prediction for *R/t* = 28

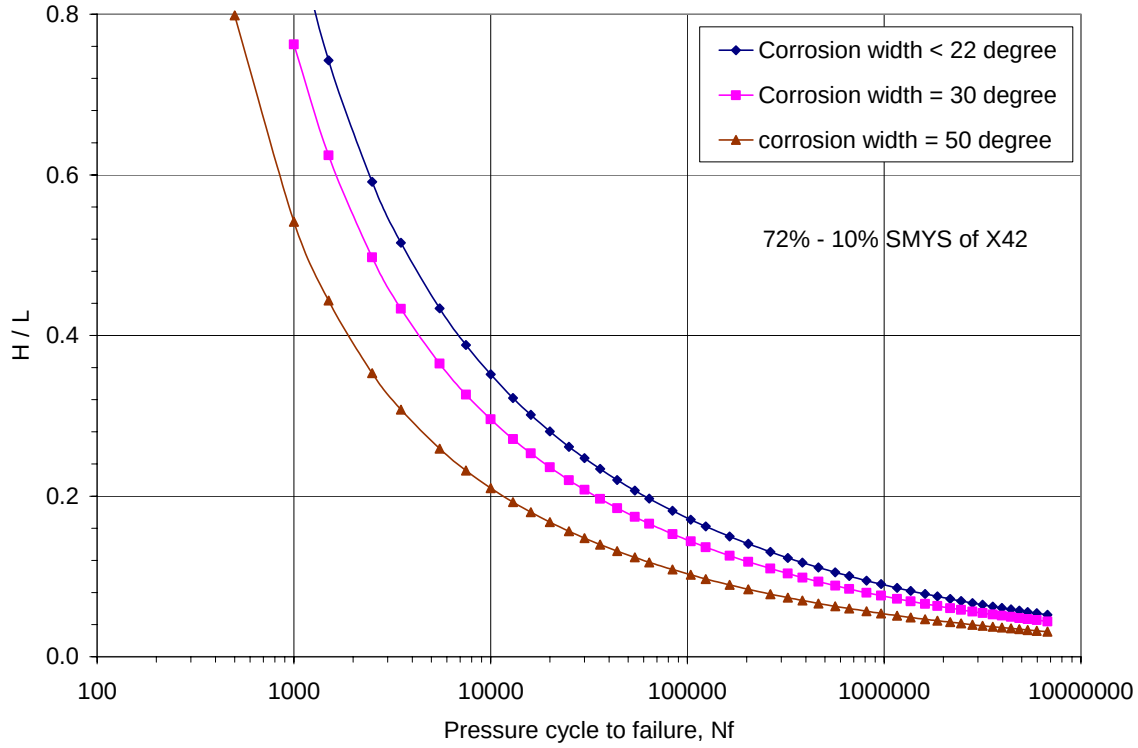

(a) cyclic pressure from 72 to 10 percent of SMYS

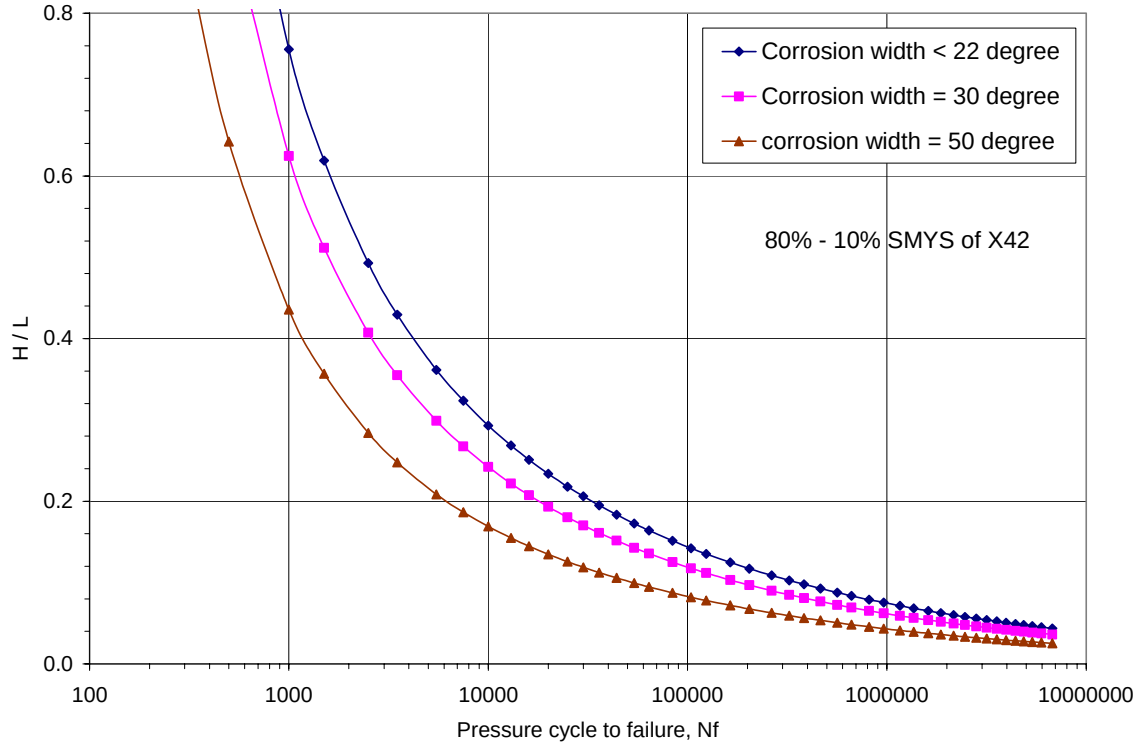

(b) cyclic pressure from 80 to 10 percent of SMYS

Figure 24. Wrinkle life prediction for *R/t* =21

pressure cycling from of MAOP at 72 to 10 percent of SMYS from 80 to 10 percent of SMYS for X42 line-pipe steel. These figures indicate that:

- the corrosion defect has no effect on the wrinkle life if the defect size is small in its width or the width arc is less than 22 degrees.
- for larger corrosion defects with an arc larger than 22 degrees, the corrosion defect decreases the wrinkle life. This is expected because a large corrosion defect decreases the local stiffness of a wrinkle, which increases the wrinkle damage and thus reduces its service life under otherwise similar conditions.
- corrosion width is a primary parameter while the length is secondary.
- corrosion defects have relatively larger effect on wrinkles for R/t =21 than R/t=28.
- for the same corrosion size or width, wrinkle damage for R/t = 21 is less than that for R/t = 28, and thus the wrinkle life for R/t = 21 is larger than that for R/t =28.

Parametric Evaluation of Constraint Applied Locally to the Wrinklebend

Because the approach adopted deals with local stresses and strains at the most highly damaged location within the flexing crown of the wrinklebend, aspects of the pipeline system that contain this wrinklebend influence the damage induced by the service loading. To date, the response of wrinklebend has been characterized in regard to pressure loadings and the effects of corrosion for wrinklebends in pipe that is free to deform in response to the pressure loading. Consequently, the initial shape of the wrinklebend changes because the bent pipe tends to straighten under the axial tension caused by the end-cap loading due to pressure. The amount of this local shape change due to straightening varies nonlinearly with the pressure, increasing with the pressure. For this reason, the effect of pressure and any constraints to the straightening of the bent pipe segment influence the amount of damage characterized by the SWT damage parameter.

Constraint to wrinklebend deformation develops locally because of strain hardening and related residual stresses and deformations. The extent of these localized effects has been evaluated by isolating the stresses and strains that develop purely due to shape, characterized by H/L, in contrast role of the shape independent of the constraint that develops from the surrounding pipe. This is akin to contrasting a simple one-dimensional (1D) analysis of wrinkle shape to the 3D formulation used herein.

The effect of pure geometric shape is evaluated by contrasting the damage developed in a 1D model subject to the same nominal stretching as experienced by the same initial wrinkle shape located at the crown of a wrinklebend in the cross-section of a pipeline. The same steel and wall thickness apply for both scenarios in the context of the same combined hardening model used throughout the prior analyses. As before, the analysis considers cold-formed wrinkles – that is the properties of the steel reflect the typical room temperature elastic-plastic response of the steel. The 1D analysis of pure geometric wrinkle shape was contrasted to the 3D analysis of wrinklebend shape and its local constraint for X42 line-pipe steel with thickness of 0.283 inch developing in a 16-inch-diameter line pipe with an initial wrinkle shape at H/L = 0.48. The loading considered involved cycling from 72 to 10 percent of SMYS.

Figure 25 presents the results in terms of the SWT damage parameter for pressure cycling from 72 to 10 percent and from 80 to 10 percent of SMYS. From this figure it is apparent that the pure effect geometric wrinkle leads to much higher fatigue damage for the same wrinklebend shape under the same cyclic loading. The essential difference between the results for pure

geometric wrinkle shape and that of the cold formed wrinkle lies in constraint to wrinkle response induced by the circular cross-section of the pipe and the residual plastic deformations and related redistribution of stress and strain that develop in the cold formed wrinklebend first during its forming and then during its cyclic pressure loading. For such reasons, the pure geometric wrinkle has less local geometric constraint and stiffness during the cyclic loading, and thus leads to a significant overestimate of the fatigue damage. This means that wrinklebends cannot be simply represented by a 1D model without resulting in a significantly conservative estimate of the damage, and a correspondingly shortened life. Given the difference between the simpler 1D model and the present 3D approach was linear or simply characterized, this difference could be simply accounted for. However, the present results indicate this difference can be strongly nonlinear depending on the circumstances, and depends on the geometry of the both the wrinkle and the pipe, and the grade and elastic-plastic mechanical response of the steel. It follows that any benefits from the use of simple 1D pure geometric wrinklebend models are more than offset by their shortfall in representing reality. Consequently, the use of 1D "strip" models should be avoided when evaluating wrinklebend.

To the extent it is useful to understand the effect of cold forming on wrinklebend behavior in contrast to consideration of only the shape that forming creates, the response in Figure 25 can be represented for pressure cycling from of MAOP at 72 to 10 percent of SMYS in terms of the simulated effects of cold forming an X42 wrinklebend as:

$$D_f = 0.565(H/L) \tag{34a}$$

while, for the same scenario but considering only the pure effects of the wrinklebend geometry one obtains:

$$D_f = 1.575(H/L) \tag{34b}$$

Similarly, the response in Figure 25 for pressure cycling from of MAOP at 80 to 10 percent of SMYS can be presented in terms of the simulated effects of cold forming an X42 wrinklebend as:

$$D_f = 0.678(H/L) \tag{34c}$$

while, for the same scenario but considering only the pure effects of the wrinklebend geometry one obtains:

$$D_f = 1.895(H/L) \tag{34d}$$

Parametric Evaluation of Constraint Applied Remote to the Wrinklebend

As noted for the preceding section on local constraint, any factor that influences the response at the most highly damaged location within the flexing crown of the wrinklebend must be assessed to determine its practical significance. Also as noted above, the initial shape of the wrinklebend changes because the bent pipe tends to straighten under the axial tension caused by the end-cap loading due to pressure. It follows that the boundary conditions imposed by both the pipeline system and the surrounding soil influence what occurs at the critical location in the wrinklebend in a potentially significant way. This has practically significant implications for rehabilitation of wrinklebends and related pressure reduction, as digging the wrinkle can remove this restraint and

possibly develop circumstances that can promote failure during or subsequent to digging the bend.

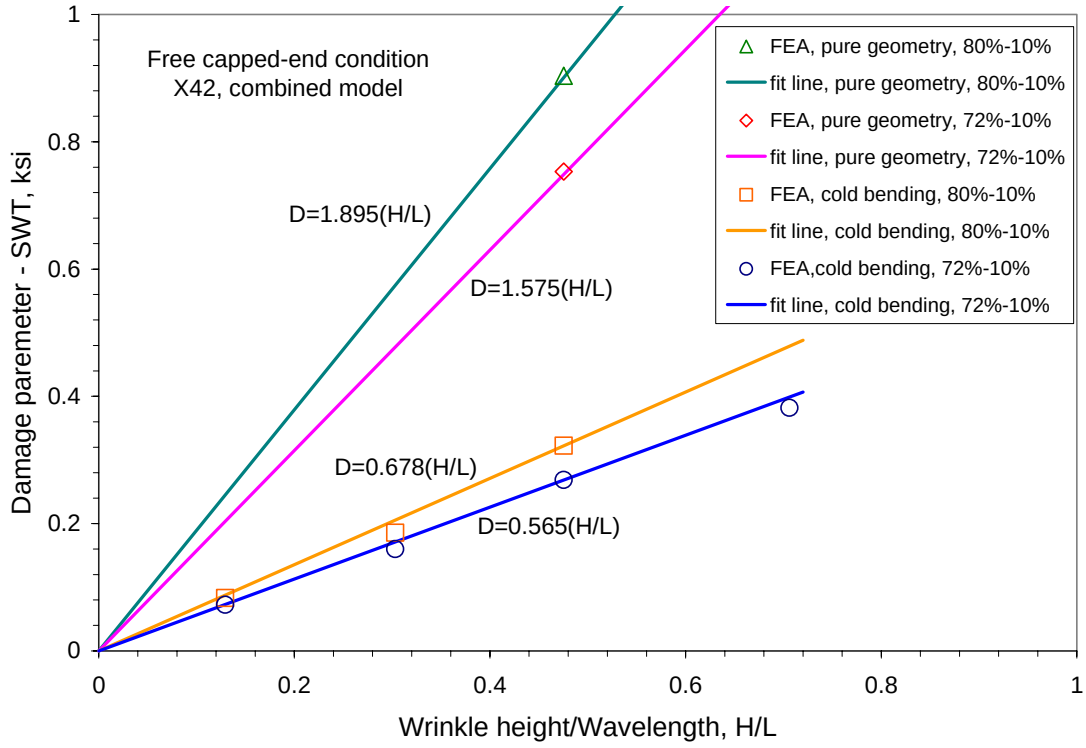

Figure 25. Fatigue damage between cold bend and pure geometric wrinkle shapes

This section simulates a range of "boundary conditions" imposed on the wrinklebend – with the practical realization that analysis of such idealized conditions is difficult to map into the field and the range of constraint that could be applied remote to the wrinkle. Up to this point, all results have been presented for the idealized condition noted in the figures as "free end-capped" conditions. Such boundary conditions reflect the pressure in the pipe under conditions where the pipe is free to move in response to the end-cap loading. The initial wrinklebend shape becomes less severe as the pipe segment rotates local to the wrinkle and acts to straighten the pipe in response to the pressure acting on the end-caps. As such the results presented to date do not necessarily reflect worst-case service conditions in reference to the initial wrinklebend shape. However, they do represent the response for the wrinklebend shape as found in service and so are relevant to all field scenarios – except where the historical constraint is disturbed. Historical constraint remote to the wrinklebend can change during rehab when the wrinkle is dug, allowing the bend to straighten, or during soil slips that can significantly change the remote loadings, whose effects on wrinklebend depend on its location and orientation relative to the soil slip.

The effects of remote boundary constraint are considered in this section for three boundary conditions, i.e., free capped-end conditions, simply supported-end conditions that maintain position but allow end rotation, and fixed-end conditions that preclude both end movement and rotation – all with end-caps. Recognizing that the relative effects of grade, line-pipe geometric properties, and service conditions can be dealt with as discussed earlier, this section continues

the focus on the same wrinklebend scenario considered in he last several sections. Thus, this evaluation deals with X42 line-pipe steel and wrinkles made in a 16-inch-diameter pipeline with wall thickness of 0.283 inch under pressure cycling from 72 to 10 percent of SMYS and from 80 to 10 percent of SMYS.

The FEA results are presented in Figure 26a for pressure cycling from 72 to 10 percent and from 80 to 10 percent of SMYS. These results show that a wrinklebend in pipe with simply supported-end conditions behaves similarly to bends in pipe with free capped-end conditions. This implies that end rotation does not significantly affect constraint sensed in the crown of the wrinkle – at least for the model length considered. In contrast, a wrinkle with fixed-end conditions is found to be much stiffer – such that the crown of the wrinkle flexes less under the action of the pressure loading, developing much lower damage. The results in Figure 26a indicate the fixed-end conditions limit this flexing so effectively that the near-worst case pressure cycling considered creates little practical concern for the integrity of wrinklebends, even for quite severe bends.

The present results indicate fully fixed conditions produce as much as a factor of 10 less damage as compared to the other end conditions. In this context, the results for the end conditions used to this point can be significantly conservative for field scenarios where the wrinklebend is highly constrained against movement by the surrounding soil, as could occur for hard clays. On the other hand, bends that lie in soft soils exist under conditions much more like those represented by the free boundary conditions that reflect the bulk of the analysis presented. Obviously, operating pipelines can experience boundary conditions that vary between the fixed-end conditions and the free capped-end conditions. Unless there is clear evidence for high soil-induced constraint, it is appropriate to consider the application to involve free capped-end conditions. In other scenarios where historically the wrinklebend has experienced significant constraint, these results suggest that rehabilitation open a hole as tight as practical to limit potential opening of the wrinkle. As line pressure drives this process, its role should be considered and the maximum pressure set accordingly.

Trend Constraint Effects and Embed in Severity Criterion

Figure 26a illustrates the fatigue damage equations for free end-capped conditions versus those for fixed-end end-capped conditions. The results shown therein for these remote constraint conditions can be expressed for pressure cycling of X42 wrinklebends from MAOP at 70 to 10 percent of SMYS as:

$$D_f = 0.565(H/L), \quad \text{for free capped-end conditions} \tag{35a}$$

$$D_f = 0.304(H/L), \quad \text{for intermediate end conditions} \tag{35b}$$

$$D_f = 0.042(H/L), \quad \text{for fixed-end conditions} \tag{35c}$$

Similar fatigue damage equations have been developed for pressure cycling of X42 wrinklebends from MAOP at 80 to 10 percent of SMYS for these remote constraint conditions, which can be expressed as:

$$D_f = 0.678(H/L), \quad \textbf{for free capped-end conditions} \tag{35d}$$

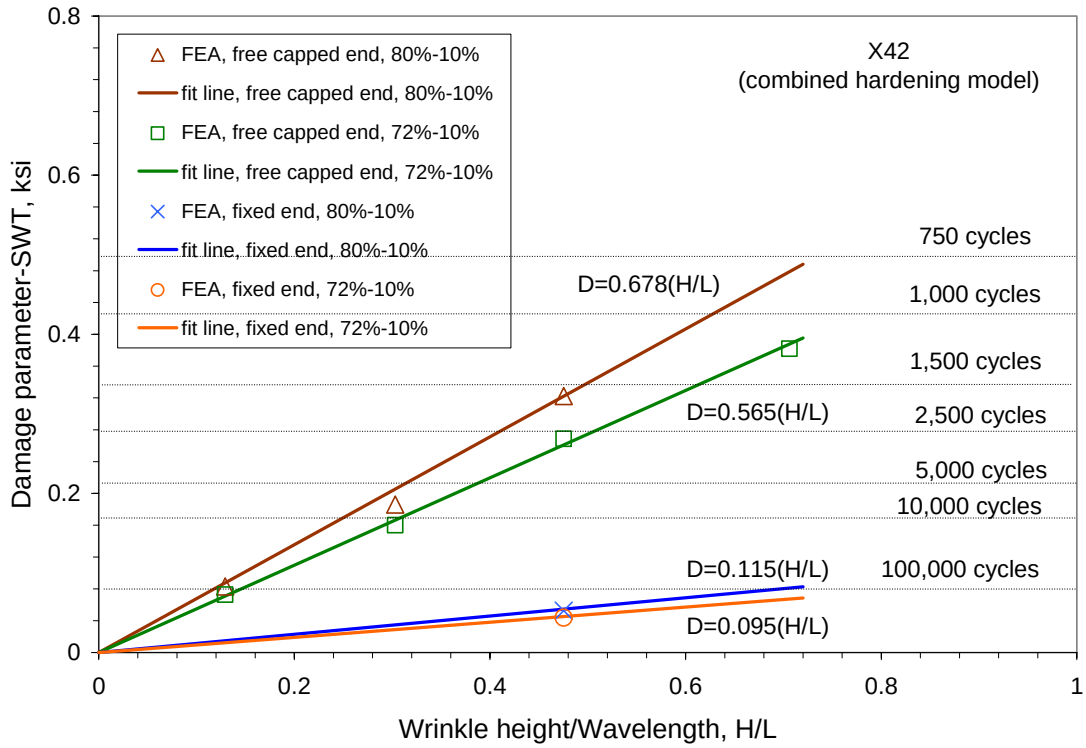

(a) relative effect of constraint

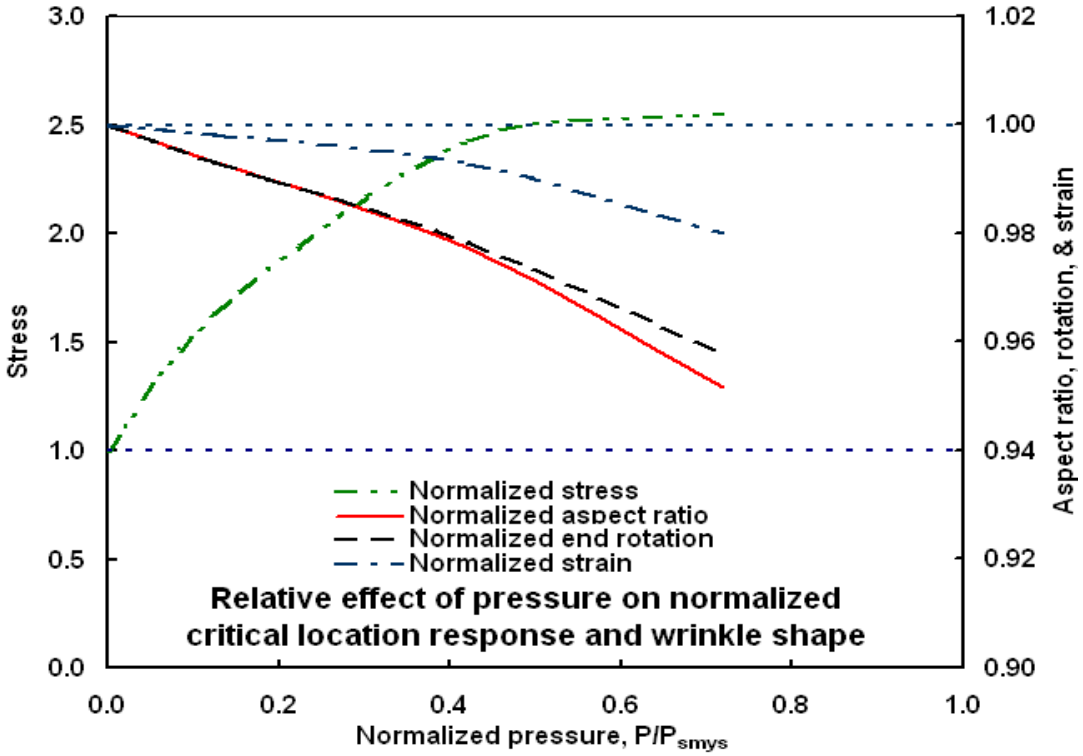

(b) relative effect of pressure on damage and wrinklebend shape

Figure 26. Field and service factors influencing the life of wrinklebends

$$D_f = 0.396(H/L), \quad \text{for intermediate end conditions} \tag{35e}$$

$$D_f = 0.115(H/L), \quad \text{for fixed-end conditions} \tag{35f}$$

From these equations and the material fatigue resistance curve of Equation A16, one can deduce the following criteria for service life for each of the three boundary conditions for pressure cycling of X42 wrinklebends from MAOP at 72 to 10 percent of SMYS:

$$\frac{H}{L} = 483.19(2N_f)^{-1.02} + 3.72(2N_f)^{-0.28}, \quad \text{for free capped-end conditions} \tag{36a}$$

$$\frac{H}{L} = 898.03(2N_f)^{-1.02} + 6.91(2N_f)^{-0.28}, \quad \text{for intermediate end conditions} \tag{36b}$$

$$\frac{H}{L} = 6500(2N_f)^{-1.02} + 50(2N_f)^{-0.28}, \quad \text{for fixed-end conditions} \tag{36c}$$

Similarly, one can deduce the following criteria for service life for each of the three boundary conditions for pressure cycling of X42 wrinklebends from MAOP at 80 to 10 percent of SMYS:

$$\frac{H}{L} = 402.65(2N_f)^{-1.02} + 3.10(2N_f)^{-0.28}, \quad \text{for free capped-end conditions} \tag{36d}$$

$$\frac{H}{L} = 689.39(2N_f)^{-1.02} + 5.30(2N_f)^{-0.28}, \quad \text{for intermediate end conditions} \tag{36e}$$

$$\frac{H}{L} = 2373.91(2N_f)^{-1.02} + 18.26(2N_f)^{-0.28}, \quad \text{for fixed-end conditions} \tag{36f}$$

In practice all wrinklebends operate between these extremes, with the results for the free capped-end conditions being relevant unless clear evidence exists to support the use of results biased toward the fixed-end condition. Figures 27a and 27b respectively illustrate the effects of boundary condition on wrinklebend life as characterized by Equations 36 for pressure cycling from 72 to 10 percent and from 80 to 10 percent of SMYS. It is obvious that the wrinklebend with the fixed-end condition has the highest life, indicating as noted above that an earth-anchored pipeline enhances wrinklebend life and the related pipeline integrity.

Quantify the Interaction between Pressure, Constraint, and Wrinkle Shape

The mechanics of wrinkle response to pressure discussed above in regard to constraint indicates an interaction between pressure and constraint on wrinklebend shape and its influence on the critical location. From the results developed in the above sections it is apparent that (a) the internal pressure and current wrinkle shape are primary parameters affecting wrinklebend life, (b) changes in local constraint due to corrosion defects has a negative effect on wrinklebend integrity only when the corrosion defect size or width is large, (c) corrosion pits can significantly reduce wrinklebend life without major effects on local constraint, and (d) constraint due to the remote boundary condition has a significant effect on the wrinkle life. Because the prior sections quantified these aspects, it is necessary here to simply indicate the relative role of pressure.

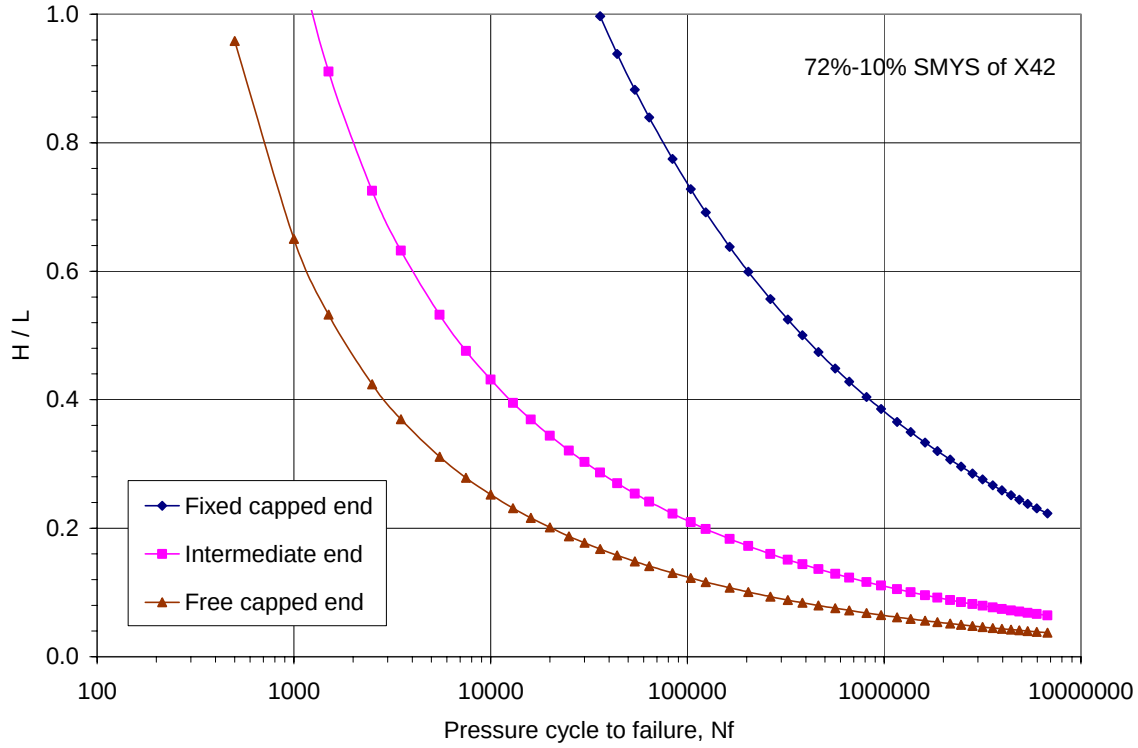

(a) cyclic pressure from 72 to 10 percent of SMYS

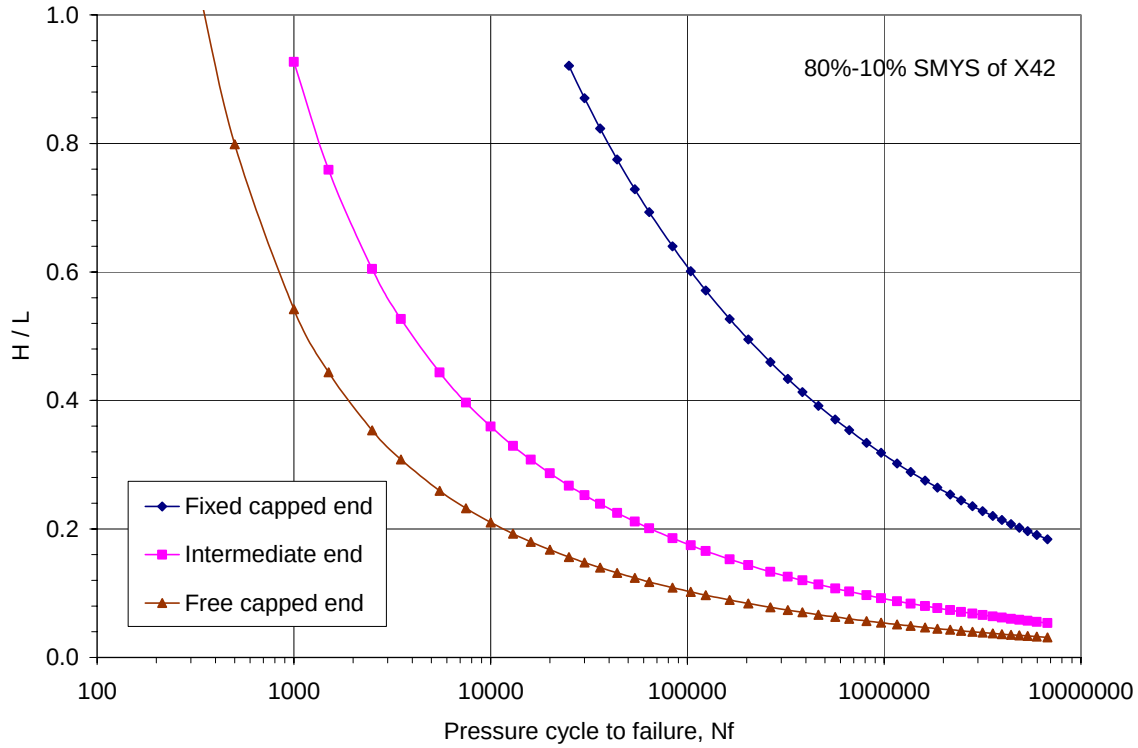

(b) cyclic pressure from 80 to 10 percent of SMYS

Figure 27. End boundary condition effects on the wrinkle life

Figure 26b serves to illustrate the relative effect of pressure on wrinklebend shape for one of the many scenarios considered to this point. From this figure it is apparent that in wrinkles free to flex as pressure increases the stress increases with pressure at lower pressure levels, but this contribution to critical-location damage saturates at and above pressures the order of 0.5 P/P_{smys}. The effects of increasing pressure on deformations are seen to decrease continuously in this figure, as is modestly evident for wrinkle aspect ratio (*H/L*), end rotation, and local strain. Thus, the contribution to the damage due to these aspects tends to diminish the damage as the pressure increases. Unfortunately, there is no simple pattern in this response, which precludes drawing specific conclusions. Suffice it to note the saturation in the role of local stress, the implication being that there is little difference in its role in applications where the nominal pressure exceeds about 50-percent of SMYS. As such typical pressure reductions, for example the order or 20-percent, would have little impact on this contribution to damage during rehabilitation for operations at higher nominal pressures, whereas for operations at lower pressures for which there is already less threat to safety this metric shows value. In contrast, where rehabilitation is planned for earth-anchored wrinklebends with high soil constraint, reducing the pressure has obvious benefits in offsetting the change in current wrinkle shape..

Quantify the Effect of Hot Forming on Mechanical and Fatigue Properties

It is well known from empirical data that temperature has a significant effect on the physical and mechanical properties of ductile steels. For hot-formed wrinkles these effects alter the damage analysis done to date, all of which reflects mechanical and fatigue properties developed at room temperature, as detailed in Reference 24. As shown in Figure 28a, which reflects the typical temperature dependence for the mechanical properties of steel, as the temperature increases the yield strength, ultimate tensile strength, and modulus decrease gradually, particularly at higher homologous temperatures. Fatigue resistance likewise decreases – but only for exposures at temperatures approaching the critical temperature (~1330 F for typical line-pipe steels used when wrinklebends were employed). Therefore, it is appropriate to assess the extent of these effects for typical wrinklebend hot-forming conditions (see Appendix A).

The effects of hot forming history on the wrinklebend damage have been simulated for X42 in regard to the mechanical properties shown in Figure 28b, which derive from use of the trends in Figure 28a. These temperature dependent steel properties were used along with a hot-forming history derived for wrinklebends based on the discussion of Appendix A. Limited data do not indicate as significant reduction in fatigue resistance for steels pre-exposed to thermal hot-forming histories inferred from Appendix A, such that the fatigue resistance characterized by Equation A16 is viable for such analyses.

Quantify Differences between Hot and Cold Formed Wrinklebends

Based on Appendix A, simulating the effects of hot forming on wrinklebends requires simulating the temperature field produced by a wood fire focused in the vicinity of where the wrinkle was to be formed, located a fixed distance from the pipe. The temperature gradient developed by this fire was rationally assumed to appear similar to the temperature distribution during conventional arc welding for low-carbon steels, but scaled in proportion to the size of the fire. Based on literature for wood-fired fires, the highest metal temperature is ~1000^{o}F, which was assumed near the wrinkle crown, with the temperature reduced gradually to ambient at 70^{o}F remote to the wrinkle. After the wrinklebend was formed, the wrinkle and pipeline were cooled to ambient conditions. This thermal gradient field was coupled with the properties for carbon steel shown in

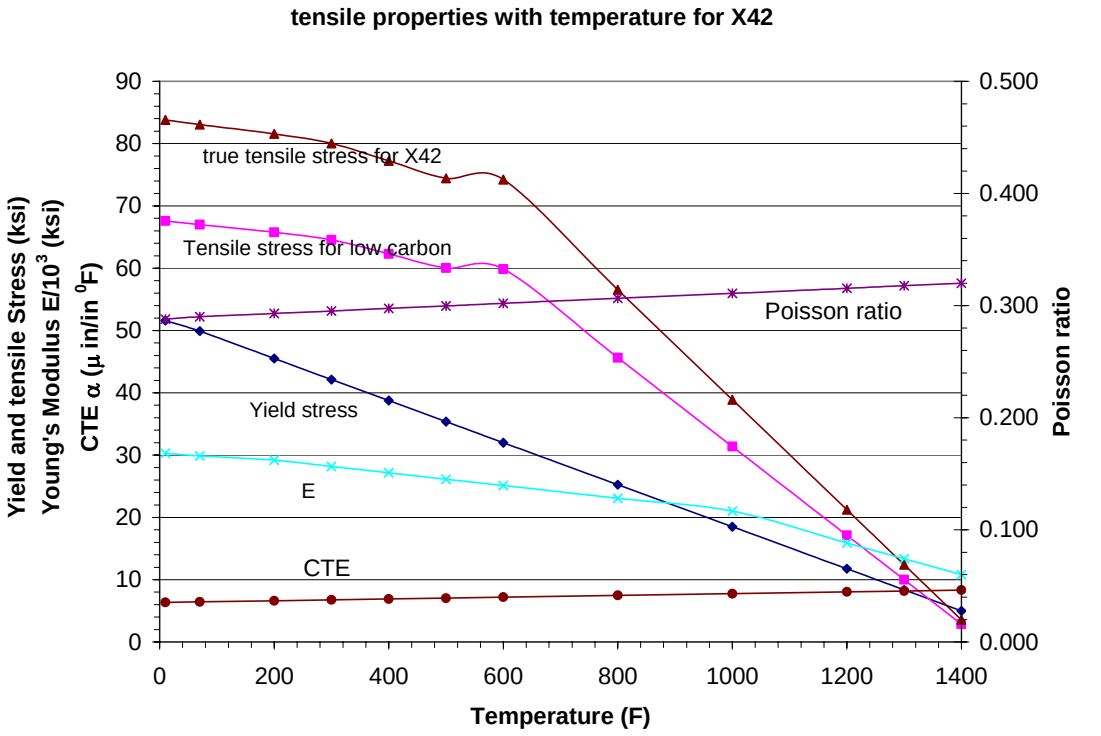

(a) normalized temperature dependence of properties

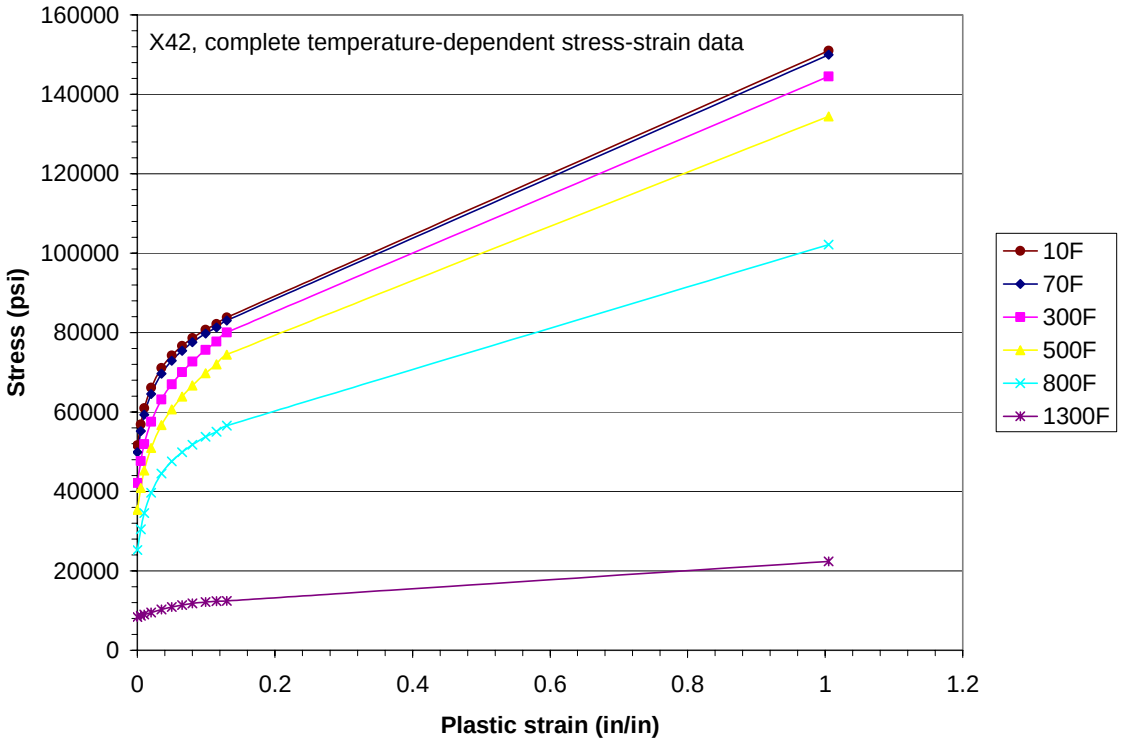

(b) temperature dependence of the true stress-true plastic strain response for X42

Figure 28. Temperature dependent properties response of steel

Figure 27 in simulating wrinkle-bending and wrinkle formation, which after cooling was subject to the same pressure cycling considered earlier, with the entire process dealt with via FEA. This analysis considered wrinklebends made in a 16-inch-diameter pipeline with wall thickness of 0.283 inch made of X42 steel subject to pressure cycling from 72 to 10 percent of SMYS and from 80 to 10 percent of SMYS.

Figures 29 present the effect of hot versus cold formed wrinkles on wrinklebend damage for X42 steel subject to pressure cycling respectively from 72 to 10 percent of SMYS and from 80 to 10 percent of SMYS for $R/t = 28$. These figures indicate that for the *same end rotation angle*, the hot-formed wrinkle shape finishes smaller than that for a cold-formed wrinkle. This apparently occurs because the steel at the crown of the wrinkle as well as surrounding this area is less stiff and weaker as compared to the cold-formed scenario. Consequently, all else being equal, it requires less force to create the wrinkle – and with less force driving the instability a smaller wrinkle develops in response to the imposed end rotation. Although the hot-formed wrinkle is physically smaller than its cold-formed counterpart, the strength of the steel following this thermal history develops larger plastic strains and correspondingly larger damage per cycle as compared to the cold-formed wrinkle developed for the same end rotation. Because the fatigue

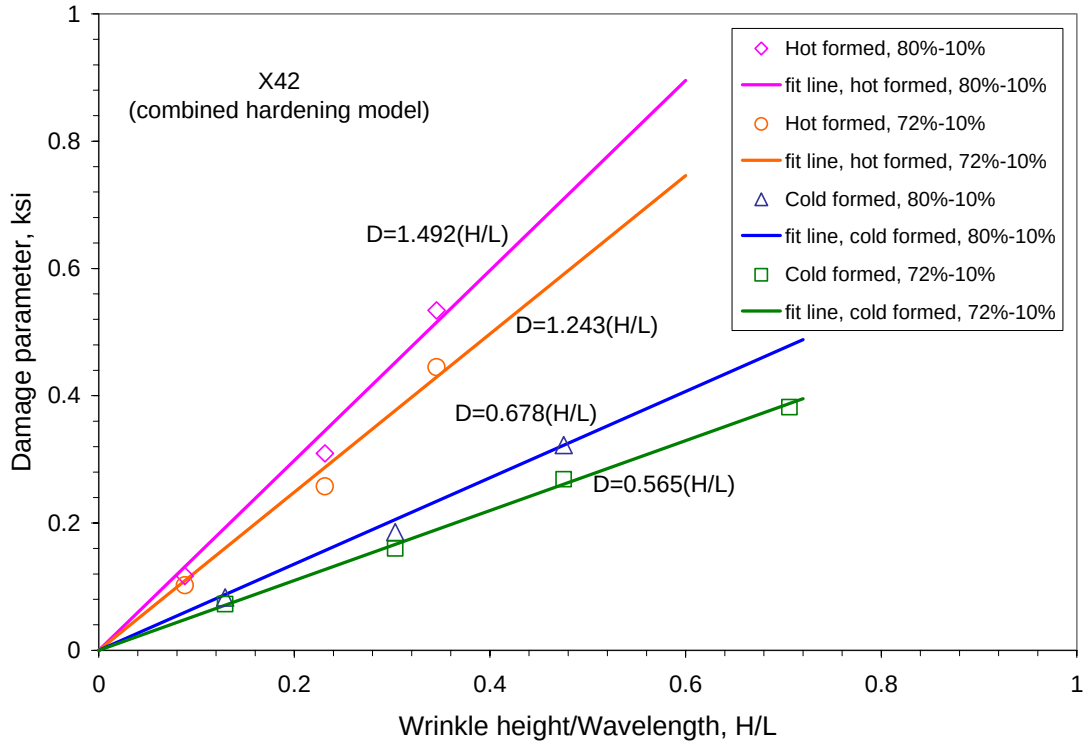

Figure 29. Effect of hot vs. cold formed wrinkles on wrinklebend damage

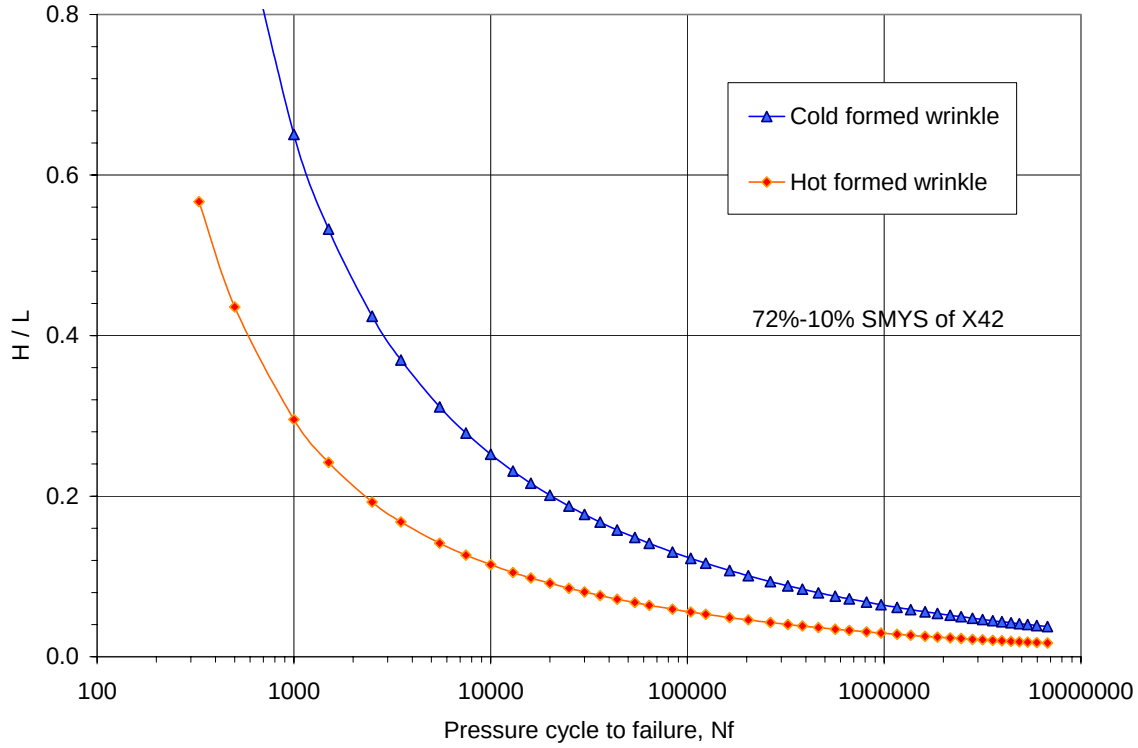

(a) cyclic pressure from 72 to 10 percent of SMYS

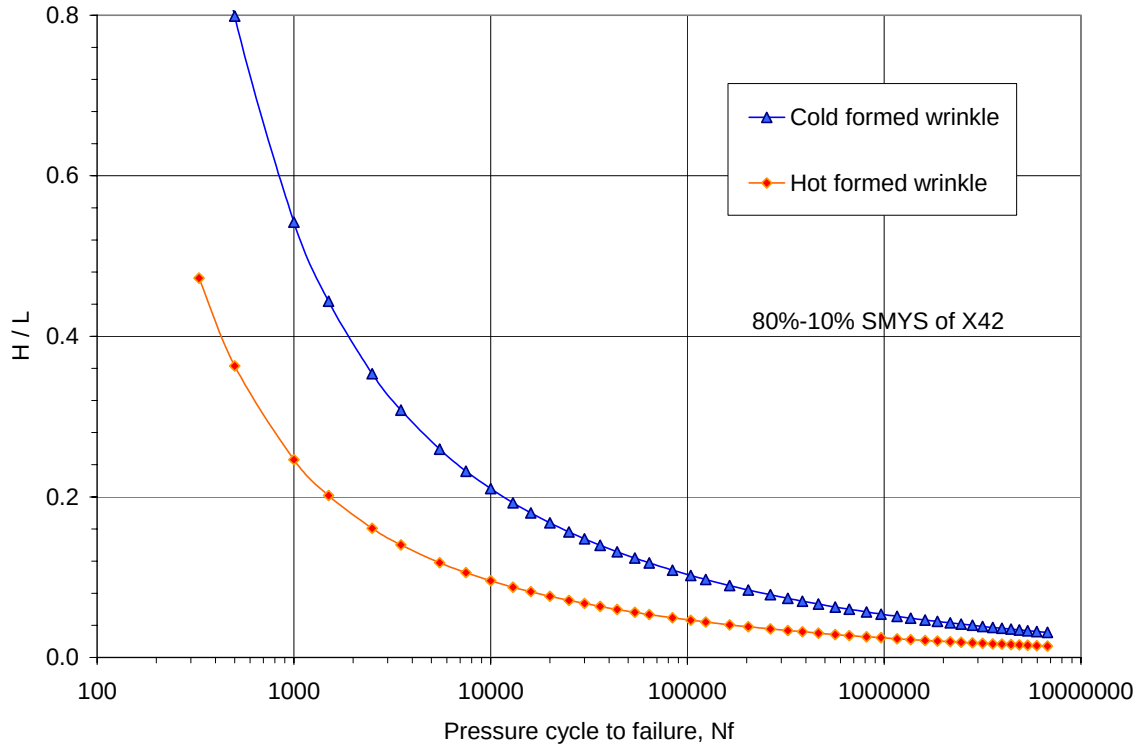

(b) cyclic pressure from 80 to 10 percent of SMYS

Figure 30. Effect of hot vs. cold formed wrinkles on wrinklebend life

resistance is unchanged due to this thermal pre-treatment, this increased damage per cycle when referenced to Equation A16 leads to shorter lives as compared to the cold-formed wrinkle at the same end rotation. As the disparity between hot and cold formed wrinklebends is significant, leading to a reduction in life by a factor of ~7 for these data, it is essential to address the integrity management of such wrinkles differently. Accordingly, company files and the corporate memory should be evaluated to determine whether hot-formed wrinklebends were used. Where uncertainty prevails, or the results point to the use of hot-formed wrinkles, the lives predicted based on the cold-formed results presented this far should be reduced by a factor of ~7, which can be analytically accomplished as dealt with next.

Embed Effects of Forming History in the Severity Criterion

In light of the trends in Figure 29, the effects of hot forming history on wrinklebend severity criteria can be expressed for cold- and hot-formed X42 steel wrinklebends subject to pressure cycling from 72 to 10 percent of SMYS as:

$$D_f = 0.565(H/L), \text{ for cold-formed wrinkle} \tag{37a}$$

$$D_f = 1.243(H/L), \quad \text{for hot-formed wrinkle} \tag{37b}$$

Similarly, the effects of hot forming history on wrinklebend severity criteria can be expressed for cold- and hot-formed X42 steel wrinklebends subject to pressure cycling from 80 to 10 percent of SMYS as:

$$D_f = 0.678(H/L), \quad \text{for cold-formed wrinkle} \tag{37c}$$

$$D_f = 1.492(H/L), \quad \text{for hot-formed wrinkle} \tag{37d}$$

Using these equations in conjunction with the fatigue resistance curve in Equation A16 to eliminate the damage parameter one obtains expressions between wrinkle aspect ratio (*H/L*) and the service life. Thus, wrinklebend life can be expressed for cold- and hot-formed X42 steel wrinklebends subject to pressure cycling from 72 to 10 percent of SMYS in the form:

$$\frac{H}{L} = 483.19(2N_f)^{-1.02} + 3.72(2N_f)^{-0.28}, \quad \text{for cold-formed wrinkle} \tag{38a}$$

$$\frac{H}{L} = 219.6(2N_f)^{-1.02} + 1.69(2N_f)^{-0.28}, \quad \text{for hot-formed wrinkle} \tag{38b}$$

Similarly, wrinklebend life can be expressed for cold- and hot-formed X42 steel wrinklebends subject to pressure cycling from 80 to 10 percent of SMYS in the form:

$$\frac{H}{L} = 402.65(2N_f)^{-1.02} + 3.10(2N_f)^{-0.28}, \quad \text{for cold-formed wrinkle} \tag{38c}$$

$$\frac{H}{L} = 182.97(2N_f)^{-1.02} + 1.41(2N_f)^{-0.28}, \quad \text{for hot-formed wrinkle} \tag{38d}$$

Figures 30a and 30b respectively plot these functions for pressure cycling from 72 to 10 percent and from 80 to 10 percent of SMYS. As anticipated from the above discussion these figures indicate that cold and hot wrinkle-forming processes develop significantly different lives, with hot-formed wrinkles being less resistant.

Evaluate Differences between Wrinkles and Large-Scale Buckles

Evaluation of the literature[e.g., 41-47] indicates that the form of equations that characterize local features like wrinkles and larger-scale features like buckles are similar. The essential difference between a localized feature like a wrinkle as compared to a larger-scale buckle is the constraint provided to the smaller-scale feature by the surrounding stiffer cross-section of the pipeline. Such constraint locks in residual displacements, strains, and stresses, which contribute to the damage. In contrast, the larger-scale features are anticipated to develop less severe damage, all else being equal. This possibility and the plausible utility of the present analyses to assess the integrity or significance of buckles can be examined by comparing results for larger-scale features whose size is more comparable to the pipeline's diameter in contrast to the physically smaller wrinklebends. Wrinkles were considered in this context to be small-scale buckles for which the length (pitch) of the feature was less than four inches. In contrast, buckles were considered to be large-scale features with a length greater than four inches, but with a reduced wave height in comparison to wrinkles. Accordingly, for the same wave height, H, the curvature for this larger-scale feature is not so localized and smaller than that for a wrinkle. The "reach" of such features around and along the pipeline is greater than for the smaller wrinkles considered to date, suggesting as noted above less influence of local constraint.

Generating larger-scale features as compared to the cold-formed wrinkle process required artificial control of wrinkle aspect ratio while end-rotation was imposed corresponding to levels achieved in forming the wrinkles. FEA was conducted for large-scale buckles considered in the same reference case considered earlier – that is a 16-inch-diameter pipe with a wall thickness of 0.283 inch made of X42 subject to cyclic internal pressure from 72 to 10 percent of SMYS.

Parts a and b of Figure 31 respectively present the results in terms of fatigue damage of wrinkles versus buckles for the same pipeline and operational scenario for pressure cycling from 72 to 10 percent. Likewise, parts a and b of Figure 32 respectively presents the measure of damage from Figure 31 directly in terms of service life for pressure cycling from 80 to 10 percent and from 80 to 10 percent of SMYS.

The trends in Figure 31a for fatigue damage for these wrinkle and buckle features can be approximately expressed for pressure cycling from 72 to 10 percent as:

$$D_f = 0.565(H/L), \qquad \text{for wrinkle} \tag{39a}$$

$$D_f = 0.485(H/L), \qquad \text{for buckle} \tag{39b}$$

Similarly, the trends in Figure 31b can be approximately expressed for pressure cycling from 80 to 10 percent as:

$$D_f = 0.678(H/L), \qquad \text{for wrinkle} \tag{39c}$$

$$D_f = 0.579(H/L), \qquad \text{for buckle} \tag{39d}$$

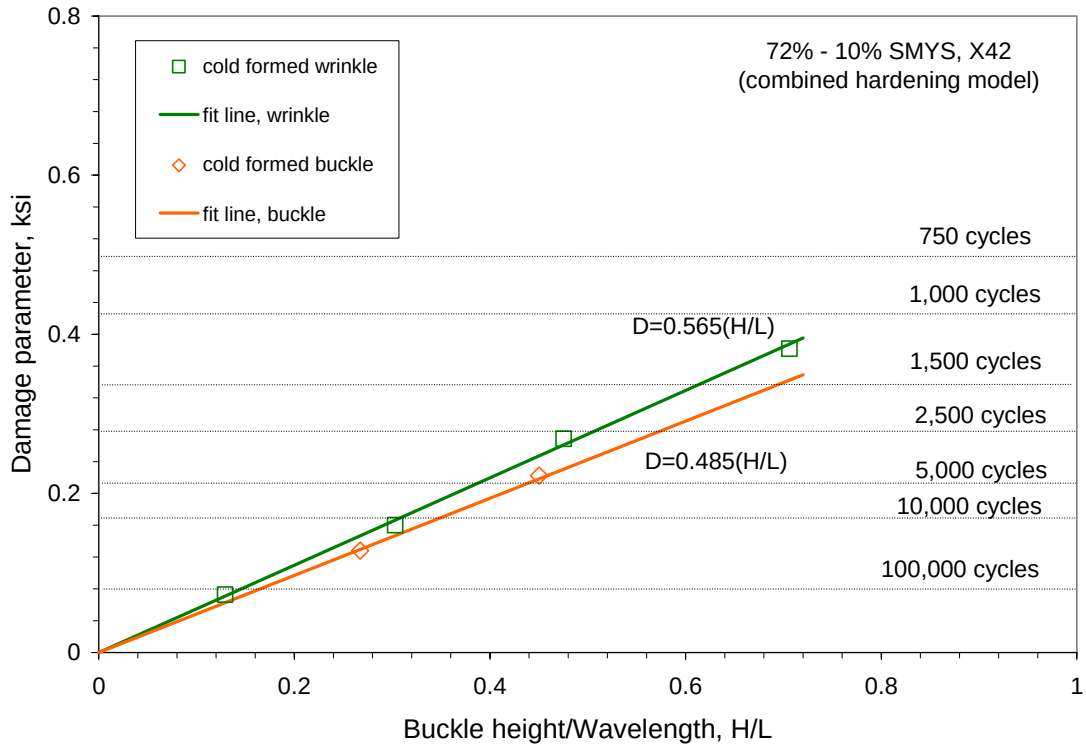

(a) cyclic pressure from 72 to 10 percent of SMYS

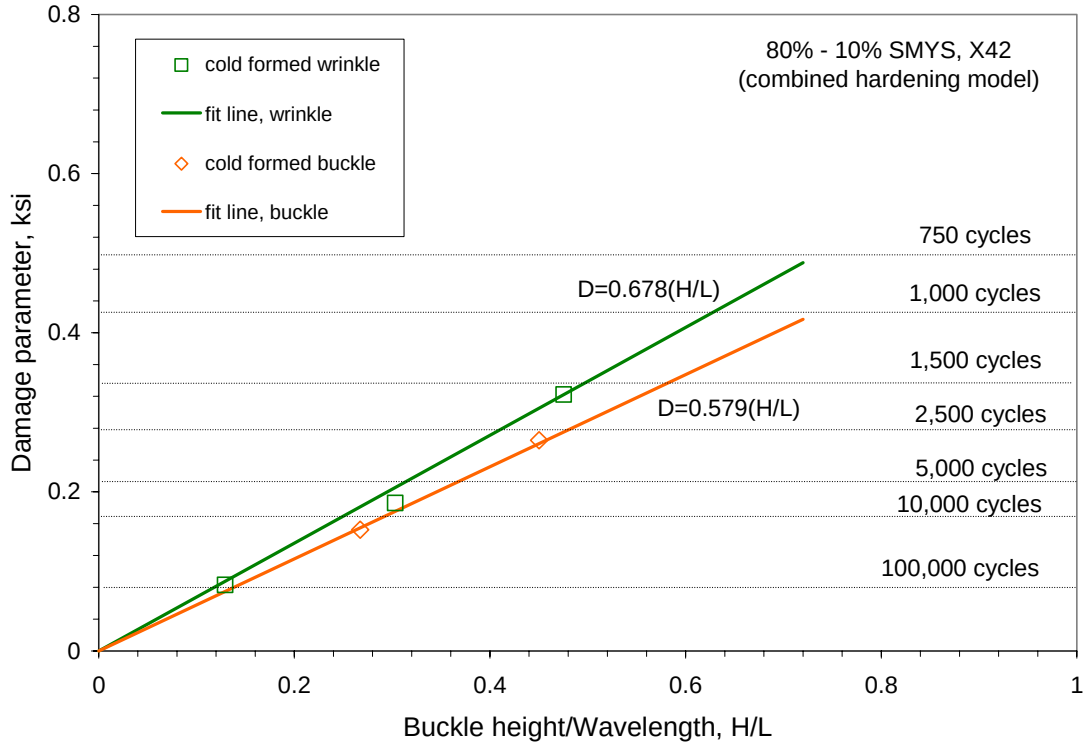

(b) cyclic pressure from 80 to 10 percent of SMYS

Figure 31. Buckle damage in comparison to wrinkle damage

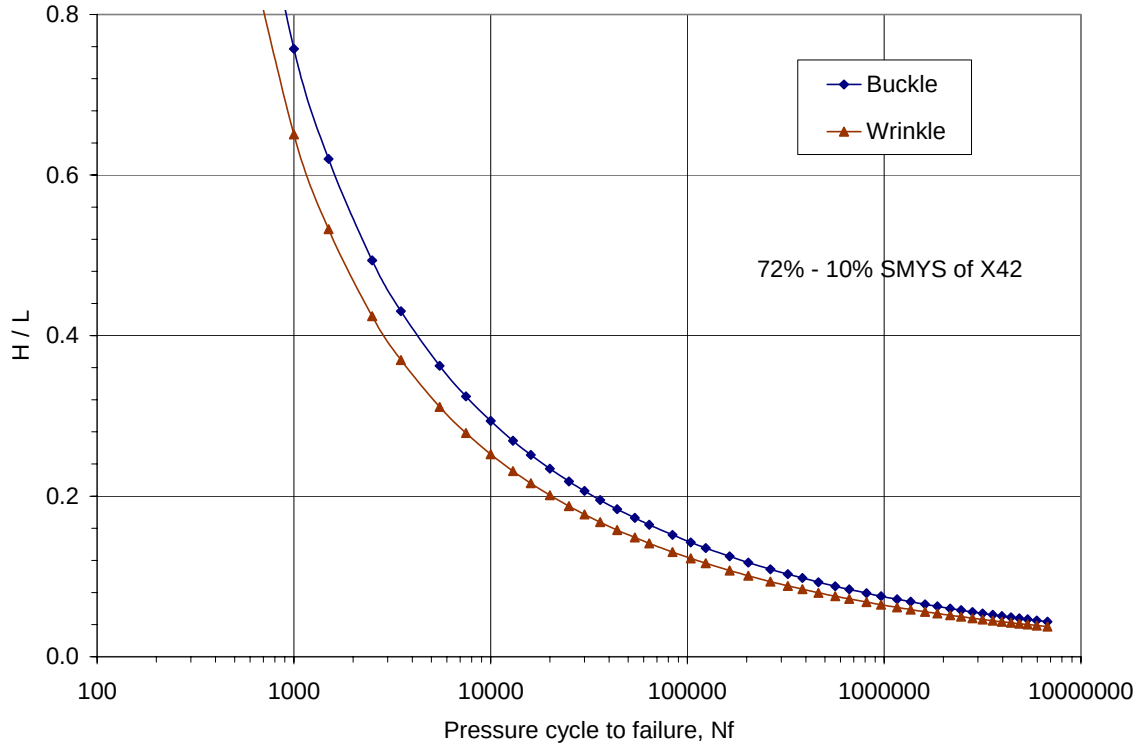

(a) cyclic pressure from 72 to 10 percent of SMYS

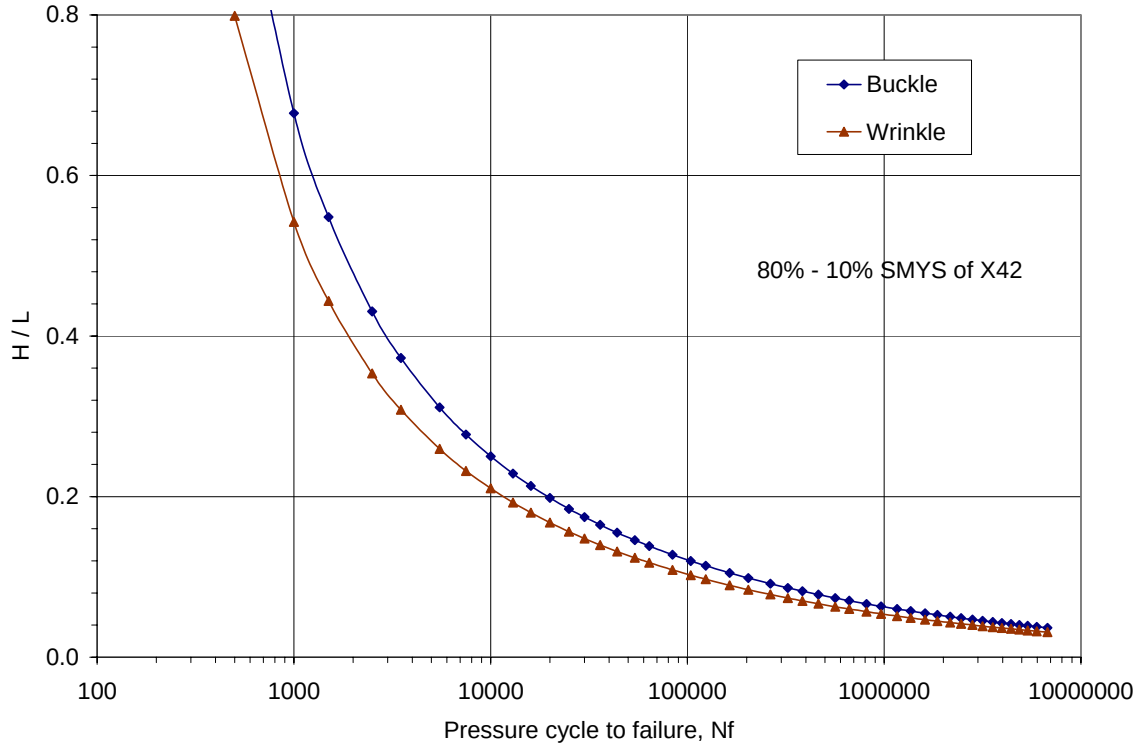

(b) cyclic pressure from 80 to 10 percent of SMYS

Figure 32. Buckle life versus wrinkle life

From these equations and the fatigue resistance curve in Equation A16 the damage parameter can be eliminated leaving direct expressions between *H/L* and service life for pressure cycling from 72 to 10 percent of the form:

$$\frac{H}{L} = 483.19\left(2N_f\right)^{-1.02} + 3.72\left(2N_f\right)^{-0.28}, \qquad \text{for wrinkle} \tag{40a}$$

$$\frac{H}{L} = 562.89\left(2N_f\right)^{-1.02} + 4.33\left(2N_f\right)^{-0.28}, \qquad \text{for buckle} \tag{40b}$$

Similarly, the damage parameter can be eliminated leaving direct expressions between *H/L* and service life for pressure cycling from 80 to 10 percent of the form:

$$\frac{H}{L} = 402.65\left(2N_f\right)^{-1.02} + 3.10\left(2N_f\right)^{-0.28}, \qquad \text{for wrinkle} \tag{40c}$$

$$\frac{H}{L} = 471.50\left(2N_f\right)^{-1.02} + 3.63\left(2N_f\right)^{-0.28}, \qquad \text{for buckle} \tag{40d}$$

Parts a and b of Figure 32 compare the service life between these wrinkles and buckles for pressure cycling from 72 to 10 percent and from 80 to 10 percent of SMYS respectively. These results indicate that the buckle service life is marginally greater than for the wrinkle.

As expected from the above discussion on local constraint, under the same cyclic loading, the residual plastic stress and strain decrease for the larger-scale features, and the fatigue damage decreased. As the buckle shape becomes flatter, the damage decreases still further. While these results show the expected trend, the difference is only marginal. This outcome suggests that when such features are formed asymmetrically as occurs herein the remaining circular cross-section asserts local constraint regardless of the scale of the feature – until the cross-section becomes unstable and collapses under the wrinkle or buckle forming loading.

It follows that the analysis and trends developed for all aspects, including factors like corrosion are applicable to "ripple" bends, such as those formed in modern bending machines[25]. However, once the cross-section becomes unstable and collapses under the loading causing the wrinkle or buckle, the smooth and gradual change in curvature evident in Figure 2 gives way to localized bending and the formation of kink-like features. To the extent that local curvature still describes the strains in such features the present analysis remains conceptually viable – as was evident in Reference 24.

However, the premise that *H/L* is a surrogate for curvature central to the present project becomes questionable once collapse occurs at the wrinklebend. This is evident in Figure 33, which presents results for a broad range of pipe geometries on the usual coordinates of damage as a function of wrinkle size, *H/L*. In contrast to prior cases using these coordinates, this figure includes results for a wide range of grades, line-pipe geometries, and values of *R/t* bounded as $15 \le R/t \le 45$, all for pressure cycling from 72 to 10 percent of SMYS. The key difference for this figure as compared to the prior cases lies in the range of *H/L* covered, which ranges from $\sim 0.05 \le H/L \le \sim 1.05$. In this context this figure shows the linear tendency evident in prior use of this format clearly breaks down as *H/L* increases beyond ~0.6, with this breakdown coming earlier for smaller-diameter line pipe for otherwise similar wrinkle severity characterized by *H/L*.

While the results as yet remain too sparse to draw quantitative conclusions, the fact that *H/L* fails to uniquely characterize wrinkle severity as wrinkle severity increases apparently traces to the dependence of the circumferential extent of the wrinkle on *H/L*. That is, the distance that a wrinkle propagates around the circumference as the wrinklebend is formed depends directly on *H/L*, and has the dimension of length rather than a nondimensional form. This indicates that for larger more severe wrinkles the wrinkle can propagate fully around the cross-section for smaller-diameter line pipe at smaller values of *H/L*, whereas it traverses proportionally less of the circumference for increased diameter. This means that the cross-section becomes unstable and collapses under a given loading at increasingly lower values of *H/L* as the line-pipe diameter decreases. As indicated above, once the cross-section collapses the nondimensional parameter *H/L* no longer serves as a surrogate for the curvature at the critical location in the crown of the wrinkle. Accordingly, the breakdown evident in Figure 33 is expected, and should develop first for smaller-diameter line pipe, which is evident by inspection of the trends in this figure. Under such circumstances, the smooth and gradual change in curvature evident in Figure 2 gives way to localized bending and the formation of kink-like features.

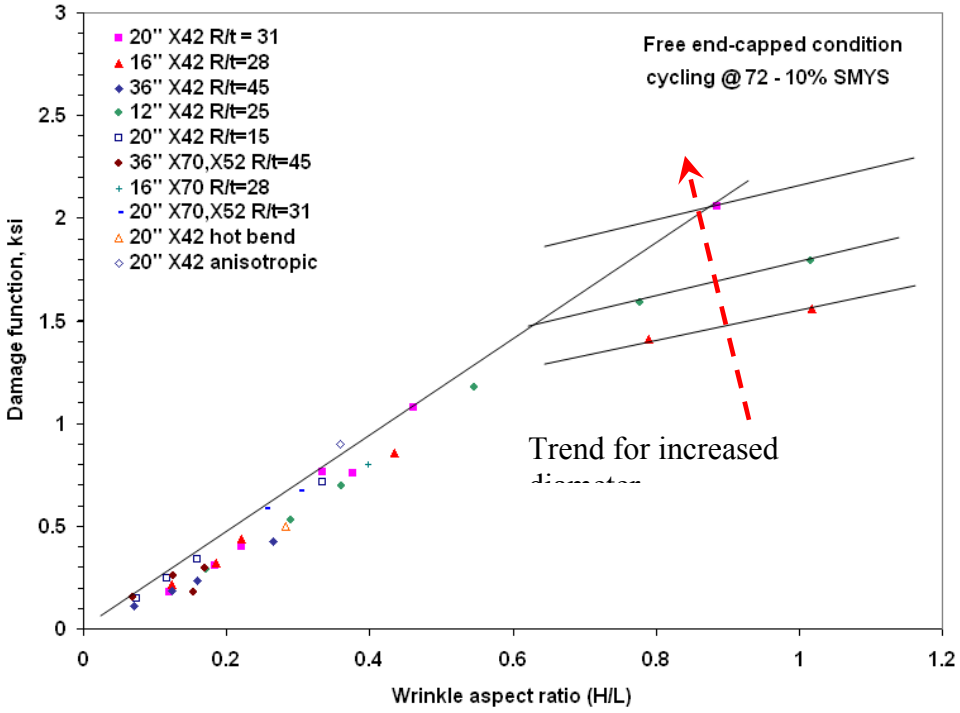

Figure 33. Apparent response of very severe wrinklebends

The limited results for very severe wrinklebends in the two smaller-diameter line pipes evident in Figure 33 show a much reduced slope in contrast to the band of results for the less severe (smaller) wrinklebends. Evaluation of the results for these few cases suggests this occurs because strain-hardening in the crown of the wrinkle and load transfer across the collapsed cross-section shift the deformation out of the crown into lower strained areas.

Validation of Criteria Based on Field Data

To date generic wrinklebend severity criteria have been developed, with validation considered in reference to limited full-scale testing for modern GrB and X42 line-pipe steels, with this

validation equally applicable to vintage line-pipe steels provided care is taken to account for the degraded surface condition. But, as such results reflect new line pipe free of corrosion no data exist to assess the viability of these severity criteria in applications to wrinklebends with local corrosion – either on the ID or the OD.

The present section develops results via laboratory work done to provide go –no-go validation data for wrinklebends with pitting and areal corrosion situated local to the crown of the wrinkle for wrinklebends removed from service. The pitting corrosion reflects the effects of moisture and modest levels of CO_2 present as impurities in the gas stream, which led to pitting on the ID local to the wrinkle – presumably because local eddies caused liquid dropout in that area. The second scenario reflects problems with the coating local to the wrinkle, which can be the cause of OD corrosion.

The Wrinklebend Samples

A total of six segments of line pipe some containing multiple wrinklebends were examined to develop field validation data, as detailed in Table 2.

Table 2. Dimensions and other details of the wrinklebends evaluated

Pipe Parameters				# of Wrinkles within a diameter spacing	Wrinkle Parameters							Ovality inch[5]
ID	Grade	OD inch	Local WT inch		ID	Bend Angle, degrees	Crown Radius @ OD, inch	Height, inch	Length, inch	Aspect Ratio, H/L	Length around pipe, inch	
Failure	X42	20	0.310	1				0.88	4.01	0.22		(1)
A	X50?	18	0.247	1		5.1	0.41	1.1 (2)	3.1	0.355	46	0.5
B	X52	20	0.291	5	B3	4.5	2.75	0.4 (2)	5.0	0.08	25	0.13
C[3]	X52	20	0.347	1								
D	X50?	18	0.258	2	D1	3.8	0.56	1.0	3.54	0.283	44	(1)
					D2	5.3	0.56	1.2	3.27	0.367	44	0.25
E	X52	30	0.281	4	E1	4.2	1.75	0.87(1)	5.8	0.15	47	0.50
					E2	4.3	1.75	0.81(4)	6.1	0.13	47	0.22
					E3	3.9	1.75	0.94(1)	5.8	0.16	45	0.46
					E4	2.5	2.25	0.75(4)	6.3	0.12	43	0.12

1 near pipe sample end – ovality measurement validity questionable

2 reflects the dimension "H"

3 wrinkle not considered in analyses

4 reflects the dimension "H_0"

5 difference between the major and minor local diameters

One segment containing multiple wrinkles spaced well more than a diameter apart and from the failure came from an in-service double-ended break (i.e., a guillotine rupture) in seamless (SMLS) 20-inch-diameter X42 grade pipe. The wall thickness in the vicinity of the rupture was about 0.310 inch (~7.9 mm). One of the wrinkles failed, while the second less severe wrinkle did not. This 20-foot-long segment, which came from a pipeline built in the early 1930s, is labeled "failure" in Table 2. Four segments that were removed in rehabilitation came labeled as Pipe Segments #1 through #4. Although each of these segments came numbered, because they also contained multiple wrinkles that also were numbered, each segment has been identified for purposes of tracking in Table 2 by a letter, with #1 designated as A, #2 designated as B, #3 designated as C and #4 designated as D. What came as Segments #1 and #4 were removed from

the same 18-inch-diameter electric-resistance welded (ERW) pipeline, which had a 0.25-inch-thich wall and noted as 1944 construction. Both of these segments were 14 feet long. While the grade was unknown, SMYS was indicated at between 50 and 52 ksi. What came as Segments #2 and #3 were removed from the same 20-inch-diameter X52 ERW pipeline reportedly constructed in 1947, which had a wall thickness indicated as 0.25-inch. Each of these segments was about 15-feet long. A final segment also removed from service came from a 30-inch-diameter X52 submerged-arc welded (SAW) pipeline reportedly constructed in 1947, which had a wall thickness indicated as 0.281-inch (7.14-mm). This segment contained four wrinkles and was about 15-feet long. For purposes of tracking this segment has been labeled as E in Table 2. Note that for Sample E, the wrinklebends identified as E1, E2, and E3 were not appreciably corroded whereas that designated as E4 showed extensive corrosion.

Some of the nominal dimensions described in the shipping correspondence that came with these segments conflicted with the measured parameters developed in this project. Logically, where this occurred the measured parameters reported in Table 2 were used as needed in the analyses.

Validation Data for Local ID Pitting

The Wrinklebend: The dimensions of the failed wrinkle were determined by reassembling the adjacent fracture faces, which were separated at three symmetric sites by thin softwood spacers of equal thickness to avoid damage to the fracture features. The height (amplitude) of the wrinkle was ~0.88-inch over a length (pitch) of ~4 inches, leading to an aspect ratio of 0.22. The wrinkle was smooth and without creases, and traversed about 45 percent of the pipe's diameter. There was no evidence of reversed curvature leading to a adjacent wrinkle oriented toward the interior of the pipe. Several wrinkles located downstream from the wrinkle that failed had similar shapes, although none was as severe and some were situated quite close together, indicating that these wrinkles were not made with shoes or mandrels on both sides of the wrinkle. Views of the ID of this SMLS pipe did not show evidence that a mandrel was used in forming these wrinkles. Some of the adjacent wrinkles did show significant reversed curvature leading to adjacent wrinkles whose amplitude was oriented toward the inside of the pipe, in contrast to the rest of the wrinkles evident in the adjacent pipe. None of the adjacent less severe wrinkles showed evidence of cracking. It is emphasized that multiple wrinkles located within about a diameter are locally more compliant and less prone to crack as compared to a single wrinkle, all else being equal. However, as these wrinkles were more widely spaced, their response can be considered typical of a single bend.

Rupture Origin: Rings were cut from the ends of the double-ended break from which pieces were cut containing the crown of the wrinkle and the fracture origin based on macroscopic evidence. These pieces were examined using low-power stereo optical microscopy (SOM), and then cut down relative to the apparent origin into pieces less than about 8 mm in length for examination using scanning electron microscopy (SEM). The inside of the pipe, the outside of the pipe, and the fracture features either side of the indicated origin were examined by SOM, first on as-received samples and then on samples cleaned to better reveal the mechanisms and other features. SOM indicated that the rupture originated from the inside of the pipe through the coalescence of several larger part-through-wall (PTW) cracks centered about the crown of the wrinkle. There was no crack nucleation evident on the exterior surface of the pipe. The larger PTW cracks developed from several smaller already-coalesced thumbnail cracks whose overall length was several inches, the deepest of which was 95 percent through the wall at failure.

A view of the origin identified via macroscopic evidence is shown in Figure 34a. The possible role of fatigue and other stress-focused cracking mechanisms was assessed using SEM, with transgranular cracking observed in nested arc-segments over parts of this fracture surface. These arc-segments were evident macroscopically, and also were found nested microscopically, with clear evidence of continuity across microstructural features such as grain boundaries – one of the requirements to identify such features as striations indicative of crack advance under cyclic loading. The orientation of these striation features was consistent with the location of two dominant origins that lay in the region identified macroscopically as the origin by chevrons either side pointing back to that area. Absent evidence to the contrary the cracking process leading to this rupture involved a fatigue type of mechanism in response to pressure cycling. The apparently brittle nature of the line-pipe limited the extent of crack-tip plasticity, which in turn limited the height of the striation-like features, which made them harder to observe as compared to ductile steels.

Figure 34b is typical of the ID surface features found adjacent to the fracture plane and near the origin. Corrosion is evident on the inside of the pipe as pitting. Figure 34c also shows localized corrosion (pitting) and evidence of crack-like features. ID pitting also was evident remote to the crown of the wrinkle, however such areas did not show evidence of crack nucleation. It follows that cracking nucleated at the crown of the wrinkle because of the increased mean and cyclic stresses and higher rate of fatigue damage. The evidence indicates nucleation driven by a striation mechanism. More than twenty origins of cracking were found in the coalesced PTW defects along the inside of the pipe. Each of these origins lay in a region of pitting corrosion as illustrated in Figures 34b and 34c. Consideration of the gas analysis for this pipeline indicated past occurrences of CO_2, H_2S, and moisture that could condense locally leading to formation of carbonic and sulfuric acids, which could dropout at wrinkles depending on local flow and other conditions.

The rupture occurred in the middle 1990s, which given early 1930s construction meant the pipeline was in service for about 65 years.

The Line-Pipe: The line pipe was seamless (SMLS) 20-inch-diameter X42 with wall thickness in the vicinity of the rupture of 0.310 inch (~7.9 mm), leading to $R/t = 32$. The chemistry, microstructure, hardness, and the mechanical properties of the line-pipe steel in the failed joint were as expected for X42 steel, indicating that these aspects were not factors. The full size equivalent toughness was about 13 J (~10 ft-lb) at the service temperature, which coupled with operation below a quite high transition temperature indicates a quite brittle steel with limited tolerance for the combination of high stress and deep crack-like defects. This observation is consistent with the chevrons observed on the fracture surface, and rationalizes the apparent brittle nature of the striation-like features, which made them harder to observe.

The Loadings: Photographs documenting the right of way (RoW) in the region of the failure showed no evidence of significant slips or geological instability. Occasional rock outcroppings imply that the underlying geological formations were likewise quite stable. Thus, soil instability was not a contributory factor, although recent rehabilitation near this rupture could have disturbed the soil and reduced related constraint for this wrinklebend.

a) fracture features through-wall at the origin

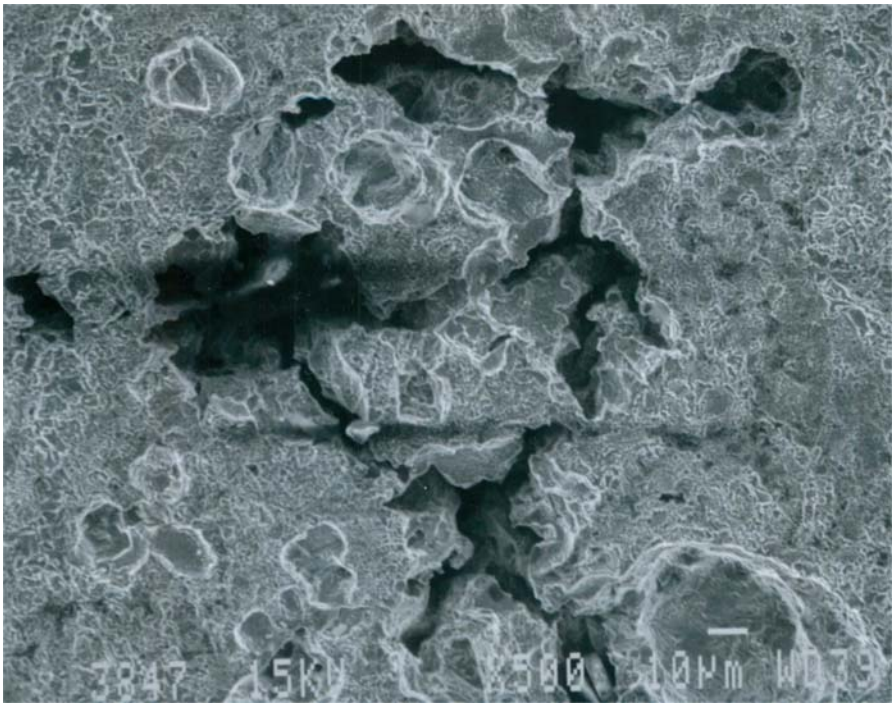

b) view of ID corrosion near the origin due to acid forming gases and water dropout

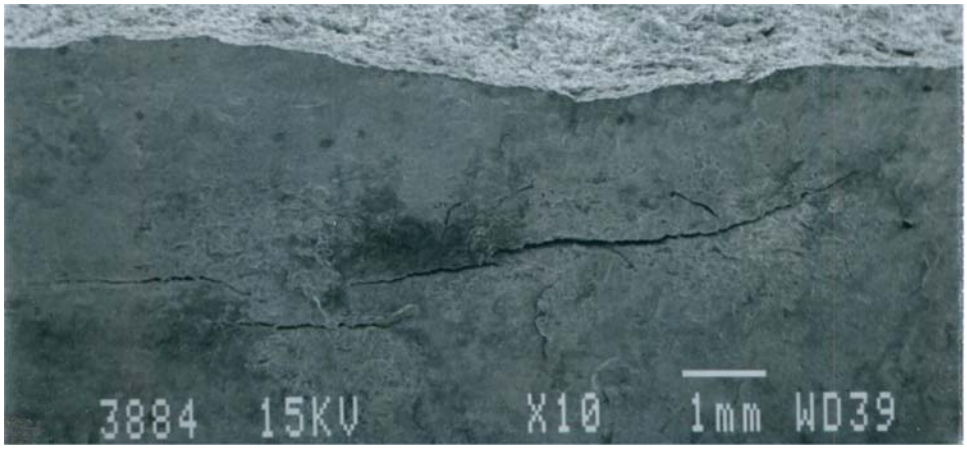

c) macroview of ID corrosion-induced cracking

Figure 34 Views at and near the origin of the guillotine failure

Thermal loading (ambient or service induced) to peak temperatures less than that at when the pipe was laid and buried would create tension on the interior of the pipe and compression on the exterior of the pipe. Conversely, thermal loading to greater temperatures would create compression on the interior of the pipe and tension on the exterior of the pipe. Given the cover apparently met code in the vicinity of the rupture, significant ambient diurnal thermal cycling was unlikely at the burial depth, which means the local temperature was controlled by service – which accounting for the distance downstream of the compressor was unlikely too different from the tie-in and burial temperatures. Given that the rupture occurred during a cold February, it is plausible that the interior of the pipe was subjected to a modest tension mean stress.

The effects of pressure cycling on this wrinklebend create tension on the ID local to the crown of this wrinkle and compression on the exterior surface. Conversely, the exterior of the pipe would have been subjected to an unknown but probably near zero mean stress with pressure cycling occurring to more compressive levels. Consequently, any cracking that nucleated due to a stress-driven mechanism is expected to continue to grow only from the inside wall of the pipeline. Records from the operating company indicate the subject pipeline operated at a maximum pressure equal to about 40 percent of SMYS and functioned in a pack and draft mode over a brief portion of its life. For the remainder of its service, operation was under much less severe cycling, such that a reasonable constant-amplitude representation of its service life is 40 to 30 percent of SMYS. As such cycling was no more frequent than daily and the pipeline was in service for about 65 years means the maximum number of service cycles can be taken at ~23,750.

Predicted versus Field Response:

The subject pipeline had been in operation for about 65 years since its construction in the early 1930s, which as indicated above reflects up to 23,750 pressure cycles – which given its unknown early service prior to its more recent pack and draft service likely overestimates the number of actual pressure cycles.

Given that $R/t = 32$ for the subject pipeline, the predicted response of the wrinklebend does not depend on the line-pipe geometry. In reference to Figure 12 and using the wrinkle aspect ratio, $H/L = 0.22$ the maximum predicted service life is indicated to be about 200,000 cycles absent the effects of corrosion for cycling from 72 to 36 percent of SMYS. The lower-bound predicted life corresponding to pressure cycling from 72 to 10 percent of SMYS is the order of 30,000 cycles absent the effects of corrosion. Where pitting occurs, the fatigue initiation life is reduced by more than an order of magnitude as discussed in reference to Figure 18. Thus, the predicted lives noted above must be reduced by about a factor of 30 to determine the corresponding life where pitting controls failure. This leads to predicted lives the order of 6700 and 1000 cycles, both of which are less than the estimated experience of up to 23,750 pressure cycles – which indicates the present criteria predicts failure for this locally pitted wrinklebend. Absent pitting at the adjacent less severe wrinklebends the present criteria not infer failure in these wrinkles, which is also consistent with the observations for these wrinklebends. Thus, both the failed as well as intact wrinklebends associated with this field failure validate the wrinklebend acceptance criteria developed herein.

Validation Data for Typical Applications

Four pipeline segments were sought to validate applications for which failure did not occur in wrinklebends free of ID or OD corrosion, except for one that had light ID corrosion. These samples were designated A to D in Table 2. The segment sought to evaluate the effects of corrosion on the wrinkle, identified as E in Table 2, provided an additional three wrinkles that were not corroded. As can be seen from Table 2, the aspect ratios of three of the wrinklebends available to represent "typical applications" free of corrosion range from values more severe than that just discussed, to levels that are less severe. Table 2 indicates that wrinklebends designated as Samples #A and #D came from 18-inch-diameter ERW pipeline with a 0.25-inch-thick wall for which the grade was unknown, although SMYS was indicated at between 50 and 52 ksi. Samples designated #B and #C came from 20-inch-diameter X52 ERW pipeline with wall thickness measured at 0.25-inch. Finally, the wrinkle samples designated E came from 30-inch-diameter X52 SAW line pipe with wall thickness measured at 0.281-inch.

The Wrinklebends: The severities of the four wrinklebends considered lie from well above to well below that for the guillotine rupture just evaluated, with aspect ratios from 0.08 to 0.367. Dimensions of the wrinklebends determined by direct measurement across the bend showed heights (amplitudes) from 0.40 to 1.2 inches over lengths (pitches) from 3.1 to 6.3 inches. All of the wrinkles considered were smooth and without creases, and traversed up to ~80 percent of the pipe's diameter. There was no clear evidence of significant reversed curvature. For the samples indicated in Table 2 to be associated with adjacent wrinkles, that is where their axial spacing was within about a diameter of each other, the analyses presented earlier indicates the local compliance was increased making them less severe as compared to a single wrinklebend, all else being equal. Figure 35 shows views of several of these wrinklebends.

Assessment of Corrosion and Possible Cracking: Rings were cut that contained the wrinklebends from which pieces were cut that contained just the crown of the wrinkle. Axial cross-sections through these pieces were polished and then examined using low-power SOM and then using higher power microscopy. Some trivial evidence of minor corrosion was evident but in no case would this be considered consequential. For all sections considered in no case did this detailed laboratory analysis show evidence of cracking from the ID or the OD. Follow-up higher power microscopy also failed to show evidence of crack nucleation.

The Line-Pipe: As noted earlier, the line pipe involved for Samples #A and #D was 18-inch-diameter ERW pipeline with a 0.25-inch-thick wall for which SMYS was indicated at between 50 and 52 ksi. Samples designated #B and #C came from 20-inch-diameter X52 ERW pipeline with wall thickness indicated as 0.25-inch, whereas samples designated E came from 30-inch diameter SAW line pipe with a wall thickness of 0.281 inch. The full size equivalent value of the toughness and the transition temperature were unknown for these samples.

The Loadings: Details along the RoW in the region where these bends were removed are unknown, although the subject pipelines do operate through earthquake-prone areas. While there is no evidence of thermal loading (ambient or service induced) there is a documented recent history of pack and draft service leading to larger pressure cycles for these wrinklebends. Records from the operating company indicate the subject pipelines operated at a maximum pressure equal to about 60 percent of SMYS with pack and draft operation most likely occurring since FERC Order 636 in the middle 1990s at a pressure ratio of about 0.8. For the remainder of its service, operation was under much less severe cycling. As such cycling was no more frequent

a) views of segments A (left) and B (right)

b) views of one of the more severe appearing wrinkles in segment A

Figure 35. Views of several typical wrinklebends examined in the validation process

than daily and the pipelines were constructed in 1944 or later and these segments were removed from service in about 2006 one can infer the maximum number of service cycles can be taken at about 24100 or less.

Predicted versus Field Response:

The worst-case scenario for all of the above-noted wrinklebends involves an aspect ratio of 0.367 located in X52 line pipe for which the predicted life is many times the above noted maximum 24100 service cycles anticipated for these pipelines. This worst-case prediction implies that no evidence of cracking should be found in any of the samples examined. Such was the case for all samples examined, which serves to more broadly validate the wrinklebend criteria consistent with the validation demonstrated for the full-scale testing of a similar wrinklebend scenario.

Validation Data for OD Areal / Pitting Corrosion

Pipeline segments were sought to validate applications for which failure occurred due to corrosion or wrinklebends were subject to widespread ID or OD corrosion. One such sample was located designated E in Table 2, specifically for the wrinkle identified as E4 in Table 2. This wrinkle was found in 30-inch-diameter X52 SAW line pipe with wall thickness measured at 0.281-inch.

The Wrinklebend: The aspect ratio for the subject wrinklebend was 0.12, which makes it among the least severe of the samples obtained whose aspect ratios ranged from 0.08 to 0.367. Its aspect ratio of 0.12 is about one-half of that for the guillotine rupture discussed earlier. The dimensions of this wrinklebend determined by direct measurement across the bend showed a height (amplitudes) of 0.75 inches over lengths of 6.3 inches. This height is the second smallest of all samples, while the pitch is the greatest. Aside from the corrosion, this wrinkle was smooth and without creases, and showed no clear evidence of reversed curvature. Also in contrast to the guillotine rupture, this wrinkle was one of four in this segment – although it was the last in this sequence as evident in Figure 36a.

Assessment of Corrosion and Possible Cracking: The nature and extent of the corrosion is apparent as-received in the views shown in Figure 36b. To facilitate observations, rings were cut that contained the wrinklebend from which pieces were cut that contained the crown of the wrinkle and the area around it. These pieces were then cleaned via light sandblasting, with Figure 36c showing a view of the corrosion after cleaning. It is apparent from this view that the metal loss is predominantly pitting.

Given that this extent of corrosion could not be broadly evaluated for possible cracking using the cross-section technique applied for other samples, following the light sandblasting the area about the crown of the wrinkle was subject to magnetic-particle inspection for evidence of cracking. Experience has shown this process to indicate the presence of even very small cracking in applications to analysis of stress-corrosion cracking, and can be viable where such corrosion occurs. Throughout this analysis did not show evidence of crack nucleation from either the ID or the OD.

The Line-Pipe: Wrinklebend E4 came from 30-inch diameter SAW line pipe with a wall thickness of 0.281 inch. The full size equivalent value of the toughness and the transition temperature were unknown for this line-pipe steel.

a) overview of segment E and wrinklebends 1 (closest) through 4 (furthest)

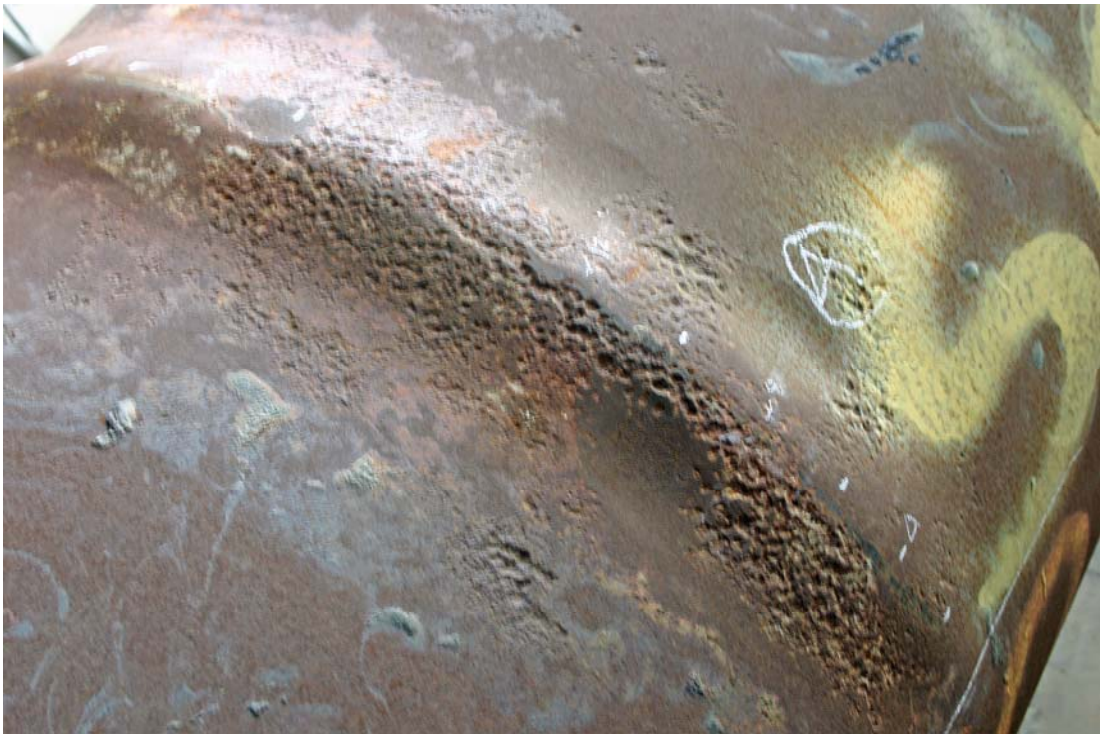

a) overview of the corrosion localized near the crown on wrinklebend 4

Figure 36. Views of the corroded wrinklebend

The Loadings: Details along the RoW in the region where this bend was removed are unknown, although the subject pipeline did operate through an earthquake-prone area. As above, while there was no evidence of thermal loading (ambient or service induced) there was a documented recent history of pack and draft service leading to larger pressure cycles for these wrinklebends. Records from the operating company indicate the subject pipelines operated at a maximum pressure equal to about 60 percent of SMYS with pack and draft operation most likely occurring since FERC Order 636 in the middle 1990s at a pressure ratio of 0.8. For the remainder of its service, operation was under much less severe cycling, such that the pressure ratio could be taken at a value of 0.9 or higher, which is more typical of historic gas transmission service. As such cycling was no more frequent than daily and the pipelines were constructed in 1947 and this segment was removed from service in about 2006 one can infer the maximum number of service cycles can be taken at about 21540.

Predicted versus Field Response:

For a corrosion-free wrinklebend with an aspect ratio of 0.12 operating in an X52 line pipe steel under cycling at a worst-case pressure ratio taken at 0.8 for this pipeline one obtains a predicted life the order of millions of cycles. If this prediction is reduced by a factor of about 30 to account for pitting according to Figure 18, then the resulting predicted life is still well beyond the anticipated 21540 cycles for the service history experienced by this pipeline. This prediction implies that no evidence of cracking is anticipated on the ID or OD of the sample examined, which was the case for the sample examined. This outcome serves to validate the wrinklebend criteria at least for scenarios like the widespread corrosion evident in Figure 36, and more broadly validate the criteria developed beyond the idealized full-scale testing considered herein.

Discussion – Trends, Field Implications, and A Useful Flowchart

Wrinklebend severity criteria for the effect of pressure cycling have been developed in the form of simple charts and equations that assess wrinkle severity using easily measured dimensions of the wrinkle that serve as a surrogate for strain where cracking will occur first. Because these dimensions can be reasonably determined using high-resolution ILI tools, there is no need to dig wrinklebends in piggable pipelines. The charts and equations developed address differences in pipe grade and size, whether the wrinkle was formed hot or cold, and the boundary conditions on the bend. When uncertain of the grade of the pipe is, or whether the wrinkle was hot or cold formed, or of bend fixity provided by the soil, the worst case scenario should be used. The underlying approach provides a measure of the useful service life based on the field-measured size of the wrinklebend. The useful remaining life follows in this context by subtracting an estimate of the prior service exposure from the total life determined for the bend. Re-inspection intervals can be assessed in reference to the remaining life and the rate at which life is inferred to diminish on yearly basis depending on the wrinkle severity, the service conditions, and the other factors that influence service life.

The presence of corrosion can be simply addressed in reference to this criterion. Where pitting is present on the crown of the wrinkle, the results indicate the service life or re-inspection interval should be decreased by a factor of about 30. Where areal corrosion overlays the crown of the wrinkle, the wrinkle should be reanalyzed considering a pipeline made of this reduced wall thickness, and that life used as the basis for integrity analysis.

The above simple process can be illustrated in regard to Figure 4a, which is used as the reference condition to assess wrinklebend integrity for this illustration. Recall that this figure reflects cold-formed wrinkles made in 12-inch-dimeter X42 line pipe with a wall thickness of 0.283-inch, subject to cycling from 72 to 10 percent of SMYS under conditions where the wrinkle was free to flex. This scenario is represented by the upper trend in Figure 4a. If service involved pressure cycling from 80 percent of SMYS, then part b of the figure is relevant, which applies here and throughout the remainder of this illustration.

If the integrity assessment deals with this same scenario, then the useful service life for a bend is determined by entering the x-axis of Figure 4a at the value of *H/L* measured via ILI or in-the-ditch. Using a quite large value of $H/L = 0.6$ for purposes of this illustration, this value is projected from the x-axis to the upper trend in Figure 4a where it intersects this trend at a life of just 1500 cycles. If the historical records point to 1500 near worst-case cycles from MAOP at 72 percent of SMYS to a minimum pressure corresponding to 10-percent of SMYS, the wrinklebend should be considered for reinforcement in the near term.

Where a wrinklebend was produced in a grade other than X42, the slope (i.e., damage / [H/L]) of the trend for X42 in Figure 4a is adjusted based on the dependence of damage on grade as was shown in Figure 9. Figure 9a indicates that GrB has the lowest slope shown there as 0.348 and so a corresponding longer life than for X42, while X52 and X60 have slopes respectively of 0.692 and 0.897, leading to higher damage than for X42 and correspondingly shorter lives than for X42. Equation 11 provides the analytical equivalent to this chart and the dependence of this slope on grade for those that choose an analytical approach in lieu of the graphical format. Such differences in damage as a function of grade indicate that the band of data for lower H/L values in Figure 33 do not reflect scatter, but rather reflect the dependence of such results on at least grade, as evident from the symbols key.

When considering different sizes of line pipe for which *H/L* is a surrogate for curvature, the effect of pipe geometry develops in reference to *R/t*. Figure 5 indicates that for $R/t \geq 25$ all line pipe exhibits similar "thin-wall" response such that no change is needed to the slope for X42 (damage / [*H/L*]) at $R/t = 21$ in Figure 4a. However, when dealing with stiffer line-pipe sections where $R/t < 25$, this slope must be adjusted in accordance with the results shown in Figure 5a, and the functional expression given for this in Equations 8 and 9. In light of the breakdown in the trend evident with increasing *H/L* apparent in Figure 33, the independence of damage on *R/t* at larger values of *R/t* shown in this figure could change as *H/L* increases beyond about 0.6.

In scenarios where the service loading differs from the near worst-case cycling from 72 to 10 percent of SMYS dealt with for X42 in Figure 4a, the results show the service life increases as the pressure ratio (R_p) decreases. As for geometry and grade, the slope (damage / [*H/L*]) for X42 shown in Figure 4a for this near worst-case cycling can be simply adjusted as a function of R_p. Equation 18 provides the analytical form of this dependence, whereas results for specific pressure histories can be found in the format of Figure 4 in Figure 11. Such analyses deal with situations where the pressure fluctuates between maximum and minimum levels that are more or less historically constant, which is termed "constant amplitude" cycling[3]. In contrast, many

[3] Since the work of Miner[48], much has been written on generalizing constant-amplitude analyses to address variable-amplitude cycling analysis, as for example see Reference 49. This topic is well beyond the scope of the

pipelines experience variable pressure conditions for which Figure 4a must be more broadly interpreted. The utility of the form of Figure 4 and the remainder of the work done for constant-amplitude cycling can be reasonably generalized through use of damage rules, such as that of Miner[48] – provided care is taken to address aspects unique to variable-amplitude pressure histories. In the simplest adaptation of such damage rules, similar pressure cycles otherwise distributed say over a typical year of service would be grouped into "blocks". Damage would then be evaluated for each block of cycles as the ratio of applied cycles at a given pressure to the number of cycles to failure based on the form Figure 4 adjusted for geometry, grade, and the other differences noted above, with the total damage being the sum of these fractions. The remaining life would then be the difference between this sum and unity, which can be used to assess the life in cycles remaining for any other combination of pressure histories. While this process is practically simple, truly complex histories should make use of the results in terms of cyclic stress-strain space – a topic well beyond the present scope.

Where hot-formed wrinklebends must be addressed, the results require that the slope determined for cold-formed bends (damage / [H/L]) shown in Figure 4a be increased by a factor of 2.2. The effect of this multiplier is to significantly increase the damage relative to that for cold-formed bends, as was evident in Figure 29, leading to correspondingly shorter lives. Equations 37 and 38 provide the analytical form of this dependence.

Finally, the effects of corrosion local to the crown of the wrinklebend were addressed relative to the reference case in Figure 4a, with the slope (damage / [H/L]) depending on whether the corrosion was pitting or areal. Where pitting corrosion was present in the crown of the bend, the trends in Figure 18 indicate the service life developed absent corrosion must be reduced by a factor of 30 to account for earlier crack initiation due to the pitting. As this factor applies to the total service life, the implicit assumption is that the corrosion was present since the wrinklebend went into service. This possibly very conservative assumption can be made more realistic for cases where a defensible estimate can be made of the timeline for the breakdown of the coating and onset of the corrosion. In such cases, the total service life is estimated absent the effects of corrosion over the time the coating is intact, with that life reduced based on the fraction of the total life for which the bend likely experienced corrosion.

For areal corrosion the adjustment to the service life absent concern for corrosion, as represented by the results in Figures 21 and 22, depends on the physical size of the corrosion relative to the size of the wrinkle. Equations 28 to 33 characterize this dependence. From these equations and the related FEA it is apparent that as the size of the areal corrosion approaches the scale of pitting the results correctly indicate a reduction in service life – consistent with the above-noted effect of pitting. However, beyond the scale of pitting, the 3D constraint and related local stiffness of the wrinkle discussed in regard to Figure 25 and Equation 34 limit the effect of local stiffness loss due to metal loss in the crown of the wrinkle. The results showed this local constraint limited the effect of areal corrosion until its circumferential extent exceeded an arc of ~22º centered at the crown of bend. For areal corrosion patches whose circumferential extent exceeds this dimension for the pipe diameter of concern (i.e., 22/360 x pipe-circumference), the

---

present project. Where complex service histories are an issue, the constant-amplitude analyses results developed herein be adapted for wrinklebends using the concepts and methods detailed in Reference 49.

service life would be assessed by considering the thickness of the line pipe as the average net-wall thickness in the corrosion. However, any decrease in thickness acts to increase *R/t* such that according to Figure 5 this locally decreased stiffness is not of consequence, except as to lead to leaks or failure as in usual pipeline applications. The limited significance of areal corrosion for wrinklebends integrity is anticipated from basic mechanics, as reduced wall thickness leads to less strain and therefore less fatigue damage, all else being equal.

An important consideration from a field perspective involves the role of boundary conditions. In reference to Figure 26, which reflects bends that lack significant end restraint, care must be taken in field applications because the response of an unrestrained wrinklebend is not typical of bends in service. Summarizing prior discussion in regard to Figure 26 there are two considerations involving boundary conditions. First, a wrinklebend will straighten under end-cap loading, reducing the severity of the as-bent wrinkle. Second, unrestrained wrinkles flex more under the action of cyclic pressure, making the unrestrained "free" boundary condition a worst-case compared to restrained bends. The degree of "fixity" provided by the soil depends on the soil, as well as on the restraint that developed against pipeline movement when the pipeline was first pressurized. Where very little soil compaction was achieved around the pipeline when it was backfilled, it is reasonable to assume that most lines operated at MAOP since their commissioning straightened to the extent possible early in their service. Fortunately, certainty in this aspect is not important as *H/L* comes from current field measurements or ILI results. On this basis, the present results indicate that Figure 4a as adjusted for grade, *R/t*, service cycling, and hot versus cold forming for wrinkles free to flex embeds the worst possible boundary conditions, so this aspect is not a field consideration.

The last consideration relative to the use of Figure 4a as a reference condition involves service life calculated from fatigue resistance developed using polished specimens whereas the surface condition for vintage line pipe steels ranged from mill-scaled through various scraped and wire brushed states depending on the over-the-ditch coating method. As noted in discussing Equations 2 and 3, there is a need to correct for surface finish beginning at lives from ~5,000 to ~20,000 cycles, with a reduction multiplier between 0.1 to 0.01 being viable for typical to most worst-case scenarios.

The flowchart in Figure 37 presents high-level guidance for the use of the wrinklebend integrity criterion, including issues such as surface finish and the appropriate life-reduction factor. Care should be taken to measure *H/L* under conditions that are conservative – which occurs at the lowest typical service pressure. While the lowest pressure might be safest for field digs and related measurements, it might be too low to effectively drive an ILI tool through the pipeline. A balance between these considerations must be sought, ensuring that the ILI tool keeps moving while tending toward the lowest pressure for this purpose. To the extent practically possible, thermal cycling where it is a consideration should be addressed under worst-case conditions, which reflect the lowest temperature in balance with the most flexible boundary conditions such as unfrozen ground as compared to frozen conditions, or soft moist soil as compared to dry hard clay.

Finally, while as noted above it is most likely that wrinklebends straighten under pressure early in their service life, it remains possible that some bends did not fully straighten, or that local soil slip has tended to "close" the bend. Because field digs to monitor bend condition or measure *H/L* where ILI is not feasible will relax soil restraint, opening the ditch at a wrinklebend for this purpose is potentially dangerous. As such, when a wrinkle is fully or even partially exposed care

should be taken to limit the extent of the disturbance, and the size of the hole. In softer soils, work on an adjacent pipeline that occurs near a wrinkle could have the same adverse effect. It is impossible to provide "rules of thumb" for this situation, but it is clear from failure experience and the present analyses that such scenarios require evaluation of soil fixity for the wrinkle, particularly if crews are working around the wrinkle or the wrinkle lies near a populated area.

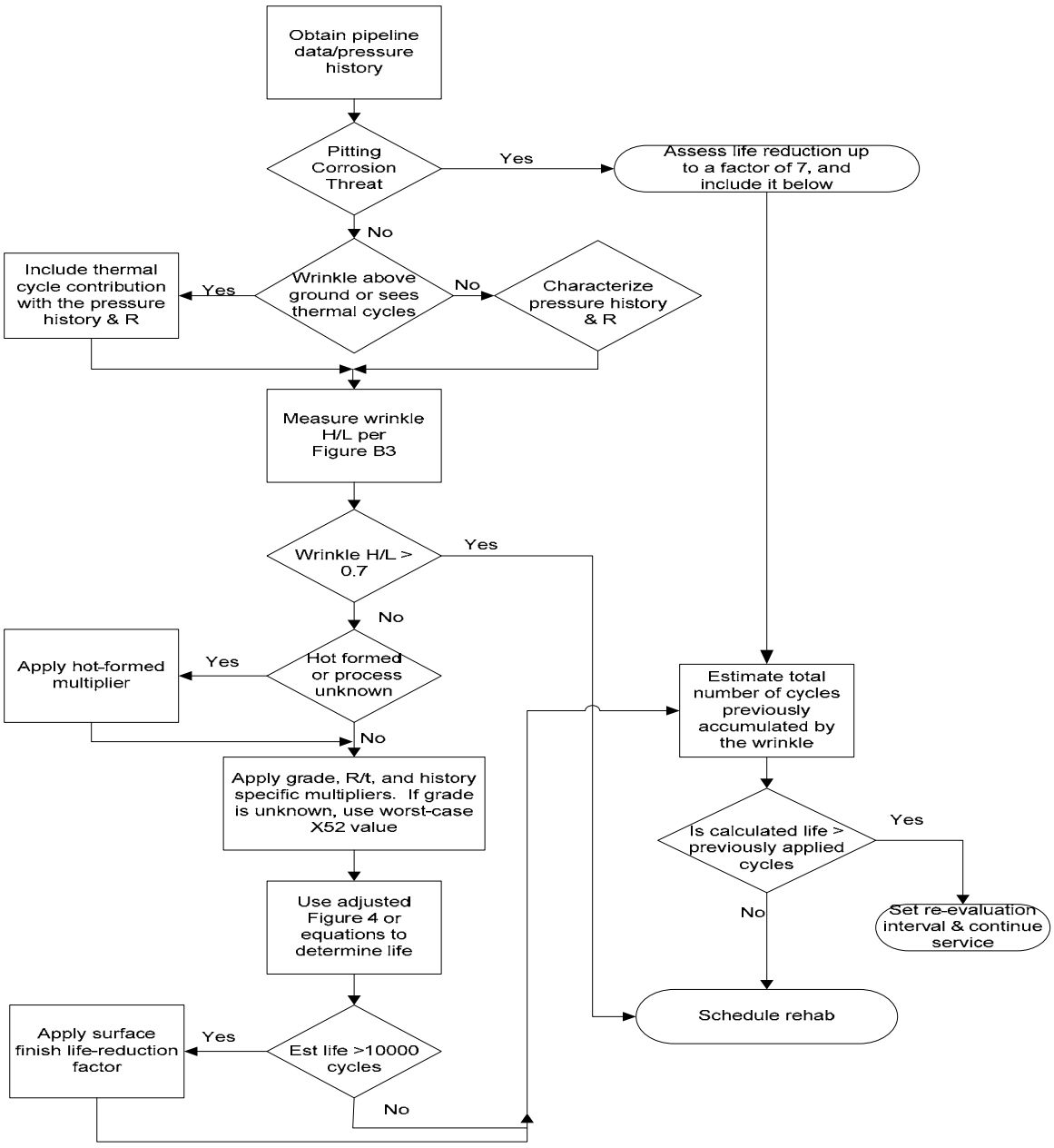

Figure 37. Flowchart for the wrinkle severity criterion (single and multiple wrinkles)

Summary and Conclusions

This report reviewed the evolution of wrinkle-bending practices, and developed technology to help formulate and evaluate integrity management plans for vintage construction that includes these features. This technology has its roots in numerical analysis developed consistent with factors identified as first-order drivers for incidents involving wrinklebends. Appendices were presented that detailed support for such aspects. Factors unique to wrinklebend integrity involve the wrinkle geometry whose severity was characterized by *H/L*, the grade and geometry of the line pipe, the production of the wrinkle as hot-formed or cold-formed, the pipeline's operation, the possible presence of pitting or areal corrosion, and the constraint on the bend provided by the pipeline's fixity in the right-of-way. The role of these factors was assessed in terms of in-line inspection measurements or field digs to determine *H/L*, whereas information on the line pipe and its service should be available from file-data and SCADA or knowledge of demand and pipeline topography. The quality of the product stream, the condition of the pipeline coating, and control of cathodic protection were noted as potentially important factors driving ID and OD corrosion. Criteria were developed to evaluate this data to identify the few wrinkles that could be potentially problematic that might remain in service – that also are located in areas of high consequence. The criteria developed should facilitate identifying wrinkles that merit removal or such consideration, or the use of an operating strategy to mange and avoid future problems.

Criteria were formulated in a manner that addresses a wide range of potential field situations, to avoid excessive conservatism that occurs through use of a one-size-fits-all approach. Criteria meeting this objective were developed and presented in graphical form, as well as analytically for those that might prefer that format. Validation was developed via close correspondence between predictions based on these criteria as compared to full-scale tests on wrinklebends.

Throughout, the emphasis has been topics central to wrinklebend integrity. Significant observations on wrinkle-bending practices and in-service performance include:

- early field practices evolved significantly from the 30s through the 50s – important dates include 1942, when "smooth bending" machines were first used and the early 50s, when track-mounted integral "vertical bending" machines are found in commercial service;
- wrinklebend quality and uniformity varied considerably even when essentially equivalent methods were being applied, which was likely due to several factors including the wide variety of wrinkle-bending methods used, material stability and limited process control when hot bending, and perhaps most importantly quality control imposed by the pipeline contractor and/or operator;
- because wrinklebend practices and quality control varied, some showed uniform wrinkle geometries spaced at regular intervals while others were essentially complex shaped buckles that significantly deformed the local pipe geometry;
- although wrinklebends were phased out in the early 50s, many pipeline systems still contain wrinklebends so it is important to understand failure incidence and their causes – incident experience indicates the rate is dropping, a trend typical of other material and construction related incidents, whereas when incidents have occurred where pressure cycling and local soil stability were major causative factors;
- wrinkle shape and size were indicated to be critical parameters in characterizing wrinklebend integrity, with shape being important because it relates to curvature, which

in turn relates to strain, while parameters defining size – the wrinkle length (pitch) and height (amplitude) of the wrinkle were found to act as surrogates for curvature at the crown (apex) of the wrinkle;

- wrinkle shape assessed via *H/L* is much less demanding of ILI tools than is curvature, such that shape can be detected and quantified through use of appropriate ILI tools, or easily characterized in the field;
- aspect ratio, *H/L*, is defined by the largest height referenced to the adjacent round pipe, divided by the length of the wrinkle, or in asymmetric wrinkles twice the shortest half-length;
- *H/L* is a viable surrogate for curvature for values the order of 0.7 in larger diameter pipelines, but this breakdowns for more severe with little further propagation around the circumference – thus, circumferential extent of a wrinkle is not necessarily an indicator of wrinkle severity;
- strains at and around the crown of the wrinkle increase as pressure increases, with end-fixity (restraint imposed on bends by the soil) being important – suggesting rehabilitation that significantly relaxes the restraint can cause potentially dangerous circumstances;
- cyclic loadings including the effects of pressure and thermal variations is the major causative factor in field failures – corrosion pitting can significantly reduce the serviceable life where it occurs whereas secondary loading due to soil/support stability also can be a factor;

Conclusions drawn in the course of this work relate to the themes of each of the appendices, as well as the focus of the work – wrinklebend integrity assessment. The most significant conclusions include:

- wrinkle shape characterized by *H/L* has been successfully related to fatigue resistance and criteria developed meeting the objective of this project including the effects of grade, line pipe geometry, and service loading;
- consideration has been given to the effect of service at 72-percent of SMYS as well as to cases where the maximum stress could be as high as 80-percent of SMYS, as can occur for some grandfathered lines: depending on the wrinkle's severity and other conditions, operation at the higher stress reduced the service life by as much as a factor of two – all else being equal;
- pitting corrosion can significantly reduce the life of a wrinklebend, with life-reduction indicated possible up to a factor of about thirty;
- the criteria were validated through successful prediction of full-scale pressure cycling of wrinklebends – and through its successful prediction of the response of ripple-bends produced in modern bending machines reported independently;
- the criteria also were validated through successful prediction of a range of wrinklebend scenarios from an in-service guillotine rupture through several wrinkles whose severity covered severe through benign, and included the effects of corrosion based on bends removed from service for a variety of reasons;
- the validated criterion can be implemented using data available from field and in-line measurements to characterize *H/L*, supplemented by file data addressing pipeline design and line pipe properties, wrinkle-bending practices, as well as its construction, operation, and maintenance – where data are uncertain, conservative fallbacks were provided;

- the criteria are simple to use and applicable on a case-specific basis if desired by the user in applications to single wrinkles – multiple wrinkles were independently found to be less severe than otherwise identical single wrinkles; and finally
- the criteria is generic in terms of pressure history – so it can be used for liquid as well as gas pipelines by reference to differences in service. Use of the criteria was illustrated in the discussion section, supported by a high-level flow chart to identify the key steps.

Further Considerations and Recommendations

The basis of the conclusions presented above and the recommendations that follow is empirical, reflecting observations made during the course of this project. As noted above, ID and OD corrosion can reduce the life significantly as compared to scenarios absent the effects of corrosion, particularly if corrosion is present in the form of pitting. In contrast; wall thinning would lead to reduced bending strain for the same local curvature. Little data were available to validate these observations. While the predicted significance of ID and OD corrosion has validated by successful prediction of field results, the available data were limited such that care should be taken when applying these criteria to field scenarios. This work also has established that constraint applied locally to the wrinkle, as well as globally to the bend, can be important factors affecting wrinklebend integrity. Because little data exist to validate the results in the context of these factors, further work should be considered to better quantify their practical significance, and to validate the results of this project.

References

1. Anon., Code of Federal Regulations, Title 49 -Transportation, Part 195.
2. Anon., Code of Federal Regulations, Title 49 -Transportation, Part 192.
3. Anon., "Managing System Integrity for Hazardous Liquid Lines", 1st Ed., API Standard 1160-2001, November 2001.
4. B31.8S Anon., ASME Code Supplement on Integrity Management for Pressure Piping, B31.8S, Revision 1, 2002.
5. Seeley F. B. and Smith, J. O., Advanced Mechanics of Materials, Wiley, 1967.
6. Chambers, A. A.; Private communications to G. A. Reinhardt regarding the construction characteristics of Youngstown Sheet & Tube line pipe versus A.O. Smith pipe, Youngstown Sheet & Tube Company, 1931 – Report 29, dated April 1931, and Reports 34 and 36, dated August 1931.
7. Bell, H. C., "Current Trends in the Multi-Flame Welding and Wrinkle Bending of Overland Pipe Lines, Proceedings of the Pacific Coast Gas Association, Vol. 30, p.94-96, 1939.
8. Stephens, M. M. Natural Gas Engineering - Volume III, State College, Pennsylvania, 1939, pp. 189, 190
9. Anon; S. R. Dresser Manufacturing Company General Catalog No. 36, Dresser Pipe Couplings, 1936.
10. Richardson, F. E.; "Modern Gas Pipe Line Construction Methods Including Short Comment on Specifications and Inspection", Proceedings-Natural Gas Department of the American Gas Association, May, 1949.
11. Wilder, A. B. and Aebersold, A. F.; "Pipeline Steels", *Mechanical Engineering*, ASME, May, 1957, pp 448-453.
12. Anon., "Panhandle Lines", Panhandle monthly employee publication, June 1964, Volume 21, No. 11, Kansas City, Mo
13. Terrell, C. E.; "Features Associated with a 14" Gas Transmission Line Designed to Operate at 1200 Pounds Pressure", Proceedings, Natural Gas Section of the American Gas Association, May, 1942.
14. Anon., Advertisement in *Pipe Line News*,
15. Quaries, W. R., "Isolated Location Adds to Contractors' Woes on Four Corners Pipeline System", *Pipe Line News*, January 1958, pp. 24-29.
16. Binckley, M. J.; "Which Bending Method", *Gas*, May 1952, pp 122-125.
17. Leis, B. N. and Lahrman, D. F., "Failure Analysis of Rupture at 4518+23", February 1996, proprietary to client.
18. Leis, B. N. et al, "Investigation of Pipeline Failure Near Peculiar Missouri", May 2001, proprietary to client.
19. Leis, B. N., Appendix VII to "Hydrostatic Testing Of Transmission Pipelines: When It Is Beneficial and Alternatives When It Is Not", PRCI Report PR-3-9523, Pipeline Research Council International, 2001.
20. Anon., Federal Power Commission Incident Database, 1950-65
21. Jones, D. J., Kramer, G. S. Kramer, Gideon, D. N. and Eiber, R. J. "An Analysis of Reportable Incidents for Natural Gas Transmission and Gathering Lines 1970 through 1984," NG-18 Report 158, March 1986.
22. Kiefner, J. F., Mesloh, R. E., Kiefner, B. A.; " Analysis of DOT Reportable Incidents For Gas Transmission and Gathering System Pipelines, 1985-1997", PRCI, PR-218-9801, 1999.

23. Leis, B. N., Chang, O. C., and Bubenik, T. A., "Leak versus Rupture Considerations for Steel Low-Stress Pipelines," GRI Report-00/0232, January 2001.
24. Leis, B. N., Zhu, X.-K., and Clark, E. B., "Criteria to Assess Wrinklebend Severity for Use in Pipeline Integrity Management," Project Report PR-003-03112, PRCI Catalog L52190, August 2004.
25. Olson, R. J., "Evaluation of the Structural Integrity of Cold Field-Bent Line Pipe, PRCI Report PR-3-9214, May 1996: see also Olson, R., Clark, T., and Odom, T., "Evaluation of the Structural Integrity of Cold Field Bent Line Pipe", 10th Biennial Joint Technical Meeting on Line Pipe Research, EPRG/PRC, Paper 6, April 1995, Cambridge
26. Becht, C., "B31.3 Appendix X Rules for Expansion Joints," *J. of Press. Vessel Technology*, ASME, Vol. 117, August 1995, pp. 283-288.
27. Morrow, J. D., Wetzel, R. M., and Topper, T. H., "Laboratory Simulation of Structural Fatigue Behavior," Effects of Environment and Complex Load History on Fatigue Life, ASTM STP 462, American Society for Testing and Materials, 1970, pp. 74-91.
28. Leis, B. N., "An Approach for Fatigue Crack Initiation Life Prediction with Applications to Complex Components", in Fatigue Life of Structures under Operational Loads, Proceedings of the 9th International Committee on Aeronautical Fatigue Meeting, ICAF Doc. 960, Laboratorium fur Betriebsfestigeit, Germany, May 1977, pp. 3.4/1-47.
29. Skeleton, R. P., "Application of Small Specimen Crack Growth Data to Engineering Components at High Temperature: A Review", ASTM STP 942: Low-Cycle Fatigue, H D Solomon, G R Halford, L R Kaisand, and B N Leis, editors, 1988, pp. 209-235.
30. Leis, B. N., Gowda, C. V .B., and Topper, T. H., "Cyclic Inelastic Deformation and the Fatigue Notch Factor", Cyclic Stress Strain Behavior-Analysis, Experimentation and Failure Prediction, ASTM STP 519, 1973, pp. 133-150.
31. Mendleson, A., Plasticity: Theory and Application, MacMillian, 1968: see also Memdleson, A. and Manson, S. S., "Practical Solution of Plasticity Problems in the Elastic-Inelastic Range", NASA TR-R28, 1957.
32. Williams, D. P., Lind, N. C., Conle, A., Topper, T. H., and Leis, B. N., "Structural Cyclic Deformation Response Modeling", Mechanics in Engineering, American Society of Civil Engineers / Engineering Mechanics Division, SMD No. 11, University of Waterloo Press, May 1976, pp 291 - 311.
33. Deiter, G. E., Mechanical Metallurgy, Third edition, McGraw-Hill, 1986.
34. Leis, B. N. and Kilinski, T. J., "Mechanical and Fracture Properties Essential in Integrity Management of Steel Transmission Pipelines," Final Report PR-3-9737, PRCI Cat. No. L51845, December 2000.
35. Chouchaoui, B.A., Pick, R.J., and Yost, D.B., "Burst Predictions of Line Pipe Containing Single Corrosion Pits Using The Finite Element Method," ASME OMAE Conf., OMAE-92-1042, 1992.
36. Leis, B. N., "An Energy-Based Fatigue and Creep-Fatigue Damage Parameter", *Journal of Pressure Vessel Technology*, Trans. ASME, Vol. 99, No. 4, November, 1977, pp. 524-533.
37. Smith, K.N., Watson, P. and Topper, T.H., "A Stress-Strain Function for the Fatigue of Metal," *Journal of Materials*, Vol. 5, pp. 767-778, 1970.
38. Leis, B. N., "Effect of Surface Condition and Processing on Fatigue Performance," ASM Handbook, Vol. 19, ASM International, 1996, pp. 314-320.
39. Novack, S. R., "Corrosion-Fatigue Crack Initiation Behavior of Four Structural Steels", in Corrosion Fatigue, T. W. Crooker and B. N. Leis editors, ASTM STP 801, 1983, pp. 26-63.

40. Dowling, N.E., "Mechanical Behavior of Materials: Engineering Methods for Deformation, Fracture and Fatigue," Second edition, Prentice Hall, New Jersey, 1999.
41. Murray, N. W. and Bilston, P., "Elasto-Plastic and Strain-Hardening Bending of Thin Steel Pipes in the Pre-Buckling Region," *The Institution of Engineers*, Paper C 91043, September 1991.
42. Murray, N. W. and Bilston, P., "Local Buckling of Thin-Walled Pipes being Bent in the Plastic Range," *Thin-Walled Structures*, 1992, p. 411-434.
43. Murray, N. W., "Stress Analyses of Wrinkle Bends in Pipelines," *Thin-Walled Structures*, 1993, p. 65-80.
44. Murray, D. W., "Local Buckling, Strain Localization, Wrinkling and Postbuckling Response of Line Pipe," *Engineering Structures*, Vol. 19, No. 5, pp. 360-371, 1997: see also Souza, L. T., and Murray, D. W., "Analysis for Wrinkling Behavior of Girth-Welded Line Pipe, *Journal of Offshore Mechanics and Arctic Engineering*, Vol. 53-61, 1999.
45. Zhou, Z. and Murray, D. W., "Numerical Structural Analysis of Buried Pipelines", Civil Engineering Structural Engineering Report No. 181, Chapters 7 and 8, University of Alberta, February 1993: see also Zhou, Z. and Murray, D. W., "Analysis of Post-Buckling Behavior of Line Pipe Subjected to Combined Loads, *International Journal of Solids and Structures*, Vol. 32, pp. 3015-3036, 1995.
46. Mohareb, M. et al, "Laboratory Testing of Line Pipe to Determine Deformation Behavior", ASME-OMAE, Volume 5, Glasgow, 1993, pp. 109-114: see also Mohareb, M., Kulak, G. L., Elwi, A., and Murray, D. W., "Testing and Analysis of Steel Pipe Segments, *Journal of Transportation Engineering*, Vol. 127: 408-417, 2001.
47. Zhou, Z. and Murray, D. W., "Behavior of Buried Pipelines Subjected to imposed Deformations", ASME-OMAE, Volume 5, Glasgow, 1993, pp. 115-122.
48. Miner, M. A., "Cumulative Damage in Fatigue," J. Appl. Mech., Vol. 12, 1945, pp. A159.
49. Fatigue Design Handbook, Second Edition, Society of Automotive Engineers, R. C. Rice, B. N. Leis, and D. V. Nelson, Editors, 1989.

Appendices

This section contains details the history of pipe and wrinklebends, aspects of the literature review relevant to wrinklebend integrity, failure experience for wrinklebends, the published literature, relevant codes worldwide, fundamental theories and models used in the numerical analyses that underlie the criteria developed. Seven appendices are included as follows:

- Appendix A – Historical Aspects of Wrinkle-Bending
- Appendix B – Archival Results from Field Studies and In-Service Failures
- Appendix C – Failure Experience with Wrinklebends
- Appendix D – Codes, Standards, and Regulations
- Appendix E – Literature on Wrinkles, Buckles, and Dents
- Appendix F – Mechanics Theories, Models, and Results
- Appendix G – Effective Plastic Hardening Models and Fatigue Damage Parameters

References cited in the body of the report are numerous, with many new references appearing in the appendices. For this reason it is convenient to adopt a numbering system with a letter-prefix to the reference number corresponding to the letter-label for the appendix. Where footnotes are used they are numbered independently from the body of the report and again use a letter-prefix. Likewise, figures and tables are labeled with a letter prefix corresponding to each appendix to the number of the figure or table. In contrast, the equations in the appendices, which occur specifically in Appendices F and G, are numbered consecutively and given the prefix A to distinguish them from those appearing in the text of the report.

Appendix A – Historical Aspects of Wrinkle-Bending

Two different practices can be used to make bends. Either the pipe is permanently stretched along the extrados, which is its largest radius – or the pipe is permanently compressed or foreshortened along the intrados, which is its smallest radius. In the first scenario, the, bend is made by stretching and thinning the pipe's wall on the tensile side of the bend. This would require supporting the pipe's shape through use of dies and mandrels enforce the stretching and avoid collapse of the cross-section. In the second case, the bend can be made by compressing and thickening of the pipe wall on the compression side of the bend, while again maintaining the pipe's shape through use of dies and mandrels. Alternatively, small buckles can be introduced to foreshorten the pipe[4]. Obviously, combinations of these scenarios also could be used.

The term "wrinklebend" has been used historically by the pipeline industry to describe bends made by intentionally creating local buckles in the line pipe. Such bends reflect the last of the above-noted schemes – as wrinklebends involve small buckles intentionally introduced to create an intrados. The formation of buckles is strongly dependent on unsupported length and thickness, as well as the presence of imperfections, as these variables are central to buckling theory(1). For this reason, pipe parameters like wall thickness, pipe diameter, and their ratio are likely significant in the formation of bends made via buckles that cause foreshortening.

In many applications the term buckle was used in reference to a significant change in shape due to instability associated with only a small increase in load(1). In contrast to this situation, the buckles that formed the intrados of wrinklebends were localized. Engineers historically used terms like cripple or wrinkle to describe a such local instabilities(1), suggesting one possible origin for the term wrinklebend.

Because mechanical couplings provided for a change in pipeline direction by up to four degrees, wrinklebends were neither necessary nor popular in early construction until welding became the preferred means to join line pipe. Thus, early use of the term in applications to larger-diameter pipeline construction dates to about the 30s, and earlier for smaller diameter line pipe. Schemes to make wrinklebends in larger-diameter pipelines were documented in some detail during the construction season of 1931 by Mr. Alfred Chambers. He made visits to various construction spreads from the east coast through the mid-west as far as Kansas. Mr. Chambers' observations were made while traveling on behalf of his employer, Youngstown Sheet and Tube. Letter reports(e.g., see 2) documenting his observations, which include some excellent photographs, eventually became the property of one of the authors (EBC) during his employment by Columbia Gas Transmission Company. Similar documentation has been assembled for construction on the west coast by Mr. Bill Amend, while working for Southern California Gas Company(e.g., see 3). Vintage bending practices of that era also can be found occasionally in books on pipelines, one example being Reference 4. This section draws heavily on these resources, and those of Battelle's library archives, which includes Pipe Line News and the Oil and Gas Journal, and

---

[4] One essential difference between formed bends used in transmission pipelines and the process industry lies in the way they are made. Stretching and thinning apparently is the preferred practice for process/plant piping. Permanently stretching the tension side, likely in combination with compression on the opposite side of the neutral plane, appears to underlie early results achieved with modern bending machines. As pipe strength increased and wall thickness decreased, it appears ripple formation occurred for modern machine-bent pipe, meaning such bends also capitalize on foreshortening the intrados.

other such industry magazines.

Background – History of Pipe Bending

From the beginning of pipeline construction, some method of accommodating necessary direction changes has been a pipeline construction requirement. Different methods have been used on early pipelines such as miter bends, bends produced by pipe manufacturers, angled couplings, and wrinklebends.

Dresser couplings were first used in 1890 and rapidly adopted for pipeline construction. A 1936 Dresser Manufacturing Company catalog[5] describes the applications and uses of their couplings including products for pipeline direction changes. Based on the information provided in the catalog, a straight Dresser coupling could accommodate a deflection of up to 4 degrees. Dresser also manufactured several versions of angled couplings that were made from mitered pipe welds and wrinkle bent pipe. These are illustrated in Figure A1. The catalog also illustrated application of Dresser couplings on a "plain end cast iron bend" in a 48-inch outside diameter (OD) gas distribution pipeline constructed from cast iron pipe. This indicates cast iron bends were being produced and joined with mechanical couplings to accommodate pipeline direction changes in the 1930's and probably earlier[5], although he pressures involved were much less than those for transmission pipelines

Bends produced by line pipe manufacturers were also being applied in the 1930's and probably earlier. For instance, A. O. Smith was providing bends for use with their pipe in the early 1930's. Pipe manufacturer produced bends were used by shaping the ditch profile to accommodate the available bend angles[2,6].

The timeframe when wrinklebends began use for pipeline construction is not well defined. The literature indicates wrinklebends has been known since about 1910-1915. However, wrinkle-bending practices likely were not widely applied for pipeline construction prior to the 1920's when larger diameter, thin wall pipeline construction began. In any case, the earliest use of wrinkle-bending practices could not have come before line pipe began being constructed from steels with sufficient ductility to tolerate the localized deformation that can occur with this bending practice. Such steels began to appear in 1887 with the production of furnace butt weld and lap welded pipe made from Bessemer steel[3,6,7].

In the 1920's, some concern existed regarding "ordinary" (undefined) bending techniques in use at the time. This concern was reportedly based on test results that indicated such bending practices were not suitable for large diameter, thin wall pipe. During this period, debate was ongoing concerning the continued use of mechanical couplings and welded joints. Because direction changes could be achieved with mechanical couplings, other methods were needed for welded pipelines. Thus, as implied earlier, the first widespread use of wrinkle-bending practices likely came with the advent of continuously welded pipelines. As construction of some early 30s cross-country larger-diameter pipelines was still coupling welded-double-joint segments[8], one can conclude the transition to all-weld construction followed this period. While this early 30s construction relied on couplings, use also was made of wrinklebends, so it is clear from Reference 8 as well as References 2-4 that such practices were in common use by the early 30s. While the microstructure of such bends implies they were cold formed[9], pipeline contractors also began using various "fire bending" methods[2], the term used to describe hot wrinklebend practices as discussed later.

Wrinkle-Bending Practices – The 30s and Earlier

Like many pipeline construction practices, wrinkle-bending evolved from various hot and cold bending practices to today's cold-bending machines. Such machines, equipped with smooth shoes and internal mandrels, produce smooth bends with little distortion of the pipe, as will become evident later this section. Hot wrinkle-bending was utilized initially, apparently because the process could be easily applied using different methods in the field with a minimum of extra equipment at low cost. Hot bending could also be applied near the ditch thereby minimizing moving pipe to another location for bending. Cold wrinklebends also were produced using a variety of methods, although because greater force was needed these practices relied on special fixtures or field fabricated frames, often with the bending force provided by heavy construction equipment such as tractors or side booms. Other reasons for preferring hot wrinklebends were that no wall thinning occurred at the bend extrados and additional stress was not introduced since bending was performed after heating the pipe. Another factor was that if the pipe was bent too much, it could be corrected by re-heating and reverse bending the pipe.

A wrinklebend consists of one or more individual wrinkles, the number depending on the total bend angle required, with as many as wrinkles observed to make one bend in the author's experience. Typically, each wrinkle created a bend angle that ranged from about 1 to 2 degrees. Occasionally, one wrinkle in a multiple wrinklebend was more severe indicating that the bending personnel were attempting to complete the total required bend angle.

Wrinkle-bending methods were applied to pipe diameters from 4 inch to over 30 inch with a range of wall thickness to make shop and field fabricated side bends and sag bends (over bends). Shop fabricated wrinklebends were also referred to as "creased bends". Accounts of various wrinkle-bending practices have circulated for years, some being documented to various degrees, others not. This section documents methods that can be quantified in reference to archives, but as it is unlikely all such methods will ever be known this section falls short of characterizing all such practices. Those that are presented provide some insight as to the in-service performance of wrinklebends and helps understand the method(s) needed to assess their integrity.

The following descriptions reflect hot and cold wrinkle-bending processes that were used during construction of a 20 inch OD pipeline in 1931[(2)]. They are based on observations made by a pipe manufacturer's employee tasked with characterizing pipeline construction and evaluating line-pipe related issues. Similar to the scenario for the cross-country pipeline discussed in Reference 10, the joining methods used included welding and mechanical joints. The welding practices included oxy-acetylene and SMA (i.e., "stick electrode"), both with backing rings.

Observations of four wrinkle-bending practices used on this project follow:

- Where over-bends of up to 2-3 degrees were required or a previously bent pipe did not properly conform to the ditch, a hot bend was made in the ditch. A fire was built on the pipe at the bending point. When the pipe became hot enough, either it sagged under its own weight or the construction personnel walked stood on the pipe to provide additional bending force.
- Hot wrinklebends intended to be greater than 3 degrees were made by supporting the pipe on skids, building a fire under and around the pipe, with the pipe sagging under its own weight. A variation of this practice supported the pipe over the ditch using the cable from a side-boom tractor. The bend produced using this variation is shown in Figure A2.

- Hot and cold wrinklebends were also produced using a saddle between the pipe to be bent and another pipe section. The bending force in this scheme is developed by a block and tackle arrangement. Such bends were made beside the ditch initially.
- Cold wrinkle-bending was done using a weld-fabricated frame that provided two round supports conforming to the pipe surface. This frame is illustrated in Figure A3, with a typical result of its use apparent in the background of this figure. This saddle was placed over the pipe in the bottom of the ditch. Wood ties were then stacked high enough to reach ground level at either end as needed, with a tractor driven over the ties to anchor the pipe. The bending force was applied by a side boom tractor that pulled up on the on the pipe.

Reference 4 also shows a photograph depicting such practices. Depending on the location and orientation of the bending couple, all of the above schemes could produce both sag-bends and over-bends. Some practices were implemented in the ditch with one of the pipe being bent already welded to the string in the ditch. Others practices were applied to individual pipe joints in work done nearby the ditch.

Hot wrinklebends made outside of the ditch were sometimes water quenched at the intrados to minimize the local instability and control the severity of wrinkles produced. It was noted that construction supervision expressed some concern regarding wall thinning at the bend extrados during hot wrinkle-bending. The possibility of embrittlement in areas where the water quench was applied also was noted. It was noted that the hot and cold wrinkle-bending practices used on this pipeline project result in considerable wrinkling and pipe deformation[(2)].

During 1931, Mr. Chambers also visited a 26-inch pipeline constructed for another pipeline operator. Both hot and cold wrinklebends were being made to complete this pipeline[(2)]. Practices used to make these bends included:

- Hot wrinklebends were made with bending fixture consisting of a straight pipe section ("strong-back") with another short pipe section placed perpendicular. This fixture is shown in Figure A4. Both ends of the short pipe section were shaped to form a "saddle" that sat on either end against the strong-back and pipe to be bent. This stub pipe served as the bend fulcrum. The pipe section to be bent was aligned on the saddle, which was anchored to the strong-back. Bending force was applied by a block and tackle at one end, while cables wrapped around the strong-back and the pipe being bent at the opposite end reacted this force. The cable and block and tackle used to apply the bending load also are evident in Figure A4. Heating was accomplished here with oil burners that were aimed at a "heat shield" located at the outside of the bend that was designed to distribute the heat, as shown in Figure A5. Once the desired heating was achieved, force was applied through block and tackle to produce the bend. The process was repeated by stepping the fixture down the pipe as necessary to produce the total required bend angle. A bend typical of the results produced using this practice is shown in Figure A6.
- Cold wrinklebends were made using a field fabricated frame that sat on the top half of the pipe similar to the method used on the 20-inch project discussed above.

Again, depending on the location and orientation of the bending couple, all of the above schemes could produce both sag-bends and over-bends. In contrast to the comments for the above-discussed 20-inch diameter project, it was noted that the wrinklebends produced on this project

were essentially smooth and did not exhibit extreme deformation observed for the 20-inch pipeline. Thus, differences in implementing otherwise comparable bending practices can lead to significant differences in the nature of the bend, for construction done during the same timeframe. It follows that the quality of a wrinklebends depends more on the crew that makes it than it does on the specific practice used, or the era in which it was made. Such is likely the case for continued use of practices discussed above, which for this discussion reflects major construction projects in the early 30s, implying they were likely practiced earlier.

- Other processes used to make hot wrinklebends beginning in the 1930's include:[11]
- Pipe was placed on skids in the bottom of the ditch. The top of the pipe was heated with torches, rolled so the heated area was at the bottom, and the skids on one end were removed. The pipe sagged under its own weight or additional loading was applied by the bending crew. A maximum bend angle of 5 to 7 degrees per wrinkle was considered acceptable. This process was used for small diameter pipe.
- Another practice relied on an "A-frame" fixture to impose the bending couple. One end of the frame was anchored to the pipe with a cable. After heating, the bending couple was created with a block and tackle loading at the opposite end. Figure A7 illustrates one A-frame bending fixture as implemented using the ground to support the frame, and the deadweight of the components to keep it stable. Figure A8 shows a wrinklebend typical of that produced with this scheme. It was stated that for "the usual low carbon pipe", the bend could be effectively arrested by water quenching at any time during the bending process, however, water quenching was not recommended for "high carbon pipe". It also was stated that heating should be concentrated 180 degrees from the longitudinal weld seam.
- A tractor equipped with a "stiff leg" was driven on top of skids surrounding the pipe to be bent. The pipe was heated and bending force was applied with block and tackle between the stiff leg and the pipe. This too utilizes A-frame loading to create the bending couple, except for this practice the A-frame is in the vertical plane and stability apparently develops via the shape of the shoe at the bottom of the stiff leg.

Wrinkle-bending into and Beyond the 40s – Advent of Early Bending Machines

Variations of the above-noted practices developed and no doubt other schemes that were less sophisticated existed, based on undocumented comments made by long-retired construction foremen and hands. As documentation is lacking, it is difficult to comment on what might have been the precursors to 20s practices that evolved into the above discussed schemes used on major early 30s construction projects. Documented examples do exist to illustrate evolution of the 30s practices. For example, one variant was used make cold wrinklebends. Described in reference to its use on a 14-inch pipeline constructed in 1941[11], this variation used a "bending block" that covered the top half of the pipe. The bending block is reminiscent of the fabricated fixture in Figure A3, except the fabrication is replaced by a block. As for the fabrication, the block was sat on the pipe after which a tractor was driven over the block as the reaction to an upward force created by a tractor with a side boom, which produced the bending couple. Reportedly, this practice produced bends without "any buckling or wrinkling". While Reference 12 is brief, it describes a contoured bending block that apparently was similar to external bending shoes that are still used when bending small diameter pipe. In turn, such shoes are the precursor to the saddles used in modern bending machines. Another variation of this 30s scheme is evident in

Figure A9, which is reproduced from an early 50s Pipeline News magazine[12]. The stiff leg described above in reference to the 30s and early 40s is evident here along with a bending block and a system of cabling to create a vertical A frame. The evolution through the 50s appears to be significant, as by the late 50s there is evidence of track-mounted integral "vertical bending" machines[13]. Figures A10a and A10b shown equipment circa 1955 through 1958, which can be seen to share some traits of the more refined and powerful equipment in use today.

The references cited above and experience of the author's evaluating pipeline wrinklebends is consistent – wrinklebend quality and uniformity varied considerably even when essentially equivalent methods were being applied. Very likely this was due to several factors. One was the wide variety of wrinkle-bending methods apparently used. Another was probably related to material stability and minimal process control especially when hot bending was performed. However, one of the major factors was the bending quality control imposed by the pipeline contractor and/or operator. Some wrinklebends exhibited uniform wrinkle geometries spaced at regular intervals while others were essentially complex shaped buckles that significantly deformed the local pipe geometry. Other hot and cold bends produced by a wrinkle-bending process have nearly smooth intrados without any significant pipe deformation[2].

The evolution of hot and cold wrinklebend practices into today's modern bending machines took a significant step ~1942, when "smooth bending" machines were used first, on the War Emergency pipelines. Broader use of smooth bending machines continued through the 1940's. But because the shift to new technology occurs gradually, wrinklebends continued in use into the early 50s. At that time, wrinkle-bending was still considered viable by some, whereas others were raising integrity concerns[e.g., see 11].

Critical Assessment of Wrinkle-bending Practices – Circa Early 50s

The early 50s saw discussion of historical wrinkle-bending practices and concern for the integrity of such practices – presumably spurred by the availability of alternative practices and the commercial appearance of equipment designed to make consistent bends.

Concerns stated in the early 50s relative to hot wrinklebends included[11]:

- Difficulty achieving the proper heating on large diameter pipe, particularly where inclement weather conditions exist,
- The effect of heating on the strength of the steel, particularly in cases where the pipe was mechanically expanded during manufacture, and
- The geometric discontinuity produced by the wrinkle introduced a "stress concentration" that would be undesirable in pipelines experiencing frequent or large pressure cycles.

Reference 16 stated that developing a cold wrinkle-bending machine was the "first important step" in developing a method that would replace hot wrinklebends. This discussion indicated wrinkle-bending machines equipped with segmented bending shoes that permit forming uniform wrinkles whose height could be controlled by the operator was desirable. Use of cold-formed wrinkle was preferred as this practice could be performed during all weather conditions.

Stated disadvantages of cold wrinkle-bending included[13]:

- Introduces cold work that could create future problems, particularly in the wrinkled area,
- Introduces a stress raiser, a concern similar to that expressed for hot wrinkle-bent pipe in

reference to the effects of pressure fluctuations,

- Cracking might occur if the pipe longitudinal weld seam was within the wrinkled section of the pipe,
- The space needed to accommodate the larger machines required for cold-forming could complicate this practice where the work area could not support the weight of bending machines, and where right-of-way (RoW) space limitations preclude its use, and
- External bending equipment can damage mill-coated pipe.

Eventually, such concerns limited use of wrinkle-bent pipe, with a timeline both for their introduction and the eventual end of their use on the timeline suggested in Figure A11 based on the present review. This timeline reflects information assembled from the references cited and the author's experience. The dashed sections of the timelines indicate periods of uncertainty, and transitions related to declining or initial usage.

Summary

Photographs and articles indicate wrinklebend practices evolved to use mechanical advantage in various forms ranging from deadweight, to "come-along" leverage, through hydraulic power. Because the amount of force is less if the pipe steel is made more compliant by heating prior to bending, wrinkles were often made hot. Based on methods of heating and other factors such as heat input versus dissipation, it appears that metal temperatures for hot-formed wrinklebends were the order of 1000 ºF, but could have reached 1200 ºF or higher. Given the scope of heating methods known, a steep temperature gradient likely developed around and along the pipe, while through-wall temperature was likely uniform. On this basis, grain coarsening occurred local to hot-formed wrinkles, as did shallow decarburization, which is confirmed by results in Battelle archives and data available from the industry.

From the photographs and other documents, it appears that early practices made wrinklebends beside the ditch, while other practices were employed in the ditch. Regardless of where the practice was implemented, all wrinklebend schemes were "force-controlled". This meant that energy stored in cables or other flexible components was available to continue the bend, which made it difficult to limit localized deformation with the onset of wrinkling. The information assembled indicates that with practice and ingenuity, coupled with mandrels and other shaped reinforcement or load spreading, smooth wrinklebends could consistently produced. Repeatable quality is evident in some quite early construction in bends comprising multiple smooth wrinkles about a diameter apart, all with similar shape. While some methods and contractors produced smooth repeatable wrinkles, others did not. On this basis, it was concluded that wrinklebend consistency and quality reflect the contractor or a crew more than they did the period of construction. With the advent of commercial bending machines, which began to appear in the 50s[5] it became easier to ensure quality cold bends typical of and the consistent smooth ripples produced with modern pipe-bending equipment.

Trending of wrinklebend incident data indicates the frequency of wrinklebend related problems

[5] Bending machines continue to evolve to deal with larger-diameter, heavier wall pipe made of high-strength grades. This evolution appears to be demand driven, as is usual in any industry.

has been low in comparison to other threats to pipeline integrity, and continues to diminish as time passes. However, recent modification of 49 CFR 192 to include integrity management provisions indicates the need to assess threats to pipeline integrity. On this basis, wrinklebend performance will require consideration in the integrity management plans of operators whose vintage systems include such features.

References

1. Seeley F. B. and Smith, J. O., Advanced Mechanics of Materials, Wiley, 1967.
2. Chambers, A. A.; Private communications to G. A. Reinhardt regarding the construction characteristics of Youngstown Sheet & Tube line pipe versus A.O. Smith pipe, Youngstown Sheet & Tube Company, 1931 – Report 29, dated April 1931, and Reports 34 and 36, dated August 1931.
3. Bell, H. C., "Current Trends in the Multi-Flame Welding and Wrinkle Bending of Overland Pipe Lines, Proceedings of the Pacific Coast Gas Association, Vol. 30, p.94-96, 1939.
4. Stephens, M. M. Natural Gas Engineering - Volume III, State College, Pennsylvania, 1939, pp. 189, 190
5. Anon; S. R. Dresser Manufacturing Company General Catalog No. 36, Dresser Pipe Couplings, 1936.
6. Richardson, F. E.; "Modern Gas Pipe Line Construction Methods Including Short Comment on Specifications and Inspection", Proceedings-Natural Gas Department of the American Gas Association, May, 1949.
7. Wilder, A. B. and Aebersold, A. F.; "Pipeline Steels", *Mechanical Engineering*, ASME, May, 1957, pp 448-453.
8. Anon., "Panhandle Lines", Panhandle monthly employee publication, June 1964, Volume 21, No. 11, Kansas City, Mo
9. Leis, B. N. et al, "Investigation of Pipeline Failure Near Peculiar Missouri", May 2001, proprietary to client.
10. Quaries, W. R., "Isolated Location Adds to Contractors' Woes on Four Corners Pipeline System", *Pipe Line News*, January 1958, pp. 24-29.
11. Terrell, C. E.; "Features Associated with a 14" Gas Transmission Line Designed to Operate at 1200 Pounds Pressure", Proceedings, Natural Gas Section of the American Gas Association, May, 1942.
12. Anon., Advertisement in *Pipe Line News*,
13. Binckley, M. J.; "Which Bending Method", *Gas*, May 1952, pp 122-125.

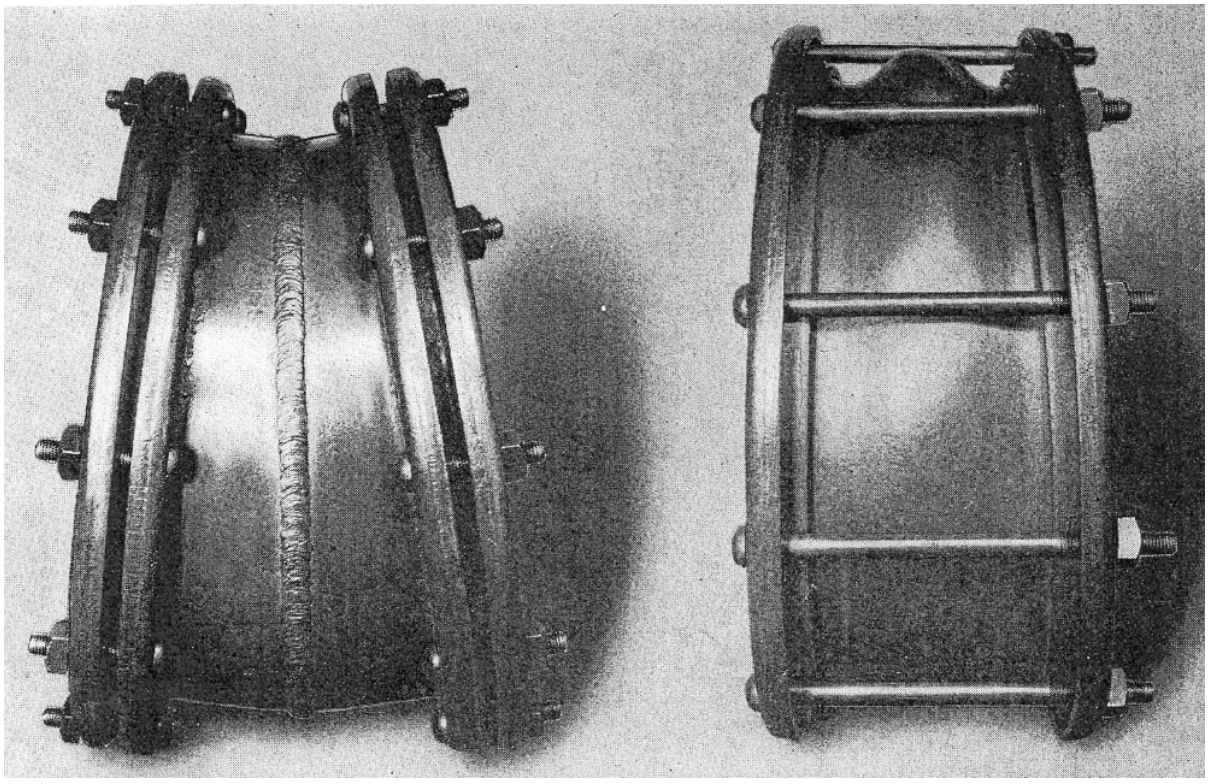

a) fabrication **b) coupled wrinklebend**

Figure A1. Dresser Angled Couplings (circa 1936, for 18-inch (457-mm) line pipe

Figure A2. Wrinkle made hot over a machined ditch by dead-weight sag method – inset view shows some significant local distortion develops in the cross-section (circa 1930s)

Figure A3. Fabricated frame used as fulcrum in making cold wrinkle-bends (circa 1930s) – view in background shows a wrinkle so produced being inspected

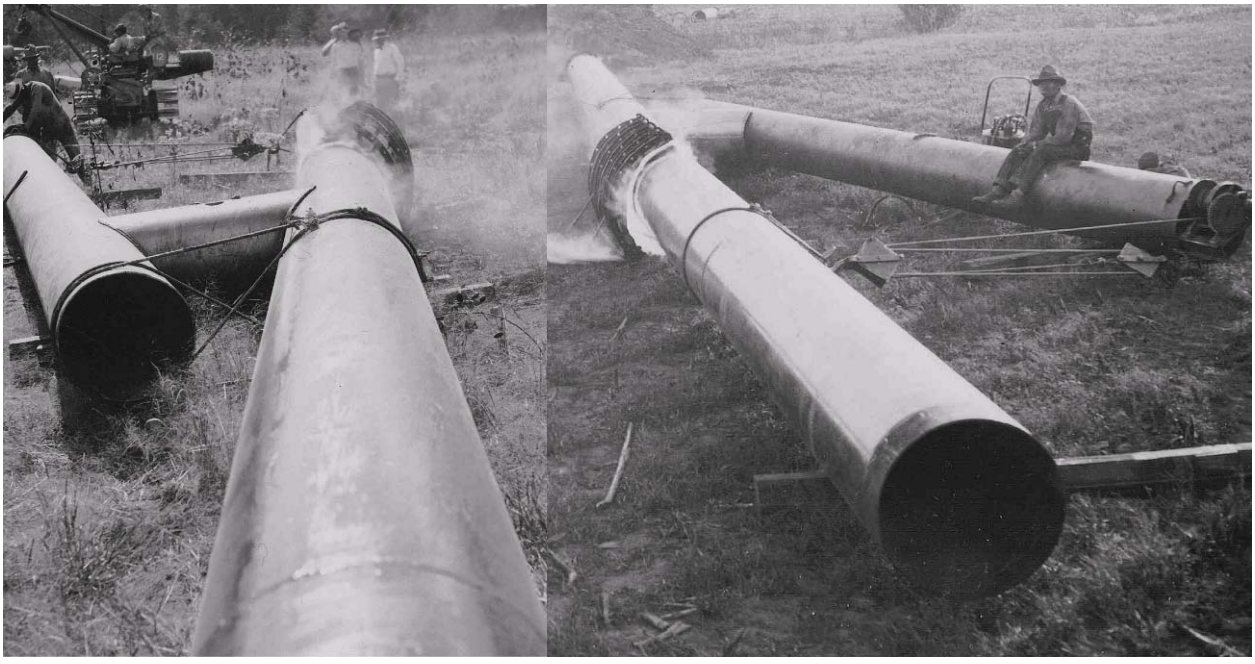

a) setup with fulcrum and tie-lineb) during heating, winch in foreground

Figure A4. Views of one hot wrinkle-bending fixture (circa 1931)

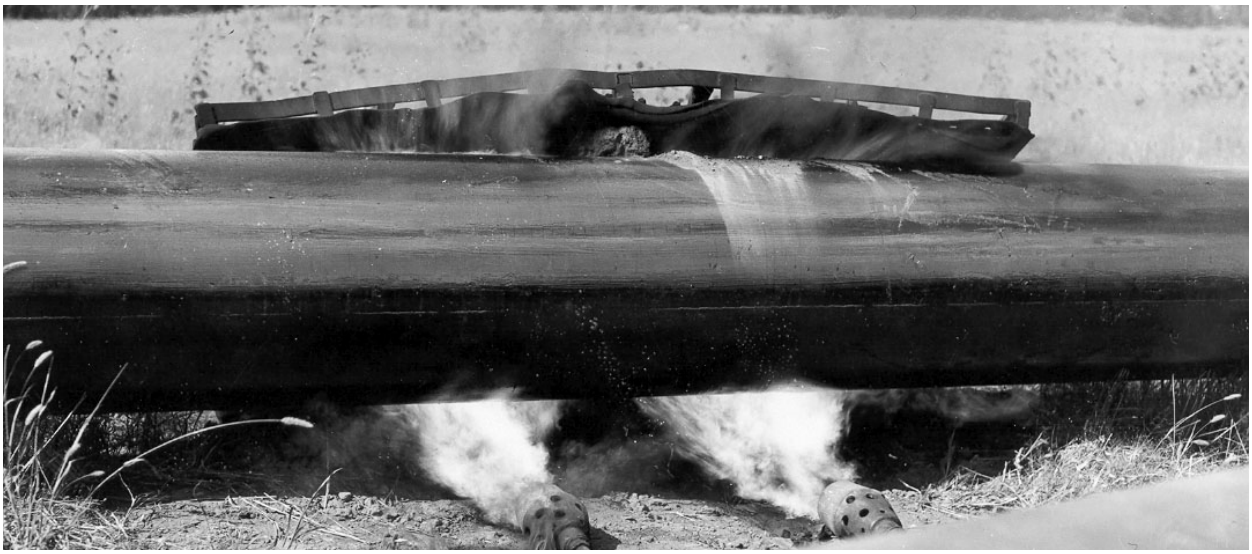

Figure A5. Heat being applied via oil burners for hot wrinkle-bending, with a fixture to distribute the heat (1930s).

a) burner oxides still intactb) smooth and free of obvious discontinuities

Figure A6. Typical bend produced by the hot wrinkle bending apparatus in Figure 5 – very little pipe distortion is evident

Figure A7. A-Frame wrinkle bending fixture (circa 1930s).

Figure A8. Typical bend produced with the A-Frame fixture shown in Figure 7.

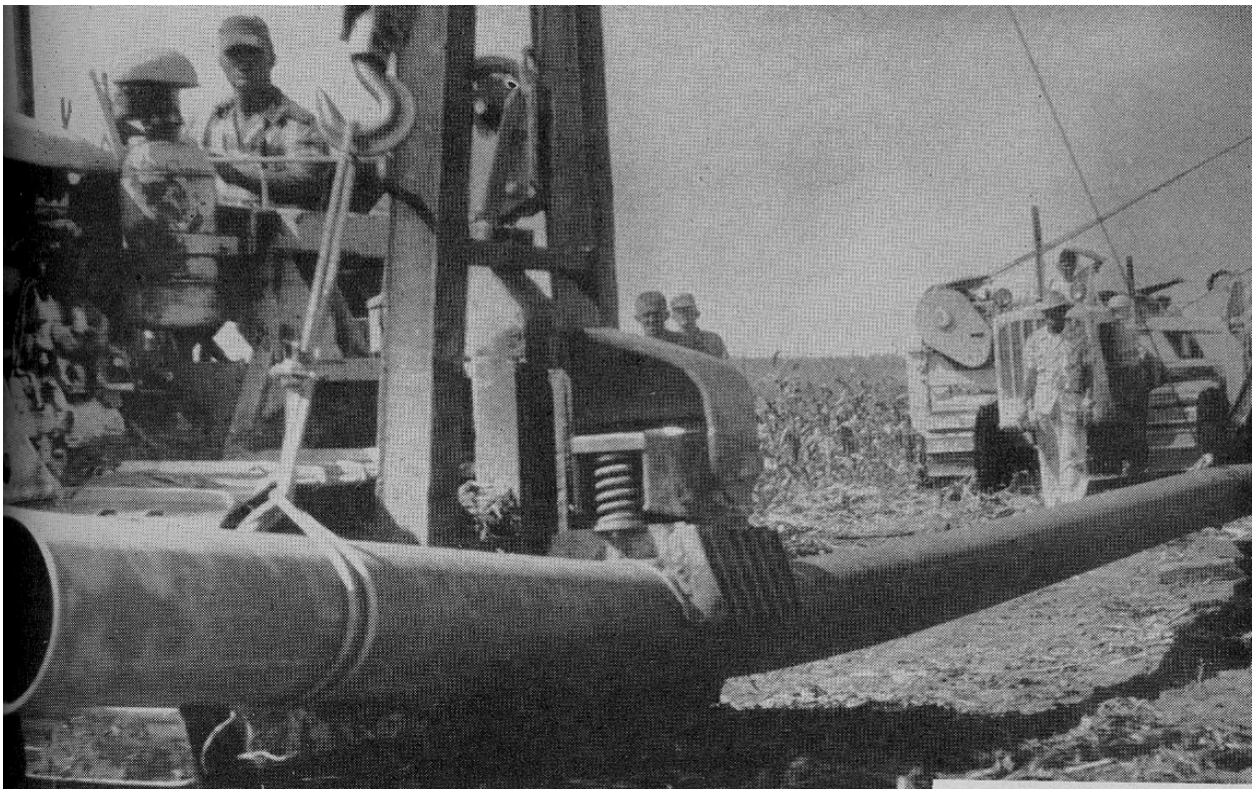

Figure A9. Side-boom stiff leg reminiscent of A-Frame fixture deployed vertically

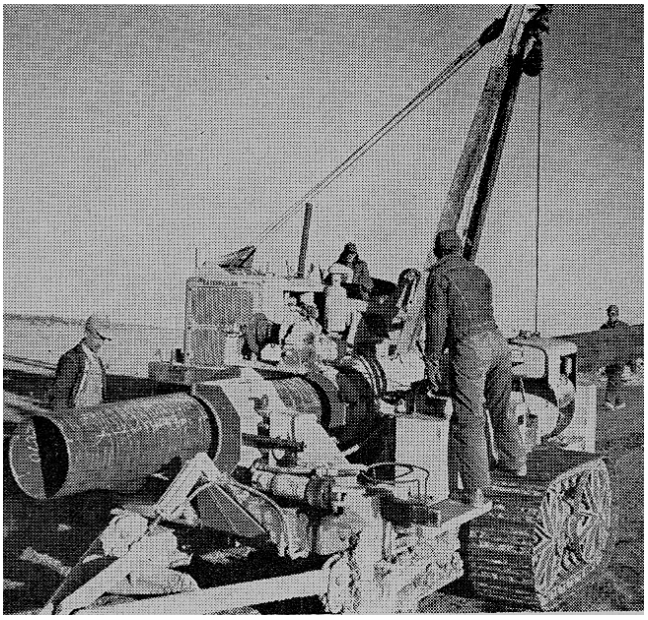

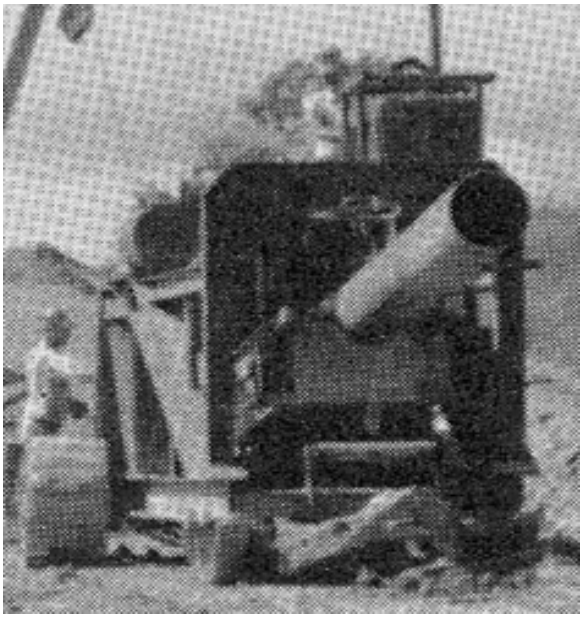

a) circa 1955 **b) circa 1958**

Figure A10. Evolution of pipe bending practices over time

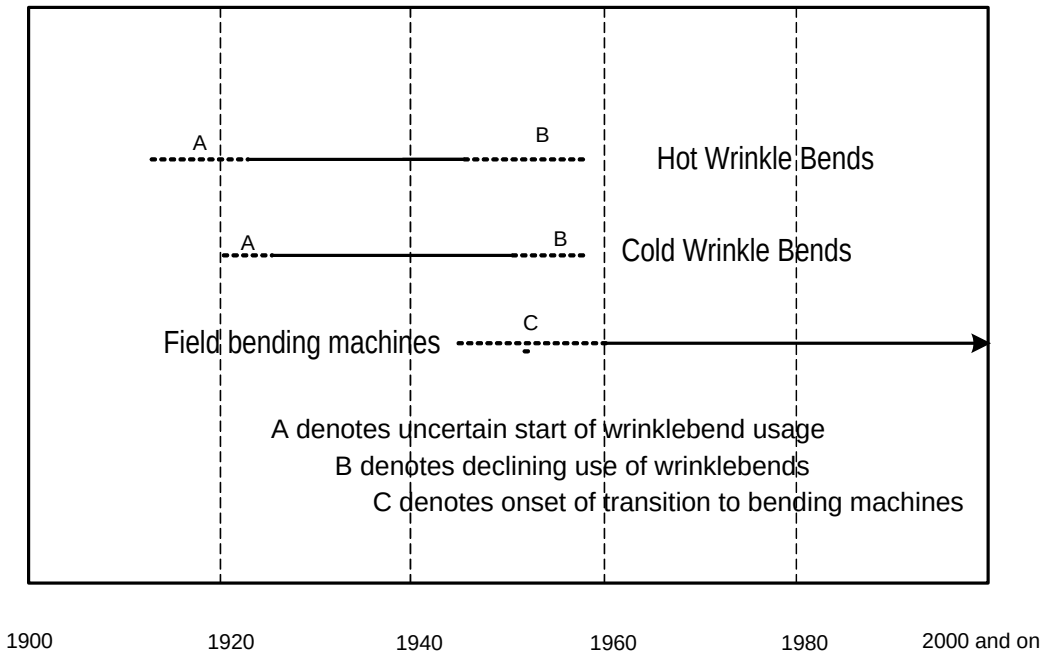

Figure A11. Timeline indicating the evolution of pipe bending practices

Appendix B – Archival Results from Field and Laboratory Studies and In-Service Failures

Aspects of this discussion involve results from historical bends as well as those made on modern bending machines. For this reason it is necessary to discriminate between these situations. This is accomplished by terming historical construction features wrinklebends – and modern machine-bent features "ripple-bends"[1].

This section identifies trends derived from reports on wrinklebend field studies and in-service failures based on Battelle archives. Topics covered include trends based on archival data on wrinklebend shapes and sizes, trends in strain that develop as a function of pressure and bend fixity based on strain gage measurements, and the results of some field failures focused on causative factors. The discussion reflects three comprehensive failure analysis, two rather focused field studies, and laboratory measurements of strains in ripples and wrinkles.

These results and trends are useful in identifying factors proven to affect wrinklebend integrity, which was essential in developing the work scope for this project. While useful to establish tendencies, the data reflect a limited scope of line-pipe geometries (i.e., diameter, d, wall thickness, t, and d/t)[2], pipe-pipe mechanical properties, wrinkle shapes and sizes, and field and in-service conditions. Thus, it is representative of wrinklebends, but not necessarily typical of all cases. Tendencies other than those presented are plausible – and where such seemed possible, the subject is avoided.

Shapes and Sizes of Wrinkles

Wrinkle shapes and sizes are critical parameters in characterizing wrinklebend integrity. Shape is important because it relates to curvature, which in turn relates to strain. Through the equal strain – equal fatigue-life hypothesis proven experimentally in the 70s for situations where only mechanical factors influence fatigue, strain can be related to fatigue resistance and life, and so is important in integrity assessment where pressure fluctuations occur. Strain likewise can be viewed as a measure of integrity for increasing load, as could stress.

Shape can be detected and quantified through use of appropriate ILI tools, or easily characterized in the field. Shape therefore offers entrée to condition monitoring for systems that can be pigged or easily made piggable, or for wrinkles uncovered in routine maintenance. Wrinkle size reflects its shape, and so provides a means to quantify local shape, which as just noted can be central to integrity assessment.

Key parameters in describing wrinkle shape and size include the length (pitch) and height (amplitude) of the wrinkle, the curvature at the crown (most peaked area, usually near the

---

[1] This term traces to Mr. Eugene (Gene) Smith of Natural Gas Pipeline Company, who as chairman of the Line Pipe Supervisory Committee (currently the Materials Committee) of the Pipeline Research Committee (PRC), (now the Pipeline Research Council International (PRCI)) suggested its use to discriminate historical wrinklebends from the ripple-like features produced by modern bending machines under study by the PRCI in the early 90s under PRCI funding[(1)].

[2] As the wrinkles or ripples reflect a local instability where "slenderness ratio" or length to thickness is a critical parameter[(e.g., 2)], one anticipates d/t to be an important variable. Unfortunately, this ratio is not well represented in the data available.

circumferential center) of the wrinkle, and the extent of the wrinkle around the circumference. Other shapes and sizes relative to wrinkles include the presence of corrosion, externally or internally, and its location and areal size relative to the crown of the wrinkle.

Shapes through the crown of the wrinkle tend to be most relevant. However, where strain hardening is significant load-shedding will occur spreading the deformation out around the pipe, outboard of this area. This could produce sharper local curvatures adjacent to the crown. Thus, the crown is not always the most critical location in regard to strain.

Profiles through the crown or elsewhere around the wrinkle along a line tracing the length of the pipe define wrinkle height and length. Their shapes tend to be similar, until the height of the wrinkle becomes large compared to the length and a kink begins to form in place of a smooth curve. Figure B1a shows some traces along a line through the crown of several wrinkles made in 20-inch diameter line pipe with a 0.310-inch thick wall. Figure B1b shows similar trends drawn in progressing around a wrinkle away from the crown for another pipeline of similar d/t. It is evident here that wrinklebends involve pipe whose cross-section extends out beyond the pipeline's profile, as opposed to dents that penetrate this profile, or buckles that often penetrate this profile. The profile of this protrusion is like a cycloid or sinusoid, the later being expected if the wrinkle process involves formation of a localized smooth buckle. That the wrinkle forms beyond the pipe's cross-section is one significant difference between wrinklebends and other local changes in pipe shape like dents, or other types of buckling.

Figure B2 presents views of typical wrinklebends removed during rehabilitation of late 40s construction of a 16-inch by 0.274-inch wall pipeline. Figure B2a is an overview of a bend with an overall angle equal to ~4 degrees. As is apparent there, this bend comprises two wrinklebends located either side of a girth weld from. It is noteworthy that wrinkles are not always symmetric about their crown, either along or around the pipeline. This is evident, for example, in the view shown in Figure B2b. Offsets much more severe than this have been seen, the worst to the authors knowledge involving a failed wrinklebend with a height to half-amplitude equal to 0.29 on one side of the "crown" and 0.42 on the other side.

With reference to Figure B3, it is possible to define wrinkle height and length several ways, only one of which can be simply evaluated based on field measurements. Fortunately, differences in the ratio of wrinkle height to wrinkle length, termed the wrinkle aspect ratio, based on these definitions is small for most practical scenarios, as will be shown much later. Thus, the definition that can be measured in the field can be adopted for general use. In regard to the traces shown in Figure B1, the wrinkle aspect ratio is the order of 0.4 to 0.5. Note from these traces that an intrusion occasionally accompanies the usually much larger protrusion. The aspect ratio in this and any case of asymmetry is the largest value of height referenced to the adjacent round pipe, divided by the corresponding half-length, which must be doubled to remain consistent with the above definition. From the author's experience, shapes like those shown in Figure B1 are not historically known to be problematic. As becomes apparent later, wrinkles that combine inward and outward components are more flexible than those that only protrude.

Figure B4 is a three-dimensional (3-D) view of another wrinkle whose shape is not likely to be problematic. While not evident in this view, this wrinkle developed around ~170-degrees of the pipe's circumference. For wrinkles that traverse half of the circumference or less, there appears to be a relationship between curvature through the crown and propagation of the wrinkle around the circumference. This relationship appears to be different for cold-formed versus hot-formed

wrinkles, but the results too sparse to state this with certainty. While a relationship between wrinkle shape and propagation around the circumference appears to exist, more severe wrinkles – that is those with higher aspect ratios – do not follow this pattern, as wrinkles can continue to become more severe with little further obvious propagation around the circumference. It follows that the circumferential extent of a wrinkle is not necessarily an indicator of wrinkle severity.

Trends in Strain

Based on a cursory survey of operators with lines with wrinklebends, few have measured strains in the field. However, to their credit some operators have made quite thorough field studies, which include in some cases results from stacked biaxial and rosette gage configurations. Even so, such potentially very instructive data are limited.

Battelle as been involved in two field studies, primarily associated with the effects of pressure on strains at and around the crown of the wrinkle. As the included angle of any bend is prone to increase as pressure increases, end-fixity and the overall restraint imposed on bends by the soil in the field can be an important factor in such studies. Experience indicates the measured strain depends strongly on the location of the gage relative to the crown, and the size of the gage relative to the steepness of the strain gradient under the gage. Precise location and use of short gage lengths thus is important in gathering useful data.

Accounting for such issues, strains measured are consistent with the effects of bending and the local curvature, subject to the end restraint. Measured field strains in all cases reflect in-service pipelines where the pressure during the measurements is reduced from the operating pressure. Where a significant amount of pipe is uncovered, strains at a given pressure were greater than when soil provided high local restraint against opening of the bend. This suggests rehabilitation that significantly relaxes the soil restraint around a wrinklebend can cause loading on that wrinkle not present before maintenance began. It is conceivable in geologically active areas that rehab local to one wrinklebend could cause loading of that wrinkle, and also that might lie in adjacent parallel lines, on the same line or those close by, either upstream or downstream. Finally, variability in the results as a function of gage placement, gage length, and bending restraint make it difficult to use such measurements to validate numerical or other models used in integrity assessment. It has been observed that the change in pressure on an operating pipeline corresponds to proportional change in strain. Such is expected for lines in service where the extent of pressure change allowed in service is relatively small. It is not anticipated for large swings in pressure for bends with limited soil restraint.

Strains have also be measured by others for line-pipe bends, but under laboratory conditions and also for cases other than wrinklebends[e.g., 1-4]. Olson et al[1] made measurements on the strains developed on modern ripple-bends made in pipe coated with fusion-bonded epoxy (FBE). The apparent purpose for the measurements was to verify results of numerical simulations, for subsequent use in predicting fatigue response. One set of measurements involved 30-inch x 0.300-inch thick X70 pipe, which contained one large wrinkle with depth of ~1.5 times the wall thickness or ~1.5-percent of the diameter, along with several smaller ripples. The second set of measurements involved 36-inch x 0.385-inch thick X65 pipe, again with one large wrinkle with depth of ~1.5 times the wall thickness or ~1.7 percent of the pipe diameter, along with several smaller wrinkles. The measurements did not involve parametric evaluation, being focused on pressure cycling following a simulated proof-pressure (hydrotest) cycle. Figures B5a and B5b, reproduced from Reference 1, show an overview of each of the bends and their instrumentation.

Arav[3] also measured strains on large-radius bends containing mild ripples made in 8-inch and 14-inch diameter pipe, where the bends had radii 4 or 10 times the pipe diameter. This is the order of the tightest radius negotiated by ILI tools, and much tighter than bend radii more typical of transmission pipelines. Ripple heights were 1 to 2 times the wall thickness or three to five-percent of the diameter. Data reported suggests that ripple crests protruded from the mean pipe surface whereas the troughs fell within the pipe mean diameter. As for the work done by Olson et al, strains were measured for use in analyses of such bends, specifically in this case to empirically determine stress-intensification factors, whose use is common in boiler and pressure-vessel codes.

Other laboratory strain measurements in ripple-bends and wrinklebends likely have been made, as for example, for use in verifying the numerical modeling work of Bilston[4]. However, the purpose here also was to validate specific modeling activities. For this reason, it appears that limited parametric results are openly available.

Causative Factors in Field Failures

Although few modern-day wrinklebend failures have occurred, Battelle has been involved in several field studies and failure analyses[e.g., 5,6], and industry personnel have provided supporting data from their experience and company archives. Such analysis was done either to understand in-service wrinklebend response to various field situations, or to identify causative factors when failures have occurred. While the reports and details of this work are proprietary to the clients involved or the companies supplying comparable data, observations and "lessons learned" can be discussed as appropriate.

Results of two detailed failure analyses of field-failed wrinklebends were available to help guide the work scope for this project. The first to occur involved a wrinkle on a 20-inch diameter seamless pipeline with 0.310-inch wall made of X42 steel[5]. This pipeline went into service in 1948, traversing hilly countryside. The second of these involved a 22-inch diameter pipeline constructed in 1931 using lap-welded pipe with 0.312-inch thick wall, with an effective yield strength of 30.7 ksi[6] (based on testing done using end-capped vessels made of this line pipe).

Failure in 1948 Construction

The wrinklebend failure in the 1948 construction occurred at a circumferential crack in a sag bend at the bottom of a large hill, in a segment of the pipeline traversing a hilly area. The wrinkle ran around ~45-percent of the pipe's circumference, being centered at 12 o'clock. Figure B6a is an overview of the failed wrinklebend following the failure, prior to its being removed for further analysis. The height of the reconstructed wrinkle was ~0.875-inch, with an overall length of ~4 inches[3]. These dimensions were considered typical by pipeline company staff involved with this investigation. The wrinkle was smooth and without creases. There was no obvious evidence of reversed curvature or inward bending. Several wrinkles downstream from the failed wrinkle had similar shapes, some of which were close together, suggesting these smooth wrinkles were not made with elongated shoes located on both sides of the wrinkle.

---

[3] The rather fracture-brittle nature of the steel, the long nearly through-wall circumferential crack-origin, the absence of external damage to the wrinkle, and the brittle ring-off that produced a guillotine break imply the reconstructed wrinkle shape reasonably characterizes its height and length prior to failure.

There was no evidence a mandrel was used. One of these downstream wrinkles did show significant reversed curvature into the adjacent wrinkle whose amplitude was oriented toward the inside of the pipe, in contrast to the others. All adjacent wrinkles were free or corrosion on the inside or the outside of the pipeline, while the failed wrinkle showed minor areal corrosion on the outside of the pipeline. Adjacent wrinkles were examined at 10 times magnification but none was found cracked. Metallography indicated the wrinkles were cold-formed. The microstructure was typical of seamless pipe for the era of construction.

Pressure cycling of this sag wrinkle caused tension at the inside wall of the pipe and compression on the exterior of the pipe. Thermal cycling to temperatures less than that at pipe laying thus creates tension on the interior of the pipe and compression on the exterior of the pipe, while the reverse occurs for cycling to temperatures greater than that at pipe laying. It follows that, given the failure occurred during a cold February, the interior of the pipe was subjected to a modest tension mean stress, with pressure cycling occurring from a tension peak stress to lower stress levels. Conversely, the exterior of the pipe was subjected to an unknown but probably near zero mean stress, with pressure cycling occurring to more compressive levels. This implies that while initiation of cracking via fatigue is possible on the inside or outside of the wrinkle, continued growth by this stress-driven mechanism was expected only from the inside wall.

Cracking in the failed wrinkle lead to a double-ended (guillotine) break, with the ends of the pipe separated axially by ~4.5 inch, as was evident in Figure B6a. After eliminating other potential causative factors, the cause of the cracking was traced fractographically to pressure cycling. Initiation of the cracking was associated with small internal corrosion pits that reflected periodic upsets in gas quality during earlier service. Cracking was transgranular and originated from the inside of the crown of the wrinkle, near the planes of symmetry along and around the pipeline. Failure was triggered by circumferential coalescence of at least three thumbnail-shaped cracks to create one longer nearly through-wall crack. An overview of this area is shown in Figure B6b. More than twenty such origins were found in co-parallel cracking between the 11 and 1 o'clock positions on the inside of the crown of the wrinkle. Such cracking is typical of results supplied from failure analyses of other wrinklebends that experience significant pressure cycles due to their service. Some evidence of cracking also was found on the outside of the crown of the wrinkle at the 12-o'clock position. This cracking was located in an area of shallow corrosion under disbanded coating. These features were very short and shallow, with lengths that were a small fraction of the wall thickness.

It was concluded pressure cycles associated with pipeline operation drove the cracking that caused the failure, although seasonal thermal cycles also could have been a factor. Absent corrosion pitting, the serviceable life of the wrinkle would have been much longer based on typical corrosion-fatigue data that show pitting appreciably reduces the life compared to the absence of pitting[(7)4]. The failure occurred through the stable coalescence of circumferential PTW cracks until a critical flaw size was reached. Formation of the guillotine failure and the axial shortening evident upon reconstruction indicate soil stability was a contributory factor, which is supported by the presence of large soil-slips in areas adjacent the failure.

---

[4] Given pitting often accounts for an order of magnitude decrease in life[(7)], one could reasonably assert this failure would not yet have occurred absent the corrosion.

Failure in 1931 Construction

Failure of the wrinkle in the 1931 construction occurred immediately upstream of a drainage ditch, the bottom of which lay approximately 12 feet below its crest on either side. The bottom of this ditch dropped about 25 feet over a distance of several hundred feet to the lake into which it drained. There was evidence of soil-slips along this area. The pipe on either side of the ditch was buried quite deep apparently in anticipation of crossing the ditch. It was apparently bedded in native soil as deep as the smooth, flat sedimentary rock ledges either side of the ditch would permit. A geological expert retained for this investigation noted the ledges were sedimentary rock with relatively low strength and low but variable resistance to erosion. This low and variable resistance to erosion was evident in rock cuts through the same geological structure made for nearby road construction.

The failure originated circumferentially in the body of the pipe at an over-bend in the upstream bank of the drainage, as is apparent from Figure B7a. The failed wrinkle had slightly reversed curvature, the majority of which protruded from the pipe's nominal cross-section. Measurements indicated the wrinkle ran roughly 50-percent around the pipe's circumference and had a maximum reconstructed peak to trough height of ~1.15-inch and length of ~5.5 inches[5]. Similar wrinkle-like features, one almost imperceptible as well as a more severe wrinkle, were found in adjacent downstream pipe joints. These wrinkles were smooth and without creases. There was no evidence of corrosion on any of the wrinkles, nor was there evidence of cracking in areas of high tensile stress when the adjacent features were inspected using the dry powder magnetic particle practice – even though one was more severe than the failed wrinkle. The absence of cracking at this more severe feature implied fatigue was unlikely a factor, all else being equal. Metallography indicated the wrinkle was cold-formed and made in steel typical of the construction era, the latter being confirmed by appropriate testing.

This pipeline experienced limited pressure cycling based on recorded service histories, so it was not surprising fractography did not identify striations or other features found where fatigue causes crack growth. The origin was remote to the lap weld, and the chemistry and strength properties were as expected, which eliminated them as causative factors. Cracking in the failed wrinkle resulted in a double-ended break, but, because the pipe broke up and was ejected from the ditch it was not possible to determine if axial loading of the pipeline would have caused an axial gap between the pipe ends. Accordingly, it was not possible to directly establish the role of soil/support instability for this failure.

The origin, which was located via chevrons and other macrofracture features, lay across the crown of the wrinkle. Fractography in the origin indicated failure occurred by circumferential coalescence of multiple thumbnail-shaped transgranular cracks growing from the outside of the pipe. This area is shown in Figure B7b. Cracking originating from the outside of an over-bend indicates line tension, or the bend is settling, or pressure or thermal cycles are causing the wrinkle to flex. Of these, the last was not supported by either the service history or the fractography. Coalescence created one PTW crack about eight-inches long. Some very deep

[5] Again, the rather fracture-brittle nature of the steel, a long nearly through-wall crack-origin, the absence of external damage to the wrinkle, and brittle-like failure make it possible to reconstruct the wrinkle shape, but in this case the dimensions are at best estimates.

portions of the origin were covered with heavy rust indicating the cracking was stable, and possibly through-wall over parts of this length prior to the failure. Shear-lips within the origin were small in comparison to that expected for this steel if high local stress under load control caused the cracking. This implied the thumbnails formed and grew under relatively low local stress, or displacement control, both of which admit stable cracking and time enough for corrosion within the origin. No co-parallel cracking was found on the outside of the pipe, nor was there evidence of cracking on the inside of the pipe, as would be expected if the stresses were high or low-cycle fatigue was involved.

Based on a site visit and review of the evidence after the fractography was completed, it was determined additional testing was needed to explore other plausible explanations of the evidence. Once completed, it could be concluded that stable coalescence of circumferential PTW cracks was due to the gradual opening of the bend caused by log-term erosion of the rock ledge that terminated below the wrinkle and draining toward the ditch. While no evidence remained to support the hypothesis, the results indicate the drainage prompted a soil-slip that opened the bend enough to trigger the failure. Whether or not this differential displacement led to axial tension that would be contributory to the failure could not be determined because necessary evidence was destroyed with the rupture.

Summary

Wrinkle shapes and sizes can be critical parameters in characterizing wrinklebend integrity, because shape relates to curvature and strain – which are indirect measures of wrinkle severity. Shape and size can be defined by the length (pitch) and height (amplitude) of the wrinkle, the curvature at the crown (most peaked area, usually near the circumferential center) of the wrinkle, and the extent of the wrinkle around the circumference. While it is possible to define wrinkle height and length several ways, only one of these can be simply evaluated based on field measurements. Fortunately, differences in the ratio of wrinkle height to wrinkle length, termed the wrinkle aspect ratio, based on these definitions is small for most practical scenarios, as will be shown much later. For wrinkles that traverse half of the circumference or less, there appears to be a relationship between curvature through the crown and propagation of the wrinkle around the circumference. This relationship likely is different for cold-formed versus hot-formed wrinkles, but the results too sparse to state this with certainty. It follows that the circumferential extent of a wrinkle is not necessarily an indicator of wrinkle severity.

A cursory survey of operators with lines with wrinklebends indicates few have measured strains in the field, and little has been done under laboratory conditions. Thus, while potentially very instructive, such data are limited. The limited data indicate the included angle of any bend is prone to increase as pressure increases, so end-fixity and the overall restraint imposed on the bend can be important in establishing wrinklebend integrity. This suggests field activities that significantly relax soil restraint around a wrinklebend can cause loadings not present before the work began. In turn, this suggests care must be taken when exposing wrinklebends for any reason, which is one explanation for the absence of field-measured strains. Finally, because measured strain depends strongly on the location of the gage relative to the crown, and the size of the gage relative to the steepness of the strain gradient under the gage, it can be difficult to use such data to characterize wrinkle severity, or as a generic basis to validate models of wrinkle severity. Other laboratory strain measurements in ripple-bends and wrinklebends likely have been made. However, their purpose was to validate their modeling activities, which limits their utility to guide this project.

As for the two failures considered, other less-well documented failures in Battelle archives show similar tendencies – the effect of cyclic loading is prevalent as is the role of outside forces involving pipe or movement. The presence of internal or external corrosion is not as common, although it is not uncommon when wrinklebends are uncovered in the course of maintenance or rehabilitation. It follows that wrinkle shape can be an indicator of potential problems, but it is equally clear that other factors like outside forces and wrinklebend restraint or internal or external corrosion can be important when assessing wrinklebend integrity.

References

1. Olson, R. J., "Evaluation of the Structural Integrity of Cold Field-Bent Line Pipe, PRCI Report PR-3-9214, May 1996: see also Olson, R., Clark, T., and Odom, T., "Evaluation of the Structural Integrity of Cold Field Bent Line Pipe", 10th Biennial Joint Technical Meeting on Line Pipe Research, EPRG/PRC, Paper 6, April 1995, Cambridge
2. Seeley F. B. and Smith, J. O., Advanced Mechanics of Materials, Wiley, 1967.
3. Arav, F., "Evaluation of Pipe Bends Having Local Corrugations", 3rd International Conference on Pressure Vessel Technology, ASME, 1977, pp. 193-205
4. Bilston, P., "The Modelling of Compression Buckles Formed During the Cold Field Bending of Line Pipe," Thesis for degree at Monash University, December 1993: see also Murray, N. and Bilston, P., Final Report of APIA Cold Field Bending Research Team, Monash University, July 1993 – proprietary to APIA/PRCI.
5. Leis, B. N. et al, "Investigation of Pipeline Failure Near Peculiar Missouri", May 2001, proprietary to client.
6. Leis, B. N. and Lahrman, D. F., "Failure Analysis of Rupture at 4518+23", February 1996, proprietary to client.
7. Novack, S. R., "Corrosion-Fatigue Crack Initiation Behavior of Four Structural Steels", in Corrosion Fatigue, T. W. Crooker and B. N. Leis editors, ASTM STP 801, 1983, pp. 26-63.

a) traces along the crowns of five different wrinkles

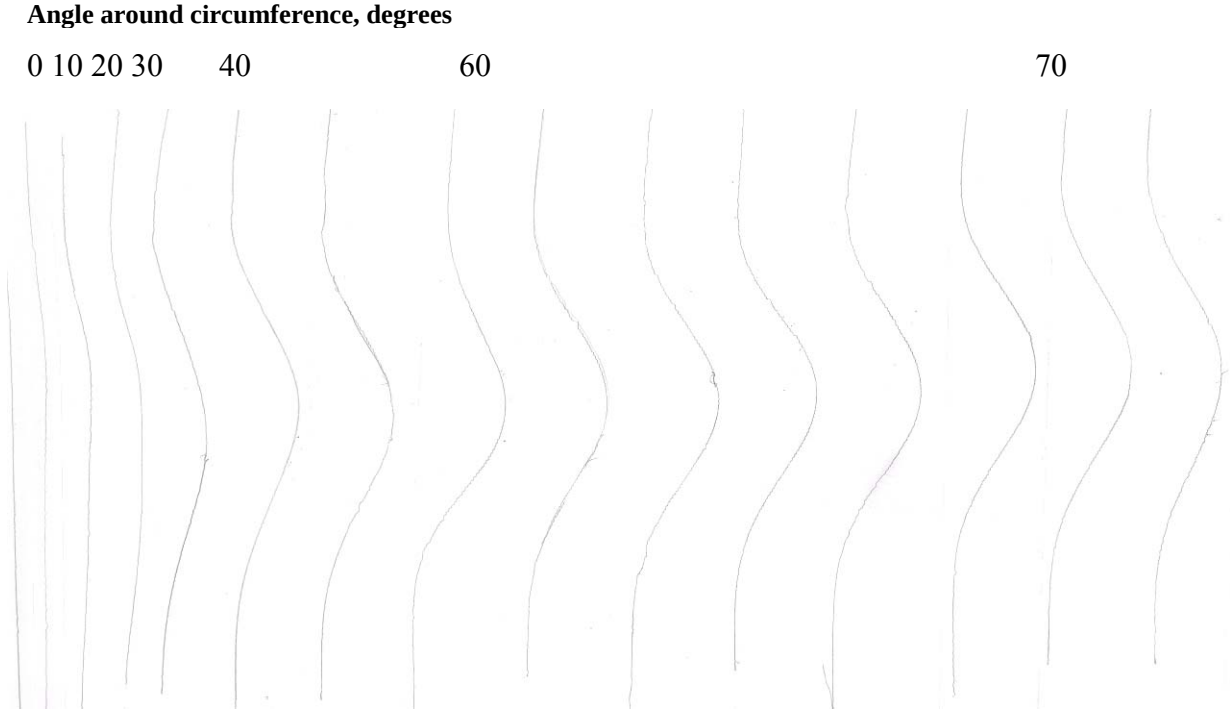

b) traces made incrementally around the wrinkle, moving from the crown

Figure B1. Traces of wrinkle shape for wrinkles in 20-inch x 0.310-inch X42 line pipe

a) bend with angle equal to ~4 degrees comprises two wrinkles either side of a girth weld

b) wrinkle that is asymmetric lengthwise along its crown

Figure B2. Typical wrinkle-bends in early vintage construction

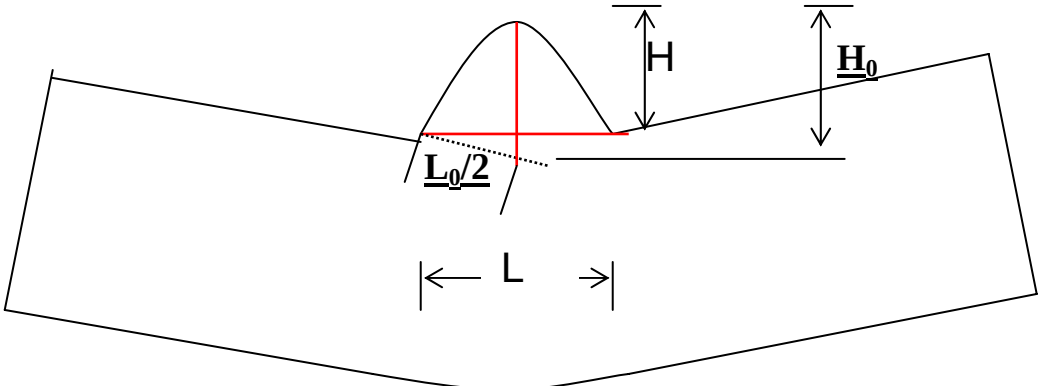

Three definitions considered:

H/L (adopted as it is easiest measured in the field)
H_0/L_0
H/L_0

Results show that the three definitions are not significantly different for typical wrinklebends.

Figure B3. Definitions of wrinkle height and length, and their ratio

Figure B4. "Cast" of a wrinkle-bend running ~160-degrees around the circumference

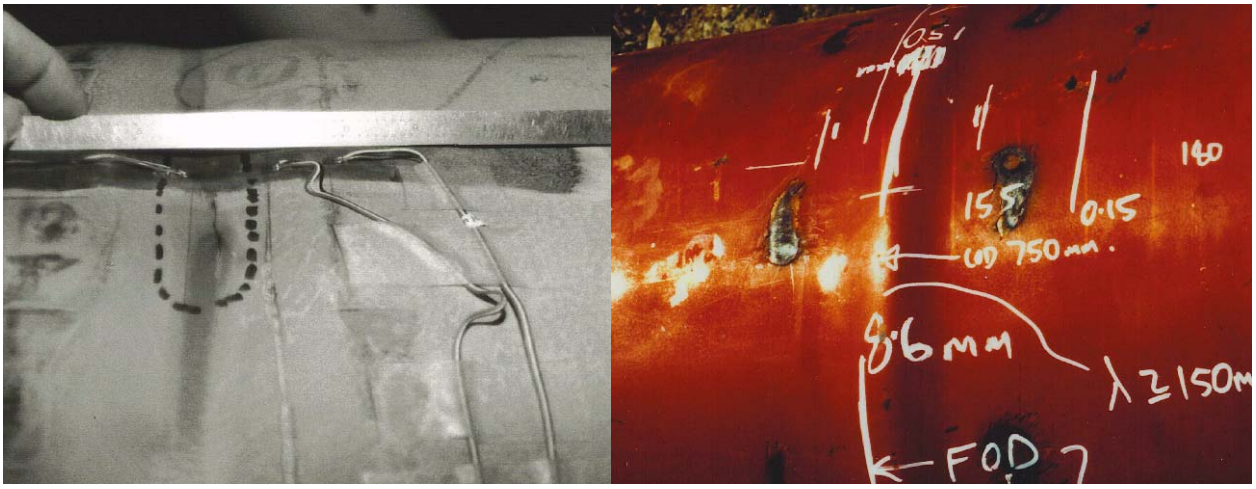

a) Specimen A: 30-inch x 0.300-inch X70b) Specimen B: 36-inch x 0.385-inch X65

Figure B5. Views of Olson's largest ripples and strain gage locations for Specimen A

a) overview of failure

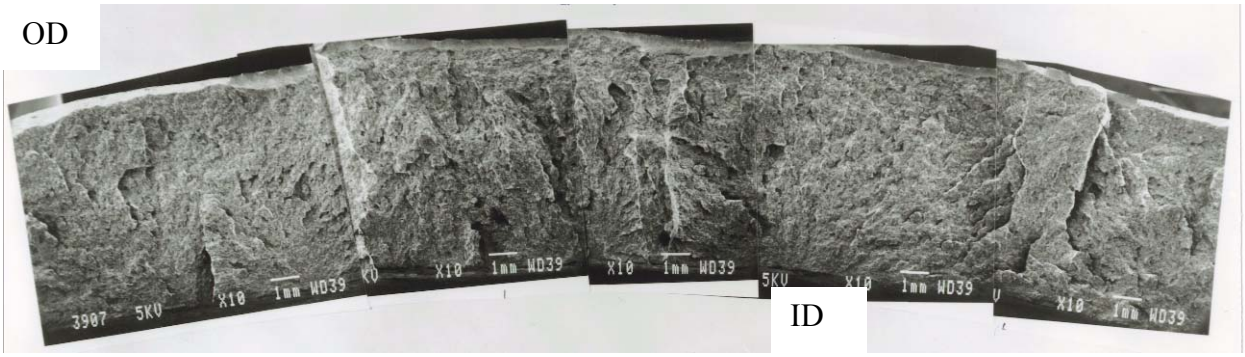

b) circumferential coalescence of several smaller thumbnail-shaped origins

Figure B6. Failed wrinklebend in 1948 construction

a) view uphill toward the location of the failed wrinklebend

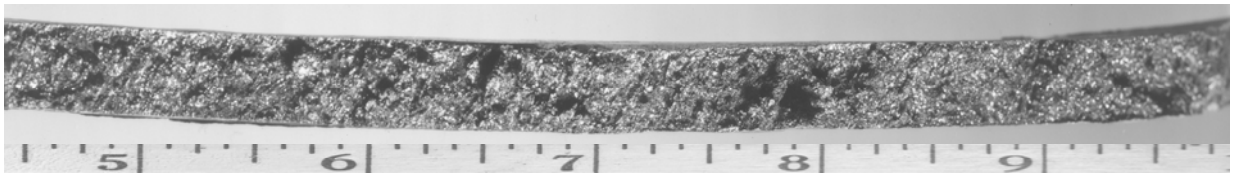

b) overview along origin, indicating multiple thumbnail-shaped cracks

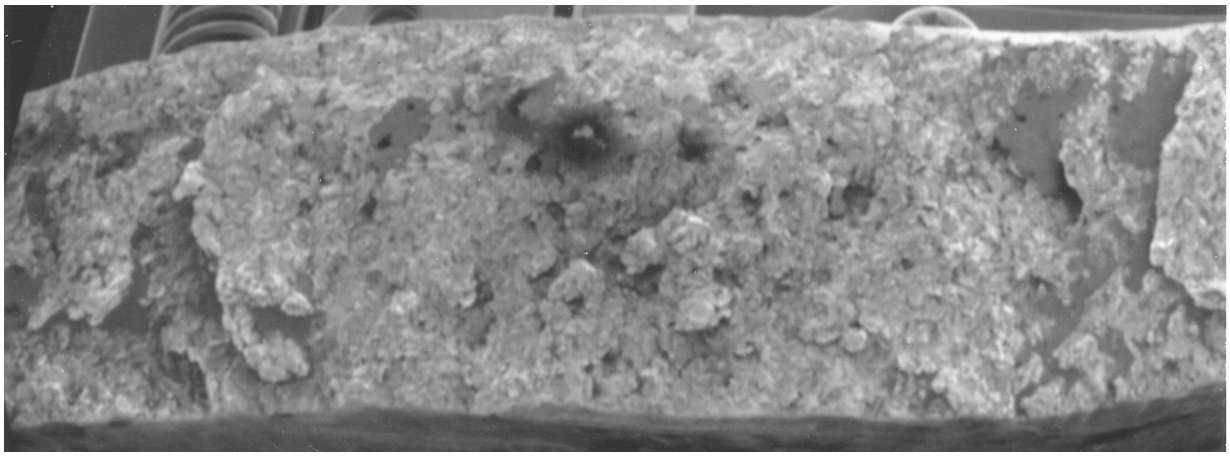

c) detail of a typical thumbnail-shaped crack– near left end in the overview in part b)

Figure B7. Failed wrinklebend in 1931 construction

Appendix C – Analysis of In-Service Failure Experience

Concerns for structural integrity noted above were in balance with views that wrinklebends were acceptable as late as 1952[1], with the exception of liquids pipelines where cleaning pigs were frequently run, and pressure fluctuations are more common. Better understanding wrinkle-bending as a viable practice versus an integrity concern is useful in evaluating wrinklebend integrity – which is important because many pipeline systems still contain wrinklebends, even though use of wrinklebends was phased out apparently in the early 50s.

Unfortunately, little quantitative data could be found for the period prior to the 1950, so it is not possible to quantify the service experience that underlies the concerns noted above. However, as such data has been assembled under Government purview since 1950, it is possible to evaluate the serviceability of wrinklebends since 1950. As with all construction-related concerns, such features are not an integrity threat in pipelines where they remain benign. It follows that a useful measure of wrinklebend integrity is evaluation of trends in wrinklebend service incidents, both in absolute numbers and in comparison relative to other threats to pipeline integrity. As these bends tend to be largely absent from liquid/products pipelines, incident data for gas pipelines provides the best historical measure of this aspect.

Databases Considered

The ensuing paragraphs make use of available incident data evaluated in terms of failure rate relative to that of other known threats for gas transmission pipelines. Experience as well as ASME B31.8S underlies selection of other potential threats for use in this relative evaluation. Three open-access incident history datasets[2-4] are needed to construct a continuous timeline for use in this comparison, data for which are summarized in Table A1. The first of this is data assembled by the Federal Power Commission (FPC), while the second and third datasets were assembled under the auspices of the US Department of Transportation (DoT), in its Office of Pipeline Safety (OPS). With reference to the table, the time interval represented begins in 1950, and continues through the present. Accordingly, the data can be viewed as complete in time in regard to the future as well as past frequency of occurrence of incidents.

Table A1. Available incident experience in US gas-transmission pipelines

Description	Time Period	Number of Incidents	
		Total	Wrinklebend
FPC	January, 1950 – June. 1965	1067	26
DoT/OPS	1970 – mid 1984	7864	4
DoT/OPS	mid 1984 – mid 2002	1455	7

Integrity Trending

Each of the databases in Table A1 was evaluated with consideration given to different reporting categories, scope of data reported, general descriptions provided, and timeframe represented by each. For instance, the DoT/OPS database from mid 1984 to mid 2002 contained 10 wrinklebend/buckle incidents. Of these, two incidents involve pipelines constructed in the 1980's, which reflect failures at buckles formed due to abnormal loading in service, and not

wrinklebends. A third incident involved a pipeline constructed in 1949, where the incident was attributed to impact from an in-line inspection (ILI) tool. This incident reflects aspects other than pipeline service. Because this incident was not due to changing operating conditions or external loading variation, it was not considered in estimating the failure rate. However, this incident does represent an issue when a company considers running an ILI tool in a pipeline containing wrinklebends or buckles. Failure causes provided in the database and covered in the present evaluation included overstress, fatigue, and thermal expansion stress.

Consideration of the DoT/OPS gas transmission pipeline incident database showed only four incidents that could be conclusively traced due to wrinklebends. Comparison of the number of wrinklebend incidents or the relative fraction of such incidents and the timeline involved for the DoT data from 1970 to 1984 with the same results for other two datasets suggests that incidents attributed to wrinklebends may not be properly identified. Such is plausible, as much of the information included in the most recent of the datasets is generic, and specific cause-identifiers have not been provided for many of the incidents.

The FPC dataset contained the largest number of wrinklebend related incidents as shown in the above table. This dataset includes the end of the era when wrinklebends were still in use (i.e., ~1955 and earlier). For this reason, and because problematic features can be expected to fail first and quite early (i.e., show infant mortality), it reasonable to expect a higher fraction of related incidents.

Because of inherent differences in the scope of the data reported between these data sets, analysis of the pooled data was not considered as a basis to identify causative factors. However, the data can be pooled to make relative comparison of factors such service life until failure. Failure rate have been estimated for each dataset, as well as jointly, to isolate possible differences in failure rate between 1950 and 2002.

Table A2. Incident rate for all incident causes in the datasets of Table A1

Description	Time Period	Incident	
		Percentage	Rate(per mile-year)
FPC	January 1950 – June 1965	2.44	$1x10^{-5}$ (b)
DoT/OPS	1970 – mid 1984	0.051	9.8×10^{-7} (a)
DoT/OPS	Mid 1984 – mid 2002	0.481	1.4×10^{-6} (a)

(a) Based on the average number of transmission pipeline miles in the time interval noted.
(b) Based on approximate pipeline mileage in FPC data (150,000 miles)

Comparison of the results for wrinklebend incident rates in Table A2 all three datasets are much less than incident rates for other pipeline threats[e.g., 4,5]. This is evident from Figure C1, developed from data in References 2 to 4. Figure C1 presents the failure rate for US gas transmission pipelines for the four incident categories used by the DoT for incident reporting for the period from 1984 through 2000. Wrinklebend failures fall into the construction category. It is apparent from the trends in Figure C1 that the failure rate for these reporting categories is the order of 10-5, which is similar to the rate shown early on in the use of wrinklebends (see Table A2). References 3 and 4 indicate there is a continuing reduction in the failure rate associated with construction-related threats. This trend also is evident for wrinklebends, as shown in Figure C2. This figure plots the number of wrinklebend failures per year as a function

of their in-service life. It is evident from Figure C2 that over 80-percent of the wrinklebend failures occurred within the first 50 years of service, at a rate that was roughly constant over that period. In contrast, beyond 50 years the failure rate drops sharply, and is asymptotically approaching zero.

The apparently low failure rate for wrinklebends in contrast to other threats does not diminish the need to address their serviceability in systems that incorporate such bends, although it does imply this construction feature is potentially less significant than other threats on average. This average result must be viewed in light of systems incorporating a significant number of such bends.

For example, consider the behavior of wrinklebends operating in a 20-inch gas-transmission pipeline installed in 1948, which is known to the authors. This pipeline contains wrinklebends at a frequency greater than one per mile on average, and so is much different than the average scenario represented by the datasets that underlie Tables A1 and A2. During its continuous service to date for more than 65 years, this pipeline experienced two wrinklebend failures. One failure was related to pressure fluctuations that resulted in crack growth due to cyclic stress, with longitudinal stresses due to soil movement being a contributory factor. The second failure was reportedly due to soil movement. The resulting incident rate for this pipeline is 4.02 x10-4 incidents/mile-year. This rate is about twice that evident in Figure C1 or evident in Table A2. This somewhat higher failure rate for wrinklebends could reflect the much greater frequency of wrinklebends per mile as compared to that for the database underlying Table A2 or Figure C1. Equally, it could reflect unique soil-stability problems along portions of this pipeline, which contributed directly or indirectly to both failures. Finally, it could reflect other unique aspects of this pipeline, such as cyclic stressing and/or external loading, which were contributory factors to at least one of the failures.

In reference to Figure C2, the initially higher failure rate is to be expected, as is the eventually decline, as follows. The bulk of the shortest service lives are represented by the FPC (1950-1965) data[(2)], which encompasses the time interval when wrinkle-bending was still in use. First-to-occur failures comprise the most severe and potentially problematic wrinkles, which reflect an "infant-mortality" response including wrinkles produced during the earlier decades of pipeline construction. Over this period the average failure rate is ~0.9 incidents/year. The spike evident after ~25 years of service reflects several failures in one operator's pipeline system for wrinkles installed the same year in two neighboring states. The wrinkles failed in 16 and 18-inch pipe used in a "wrinkle expansion bend", where by virtue of its service fatigue cracking is an expectation, as evident in concerns expressed in the early 50s[(1)]. Thereafter, the average rate declines to ~0.64 incidents/ year, and beyond 50 years of service falls off sharply toward zero.

Wrinklebend Integrity Trends with Time

Table A3 quantifies trends in estimated wrinklebend incident rate normalized by pipeline mileage as a function of time in service. The results indicate that the wrinklebend incident rate is declining with increasing service time, which likely reflects the fact that the most severe and potentially problematic wrinkles have been removed from the in-service population, albeit by in-service failure at shorter lives. Analysis of the underlying database indicates that wrinklebends can be very sensitive to cyclic environments and/or increased secondary loadings, such as that due to land movement. This suggests that factors that affect wrinklebend performance should be understood for each operating system such that necessary mitigation action can be properly

identified. This report provides guidance for this activity.

Table A3. Incident rate for wrinklebends for the timeframe of the databases in Table A1

Years in Service	Incident Rate (incidents/mile-year)
0 – 25	5.4×10^{-6}
25 – 45	2.6×10^{-6}
> 45	4.4×10^{-7}

Summary

Trending of wrinklebend incident data indicates the frequency of wrinklebend related problems has been low in comparison to other threats to pipeline integrity, and continues to diminish as time passes. However, recent modification of 49 CFR 192 to include integrity management provisions indicates the need to assess threats to pipeline integrity. On this basis, wrinklebend performance will require consideration in the integrity management plans of operators whose vintage systems include such features.

References

1. Binckley, M. J.; "Which Bending Method", *Gas*, May 1952, pp 122-125.
2. Anon., Federal Power Commission Incident Database, 1950-65
3. Jones, D. J., Kramer, G. S. Kramer, Gideon, D. N. and Eiber, R. J. "An Analysis of Reportable Incidents for Natural Gas Transmission and Gathering Lines 1970 through 1984," NG-18 Report 158, March 1986.
4. Kiefner, J. F., Mesloh, R. E., Kiefner, B. A.; " Analysis of DOT Reportable Incidents For Gas Transmission and Gathering System Pipelines, 1985-1997", PRCI, PR-218-9801, 1999.
5. Leis, B. N., Chang, O. C., and Bubenik, T. A., "Leak versus Rupture Considerations for Steel Low-Stress Pipelines," GRI Report-00/0232, January 2001.

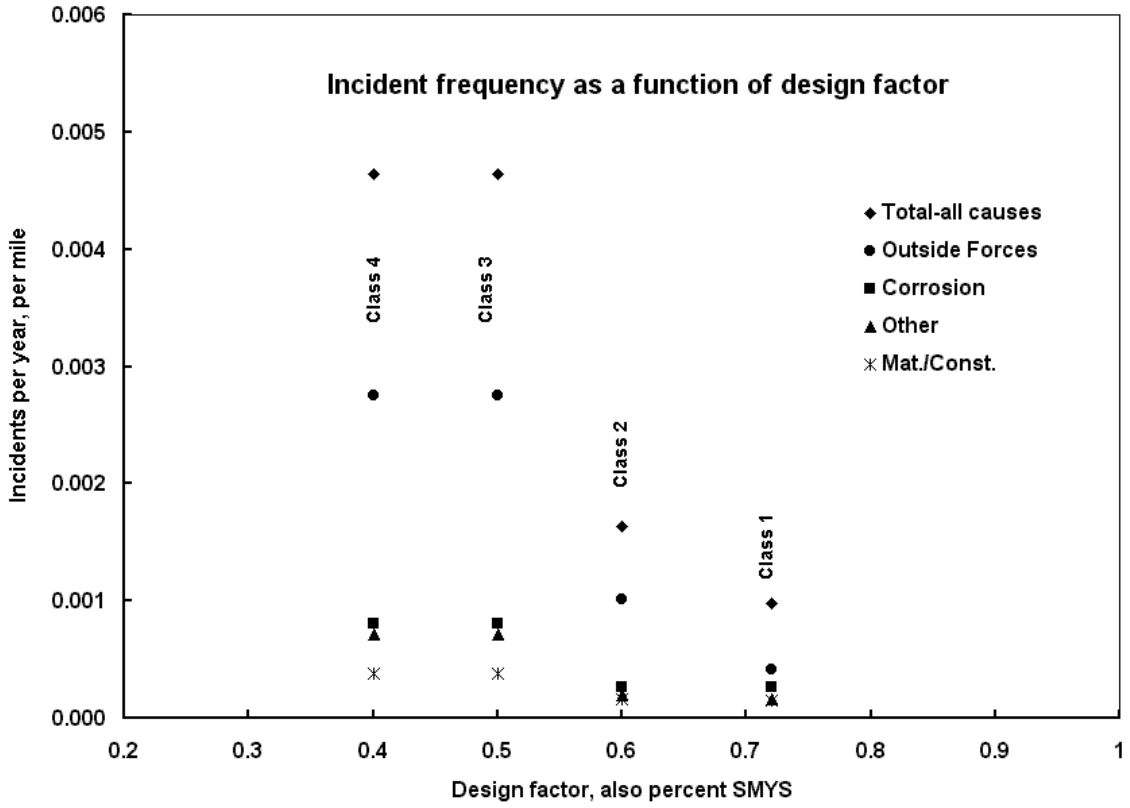

Figure C1. Incident frequency as a function of design factor (mileage uncertainty for the sample versus the total system could cause these trends to shift slightly)

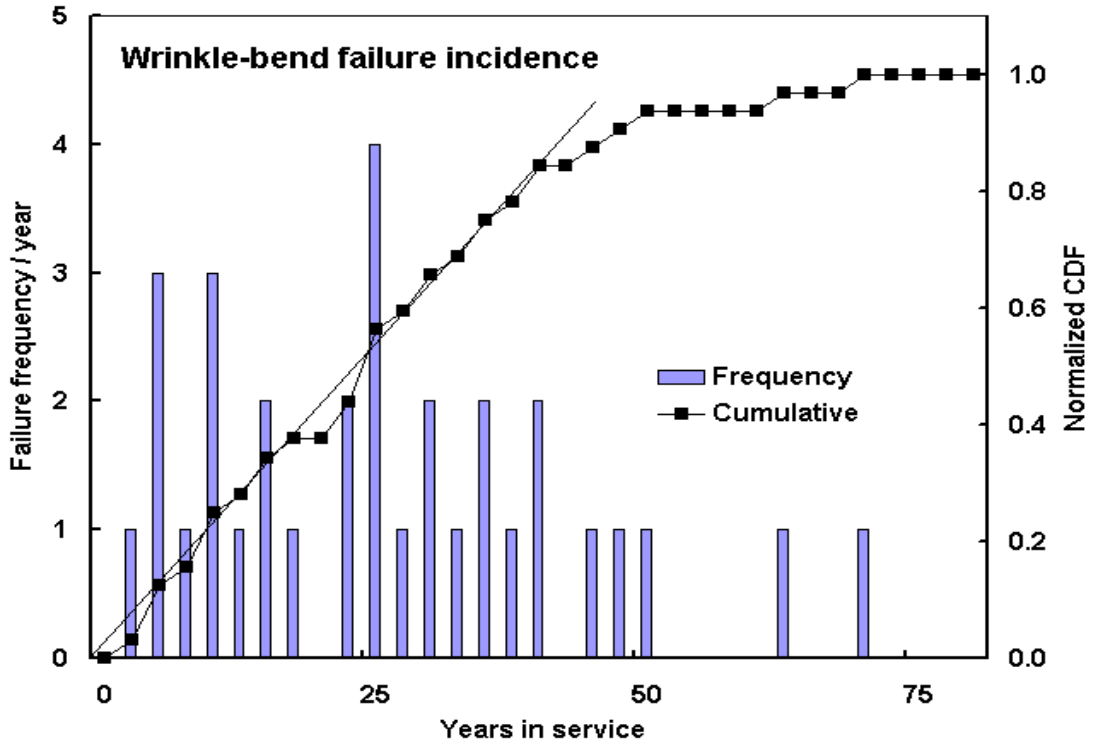

Figure C2. Failure experience for wrinkle-bends as a function of time in service

Appendix D – Codes, Standards, and Regulations

Because bends and wrinklebends are unique to pipeline construction, several industry codes, standards, and regulations address such features. This section reviews applicable industry codes and standards, and country regulations, to identify what guidance exists relative to wrinklebend integrity assessment.

Language regulating bends can be found in ASME B31.4[(1)] and B31.8[(2)], which underlie pipeline codes worldwide. This language deals with field-bend quality in generic terms, with specific paragraphs addressing wrinklebends. Language dealing with field-bend quality in generic terms likewise can be found in country codes and regulations around the world. Language for the US[(3)], Canada[(4)], Australia[(5)], and Norway[(6)] is presented in addition to that of the ASME to illustrate some typical provisions for bends in onshore and offshore applications.

The ASME B3l Code for Pressure Piping, Sections 4[(1)] and 8[(2)], address field bends in paragraphs 406.2.1 and 434.7.1 for liquid pipelines and paragraph 841.231 for gas pipelines. This language requires field bends to be free of buckles, cracks, mechanical damage, and excessive wall thinning. B31.4 further requires that the pipe diameter may not be reduced by more than 2.5 percent, with the further stipulation that bends must pass a sizing pig. Wrinklebends are permitted in gas pipelines with severe restrictions on their application, but are prohibited in liquid pipelines. Both standards are silent on minor ripples. Regarding wrinkles, ASME/ANSI B31.8 paragraph 841.231 (f) contains the same language that is applied to new designs, while as expected paragraph 406.2.4 of ASME/ANSI B31.4 excludes their use.

US federal regulatory codes are set forth in Parts 192 and 195 of Title 49 of the Code of Federal Regulations (49 CFR)[(3)]. Language addressing field bends is found in paragraphs 192.313 (gas) and 195.212 (liquid). Both regulations state that bends must not “impair the serviceability” of the pipe, and must be free of buckles, cracks, or other mechanical damage, and must have a "smooth contour". Neither “impair serviceability” nor “smooth contour” have clear prescriptive interpretation in the regulations. Impair serviceability pushes toward exclusion of features like wrinklebends whereas smooth contour could be viewed less stringent. It is possibly because of concern for impairing serviceability that wrinklebends are excised from gas pipelines when they are exposed, whereas their failure history does not suggest such is always necessary.

Paragraph 192.315 (gas) applies specifically to wrinklebends. It limits use of wrinklebends to steel pipe operated at a wall stress less than 30-percent of SMYS, and further states bends must be free of sharp kinks, and that adjacent wrinkles must be separated by at least one diameter. It imposes a maximum wrinkle height for larger-diameter pipe, and stipulates that in seamed pipe the seam must lie close to the neutral bending plane. While Part 192 allows wrinkles for gas pipelines, the opening sentences of paragraph 195.212 preclude their use in liquid pipelines.

The Canadian regulatory position for oil and gas pipelines is the Canadian Standards Association (CSA) Standard Z662[(4)]. Paragraph 6.2.3 of this industry consensus contains language for field bends. It states that bends must be free of buckling, cracks, and other mechanical damage, and requires they pass internal inspection tools and scrapers. Such performance-based language is consistent with the National Energy Board approach, which embeds adopts this philosophy. With a view to piggability, this standard also includes a prescriptive limit on bend dimensions, limiting the difference between maximum and minimum diameters to less than 5-percent of the specified diameter.

The Australian pipeline code, Australian Standard (AS) 2885[5] is an industry consensus standard built on a performance philosophy similar to the approach adopted in Canada. This standard permits mild ripples in field bends within limits that trace to the work done by Murray and Bilston[e.g., 6-8]. The ripples must not exhibit a peak-to-valley dimension in excess of 5 percent of the center-to-center dimension between ripples. Alternatively, the ratio of ripple pitch to amplitude must exceed 20. This code also includes a practical limit on strain to avoid damage to mill-applied coatings, which requires the strain to be the lesser of the tolerance of the pipe coating, or 10 percent.

The standard Norway's offshore pipelines that also is broadly adopted offshore pipelines, Det Norske Veritas (DNV) OS-F101[9], currently permits "minor buckles". Such features are permitted in the inside radius profile of the bend under three conditions. Their height and depth must be less than 1-percent of the pipe's nominal inside diameter, their length-to-depth ratio must be greater than 12, and their spacing must be greater than one nominal diameter.

The ASME, CSA, and AS codes include indices of fatigue performance for bends (and wrought elbows) in the form of Markl-type stress intensification factors, often denoted SIFs or i-factors [1], in the manner of the ASME Boiler and Pressure Vessel Code. These factors consider the basic dimensions of pipe diameter, pipe wall thickness, and bend radius, being are applicable to flexibility analysis for thermal expansion or other displacement controlled loadings on unrestrained piping systems. Continuing in the vein of plant piping, the Pipe Fabrication Institute (originally the Power Piping Society) maintains engineering and fabrication standards for shop-fabricated bends. This standard[10] permits "mild ripples" to create bends if the maximum peak-to trough height is less than 3-percent of the nominal pipe size, and ratio of distance between ripple crests to ripple height exceeds 12. While reflecting workmanship rather than performance, this requirement is less stringent than aspects of both the Australian and Norwegian standards for transmission pipelines.

Summary

Industry codes, standards, and regulations address bends in generic quality-related language and comment specifically on wrinklebends selectively, they fall short of quantitative guidance in reference to wrinklebend integrity assessment. Some codes incorporate indices of fatigue performance for bends in the form of stress intensification factors in the manner of the ASME Boiler and Pressure Vessel Code, which would support such analysis if deemed adequate.

References

1. Anon., ANSI/ASME Code for Pressure Piping – B31.4 Liquid Petroleum Transportation Piping Systems, ASME.
2. Anon., ASME/ANSI Code for Pressure Piping – B31.8 Gas Transmission and Distribution Piping Systems, ASME.

---

[1] i-factors originally were developed empirically by Markl[e.g., 11] from a large number of displacement-controlled cyclic bend tests for circumstances that simulate flexural loadings in piping expansion loops for use in plant piping and pressure vessels rather than transmission pipelines.

3. Anon., Code of Federal Regulations, Title 49 -Transportation, Parts 192 and 195, October 2001
4. Anon., Oil and Gas Pipeline Systems, Canadian Standards Administration, CSA Z662, 1999.
5. Anon., Pipelines -Gas and Liquid Petroleum, Council of Standards, Australian Standard AS 2885.
6. Murray, N. W., and Bi1ston, P., "Rational Acceptance Limits for Field Bends in Oil or Gas Pipelines", International Conference on Pipeline Reliability, Paper V-2, CANMET, Calgary, June 1992: see also Murray, N. W. and Bilston, P., "Local Buckling of Thin-Walled Pipes being Bent in the Plastic Range," *Thin-Walled Structures*, 1992, p. 411-434.
7. Bilston, P, and Murray, N. W., "Evaluation of Factors Affecting Field Bending, Characteristics of Line Pipe", 9th Biennial Joint Technical Meeting on Line Pipe Research, PRC/EPRG, Paper 6, Houston, May 1993.
8. Bilston, P, and Murray, N. W., "The Role of Cold Field Bending in Pipeline Construction", 8th Symposium on Line Pipe Research, PRCI, Paper 27, Houston, September 1993.
9. Anon., DNV OS-Fl01, Submarine Pipeline Systems, Det Norske Veritas, January 2000
10. Anon., PFI ES 24, "Pipe Bending Methods, Tolerances, Process and Material Requirements", Pipe Fabrication Institute, Revised 1992, pp. 1-6.
11. Markl, A. R. C., "Fatigue Tests of Piping Components", Paper No. 51, PET-21, Transactions, ASME, 1952.

Appendix E – Literature on Wrinkles, Buckles, and Dents

While not dealing specifically with wrinklebends, there is an extensive literature that helps to characterize stresses and strains associated with wrinkles and buckles, which could be useful in developing criteria to assess wrinklebend integrity. This section reviews the literature as a supplement to trends derived from reports on wrinklebend field studies and in-service failures as presented in Appendix B. The objective is to identify what has been done to date in mechanics analysis potentially relevant to wrinklebend integrity assessment.

The most comprehensive prior review of this literature was relevant to specifically to ripple-bends and done by Bilston[1]. His work began in 1990 as part of a Doctoral thesis developed under funding from the Australian Pipeline Industry Association (AIPA). In 1991 the PRC joined this effort. Bilston's work, reported in collaboration with his thesis advisor[e.g. see 1-4], was directed at allowable limits for ripple-bends made with modern bending machines. About the same time, Olson et al[5] began an independent evaluation of comparable features under funding from the PRC (now the PRCI). These efforts became collaborative under the direction of the funding organizations, to limit duplication. As AIPA's efforts preceded those of the PRCI, Olson's literature review relies on that by Bilston.

The PRCI work as well as that funded by the AIPA effort was motivated by the same issue – field bending difficulties experienced when using modern bending machines. This same issue also motivated earlier PRCI work by Williams and Eiber[6], and its follow-on project[7]. The work done for the AIPA and the PRCI directed at ripple-bends in transmission pipelines was subsequently more broadly published[8,9]. Rosenfield[10] has recently summarized much of the above literature, and thereafter developed an approach to assess ripple-bend integrity[12].

In contrast to work motivated by pipe-bending problems, analysis work by Murray specifically addressed wrinklebend integrity[11]. Other analytical work dealt with buckles formed in pipelines under settlement and such loads[12-15], although their experiments[e.g., see 13,14] produced features comparable to the wrinkles shown earlier in Figures B1, B2, B4 and B5. Experiments on wrinklebends also was the focus of work by Keifner and Alexander[16] that was funded by the American Petroleum Institute (API).

Work potentially relevant to failure at wrinkles and ripples done for transmission pipeline steels involves the integrity of dents. Keifner and Alexander[17] evaluated dent fatigue resistance in work funded by the API. Leis and Hopkins[18] completed a gaps analysis for mechanical damage for the PRCI that included consideration of dent-acceptance criteria, including comments on wrinkled or kinked dents. Rosenfeld[19] has discussed dent acceptance criteria. Battelle[20] and others[e.g., see 21] have done work on kinked dents that might be particularly relevant to kinked bends. Work directed more at bends in plant piping also has been done[22-24].

[12] Reference 40 limits its coverage to ripple-bends and explicitly excludes wrinklebends.

Work Under the Auspices of the AIPA

The AIPA carried out a series of investigations concerning the formation of ripples in field bends. One of the early publications[2] considered possible modes of deformation during field bending, including ovalization, wall thickness variation, wrinkling or rippling, as well as the formation of a nonuniform bend radius (kinking/buckling). Rather basic analysis was done to identify limits on deformation. The adverse effect of wrinkling on coating integrity was recognized as well, but there was no evaluation of the effect of wrinkles/ripples on pipe integrity.

Subsequent work[1,3,4] evaluated the effects of ripples on pipe integrity in terms of elastic buckling theory. Theoretical predictions of buckle wavelength made based on the elastic theory were a poor match for those actually measured. However, after a simple allowance for inelastic effects the actual wavelength were accurately predicted. A prototypical ripple, termed a buckle in Bilston's work, was used to characterize the ripple shape. This shape was the basis to evaluate integrity aspects of ripple-bends. Their prototypical shape looked like an outward smooth ripple with respect to the bend surface, whose shape was apparently influenced strongly by what was observed in field bends. Figure E1, reproduced from Reference 1, illustrates this ripple and related geometric details. This sinusoidal profile was used to develop a relationship between bending angle and length change in the bend's intrados. From this and the underlying assumed ripple geometry, relationships were developed between strain at the crown of the ripple and the ripple height, as well as the residual bend angle. Predictions with the results of this deformed-shape analysis were found to agree reasonably well with laboratory-scale experiments made using 3.5-inch diameter thin-wall pipe, and limited full-scale results. Figure E2 illustrates Bilston's laboratory bending machine, which was designed to replicate commercial equipment. Typical relationships developed between the ripple parameters defined by Bliston et al based on their analyses are presented in Figure E3.

Full-scale tests done in part to validate the modeling provide insight into the integrity of ripple-bends under pressure loading. By way of example, one bend in 16-inch x 0.25-inch wall pipe made of X42 pipe produced mild ripples about 0.21-inch high. At a pressure corresponding to a hoop stress of 115 percent of specified minimum yield stress (SMYS) the measured strain in the crown of the ripple was only 0.4 percent. Not surprisingly, continued pressurization caused failure remote to the ripples at a pressure corresponding to a hoop stress of 140 percent of SMYS. The results of this work evidently led to acceptance of mild ripples up to 50 percent of the wall thickness in the Australian pipeline code.

With reference to ways to produce bends noted much earlier, Bilston's model reflects bends created by foreshortening the intrados through formation of small buckles. As pipe diameter, wall thickness, and their ratio contribute to the extent of this buckling all else being equal, it is possible that behavior different than that characterized in Figures D3a and D3b will develop. As will thickness increases one can anticipate a contribution of stretching and thinning along the extrados whose influence is not embedded in this model of ripple-bending.

Work Under the Auspices of the PRCI

The PRCI also funded work on ripple formation and integrity in bends in the late 80s, and into the early to mid 90s. The initial empirical work[6,7] focused on field reports of increased

susceptibility to wrinkles formed during cold bending of pipe coated with fusion-bonded epoxy[13]. The earliest work[6] suggested the possible role of discontinuous yielding, while the follow-on effort evaluated that possibility[7]. The latter effort characterized mechanical properties and wrinkling tests were performed using four combinations of pipe geometry and properties. This included samples of 8-inch NPS by 0.172-inch wall API 5L Grade X42 pipe, l2-inch NPS by 0.203-inch wall X42 pipe, l2-inch NPS by 0.250-inch wall X52 pipe, and 24-inch by 0.375-inch wall X52 pipe. The properties tests indicated discontinuous yielding was not a factor whereas residual stresses introduced by the coating process were considered a potential contributor. However, the work did not consider the effect of wrinkles on pipe integrity.

The integrity of these ripple-bends was addressed in the subsequent work of Olson et al[5] and in the parallel and initially independent work of Bilston. Olson et al supplemented Bilston's work with full-scale tests that evaluated the fatigue resistance of ripples created in two cold field bends made in large-diameter line pipe coated with FBE. One pipe, designated "A", was 30-inch x 0.300-inch wall X70 pipe. This pipe contained one large wrinkle whose depth was 1.5 times the thickness or 1.5-percent of the pipe's diameter, and several smaller wrinkles. A second sample designated "B", involved 36-inch x 0.385-inch wall X65 line pipe. This pipe contained one large wrinkle having a depth of 1.5 times the thickness or 1.7-percent of the pipe's diameter, and like the first had several smaller wrinkles as bent but these were removed prior to testing. The ripples in both specimens appear to consist of primarily inward deformations, as was shown earlier in Figure B5. File records indicate the residual bend angles ranged from 0.51 degrees (~no ripples) to 7.26 degrees (significant rippling). The as-made sizes of the largest ripples in both bends would have been rejected for use in pipeline construction.

Each bend was end-capped, filled with water, and subjected to a simulated hydrotest, after which they were subjected to pure-bending fatigue. Pressure loading to wall stresses comparable to hydrotest levels opens the ripples on unrestrained bends. This decreases their heights and increases their lengths as compared to the measurements noted above. Ripple dimensions were not measured again following the simulated hydrotest. The hydrotest for Specimen A was to 100-percent of SMYS, while that for Specimen B was to 108-percent of SMYS. The pressure volume plot for Specimen A was linear, while that for Specimen B was nonlinear beyond ~85-percent of SMYS.

Four- point (pure) bending was used to create a uniform stress field over the region of the bend, being imposed using the load frame is shown in Figure E4. Specimen A was cycled for 75,864 cycles at a tension-tension peak (exterior surface) stress range equal to 19,775 psi, which then was increased to 24,375 psi for an additional 9,133 cycles. Failure occurred at a circumferentially oriented fatigue crack at a valley between ripples. Specimen B was cycled for 75,000 cycles at a tension-tension peak (exterior surface) stress range equal to 21,125 psi, and then 67,726 cycles of a stress range equal to 29,675 psi. This specimen failed at a circumferentially oriented fatigue crack located in a girth weld about one diameter from the

---

[13] Depending on coating conditions that involve heating the pipe's surface to about 240ºC (~460ºF), strain aging and other changes in mechanical properties can occur. Such temperatures are too low and imposed for too little time to appreciably effect residual stress fields developed during pipe making, but, depending on the heating practice and prior pipe temperature could induce a near-surface compressive residual stress field.

ripples. This weld was included in the test section with the view to illustrate failure there was more likely than at the ripple.

Olson et al applied Bilston's for an isolated ripple to estimate local strains for use in a critical-location analysis[25] of fatigue resistance. As with most analysis methods, when the data needed to implement this approach is available it accurately predicts fatigue resistance. This has been demonstrated in blind predictions made for structural components under random service histories[e.g., 26], which is far more complex than the present almost constant amplitude experiments. Recognizing the need for relatively accurate local strains and stresses for inputs to this approach, Olson et al modified Bilston's isolated ripple model with a flexibility factor empirically calibrated for this application to account for the adjacent ripples. Good comparison was achieved between predicted and measured strains – although this might be expected given foreknowledge of the correct answers and provision for "calibration" through disposable coefficients embedded in the flexibility factor. Calculated strains were used in conjunction with a damage parameter[27] that was developed to account for mean stress effects like that likely in the area where cracking originated. Mean stress for this purpose was developed using typical mechanical properties for the two steel grades involved, and hysteresis analysis of the pressure cycling imposed. The resulting mean stresses were near yield, which is anticipated for these pressure histories. Fatigue resistance was characterized in terms of this damage parameter based on polished smooth-specimen fatigue test data, with no effort made to account for differences in surface quality between the pipe surface where cracking initiated and the specimens. Literature guidance[e.g., 28] indicates such differences at long lives make smooth-specimen data conservative by factors the order of 10 to 100 depending on the relative differences in surface quality.

The effort invested in accurately estimating stresses and strains for use in fatigue analysis was rewarded as the approach developed correctly predicted the failure site in the valley between two ripples. While the failure site was correctly predicted, the fatigue life was over-predicted by a factor of ~50. In a world where duplicate experiments often scatter by this amount or more at long lives[29], these predictions are viable. Likewise, they are viable in that predicted life was based on polished smooth-specimen data without adjustment for the typical pipeline surface conditions, where such differences are known to cause differences in fatigue life of the same order[28]. Retrospective analysis that was done as part of this project indicates almost exact predictions result when differences in surface-quality are addressed.

Also working under funding from the PRCI, Rosenfield et al[10] have developed an approach to assess ripple-bend integrity that according to constraints reported therein preclude its use for the analyses of fatigue in wrinkles. This work, were it reported by the middle 90s, might have had an impact on the present work-scope.

Rosenfeld et al combined insight from numerical methods with traditional strength-based fatigue analysis to develop their method, whose virtue lies in its direct utility in field problems. As yet, their formulation has not been broadly validated, although this aspect was addressed in their report. Such utility, coupled with blind experimental validation, were among the objectives of the joint-industry project team that originally funded the present work dealing with wrinklebends.

Work Under the Auspices of the API

Kiefner and Alexander[8] conducted pressure-cycle fatigue tests on three pipe specimens that were field-bent with intentional wrinkles of different severities under funding from the API. The

specimens were formed from 36-inch by 0.281-inch wall X60 line pipe using a standard pipe-bending rig, but without use of the internal mandrel. Wrinkles having depths of 1.7, 3.7, and 6.9 percent of the pipe diameter were produced. Measured profiles for the wrinkles are shown in Figure E5, which is usual of Euler buckling and are not anticipated normally if a mandrel is used. While the work of Rosenfeld et al[10] was not directed at wrinklebends, they comment therein on these tests, noting the "features went far beyond what is envisioned as potentially acceptable, but served adequately for test purposes".

The pipe bends were capped and the pups pressure cycled to produce a hoop stress range between 12 and 84 percent of SMYS. The 6.9-percent wrinkle failed by fatigue in 1,086 cycles, that at 3.7 -percent wrinkle failed in 2,791 cycles, whereas the 1.7 -percent wrinkle survived 44,541 cycles without failure or evidence of cracking. These results show a pronounced adverse effect of severe wrinkle-like deformations on the fatigue life under internal-pressure cycling. Such occurred for pressure cycles a maximum stress beyond code acceptable levels, coupled with a stress ratio of ~0.14. Were such cycling done at a stress ratio the order of 0.7 or higher, the lives in the cases where failure occurred would have been orders of magnitude longer, tending to produce no failure as occurred in the experiments for the least severe wrinkle. Absent a means to generalize these test results for application to other wrinkle sizes in other pipe geometries, such tests provide only insight – with potential value as data to test the means to predict such behavior once it is developed. The means to predict failure at wrinkles subject to pressure cycles was another objective of the joint-industry project team that originally funded the present work dealing with wrinklebends.

Related Work on Deformation in Pipes

Murray[11] recently has addressed wrinklebend integrity. His approach is an adaptation of bellows technology[e.g., see 30] and his earlier work with Bilston. Murray developed results that characterized the maximum stress due to bending for a variety of bellows configurations. As the shape of the convolution in a bellows is much different than a wrinklebend, the results are of interest but unlikely of great value for the present project. Nevertheless, this work was considered in formulating the approach used later to evaluate wrinklebend integrity.

Other analytical work has dealt with buckles formed in pipelines under settlement and such loads[12-15]. The experiments[e.g., see 13,14] done in support of validating this work has produced features that are comparable to the wrinkles shown earlier in Figures B1 to B3. A very robust numerical approach underlies the analyses, which appears sufficiently general to be adapted to wrinklebends, as well as ripple-bends. Parametric analyses were conducted focused primarily on geotechnical issues such as differential settlement. Criteria are presented for various limit states developed in reference to such applications[13]. These address concerns such as ovality, and wrinkling due to buckling, which for the problem address could involve some soil-induced restraint. They note strain is a better criterion for wrinkling that deformation, particularly in reference to the onset of the phenomenon, but fall short of presenting results specifically useful for present purposes. However, the work is instructive in reference to pipe instability. It was considered in formulating the approach adopted later in formulating an approach to evaluate wrinklebend integrity and in developing acceptance criteria for wrinklebends.

Work on dents is potentially useful in application to wrinklebends, although some effort would be needed to demonstrate its applicability. Keifner and Alexander[17] evaluated dent fatigue resistance in work funded by the API. Leis and Hopkins[18] completed a gaps analysis for

mechanical damage for the PRCI that included consideration of dent-acceptance criteria, whereas Rosenfeld[20] has discussed dent acceptance criteria. Battelle[20] and others[e.g., see 21] have done work on kinked dents that might be particularly relevant to kinked bends. The techniques used to develop these acceptance criteria could be of value in guiding work done for wrinkles. If a criterion directly applicable to wrinkles, and more specifically wrinklebends is developed, such results might be useful to test its utility. However, because buckle formation is inherently different that that of contact-induced denting, and because their shapes are significantly different, it is unlikely one can validate methods used to analyze wrinkles or buckles by demonstrating utility in application to dents.

Work directed more at bends in plant piping also has been done. Tests on large-radius bends containing mild ripples were reported by Arav[22]. Thomas[23] carried out parametric studies at Westinghouse Advanced Reactor Division in connection with the now-defunct US Liquid Metal Fast Breeder Reactor (LMFBR) program. Finally, Wang and Cao[24] considered the wrinkling limit for tube bending.

Arav[22] did experiments on large-radius bends containing mild ripples apparently in reference to his work for a boiler manufacturer. His specimens were made of 8-inch and 14-inch pipe with bend radii equal to four or ten times the pipe diameter. Ripple heights were one to two times the wall thickness or three to five percent of the diameter. Profile data suggests that ripple crests protruded from the mean pipe surface while the troughs were reentrant. Strain gages were used to measure actual strains throughout the bends as they were subjected to static end moments. Stress intensification factors (SIFs) were reported as the ratio of stress inferred from measured strain in the ripples to the longitudinal stress in straight pipe. After some analysis, i-factors were determined whose value lay between 1.2 and 3.0. Arav also described a theoretical computation of the SIF that arises from the geometry of the ripples. His model employed a representative strip cut perpendicular to the crown of the ripple, which is comparable to the approach adopted by Bilston. The SIFs calculated on the basis of this model agreed reasonably well with the SIFs derived from strain measurements in the static load tests. SIFs are a common code approach to reflect the severity of local geometric discontinuities. This approach was considered when formulating the approach used later to assess wrinklebend severity.

Thomas[23] carried out parametric numerical studies using a finite difference technique in reference to nuclear plant piping. He evaluated the effects of geometric imperfections such as ripples on the intrados, and other aspects like ovality and longitudinal weld seam shrinkage. This was done in reference to clam-shell elbows with D/t of 40 to 80. Much of these analyses considered bends with a nominal diameter of 36 inches and wall thickness of 0.5 inch, which is comparable to some transmission pipeline applications. The effects of applied bending loads and internal pressure were evaluated. Ripples were modeled using a sinusoid pattern with respect to the mean surface (so crests were bulged outward and troughs were reentrant). Ripple size varied with position around the intrados, although the basis for this was unclear.

Thomas' results for his unique ripple geometry indicated that such ripples along the intrados whose size was three-percent of the diameter caused the in-plane bending stresses to double. While the ripple effects were indicated to be larger on stresses due to internal pressure, they appeared relatively insensitive to the ratio of bend radius to pipe radius for values lying between two and five. For high-D/t bends, the local stresses peaked for ripples about two-percent of the pipe diameter. Like Thomas, the approach adopted to evaluate wrinklebend integrity used parametric analyses.

Wang and Cao[24] considered the wrinkling limit for tube bending in reference to concerns for plant-manufactured tubing and challenges related to weight reduction and enhanced manufacturing processes. Their work considered limits on tube bending practices where the bend is produced by stretching and thinning in tensile fibers, where rippling along the intrados is apparently unacceptable. This approach represents an alternative to pipe bending. Used without consideration of foreshortening along the intrados as considered in this paper the drawbacks include a thinner cross-section and heavily work-hardened pipe wall, which might preclude the practice. However, used in conjunction with current methods, this practice might prove practical. Until such time, the technology and results of this work remain beyond present-day practical interests.

Summary

While not dealing specifically with wrinklebends, literature was evaluated to identify information and trends potentially useful in assessing wrinklebend integrity. Mechanics analyses were found specific to wrinkles under pressure[11] and bending (differential settlement) loads[12-15]. However, none of this was directly useful in meeting the objectives of this project. Data were found that are directly useful in validating any criterion for wrinkle integrity, which considered in the report text. This includes the ripple-bends tested by Olson et al[5], and wrinklebends pressure cycled by by Keifner and Alexander[16].

References

1. Bilston, P., "The Modelling of Compression Buckles Formed During the Cold Field Bending of Line Pipe," Thesis for degree at Monash University, December 1993: see also Murray, N. and Bilston, P., Final Report of APIA Cold Field Bending Research Team, Monash University, July 1993 – proprietary to APIA/PRCI.
2. Murray, N. W., and Bi1ston, P., "Rational Acceptance Limits for Field Bends in Oil or Gas Pipelines", International Conference on Pipeline Reliability, Paper V-2, CANMET, Calgary, June 1992: see also Murray, N. W. and Bilston, P., "Local Buckling of Thin-Walled Pipes being Bent in the Plastic Range," *Thin-Walled Structures*, 1992, p. 411-434.
3. Bilston, P, and Murray, N. W., "Evaluation of Factors Affecting Field Bending, Characteristics of Line Pipe", 9th Biennial Joint Technical Meeting on Line Pipe Research, PRC/EPRG, Paper 6, Houston, May 1993.
4. Bilston, P, and Murray, N. W., "The Role of Cold Field Bending in Pipeline Construction", 8th Symposium on Line Pipe Research, PRCI, Paper 27, Houston, September 1993.
5. Olson, R. J., "Evaluation of the Structural Integrity of Cold Field-Bent Line Pipe, PRCI Report PR-3-9214, May 1996: see also Olson, R., Clark, T., and Odom, T., "Evaluation of the Structural Integrity of Cold Field Bent Line Pipe", 10th Biennial Joint Technical Meeting on Line Pipe Research, EPRG/PRC, Paper 6, April 1995, Cambridge
6. Williams, D. N. and Eiber, R. J., "Cause of Wrinkling of Epoxy-Resin-Coated Pipe During Field Bending," Battelle Report to Columbia Gas Transmission Corporation, May, 1981.
7. Williams, D. N., "Investigation of Field Bending Problems in Line Pipe", NG 18/HLP Joint Technical Meeting on Line Pipe Research, Columbus, OH, American Gas Association, Paper 16, September 1984.
8. Murray, N. W. and Bilston, P., "Elasto-Plastic and Strain-Hardening Bending of Thin Steel Pipes in the Pre-Buckling Region," *The Institution of Engineers*, Paper C 91043, September 1991.

9. Murray, N. W. and Bilston, P., "Local Buckling of Thin-Walled Pipes being Bent in the Plastic Range," *Thin-Walled Structures*, 1992, p. 411-434.
10. Rosenfeld, M. J., Hart, J. D., and Zulfiqar, N., "Acceptance Criteria for Mild Ripples in Pipeline Field Bends", Draft PRCI Report PR-218-9925, December 2002: see also Rosenfeld, M. J., Hart, J. D., and Zulfiqar, N., and Gailing, R. W., "Development of Acceptance Criteria for Mild Ripples in Pipeline Field Bends", Proceedings of the 4th International Pipeline Conference, Alberta, Canada, September 29-October 3, 2002.
11. Murray, N. W., "Stress Analyses of Wrinkle Bends in Pipelines," *Thin-Walled Structures*, 1993, p. 65-80.
12. Murray, D. W., "Local Buckling, Strain Localization, Wrinkling and Postbuckling Response of Line Pipe," *Engineering Structures*, Vol. 19, No. 5, pp. 360-371, 1997.
13. Zhou, Z. and Murray, D. W., "Numerical Structural Analysis of Buried Pipelines", Civil Engineering Structural Engineering Report No. 181, Chapters 7 and 8, University of Alberta, February 1993: see also Zhou, Z. and Murray, D. W., "Analysis of Post-Buckling Behavior of Line Pipe Subjected to Combined Loads, International Journal of Solids and Structures, Vol. 32, pp. 3015-3036, 1995.
14. Mohareb, M. et al, "Laboratory Testing of Line Pipe to Determine Deformation Behavior", ASME-OMAE, Volume 5, Glasgow, 1993, pp. 109-114. Mohareb, M., Kulak, G. L., Elwi, A., and Murray, D. W., "Testing and Analysis of Steel Pipe Segments, Journal of Transportation Engineering, Vol. 127: 408-417, 2001.
15. Zhou, Z. and Murray, D. W., "Behavior of Buried Pipelines Subjected to imposed Deformations", ASME-OMAE, Volume 5, Glasgow, 1993, pp. 115-122.
16. Kiefner, J. F., and Alexander, C. R., Addendum to API Publication 1156, "Effects of Smooth and Rock Dents on Liquid Petroleum Pipelines, Phase 2", September 1999.
17. Kiefner, J. F., Alexander, C. R., and Fowler, J. R., "Repair of Dents Containing Minor Scratches", 9th Symposium on Line Pipe Research, Paper 9, PRCI, Houston, Texas, USA, 1996: see also Fowler, J. R., Alexander, C. R., Kovach, P. J. and Connelly, L. M., "Fatigue Life of Pipelines with Dents and Gouges Subjected to Cyclic Internal Pressure", PD-Vol. 69, *Pipeline Engineering*, ASME, 1995 or 10th Biennial Joint Technical Meeting on Line Pipe Research, EPRG/PRC, Cambridge, UK, 1995, pp 15-1-15-20.
18. Rosenfeld, M. J., "Proposed New Guidelines for ASME B31.8 on Assessment of Dents and Mechanical Damage", GRI 01/0084, 2001: see also Rosenfeld, M. J., "Investigations of Dent Re-Rounding Behavior," Proceedings International Pipeline Conference – 1998, Volume 1, pp 299-308, ASME, 1998.
19. Leis, B. N. and Hopkins, P., "Mechanical Damage Gaps Analysis", in 14th PRCI-EPRG Joint Symposium, Berlin, 2003, pp. 30.1-15.
20. Dinovitzer, A., et al "Geometric Dent Characterization", 4th International Pipeline Conference, pp. IPC2002-27076.1-10, 2002
21. Leis, B. N., Forte, T. P., and Zhu, XianKui, "Integrity Analysis for Dents in Pipelines", International Pipeline Congress, Calgary, October 2004, ASME, IPC04-0061, 12 pages.
22. Arav, F., "Evaluation of Pipe Bends Having Local Corrugations", 3rd International Conference on Pressure Vessel Technology, ASME, 1977, pp. 193-205
23. Thomas K., "The Effects of Geometric Irregularities on the Design Analysis of Thin-Walled Piping Elbows", Century 2 PVP Conference, 80-C2/PVP-43, ASME, San Francisco, August 1980.

24. Wang, Xi and Cao, Jian, “Wrinkling Limit in Tube Bending,” *Transactions of the ASME, Vol. 123*, October 2001, p. 430-435.
25. Morrow, J. D., Wetzel, R. M., and Topper, T. H., “Laboratory Simulation of Structural Fatigue Behavior,” Effects of Environment and Complex Load History on Fatigue Life, ASTM STP 462, American Society for Testing and Materials, 1970, pp. 74-91.
26. Leis, B. N., "An Approach for Fatigue Crack Initiation Life Prediction with Applications to Complex Components", in Fatigue Life of Structures under Operational Loads, Proceedings of the 9th International Committee on Aeronautical Fatigue Meeting, ICAF Doc. 960, Laboratorium fur Betriebsfestigeit, Germany, May 1977, pp. 3.4/1-47.
27. Leis, B. N., "An Energy-Based Fatigue and Creep-Fatigue Damage Parameter", *Journal of Pressure Vessel Technology*, Trans. ASME, Vol. 99, No. 4, November, 1977, pp. 524-533:
28. Abelkis, P. R., “Fatigue Strength Design and Analyses of Aircraft Structures: Part I, Scatter Factors and Design Charts,” AFFDL-TR 66-197, June 1967.
29. Leis, B. N., “Effect of Surface Condition and Processing on Fatigue Performance,” ASM Handbook, Vol. 19, ASM International, 1996, pp. 314-320.
30. Takezono, S., Inoue, K., Ogasawara, H., and Kato, Y., “Stress Analysis of Expansion Joints of Pressure Vessels under Internal Pressure,” *Bull. of the JSME*, Vol. 14, No. 74, p. 753-760, 1971.

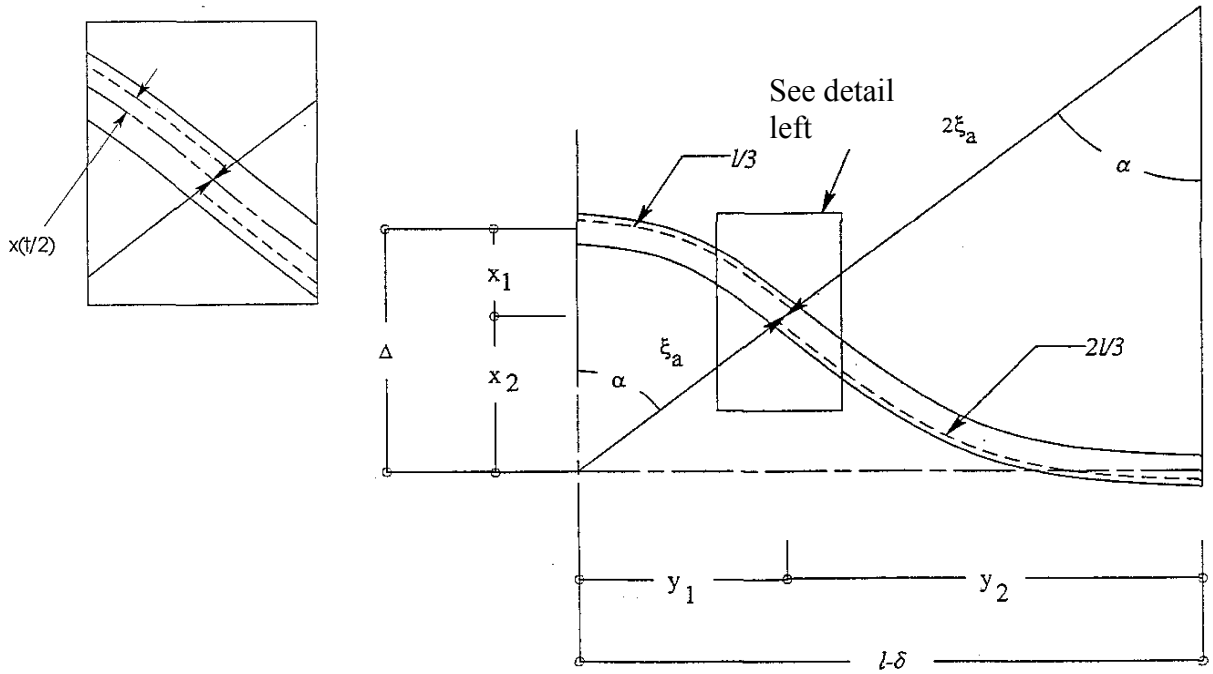

Figure E1. Bilston's ripple shape and related geometric details to determine Δ

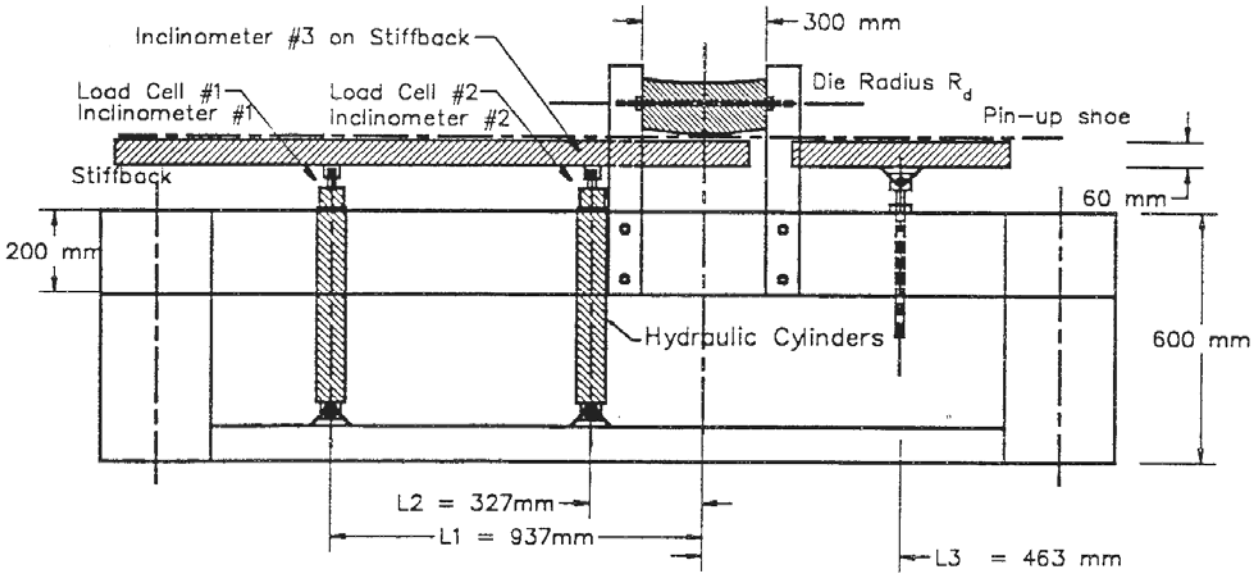

Figure E2. Bilston's laboratory pipe bending machine

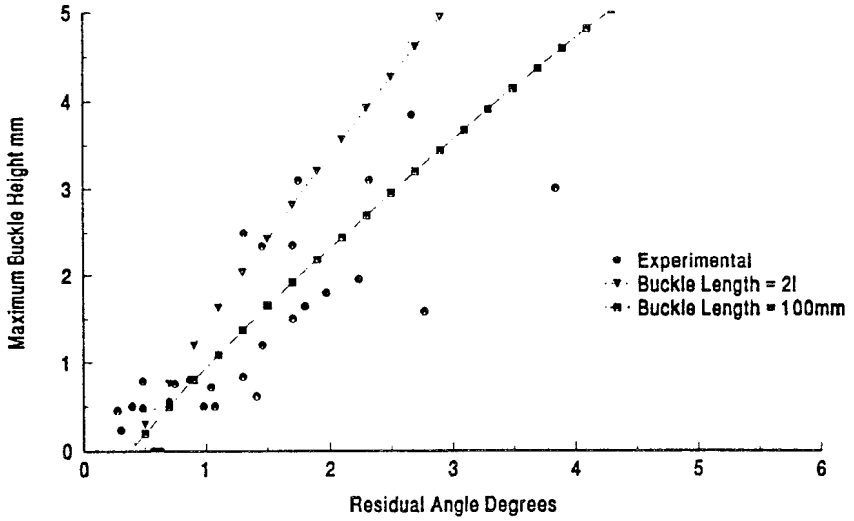

a) experimental trends in wrinkle height vs. residual bend angle

wrinkle height

$$\Delta = 3\left(\frac{l}{3\alpha} - x\frac{t}{2}\right)(1-\cos\alpha)$$

wrinkle strain

$$\varepsilon_e = -\frac{t(1+x)}{2}\frac{1}{2\zeta_a} = -\frac{t(1+x)}{2}\left(\frac{3\alpha}{2l-3\alpha xt}\right)$$

wrinkle angle

$$\alpha = \frac{2\sqrt{2}\sqrt{81t^2x^2+2l^2}\sin\left[\frac{\arctan\left(\frac{243t^2x^2(3\delta-1)-4l^3}{27tx\sqrt{1458t^4x^4-27t^2x^2(27\delta^2-18\delta l-l^2)+8\delta l^3)}}\right)}{3}\right]}{9tx}+\frac{2l}{9tx}$$

b) summary of key analytical relationships in reference to Figure E1

Figure E3. Important relationships developed by Bilston

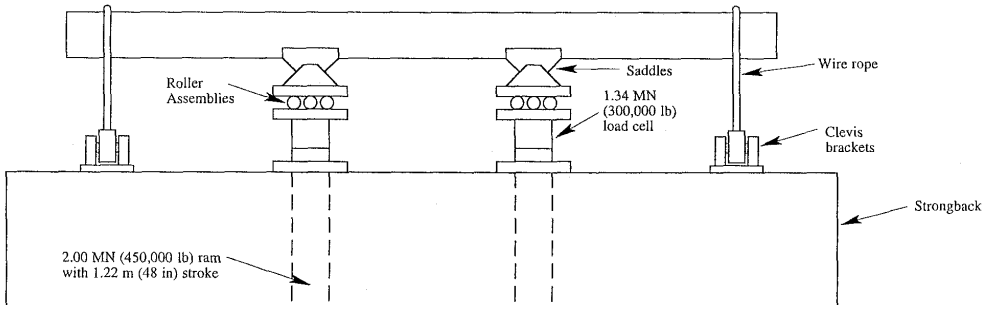

a) setup

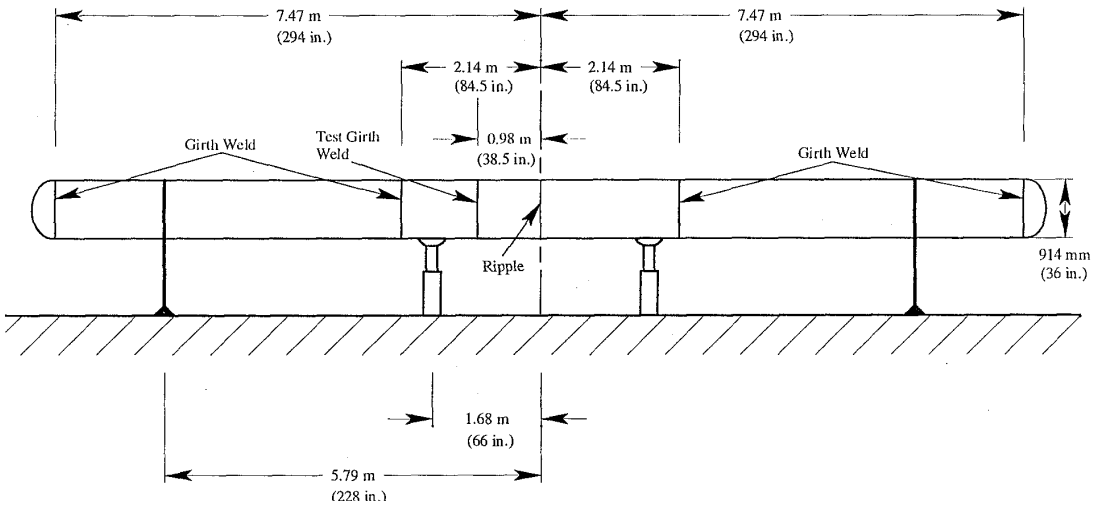

b) layout

c) photograph

Figure E4. Overview of the testing machine used by Olson et al[5]

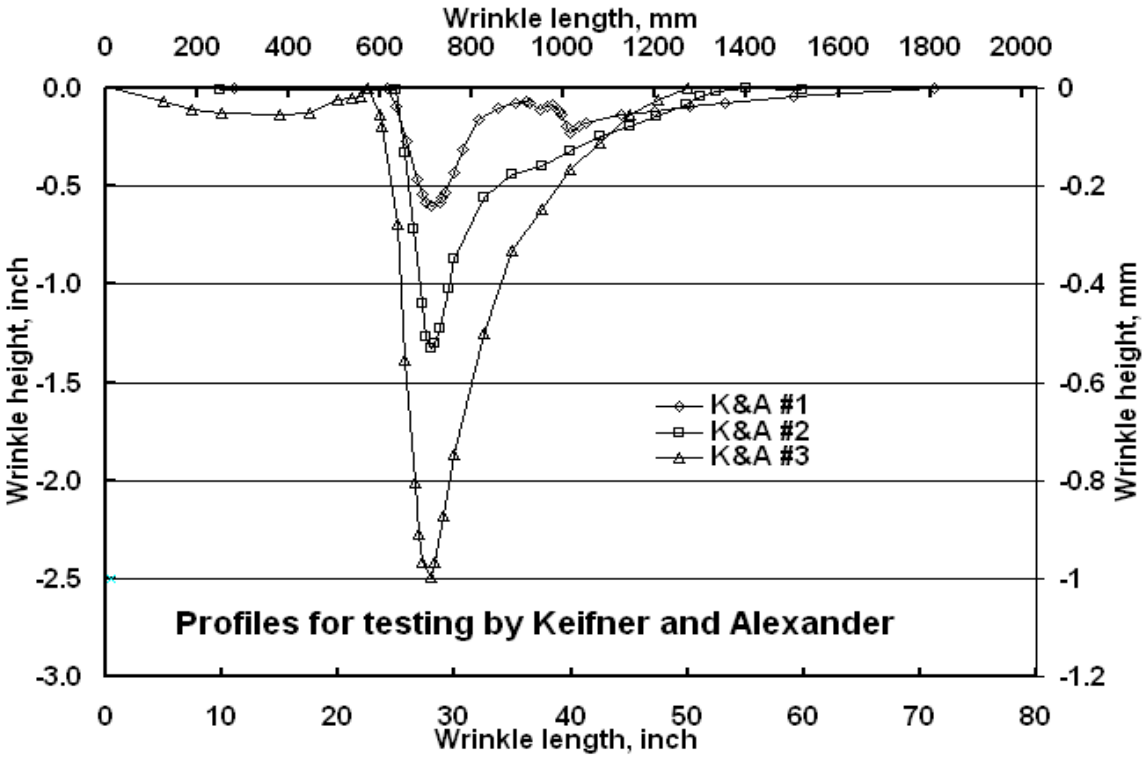

Figure E5. As-bent wrinkle profiles for the testing by Keifner and Alexander[16]

Appendix F – Mechanics Theories, Models, and Results

This wrinklebend project depends primarily on the FEA and the commercial FEA software, ABAQUS standard[(1)], to establish the wrinklebend integrity criteria for fatigue damage under various conditions. As such, accurate FEA results are the key for developing criteria for wrinklebend integrity. Therefore, before reporting our detailed results for each task or activity of the DOT project, it is necessary to present the fundamental plasticity theories, material models, fatigue damage criteria, and FEA results of their applications to simple laboratory specimens or simple components. These basic theories and analyses presented in this part provide solid confidence on the FEA simulations and results for the wrinklebends. The objective in this part is to show the theoretical and numerical validations of the proposed wrinklebend criteria for fatigue damage in the integrity management of the wrinklebends and buckles.

Plastic Hardening Models for Cyclic Loading

To effectively simulate the stresses and strains for a wrinklebend under cyclic loading, different plastic constitutive models needs to be examined in FEA as built in ABAQUS. In the following sections, the general plastic yield law, the isotropic plastic hardening model, the linear kinematic plastic model, and the combined nonlinear isotropic/kinematic plastic model are briefly introduced, and then two simple examples are followed so as to show the differences between the FEA results from these plastic hardening models for cyclic loading. Accordingly, a valid plastic hardening model is determined in the FEA calculations for wrinklebends subjected to applied cyclic loading or internal pressures.

General Plastic Yield Law

As well-known, the general plastic yield law for metals is defined by:

$$f(\underset{\sim}{\sigma}-\underset{\sim}{\alpha})-\sigma^0(\varepsilon^P)=0 \tag{1}$$

where $\boldsymbol{\sigma}$ is the stress tensor, $\boldsymbol{\alpha}$ is the backstress, σ^0 is the current equivalent stress and $\bar{\varepsilon}^{pl}$ is the accumulative equivalent plastic strain. From the flow theory of plasticity and the normalization rule, the associate flow rule with respect to the yield function *f* is:

$$\dot{\boldsymbol{\varepsilon}}^{pl}=\dot{\lambda}\frac{\partial f}{\partial \boldsymbol{\sigma}} \tag{2}$$

where $\dot{\boldsymbol{\varepsilon}}^{pl}$ is the incremental plastic strain tensor, and $\dot{\lambda}$ is the plastic flow factor. For the von Mises yield criterion, the yield function $f(\boldsymbol{\sigma}-\boldsymbol{\alpha})$ is the equivalent Mises stress:

$$f(\boldsymbol{\sigma}-\boldsymbol{\alpha})=\sqrt{\frac{3}{2}(\mathbf{S}-\boldsymbol{\alpha}')(\mathbf{S}-\boldsymbol{\alpha}')} \tag{3}$$

where $\mathbf{S}$ is the deviatoric stress tensor, and $\boldsymbol{\alpha}'$ is the deviatoric backstress tensor. Substitution of Equation 3 into Equation 2 obtains:

$$\dot{\boldsymbol{\varepsilon}}^{pl}=\dot{\lambda}(\mathbf{S}-\boldsymbol{\alpha}'). \tag{4}$$

This incremental plastic strain plus the incremental elastic strain determines the incremental total strain for the material considered. Different plastic hardening laws have been developed to describe the evolution of the backstress tensor $\boldsymbol{\alpha}$ and the equivalent stress σ^0. Three commonly

used plastic hardening models are outlined in the following sections. Detailed review of these models can be found in a treatise of plasticity theory.

Isotropic Hardening Model

This model assumes that the yield surface enlarges equally in all directions and without any kinematic shift of its yield center. Therefore, the backstress tensor is zero:

$$\boldsymbol{\alpha} = 0 \tag{5}$$

The isotropic hardening model is widely used for elastic-plastic analysis under monotonic loading. However, it is inappropriate to use this model for cyclic plastic loading because it can not simulate the Bauschinger effect and anisotropy induced by work hardening.

Linear Kinematic Hardening Model

This model is a simple kinematic hardening model that assumes a constant hardening modulus. When temperature dependence is omitted, the evolution of the backstress tensor $\boldsymbol{\alpha}$ is defined by the following Ziegler hardening law:

$$\dot{\boldsymbol{\alpha}} = C\frac{1}{\sigma^0}(\boldsymbol{\sigma} - \boldsymbol{\alpha})\dot{\bar{\varepsilon}}^{pl} \tag{6}$$

where $\dot{\bar{\varepsilon}}^{pl}$ is the equivalent plastic strain rate and *C* is the kinematic hardening modulus. For the uniaxial tension, *C* is the tangential modulus of the stress-strain response, $E_p = \frac{d\sigma}{d\varepsilon^{pl}}$. In this model, the equivalent stress defining the size of the yield surface remains constant, i.e. $\sigma^0 = \sigma_0$, where σ_0 is the initial yield stress at zero plastic strain. The linear kinematic hardening model can consider the Bauschinger effect and anisotropy. In the current version of ABAQUS, this model is used only for bilinear hardening materials, and thus good for small plastic deformation.

Combined Nonlinear Isotropic/Kinematic Hardening Model

This model was developed based on the work of Lemaitre and Chaboche[2]. The evolution of this model consists of two components: an isotropic hardening component and a nonlinear kinematic hardening component. The isotropic hardening behavior defines the equivalent stress, describing the yield surface size, as a function of the equivalent plastic strain. This evolution can be expressed as the simple exponential law:

$$\sigma^0 = \sigma_0 + Q\left(1 - e^{-b\bar{\varepsilon}^{pl}}\right) \tag{7}$$

where *Q* and *b* are the material parameters that must be calibrated from cyclic test data. *Q* defines the maximum change in the size of elastic range and *b* is the rate at which the size of the yield surface changes as the plastic strain develops. If $\sigma^0 = \sigma_0$, this model reduces to a nonlinear kinematic hardening model.

The nonlinear kinematic hardening component of this combined model describes the Bauschinger effect by describing the translation of the yield surface in stress space through the backstress such that straining in one direction reduces the yield stress in the opposite direction. This law is defined as an additive combination of a purely kinematic term and a relaxation term, which introduces the nonlinearity:

$$\dot{\boldsymbol{\alpha}} = C\frac{1}{\sigma^0}(\boldsymbol{\sigma}-\boldsymbol{\alpha})\dot{\bar{\varepsilon}}^{pl} - \gamma\boldsymbol{\alpha}\dot{\bar{\varepsilon}}^{pl} \tag{8}$$

where C and γ are the material parameters that must be calibrated from cyclic test data. C is the initial kinematic hardening modulus, and γ defines the rate at which the kinematic hardening modulus decreases as plastic deformation develops. If C and γ are zero, Equation 8 reduces to Equation 5 for the isotropic hardening model. If γ is zero, Equation (8) reduces to Equation 6 for the linear kinematic hardening model.

Integration of the kinematic hardening law in Equation 8 over a half cycle of uniaxial stress-strain curve gives:

$$\alpha = \frac{C}{\gamma}\left(1-e^{-\gamma\bar{\varepsilon}^{pl}}\right) \tag{9}$$

and the uniaxial stress can be expressed as:

$$\sigma = \sigma_0 + Q\left(1-e^{-b\bar{\varepsilon}^{pl}}\right)+\frac{C}{\gamma}\left(1-e^{-\gamma\bar{\varepsilon}^{pl}}\right). \tag{10}$$

In general, the combined hardening model can account for the Bauchinger effect, ratcheting, relaxation of the mean stress and cyclic hardening with plastic shakedown. This plastic constitutive model incorporates several material parameters that are usually determined from cyclic test data. In Chapter 11 for inelastic mechanical properties, theABAQUS standard user's manual provides detailed calibration methods for these parameters, and input methods of the cyclic test data for the plastic hardening models.

Fatigue Damage Parameters and Properties

The general definitions and concepts in fatigue analysis are proposed as follows for stress and strain, respectively:

Stress range: $\Delta\sigma = \sigma_{\max} - \sigma_{\min}$

Mean stress: $\sigma_m = (\sigma_{\max} + \sigma_{\min})/2$

Stress amplitude: $\sigma_{amp} = \Delta\sigma/2 = (\sigma_{\max} - \sigma_{\min})/2$

Maximum stress: $\sigma_{\max} = \sigma_m + \sigma_{amp}$

Minimum stress: $\sigma_{\min} = \sigma_m - \sigma_{amp}$

Applied stress ratio: $R = \sigma_{\min}/\sigma_{\max}$ (A completely reversed cycle is R = -1.)

For an applied load P with the minimum load, P_{min} and the maximum load P_{max}, the applied stress ratio can be expressed as the applied load ratio as $R = P_{\min}/P_{\max}$.

Strain range: $\Delta\varepsilon = \varepsilon_{\max} - \varepsilon_{\min}$

Mean strain: $\varepsilon_m = (\varepsilon_{\max} + \varepsilon_{\min})/2$

Strain amplitude: $\varepsilon_{amp} = \Delta\varepsilon / 2 = \left(\varepsilon_{\max} - \varepsilon_{\min}\right)/2$

Maximum strain: $\varepsilon_{\max} = \varepsilon_m + \varepsilon_{amp}$

Minimum strain: $\varepsilon_{\min} = \varepsilon_m - \varepsilon_{amp}$

From these fatigue concepts, different fatigue damage parameters or variables and the corresponding fatigue damage criteria have been developed. Commonly used fatigue life criteria are summarized as below.

Stress controlled fatigue (S-N curve)

$$\sigma_{amp} = \sigma_f \left(2N_f\right)^b \tag{11}$$

The equation above is a stress-life curve, i.e., the well-known S-N curve. The stress-based approach is good for high-cycle fatigue (long fatigue life, >10^4), and the strain-based approach is good for low-cycle fatigue (short fatigue life, < 10^4).

Strain controlled fatigue (ε-N curve)

$$\varepsilon_{amp} = \varepsilon_{amp}^e + \varepsilon_{amp}^p = \frac{\sigma_f}{E}\left(2N_f\right)^b + \varepsilon_f \left(2N_f\right)^C \tag{12}$$

The equation above is a strain-life curve, and usually used in the strain-based approach to fatigue. It considers small and large deformation in local yielding regions, and is good for ductile metals at relatively short lives. The strain-based approach differs significantly from the stress-based approach. The later emphasizes nominal or average stresses, rather than local stresses and strains, and employs elastic stress. However, Equation 12 is experimentally determined for completely reversed loading, and thus does not consider the effect of mean stress on fatigue lives. f a mean stress is present in applications, the strain-life curve needs to be modified. The following energy-based damage parameters are proposed for such purposes.

Energy-based fatigue damage parameter

Smith, Watson and Topper (SWT) [3] parameter

$$D_1 = \sigma_{\max}\varepsilon_{amp} \tag{13}$$

This approach assumes that the fatigue life for any situation of the mean stress depends on the product of the maximum stress and the amplitude of strain. For completely reversed fatigue ($\sigma_m = 0$), $D_1 = \sigma_{\max}\varepsilon_{amp} = \sigma_{amp}\varepsilon_{amp}$. Thus the fatigue life is expected to be the same for completed reversed loading where the product has the same value. Dowling[4] pointed out that the SWT parameter appears to give good results for a wide range of materials, and is good choice for general use. *For multiaxial stress states, a reasonable approach for tensile stress dominated cracking or failure is to simply apply the SWT fatigue damage parameter with ε_{amp} being the maximum amplitude of normal strain, and $\sigma_{\max}$ being the maximum normal stress on the same plane as ε_{amp} during that ε_{amp} cycle.*

Except for the SWT parameter, there are two other useful fatigue damage parameters, i.e., the Leis[5] parameter and total energy parameter. These are also energy-based damage parameters and can consider the mean stress effect on the fatigue life.

Leis parameter

$$D_2 = (\sigma_m + \Delta\sigma)\Delta\varepsilon/4 = (\sigma_m/2 + \sigma_{amp})\varepsilon_{amp} = (\sigma_{\max} + \sigma_{amp})\varepsilon_{amp}/2 \tag{14}$$

Total energy parameter

$$D_3 = \sigma_{amp}\varepsilon_{amp} = \Delta\sigma\Delta\varepsilon/4 \tag{15}$$

For completely reverse fatigue, $\sigma_m = 0$ and thus from Equations 13 to 15, the three damage parameters become identical. As a result, for such completely reversed (R = -1) fatigue tests between constant strain limits for various pipeline steels, as shown in Figure 1, we can determine a fatigue damage versus life curve as the material property of fatigue resistance. In Figure 1, using best-curve fitting, the following equation is determined as the material fatigue resistance curve for extensive pipeline steels ranged from Grade B to X70:

$$D = 273(2N_f)^{-1.02} + 2.1(2N_f)^{-0.28} \tag{16}$$

or

$$\begin{aligned} D &= 132(N_f)^{-1.}, && D \geq 2 \\ &= 2418(\ln(N_f))^{-3.333}, && D < 2 \end{aligned} \tag{17}$$

With the above fatigue resistance curve, service life of any structural components subjected to cyclic loading can be estimated for small and large plastic deformation, provided that the local stresses and strains at critical locations are determined using the FEA calculations. The discussions above provide a guideline for this project to perform the fatigue damage evaluation using the FEA simulations, and to develop damage criteria for the wrinklebend integrity.

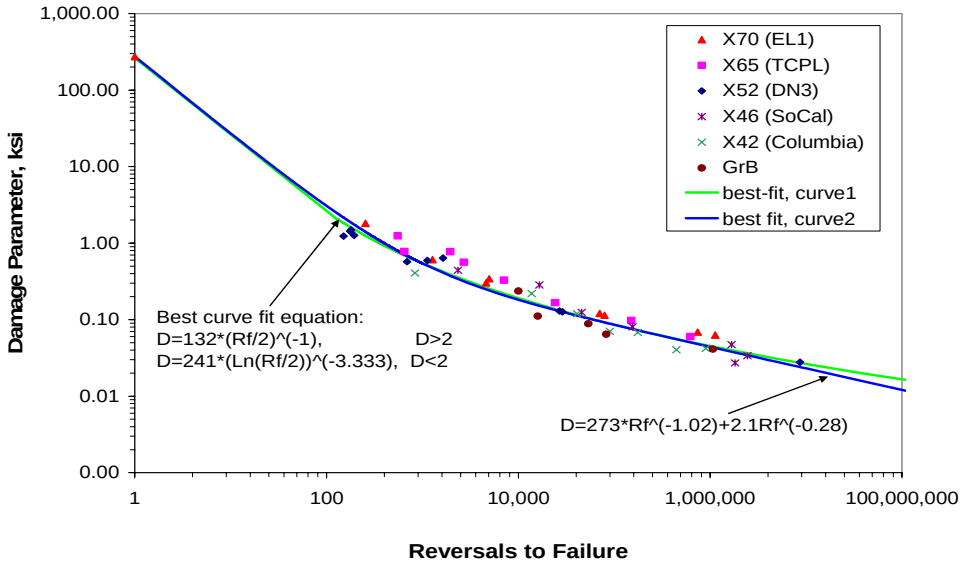

Figure 38. Fatigue damage parameter versus reversals to failure

Two Example Applications of the Cyclic Plastic Hardening Models

To show the difference of FEA results between three cyclic plastic hardening models and to identify an effective plastic hardening model to simulate the wrinklebend under cyclic internal pressure, the following sections will examine two application examples. One is a simple rectangular beam under cyclic bending, and the other is a bend pipe or elbow under combined internal pressure and cyclic tension. Both the beam and elbow are simulated using ABAQUS in conjunction with the three cyclic plastic hardening models. Cyclic stress and strain relations from the FEA calculations using the different plastic hardening models are compared, and the corresponding conclusions are obtained.

Rectangular Beam under Cyclic Bending

Specimen geometry and FEA models

A beam with rectangular cross-sections subjected to pure cyclic bending is considered. The thickness, width, and span of the beam are 25.4 mm (1 inch), 50.8 mm (2 inches) and 508 mm (20 inches), respectively, as shown in Figure 2(a). Detailed elastic-plastic FEA calculations with large deformation were performed using ABAQUS standard for this beam under the plane stress conditions. Due to symmetry, only one half of the beam was modeled and the finite element

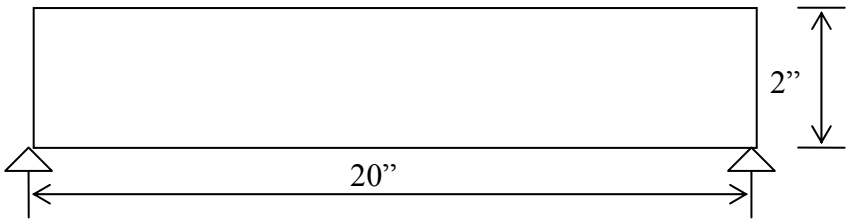

a) Geometry of beam with one inch thick

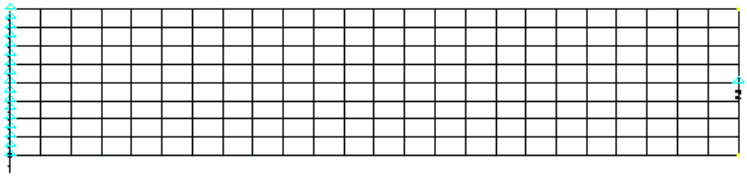

b). Plane stress FEA mesh of the beam

Figure 39. FEA Mesh for beam models

mesh is shown in Figure 2(b). This mesh involves 641 nodes and 192 eight-node plane stress elements with reduced integration (ABAQUS element type: CPS8R). The simple support constraint conditions and the symmetric boundary conditions were employed in the model. The pure cyclic bending moment with 1.25 cycles as shown in Figure 4 was applied at the end of beam. The maximum bending moment was 124 percent of the limit bending moment so as to promote large-scale yielding. It should be noted that the loading by displacement, such as the end rotation angle applied to the beam, is inappropriate for cyclic loading simulations in ABAQUS.

Material properties and ABAQUS input data

The material considered is X42 pipeline steel. The monotonic tensile true stress – true plastic strain curve is shown in Figure 3(a), and the cyclic true stress – strain loops are shown in Figure 2(b) for the X42 steel. It is seen from Figure 3(b) that after two stress cycles, the stress – strain loop approaches to be stable.

Three nonlinear plastic hardening models, i.e., the isotropic, kinematic, and combined isotropic/kinematic models were adopted in the FEA calculations. The incremental theory of plasticity with large deformation and Mises yield criterion was used. For the isotropic hardening model, only the monotonic tensile true stress – true plastic strain curve was needed in the ABAQUS input data in conjunction with the Young's modulus of 207 GPa, and the Poison ratio of 0.3. For the pure kinematic hardening model, the half-cycle test data of the fourth stress-strain loop was used to define the kinematic hardening components without including cyclic hardening which specifies isotropic components. For the combined hardening model, both the monotonic and cyclic test data were used to define the isotropic hardening components and the kinematic hardening components.

The ABAQUS input properties needed for different hardening models are summarized as follows:

(a)ABAQUS input properties for *isotropic hardening model*

Using the monotonic tensile stress – plastic strain curve.

(b) ABAQUS input properties for *pure kinematic hardening model*

Using Figure 1 and combined hardening model with data type of half cycle, but do not include cyclic hardening which specific isotropic components here.

(c) ABAQUS input properties for combined isotropic / kinematic hardening model

Using Figure 1 and combined hardening model with data type of half cycle, and include cyclic hardening which specific isotropic components here.

(d) ABAQUS input properties for combined stabilized hardening materials

Using the stabilized stress – strain curve calculated as described in ABAQUS.

More detailed methods of material property inputs for different plastic hardening models can be referenced to ABAQUS standard user's manual.

FEA results and analysis

Figure 5 shows the variations of the rotation angle at the ends of the beam with the loading time from the nonlinear FEA simulations using the isotropic, kinematic, combined isotropic/kinematic, and combined stabilized hardening models, respectively. It is evident that the plastic hardening models have significant effect on the end rotation angle. The isotropic model predicts the smallest rotation angle, while the kinematic model predicts the largest rotation angle for the beam during cyclic bending except for the stabilized model which predicts the ultimate stable state of cyclic behavior.

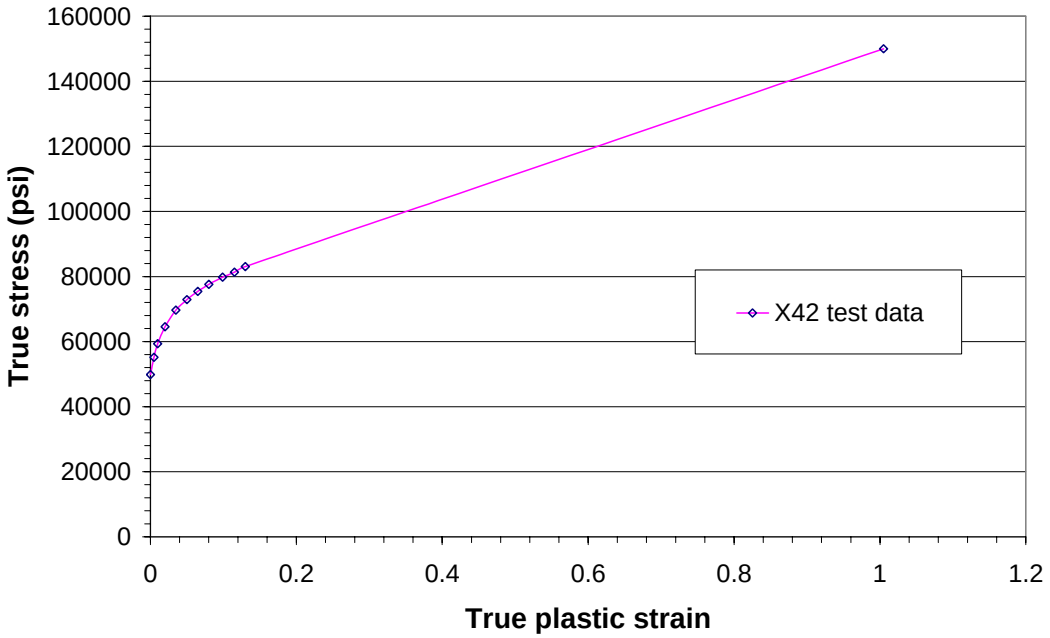

a) Tensile true stress-strain curve for X42

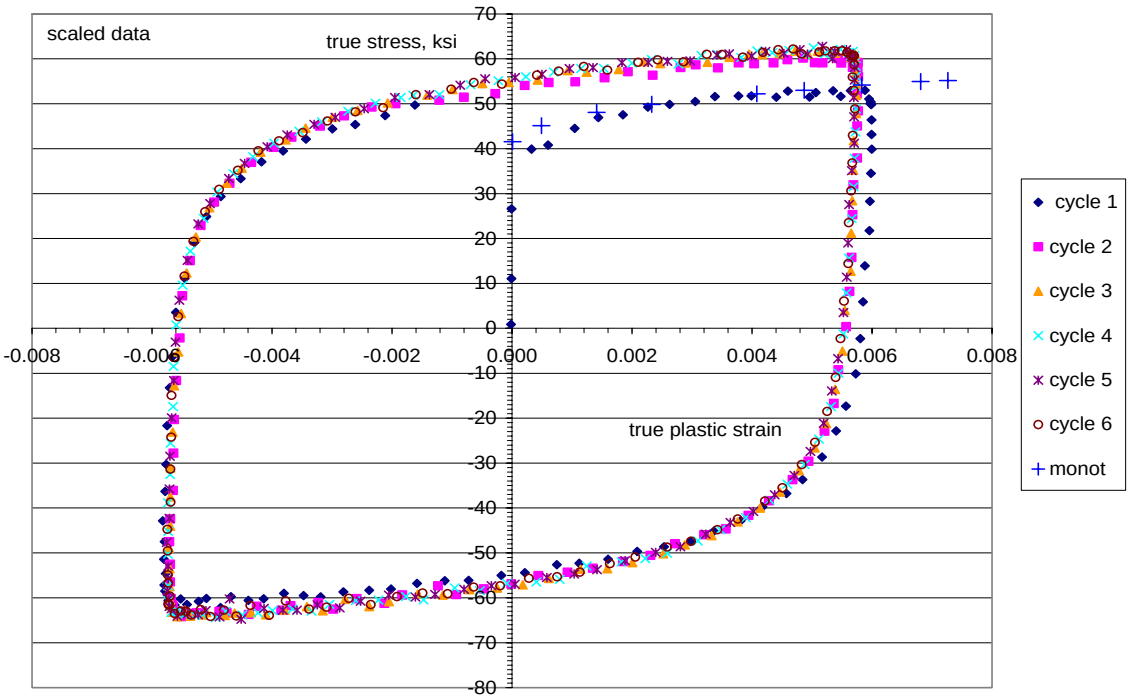

b) Cyclic true stress – strain curve for X42

Figure 40. Mechanical properties and typical hysteresis response

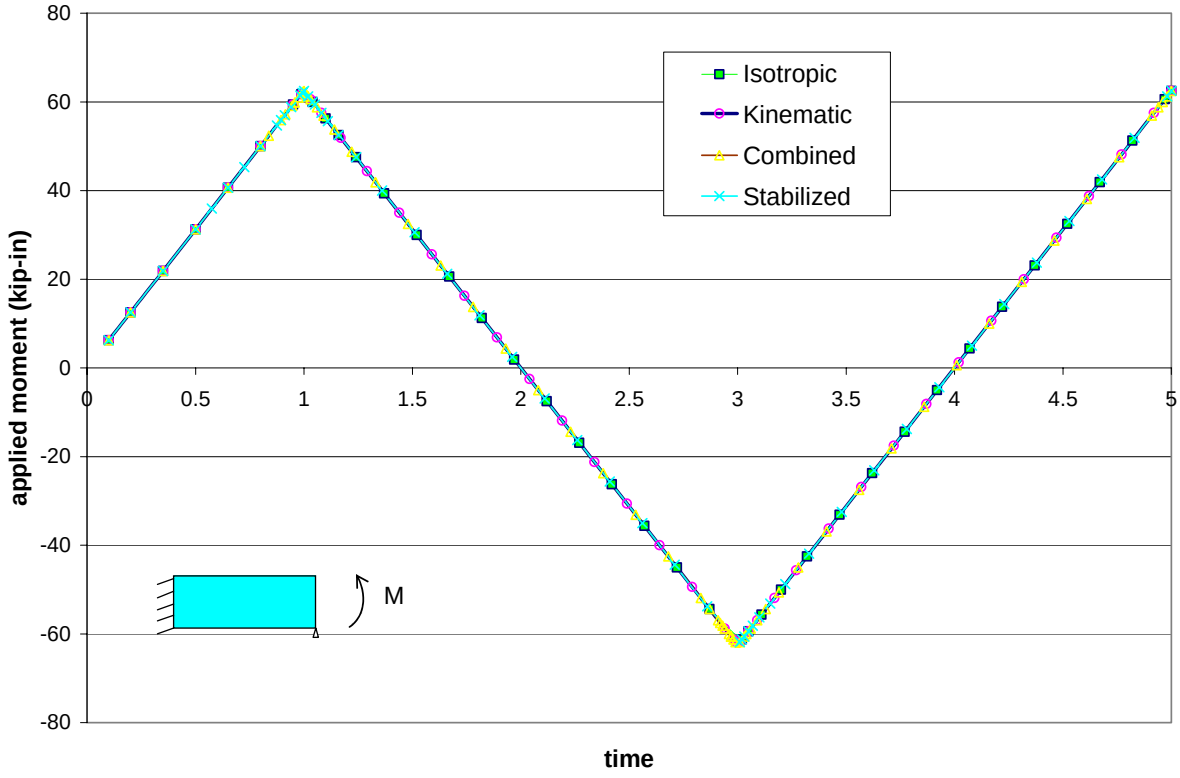

Figure 41. Cyclic loading of the beam bending moment

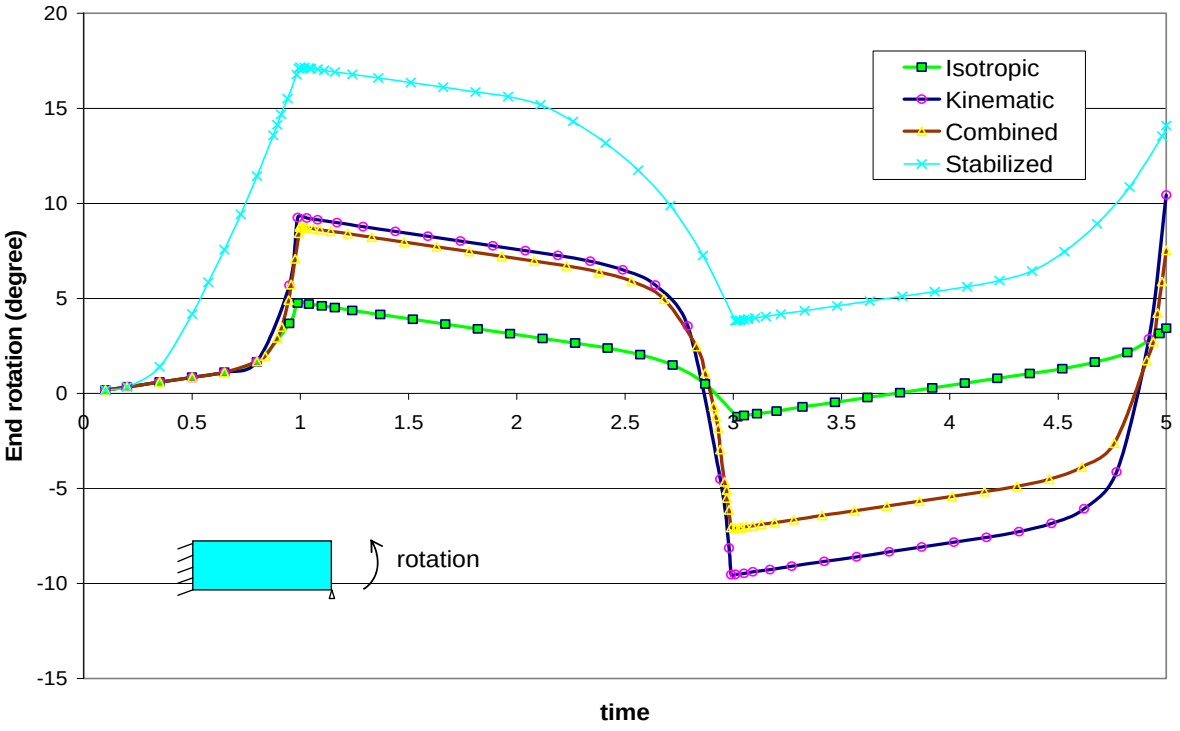

Figure 42. End rotation under different hardening models

Figures 6 and 7 show the variations of the axial stress and the axial strain at the top point on the symmetric plane of the beam with the loading time from the FEA calculations using the isotropic, kinematic, combined isotropic/kinematic, and combined stabilized hardening models, respectively. From these figures, one can find that the different plastic hardening models have relatively small effects on the axial stress, even for the stabilized plastic hardening model. However, significant effects on the axial strain are observed for the four cyclic plastic hardening modeling. Except for the ultimate case of the stabilized model, the isotropic model predicts the smallest strain, the kinematic model predicts the largest strain, and the combined model predicts the result between the isotropic model and the kinematic model.

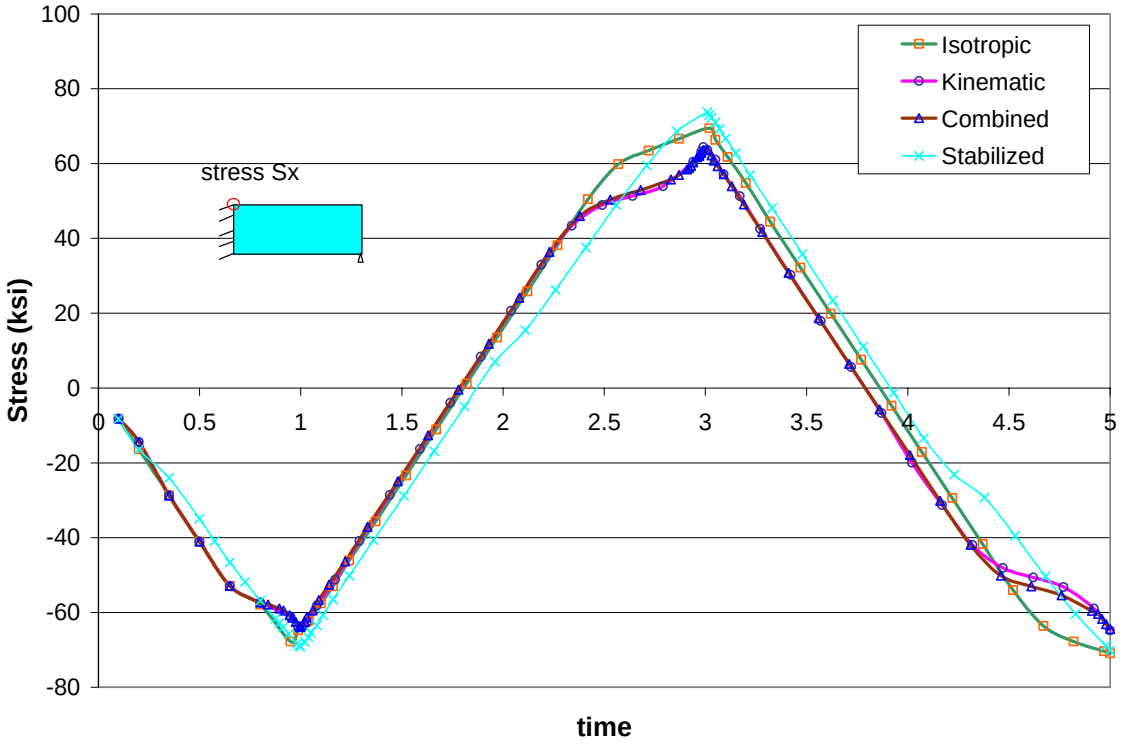

Figure 43 Axial stress versus time at the center top point

Figure 8 shows the axial stress – the end rotation angle loop, and Figure 9 shows the axial stress – the axial strain hysteresis loop using the isotropic, kinematic, combined isotropic/kinematic, and combined stabilized hardening models, respectively for the beam under the 1.25 cyclic bending. Except for the ultimate case of the stabilized model, both figures indicate that the isotropic model determines the smallest loop, the kinematic model determines the largest loop, and the combined model determines the intermediate loop. Moreover, both the kinematic and combined models predict larger plastic strain or deformation than the isotropic model. These observations are consistent to those for the springback of metal forming sheets under bending, which shows that our FEA simulations of the rectangular beam under cyclic bending are correct. Therefore, it can be said that the FEA numerical stresses and strains obtained by the combined isotropic/kinematic model in ABAQUS are the accurate results for the rectangular beam under cyclic bending.

From the FEA simulations of the plastic cyclic beam using ABAQUS, several important conclusions can be drawn:

- Plastic hardening model has small effect on stress.
- Plastic hardening model has significant effect on strain.
- The combined isotropic/kinematic hardening model is the good model to be used to simulate the stresses and strains of the beam under cyclic bending.

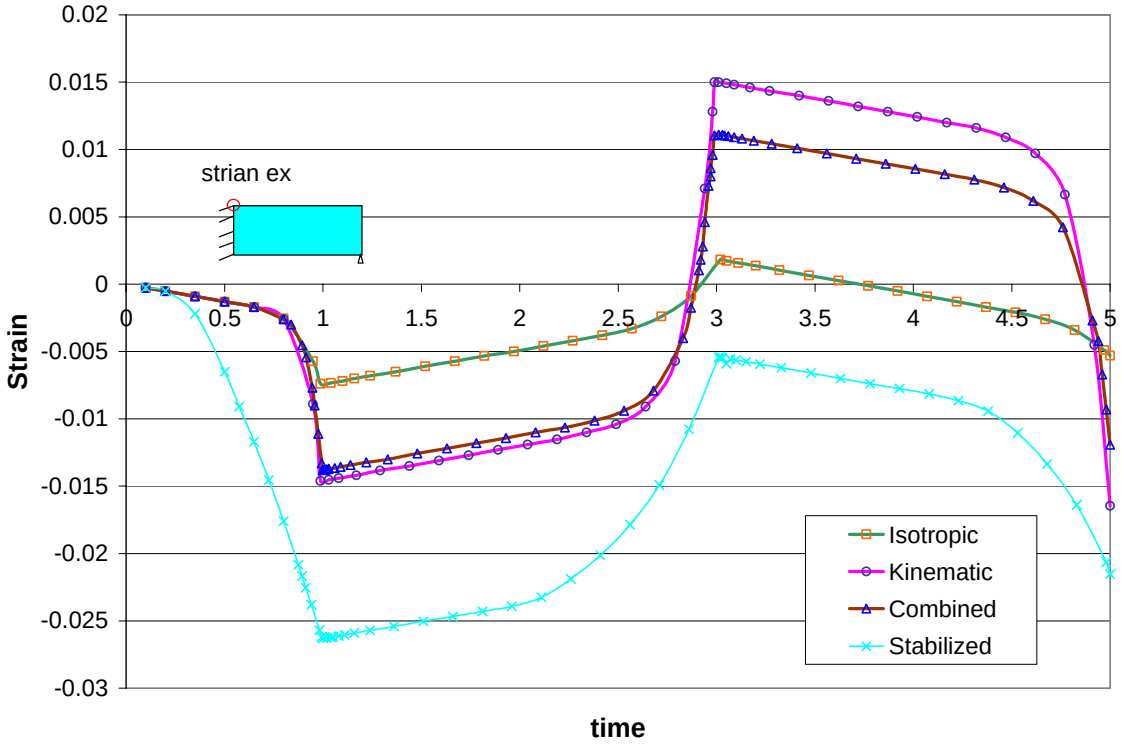

Figure 44. Strain versus time at the center top point

Fatigue damage quantification

With the maximum stress and strain amplitude obtained above by ABAQUS for the beam during cyclic bending, fatigue damage analysis can be performed. Experimental analysis indicated that the following SWT parameter is a good energy-based damage parameter to quantify fatigue damage due to large cyclically plastic deformation:

$$D_f = \sigma_{\max} \varepsilon_{amp} . \tag{18}$$

At the center top point, the SWT parameter D_f is 0.320, 0.942, 0.793, and 0.769 ksi for the isotropic hardening model, pure kinematic hardening model, combined isotropic / kinematic hardening model, and stabilized hardening model. From the relationship between the fatigue damage parameter and the fatigue life for pipeline steels, as shown in Equation 16 or 17, the predicted fatigue life for the rectangular beam under cyclic bending is estimated as 1840, 231, 308 and 324, respectively for the four plastic hardening models. Therefore, the isotropic hardening model may overly estimate the fatigue life as anticipated, while the pure kinematic hardening model may underestimate the fatigue life, and the combined isotropic/kinematic hardening model may determine the reasonable life. Although the stabilized hardening model does not consider the initial cycle behavior, it can determine the fatigue service life close to that by the combined hardening model. Therefore, the stabilized model and the combined model are

nearly equivalent for the X42 pipeline steel considered. Finally, one can conclude that the service life of the rectangular beam under cyclic bending may be 308 cycles.

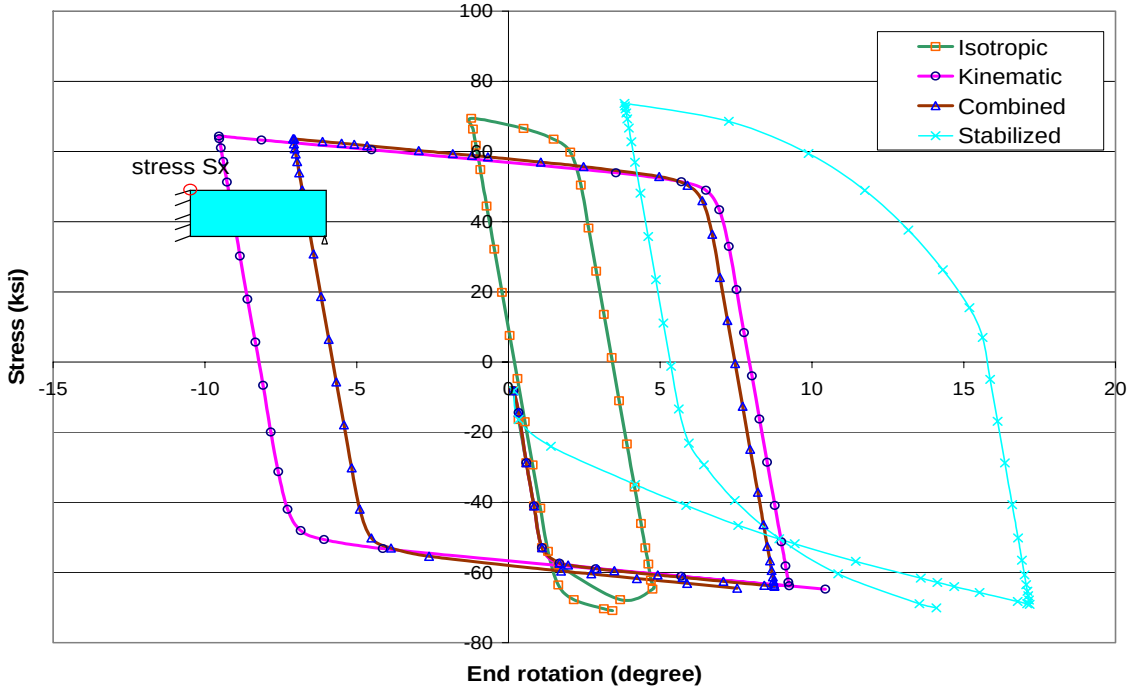

Figure 45. Stress – end rotation loop

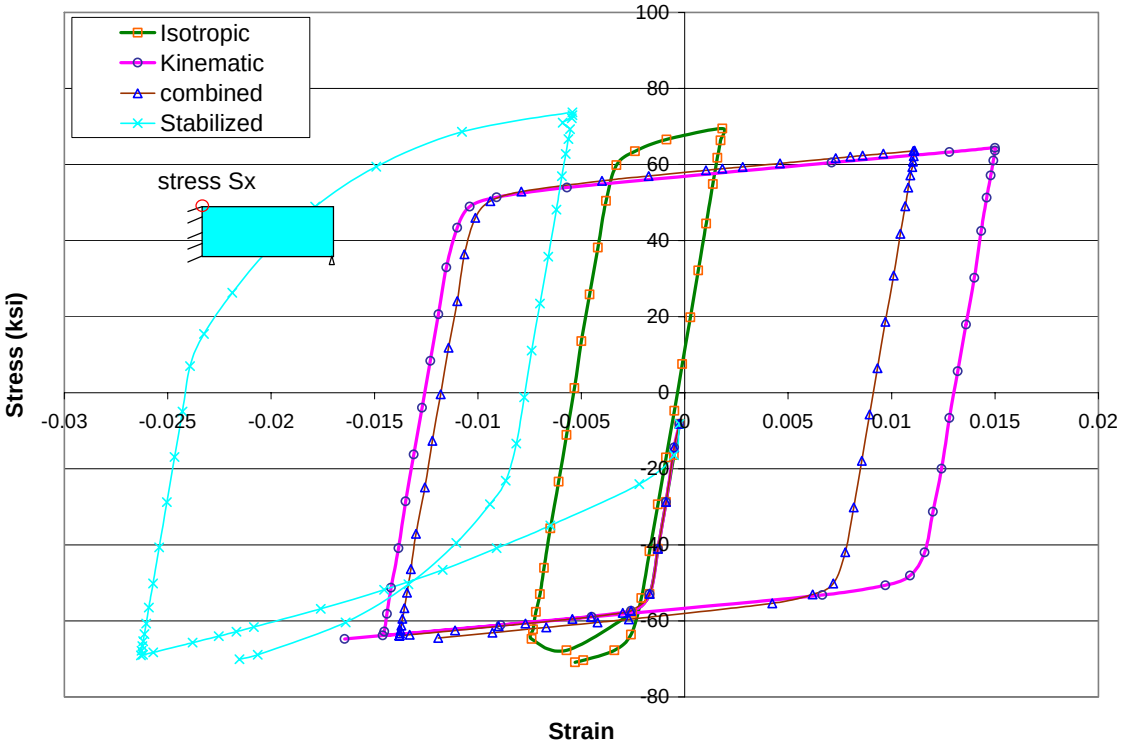

Figure 46. Stress – strain loop

Elbow under Fixed Internal Pressure and Cyclic Bending

Specimen geometry and FEA models

A 90^o elbow attached to two equal length straight pipes with capped ends is considered. The mean cross-sectional radius of the elbow is R = 203.2 mm (8 inches), the pipe thickness t = 12.7 mm (0.5 inches), the elbow radius to cross-sectional radius ratio is R_b/R = 3, and the bend parameter is $\lambda = R_b t / R^2 = 0.1875$. The length of the attached straight pipes was chosen as 10R, which was suggested by Robertson et al.[6] after a sensitivity analysis to meet the condition that the elbow response is independent of the pipe ends.

Detailed elastic-plastic FEA with large deformation is performed using ABAQUS standard for this elbow in three dimensions. Due to symmetry, only one quarter of the elbow was modeled and the finite element mesh is shown in Figure 10. This mesh involves 755 nodes and 700 four-node shell elements with reduced integration (ABAQUS element type: S8R). It should be noted that the shell elements have identical accuracy to the volume elements for thin-wall elbows. The simple support end constraint conditions and the symmetric boundary conditions are employed in the model. An operating internal pressure of 72 percent of the specified minimum yield stress (SMYS) is fixed, and a cyclic bending is applied at the elbow ends by a couple of tensile or compressive forces.

The applied cyclic equivalent bending moment with two cycles is shown in Figure 11. The maximum bending moment is the limit bending moment obtained by Chattopadhyay and Tomar[7] for defect-free elbow under the in-plane closing bending moment and internal pressure.

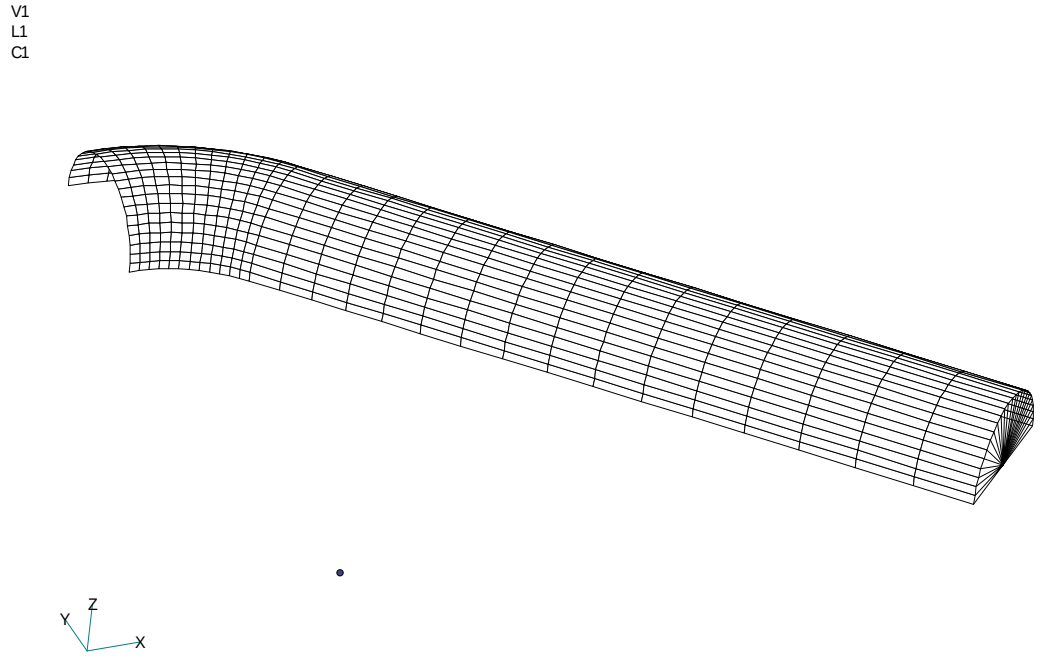

Figure 47. FEA mesh of the 90 degree elbow

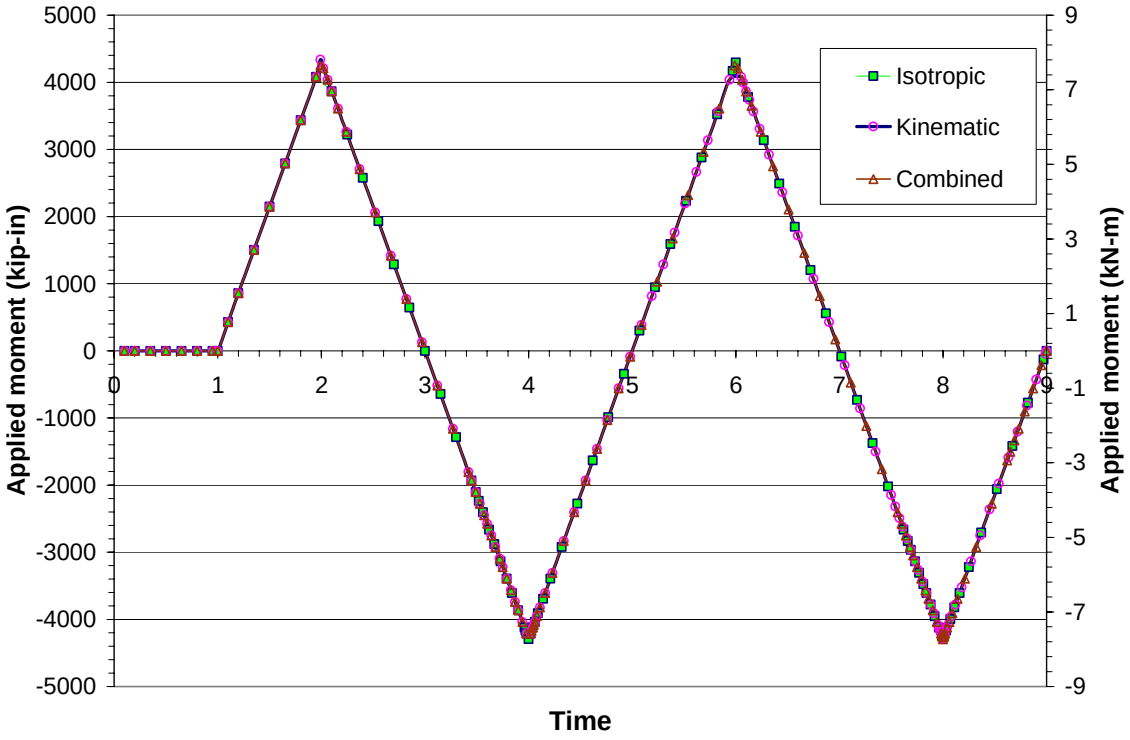

Figure 48. Cyclic bending for the elbow due to the cyclic tension

Material properties and ABAQUS input data

The material considered, its properties, and the ABAQUS input data are the same as those described in the last section for the cyclic beam. However, the combined stabilized model will not be considered in this section, and so this section will use the three plastic hardening models, i.e., the isotropic hardening model, the pure kinematic hardening model, and the combined isotropic/kinematic hardening model.

FEA results and analysis

It is necessary to know the location of the highest stresses because crack initiation will probably occur there after a certain number of cycles. Weis et al.[8] pointed out that the internal pressure or in-plane bending moment causes the maximum stresses at the intrados of pipe bends. Similarly, we find the maximum stress range and strain range at the outside surface at the intrados of the elbow under the fixed internal pressure and cyclic bending. The following analysis is focused on this point.

Figures 12 and 13 show the variations of the axial stress and strain at the outside surface point at the intrados of the elbow with the loading time from the finite element simulations for the three plastic hardening models, i.e., the isotropic, kinematic and combined isotropic/kinematic plastic hardening models, respectively. From these figures, we can find that the plastic hardening model has relatively small effect on the stress, but has significant effect on the strain, as observed for the cyclic beam.

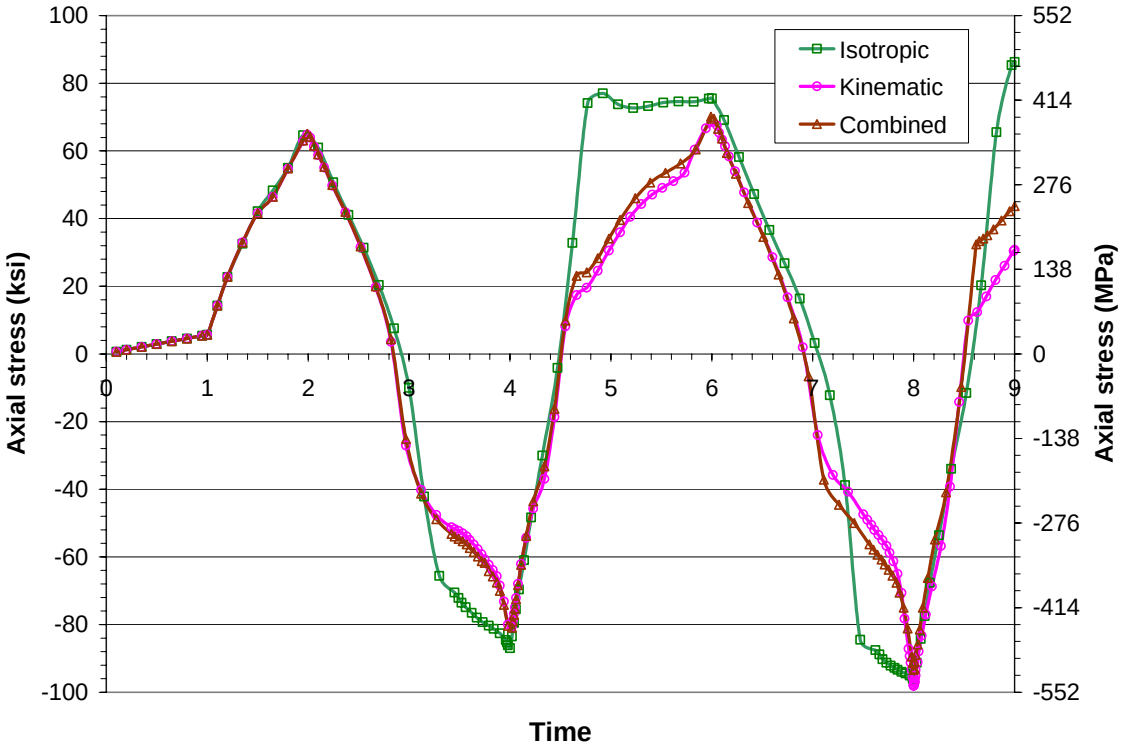

Figure 49. Axial stress versus time at the intrados point

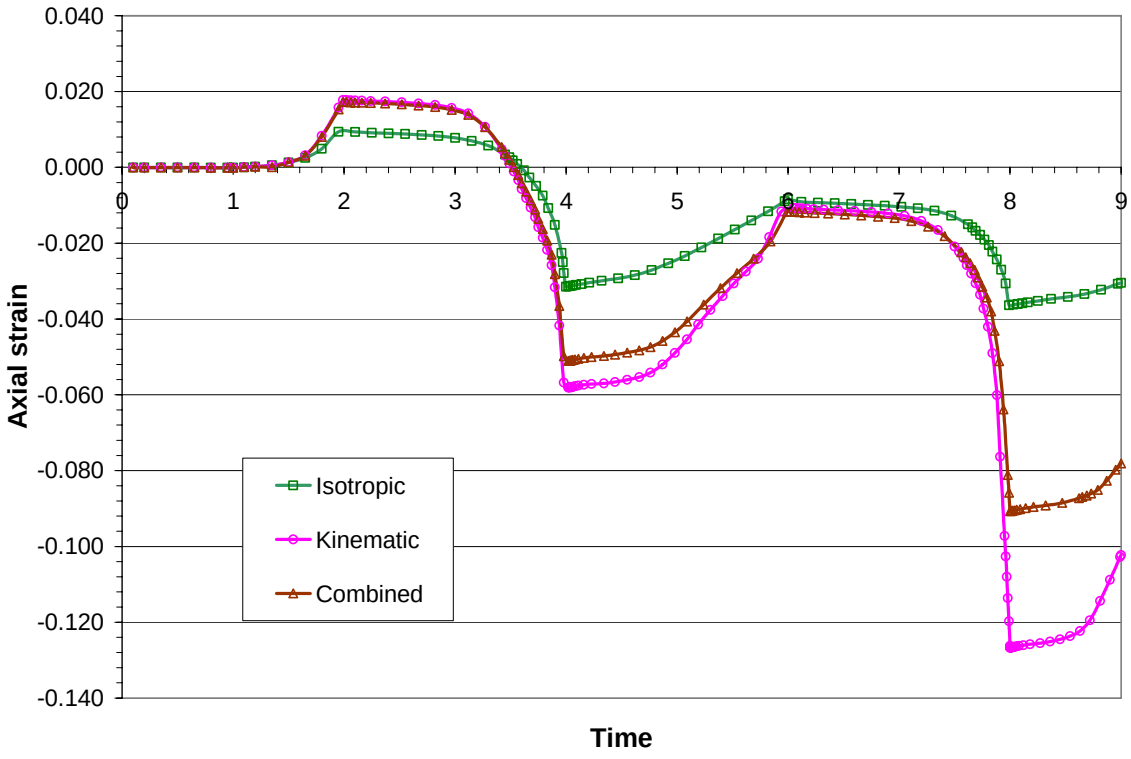

Figure 50. Axial strain versus time at the intrados point

Figure 14 shows that the axial stress – axial strain loop for the elbow under the two cyclic bending. Both figures indicate that the isotropic hardening model determines the smallest loop, the kinematic hardening model determines the largest loop, and the combined isotropic/kinematic hardening model determines the intermediate loop.

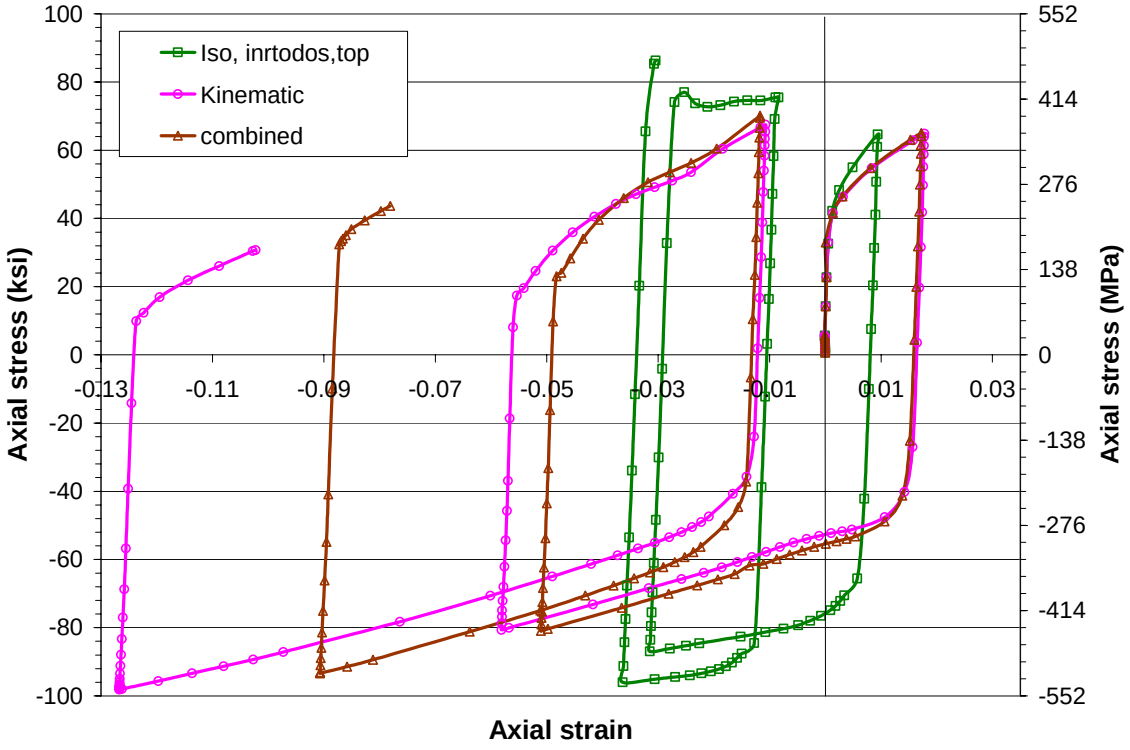

Figure 51. Stress – strain loop at the intrados point

Fatigue damage quantification

At the top point of the intrados of the elbow, the SWT parameter D_f is determined as 1.055 ksi, 3.914 ksi, and 2.743 ksi, respectively for the isotropic hardening model, pure kinematic hardening model, and combined isotropic/kinematic hardening model. From the relationship between the fatigue damage parameter and the fatigue life for pipeline steels, as shown in Equation 17, the corresponding fatigue life for the rectangular beam under cyclic bending is predicted as 192, 36, and 52 cycles, respectively for the three plastic hardening models.

Once again as anticipated, the isotropic hardening model overestimates the fatigue life, while the pure kinematic hardening model may underestimate the fatigue life. The combined isotropic/kinematic hardening model may determine the reasonable life. As a result, the service life of the elbow under fixed internal pressure and cyclic tension may be 52 cycles.

In a word, the combined isotropic/kinematic hardening model is the best one to be used to numerically simulate structures under cyclic loading.

References

1. ABAQUS Standard Users' Manual, version 6.5, ABAQUS, Inc., 2005.
2. Lemaitre, J. and Chaboche, J.L., 1990, "Mechanics of Solid Mechanics," Cambridge University Press, Cambridge, UK, pp. 161-241.
3. Smith, K.N., Watson, P. and Topper, T.H., 1970, "A Stress-Strain Function for the Fatigue of Metal," Journal of Materials, 5, pp. 767-778.
4. Dowling, N.E., 1999, "Mechanical Behavior of Materials: Engineering Methods for Deformation, Fracture and Fatigue," Second edition, Prentice Hall, Upper Saddle River, New Jersey.
5. Leis, B.N., 1977, "An energy-based fatigue and creep-fatigue damage parameter," Journal of Pressure Vessel Technology, **99**, pp.524-533.
6. Robertson, A., Li, H. and Mackenzie, D., 2005, "Plastic Collapse of Pipe Bends under Combined Internal Pressure and In-Plane Bending," International Journal of Pressure Vessels and Piping, **82**, pp. 407-416.
7. Chattopadhyay, J. and Tomar, A.K.S., 2006, "New Plastic Collapse Moment Equations of Defect-Free and Throughwall Circumferentially Cracked Elbows Subjected to Combined Internal Pressure and In-Plane Bending Moment," Engineering Fracture Mechanics, 73, pp. 829-854.
8. Weis, E., Lietzmann, A. and Rudolph, J., 1996, "Linear and Nonlinear Finite-Element Analysis of Pipe Bends," International Journal of Pressure Vessels and Piping, **67**, pp. 211-217.

Appendix G – Effective Plastic Hardening Models and Fatigue Damage Parameters

Fatigue Damage Quantification for Isotropic Hardening Model

Analysis procedures similar to that for the cyclic loading of the rectangular beam and elbow for the previous sections are continued here for wrinklebend analyses. Using FEA simulations local stresses and strains are determined at the crown of the wrinklebend, and then the corresponding damage parameters defined in Equations 13 to 15 are determined in reference to H/L, with the fatigue damage criterion expressed in terms of service life determined via Equation 16. Thus, wrinklebend service life can be estimated from a given H/L for each fatigue damage model. All FEA calculations are performed using the isotropic hardening model considering the bend to be made from X42 line-pipe steel.

Relationships between Fatigue Damage Parameter and Wrinkle Size H/L

Detailed FEA calculations were conducted for a pipeline with different wrinkle sizes. The pipe diameter was 16 inches, thickness 0.283 inches, with the length of the model taken as 2.5 times the pipe diameter. Due to the symmetry, only one quarter of the pipeline with a wrinkle was modeled using the mesh shown in Figure G1. Four node shell elements are used in all FEA calculation. Symmetric displacement boundary conditions were applied in the FEA models. The cyclic loading was the internal pressure from 72 to 10 percent of the SMYS of the X42 pipeline steel, except for simulations of full-scale testing – which considered the actual test history.

Detailed stresses and strains obtained from the FEA calculations for different wrinkle sizes lead to determination of maximum stress, stress amplitude, and strain amplitude at the critical location located in the crown of the wrinkle. Using Equations 13 to 15, three energy-based fatigue damage parameters (the SWT parameter, Leis parameter, and the total energy parameter) were determined. In addition, a strain-based fatigue damage parameter, i.e., strain amplitude as defined in Equation 12, was also included for comparison to the three energy-based fatigue damage parameters to ensure that a reasonable damage parameter is identified.

Figure G2 shows the FEA results and the corresponding curve fits for each damage parameter. These results reflect a specific wrinkle size, H/L: the SWT parameter determines the largest damage, which was followed by the Leis parameter and then total energy.

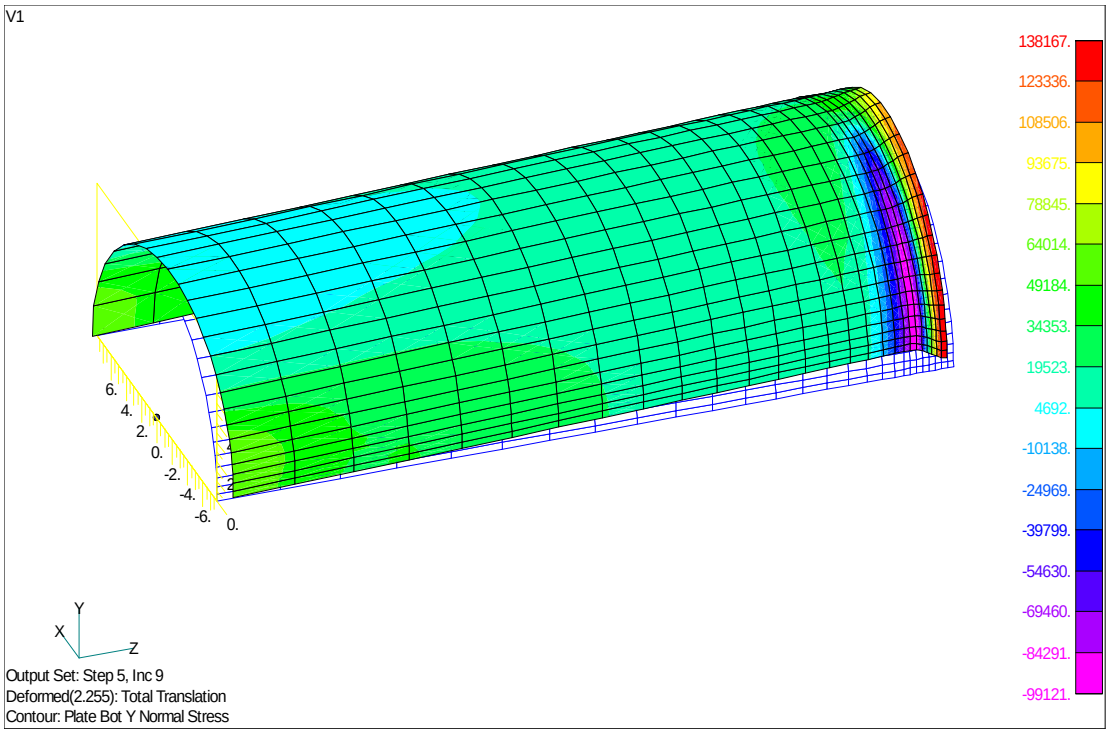

Figure 52. FEA model for a wrinklebend simulation

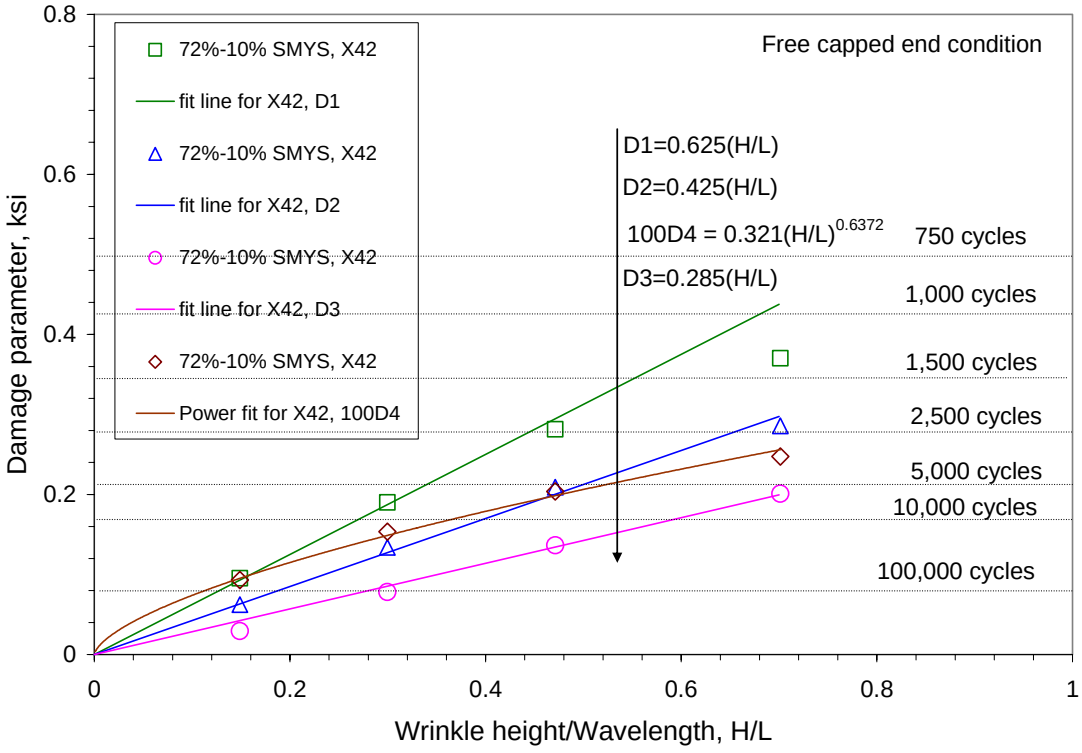

Figure 53. Four damage parameters versus wrinkle size H/L

Fatigue Life Criteria for Wrinklebends

With the FEA results of the damage parameters in Figure G2 and using the material fatigue life curve as shown in Equation 16 or 17, the mathematical expressions between the fatigue life, N_f, and the wrinkle size, H/L, can be determined as follows:

- SWT damage parameter

$$D_{1FEA} = \sigma_{\max}\varepsilon_{amp} = 0.625H / L \tag{19}$$

Substituting Equation 19 into Equation 16 obtains

$$\frac{H}{L} = 436.8\left(2N_f\right)^{-1.02} + 3.36\left(2N_f\right)^{-0.28} \tag{20}$$

- Leis damage parameter

$$D_{2FEA} = \left(\sigma_{\max} + \sigma_{amp}\right)\varepsilon_{amp} / 2 = 0.425H / L \tag{21}$$

Substituting Equation 21 into Equation 16 obtains

$$\frac{H}{L} = 642.353\left(2N_f\right)^{-1.02} + 4.941\left(2N_f\right)^{-0.28} \tag{22}$$

- Total energy damage parameter

$$D_{3FEA} = \sigma_{amp}\varepsilon_{amp} = 0.285H / L \tag{23}$$

Substituting Equation 22 into Equation 16 obtains

$$\frac{H}{L} = 957.895\left(2N_f\right)^{-1.02} + 7.368\left(2N_f\right)^{-0.28} \tag{24}$$

- Total strain amplitude damage parameter

$$D_{4FEA} = \varepsilon_{amp} = 0.00321(H / L)^{0.6372} \tag{25}$$

$$D_{4material} = 1.15\left(2N_f\right)^{-1.} + 0.04\left(2N_f\right)^{-0.25} \tag{26}$$

Substituting (25) into (26) obtains

$$\frac{H}{L} = \left[358.4\left(2N_f\right)^{-1.} + 12.5\left(2N_f\right)^{-0.25}\right]^{1.5694} \tag{27}$$

From (20), (22), (24), and (27), the predicted fatigue life versus the wrinklebend size H/L is plotted in Figure G3.

Figure G3 shows the predicted fatigue lives as a function of wrinkle size in reference to the isotropic hardening model. As noted above, the SWT parameter D_1 predicts the smallest fatigue life, which is followed by the Leis parameter D_2, with the total energy parameter D_3 predicting the highest fatigue life. The total strain parameter D_4 highly overestimates the fatigue life for the wrinklebend. This is anticipated because the deformation in the wrinklebend is controlled by both the stress and strain at the wrinkle area.

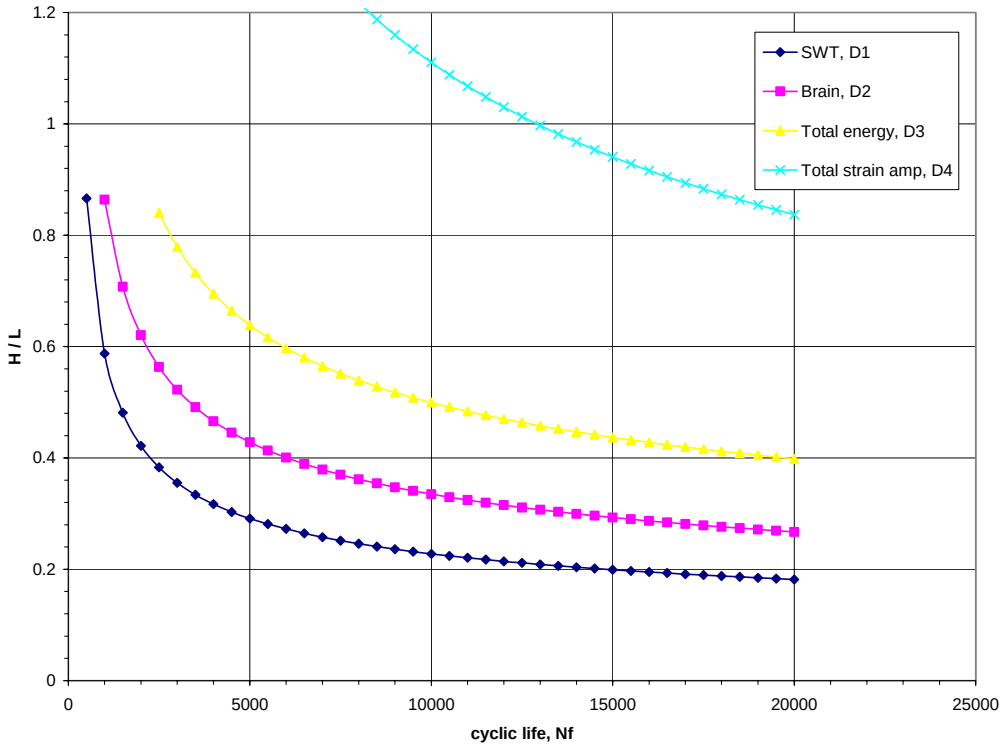

Figure 54. Predictions of fatigue life with wrinklebend size

As detailed in the following section, the three energy-based damage parameters and the corresponding fatigue life criteria, as expressed in Equations 20, 22, and 24, can be validated by a full-scale wrinklebend test under cyclic loading of internal pressure. Figure G4 shows the predictions of fatigue life from wrinklebend size H/L based on the SWT parameter D1 in Equation 20, the Leis parameter D2 in Equation 22, and the total energy parameter D3 in Equation 24 with comparison of the experimental data. Good agreement between the prediction by the SWT parameter and experimental data is observed, the Leis parameter appears viable, while the total energy parameter is less so.

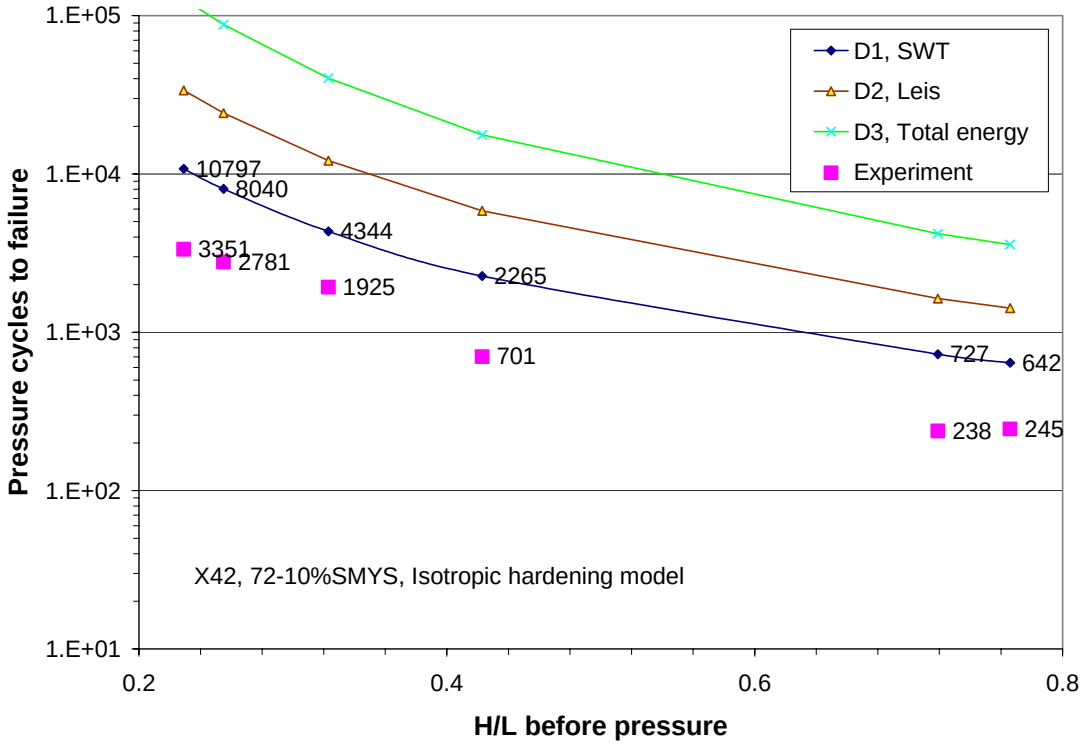

Figure 55. Comparison of pressure cycles to failure from experiments and predictions using the three damage parameters

Fatigue Damage Measures for Different Pipeline Grades

Three other vintage pipeline steels, i.e., Grade B, X52, and X60 also were considered in similar FEA calculations using the isotropic plastic hardening model, after which damage analysis was done.

FigureG5 shows the SWT damage parameter versus the wrinkle size for the four materials of Grade B, X42, X52 and X60. Figure G6 shows the Leis damage parameter versus the wrinkle size for the four materials. Figure G7 shows the total energy damage parameter versus the wrinkle size for the four materials. For all three damage models, the fatigue damage increases with increasing grade of pipeline steels for a given wrinkle size, which reflects the significant influence of stress in the damage parameters considered. For this reason, for the same pipe and wrinkle geometry, the wrinkle in a lower grade appears safer than for higher grades.

For each material and each fatigue damage model, the damage parameter can be approximated as the linear function of the wrinklebend size ratio, H/L. These linear expressions of the SWT parameter, the Leis parameter, and the total energy parameter are included in Figures G5, G6, and G7, respectively. From these damage expressions and the material fatigue curve in Equation 16, the functions between the fatigue life and the wrinkle size can be determined, and thus the fatigue service life can be predicted from the different fatigue damage models for the four pipeline steel grades.

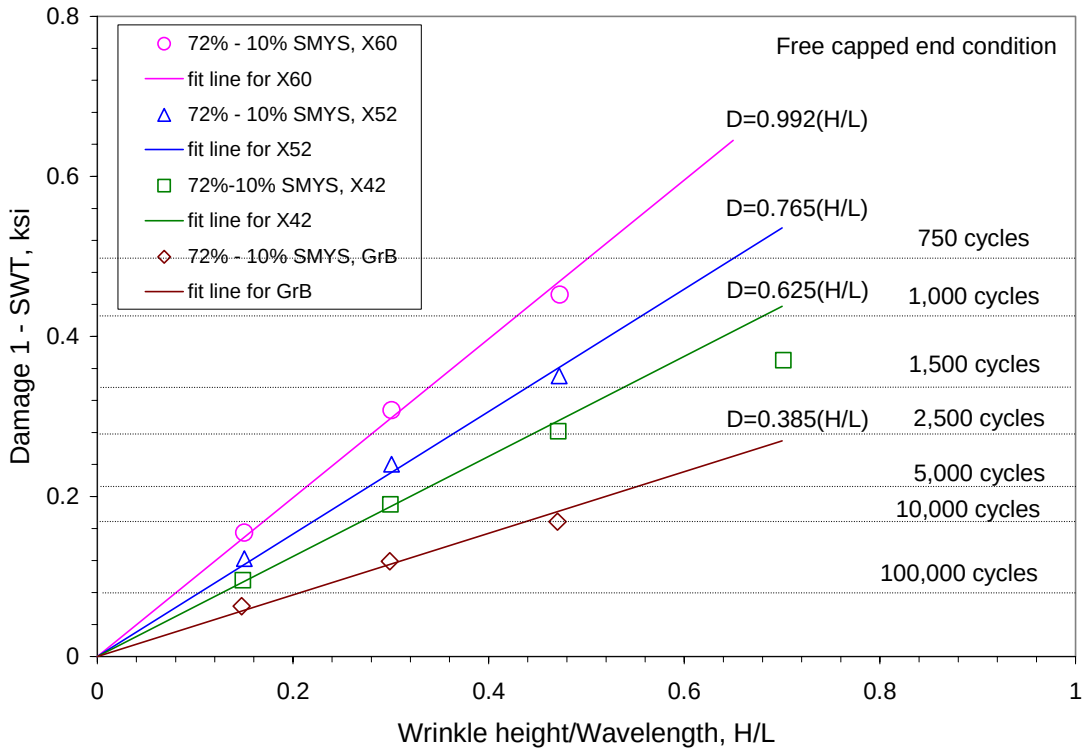

Figure 56. D1 versus H/L for the four pipeline steels

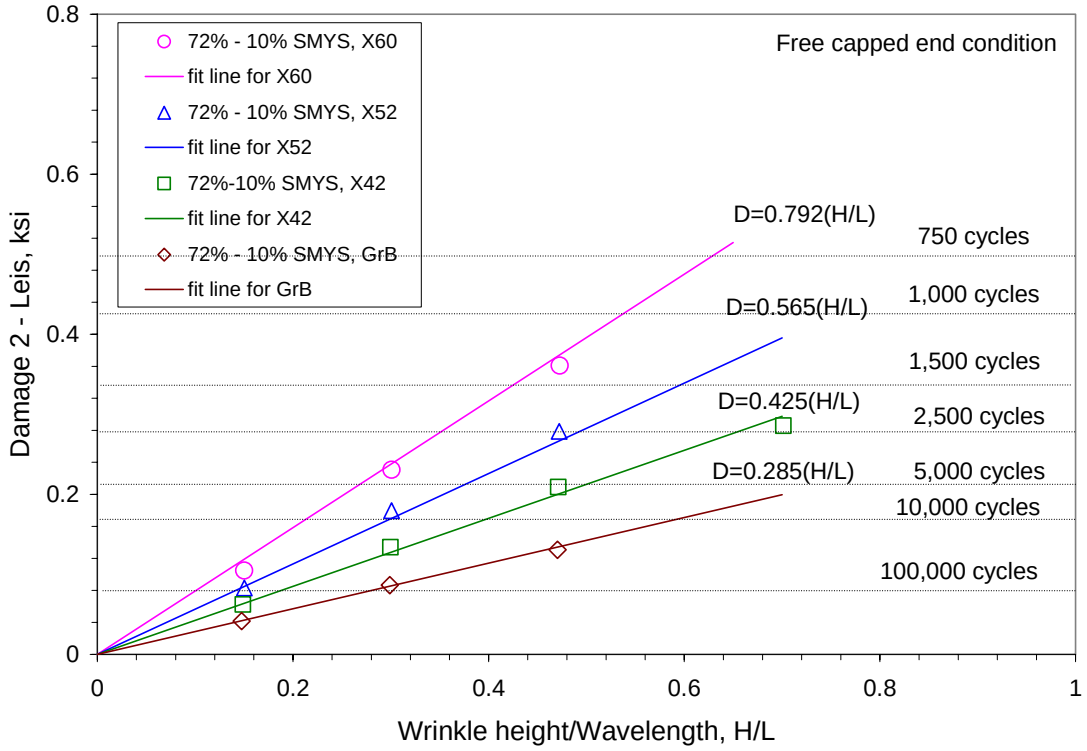

Figure 57. D2 versus H/L for the four pipeline steels

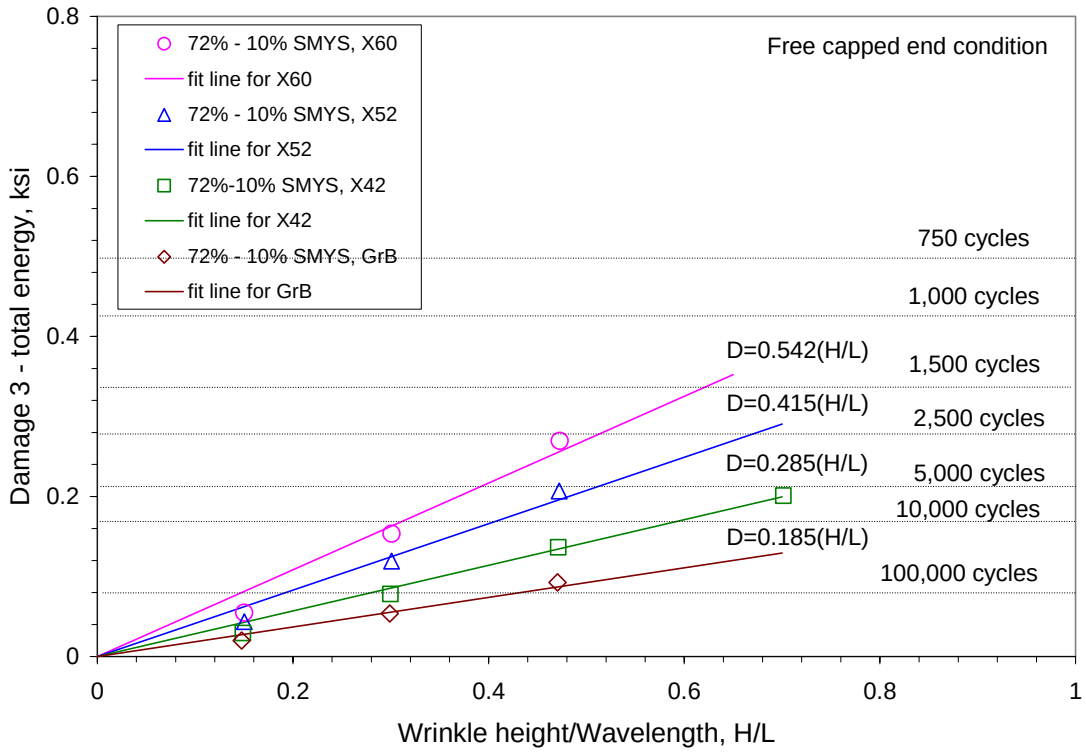

Figure 58. D3 versus H/L for the four pipeline steels

Fatigue Damage Predictions by Three Plastic Hardening Models

Fatigue Damage Comparison for the Three Hardening Models

For the X42 pipeline steel, detailed FEA calculations were repeated using the kinematic hardening model and the combined isotropic/kinematic hardening model using otherwise similar conditions.

Figure G8 shows the variations of the SWT damage parameter versus the wrinkle size from the FEA results using the isotropic, kinematic, and combined hardening models. Figure G9 shows the variations of the Leis damage parameter versus the wrinkle size from the FEA results using the three hardening models. Figure G10 shows the variations of the total energy damage parameter versus the wrinkle size from the FEA results using the three hardening models. For each plastic hardening model, the FEA results for the damage parameters were curve-fitted using a linear equation. All curve-fitted equations were included in the figures and expressed as follows:

- SWT parameter in Figure G8
  - $D_1 = 0.625(H/L)$, for isotropic model (28a)
  - $D_1 = 0.565(H/L)$, for combined model (28b)
  - $D_1 = 0.205(H/L)$, for kinematic model (28c)
- Leis parameter in Figure G9
  - $D_2 = 0.425(H/L)$, for isotropic model (29a)

- ➢ $D_2 = 0.455(H/L)$, for combined model (29b)
- ➢ $D_2 = 0.172(H/L)$, for kinematic model (29c)

- Total energy parameter in Figure G10
  - ➢ $D_3 = 0.285(H/L)$, for isotropic model (30a)
  - ➢ $D_3 = 0.355(H/L)$, for combined model (30b)
  - ➢ $D_3 = 0.159(H/L)$, for kinematic model (30c)

With these equations and using the material fatigue resistance curve in Equation 16, the wrinkle size versus the fatigue life can be determined for each plastic hardening model and each damage parameter. The details are discussed in the following section.

As compared in Figures G8 to G10 from FEA results for the wrinklebend under cyclic loading of internal pressure, it is observed that

- Kinematic hardening model predicts the smallest fatigue damage among the three damage parameters.
- For the SWT parameter, the isotropic hardening model predicts the largest damage, followed by the combined hardening model.
- For the Leis and total energy parameters, the combined hardening model predicts the largest damage, and followed by the isotropic hardening model.
- For H/L = 0, i.e., wrinkles free, the pipe is elastic under the cyclic internal pressure of 72 percent-10 percent SMYS, and strain range or strain amplitude is zero under pure elastic cyclic loading. Therefore, all three energy-based damage parameters are zero at H/L = 0, and all fitted curves go through the origin in Figures G8, G9, and G10.

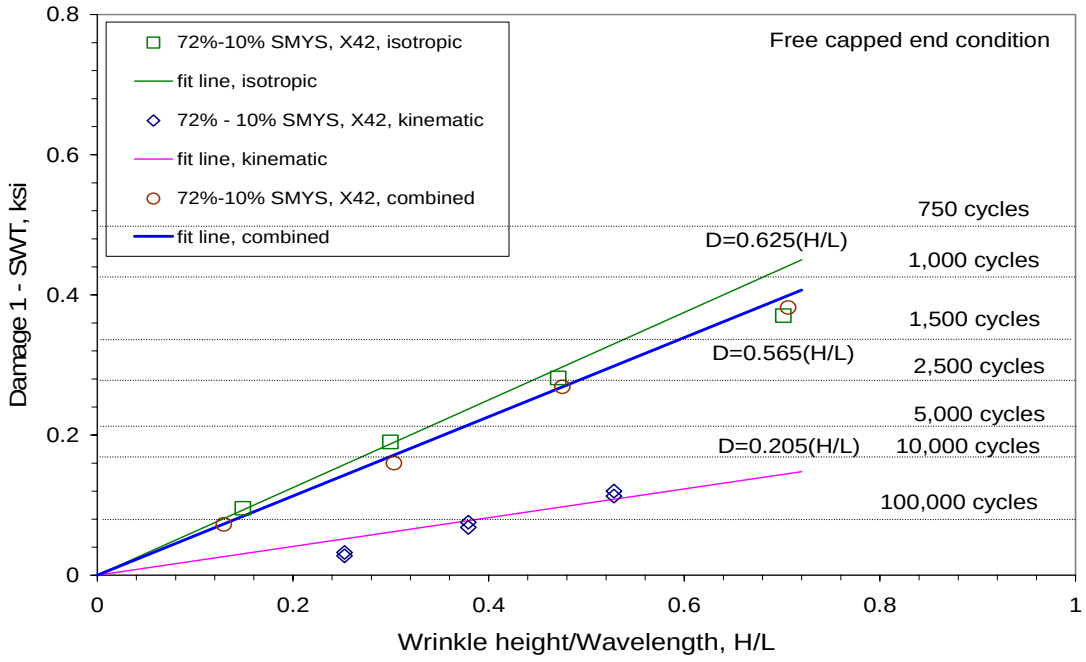

Figure 59. D1 versus H/L for three plastic hardening models

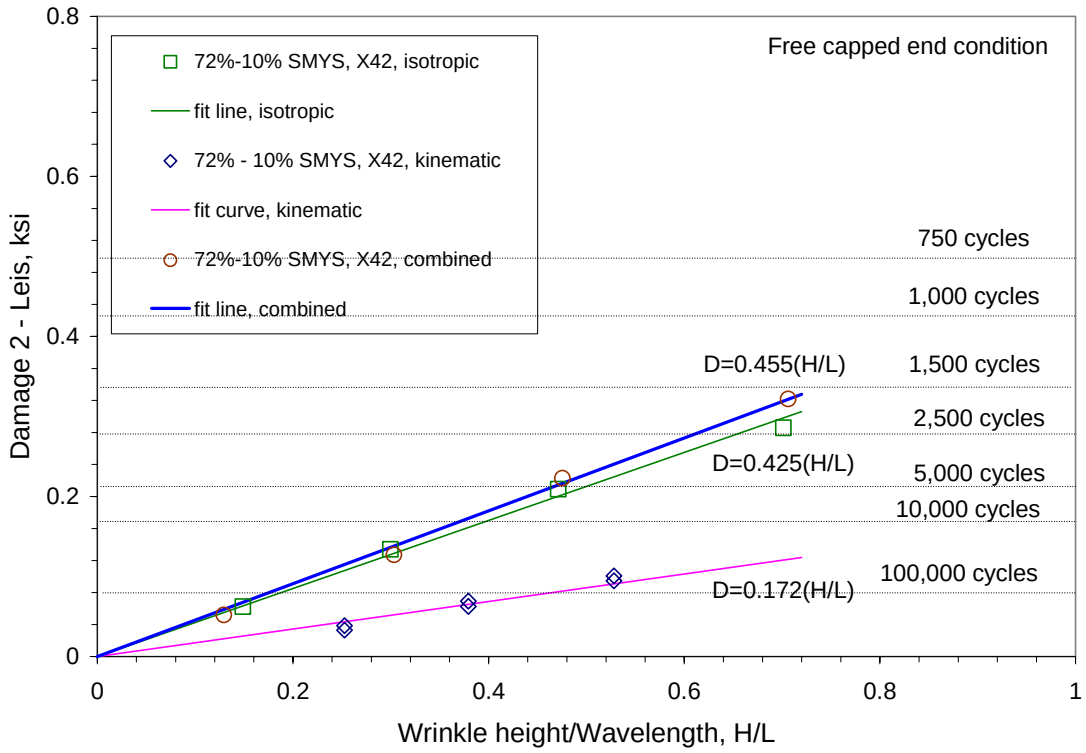

Figure 60. D2 versus H/L for three plastic hardening models

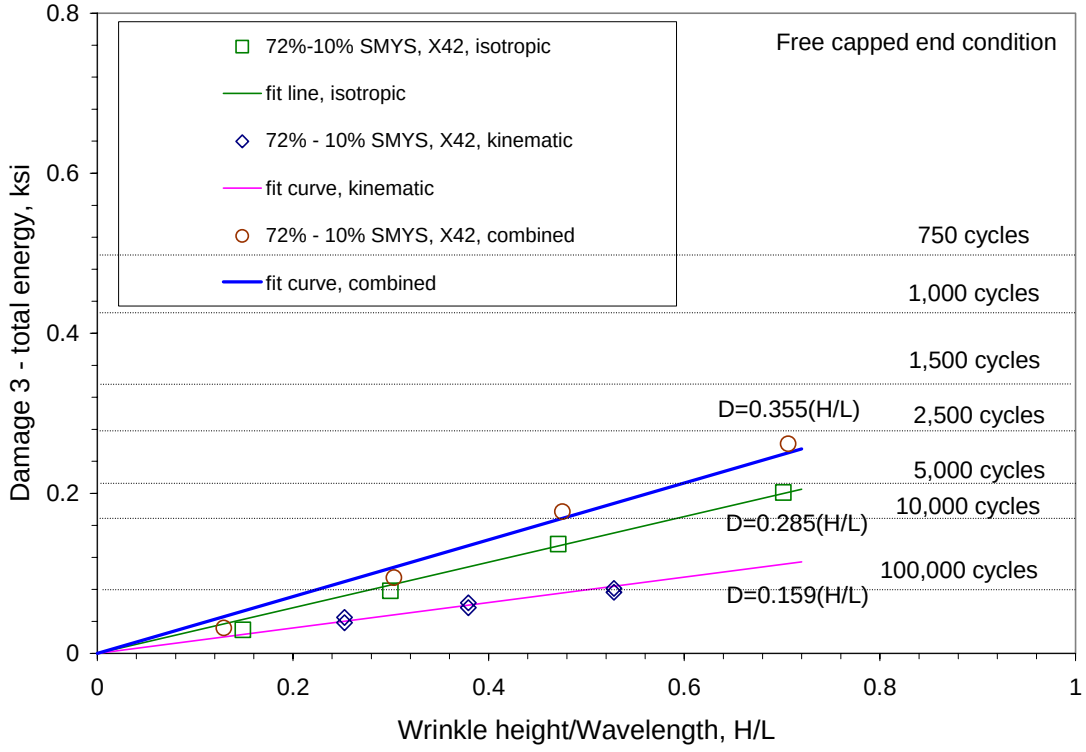

Figure 61. D3 versus H/L for three plastic hardening models

Prediction of Fatigue Life for Wrinklebend

From FEA determined damage parameters in Equations 28 to 30 and using the material fatigue resistance curve in Equation 16, the relationship between the wrinkle size H/L and the fatigue life N_f can be determined as follows:

- For SWT parameter
  - $\frac{H}{L} = 436.8\left(2N_f\right)^{-1.02} + 3.36\left(2N_f\right)^{-0.28}$, for isotropic model (31a)
  - $\frac{H}{L} = 483.2\left(2N_f\right)^{-1.02} + 3.72\left(2N_f\right)^{-0.28}$, for combined model (31b)
  - $\frac{H}{L} = 1331.7\left(2N_f\right)^{-1.02} + 10.24\left(2N_f\right)^{-0.28}$, for kinematic model (31c)
- For Leis parameter
  - $\frac{H}{L} = 642.35\left(2N_f\right)^{-1.02} + 4.94\left(2N_f\right)^{-0.28}$, for isotropic model (32a)
  - $\frac{H}{L} = 600.0\left(2N_f\right)^{-1.02} + 4.62\left(2N_f\right)^{-0.28}$, for combined model (32b)
  - $\frac{H}{L} = 1587.2\left(2N_f\right)^{-1.02} + 12.21\left(2N_f\right)^{-0.28}$, for kinematic model (32c)
- For total energy parameter
  - $\frac{H}{L} = 957.9\left(2N_f\right)^{-1.02} + 7.37\left(2N_f\right)^{-0.28}$, for isotropic model (33a)
  - $\frac{H}{L} = 769.0\left(2N_f\right)^{-1.02} + 5.92\left(2N_f\right)^{-0.28}$, for combined model (33b)
  - $\frac{H}{L} = 1717.0\left(2N_f\right)^{-1.02} + 13.2\left(2N_f\right)^{-0.28}$, for kinematic model (33c)

Figures G11, G12, and G13 show the variations of H/L versus service life using the FEA results from the isotropic, kinematic, and combined hardening models for the SWT parameter, Leis parameter, and total energy parameter, respectively. From these figures, it can be observed that:

- Kinematic hardening model predicts the highest fatigue life for all three damage parameters.
- For the SWT parameter, the isotropic hardening model predicts the smallest life, followed by the combined hardening model.
- For the Leis parameter and total energy parameter, the combined hardening model predicts the smallest life, and followed by the isotropic hardening model.
- For all three plastic hardening models, the isotropic model predictions are close to those by the combined hardening model, and these two predictions are significantly different from those by the kinematic model.

As a result, it may concluded that the fatigue damage analysis of the wrinklebends based on the isotropic hardening model is close to those from the combined hardening model, and both results and fatigue criteria can be used for the wrinklebend structural analysis. However, the kinematic hardening model predicts the fatigue life is much larger than that from the isotropic hardening

model or combined hardening model, and thus it may not be suggested for use in the wrinklebend analysis.

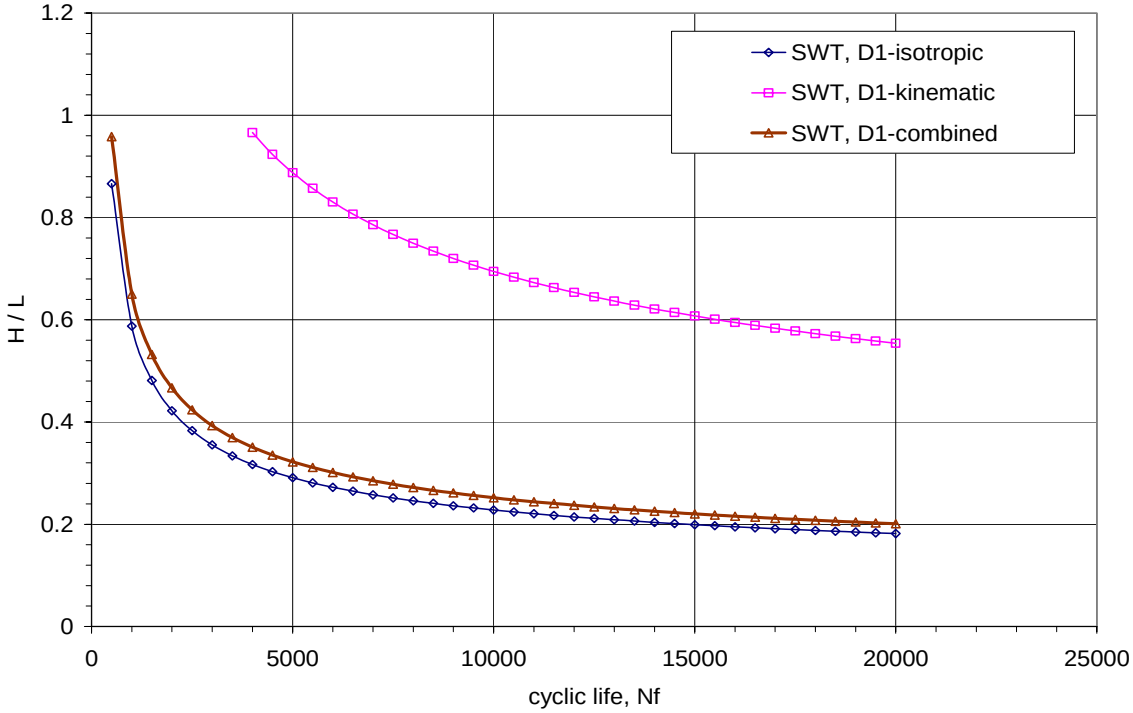

Figure 62. Predicted fatigue life with H/L via D1 for three plastic hardening model

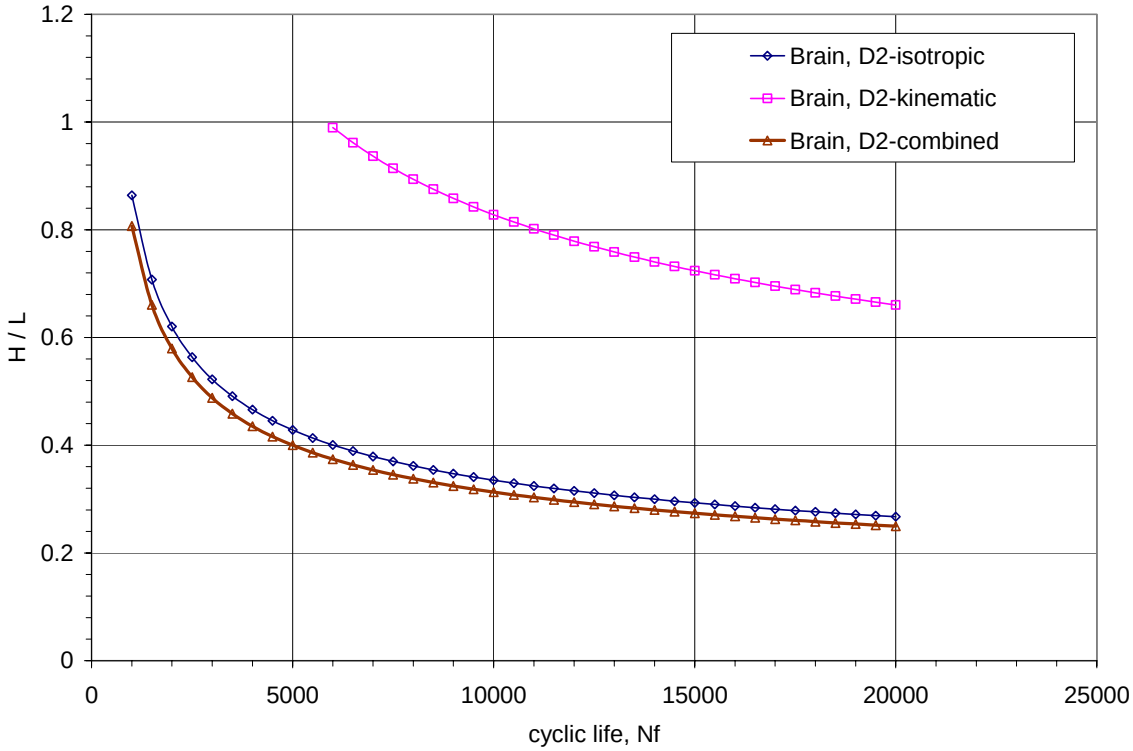

Figure 63. Predicted fatigue life with H/L via D2 for three plastic hardening model

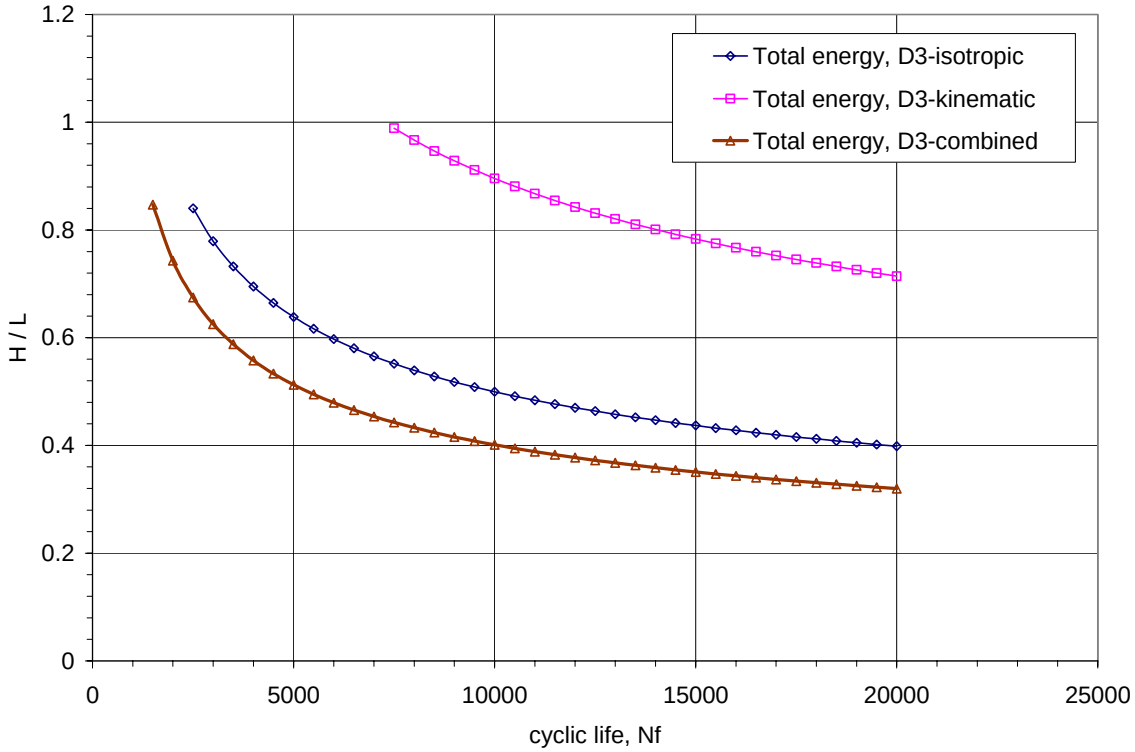

Figure 64. Predicted fatigue life with H/L via D3 for three plastic hardening model

Full-Scale Experimental Validation

Full-scale experiments for wrinklebends with different wrinkle sizes have been reported in detain in Appendix G of Reference 5. The pipe had a diameter of 20 inches and a thickness of 0.25 inches. The steels used for tests were GrB and X42 line-pipe steel. The average cyclic pressure was from 103.45 percent to 7.52 percent SMYS of X42.

FEA calculations have been done for these wrinklebends for the X42 pipeline steel under the conditions evaluated experimentally. The combined isotropic/kinematic plastic hardening model was used in the FEA calculations. Figure G14 shows the three damage parameters determined from FEA and the equations determined by the curve fitting. From the three linearly curve-fitted equations and the material fatigue curve in Equation 16, the fatigue life and the wrinkle size can be determined and expressed as follows:

- For SWT parameter, D1:

$$D_1 = 0.892(H/L) \tag{34a}$$

$$\frac{H}{L} = 306.05(2N_f)^{-1.02} + 2.35(2N_f)^{-0.28} \tag{34b}$$

- For Leis parameter, D2:

$$D_2 = 0.755(H/L) \tag{35a}$$

$$\frac{H}{L} = 361.59(2N_f)^{-1.02} + 2.78(2N_f)^{-0.28} \tag{35b}$$

- For total energy parameter, D3:

$$D_3 = 0.635(H/L) \tag{36a}$$

$$\frac{H}{L} = 429.92\left(2N_f\right)^{-1.02} + 3.31\left(2N_f\right)^{-0.28} \tag{36b}$$

From Equations 34b, 35b, and 36b, the variations of the pressure cycles to failure and the wrinkle size are shown in Figure G15 for the three damage parameters. It indicates that based on the FEA results from the combined hardening model, the SWT damage parameter can predict the fatigue life is well agreed to the experimental data. The predictions using the Leis damage parameters are good and the predictions using the total energy parameter are also reasonable.

Therefore, *it can be concluded that the FEA simulation with combined plastic hardening model plus the SWT fatigue damage parameter provides us excellent results to simulate and predict the wrinklebend fatigue life for their integrity assessment*.

Cyclic Stress and Strain at Wrinklebend

As demonstrated in the last section, the combined isotropic/kinematic hardening model is a good plastic hardening model which can be used in the FEA calculations in ABAQUS to simulate the local stress and strain in a wrinkle area of a pipeline under cyclic internal pressure. Therefore, this combined hardening model will be used to develop the wrinklebend criteria for this DOT wrinklebend project.

One FEA case is selected to illustrate the FEA results. For this case, the pipe diameter was 16 inches, the thickness was 0.283 inches, and the length of the FEA model 35 inches. The applied rotation angle was 0.0693 radian (3.84 degrees), while the applied cyclic internal pressure was from 72 to 10 percent of SMYS for X42. The FEA results are as shown in Figure G16 based on the stabilized combined hardening model. Figures G17 and G18 present the FEA results at the bottom point at the crown of the wrinkle. From these figures it is apparent that:

- After the wrinkle is formed, a large compressive residual strain and about 50 percent of the SMYS of X42 tensile residual stress are generated.
- The axial strain has small changes during cyclic loading.
- The axial stress has large changes during cyclic loading.
- The axial stress has small nonlinear behavior and has almost the linear elastic responses during the load – unload corresponding to 72 to 10 percent SMYS of X42.

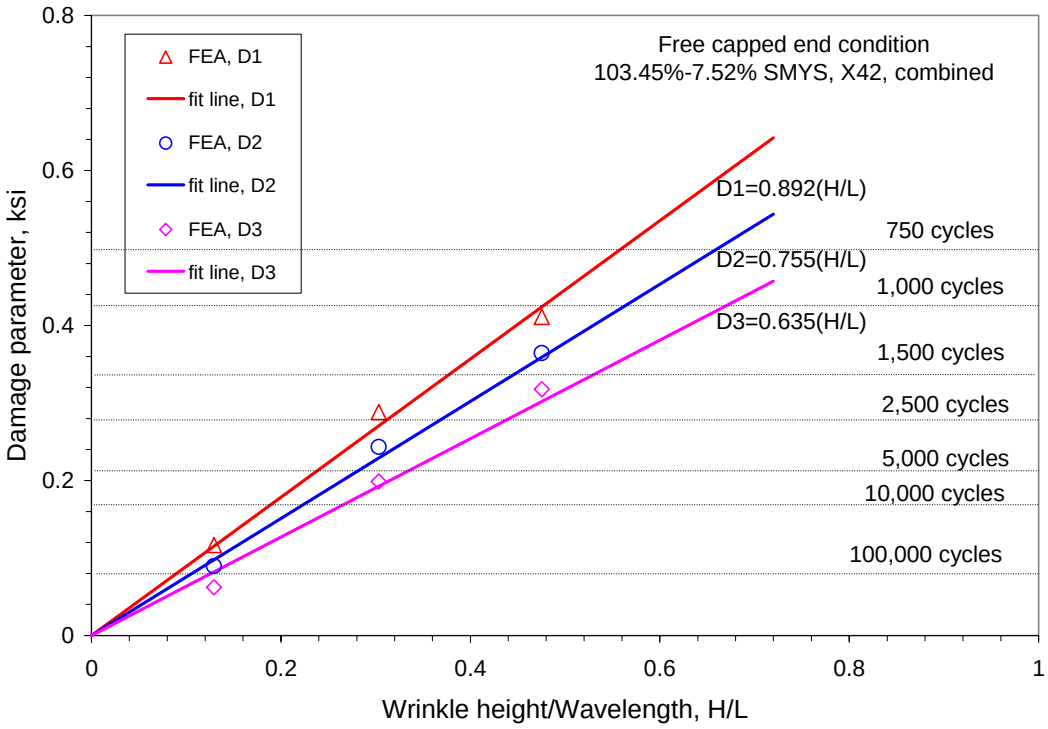

Figure 65. Three damage parameters versus H/L for Columbia Gas wrinklebends

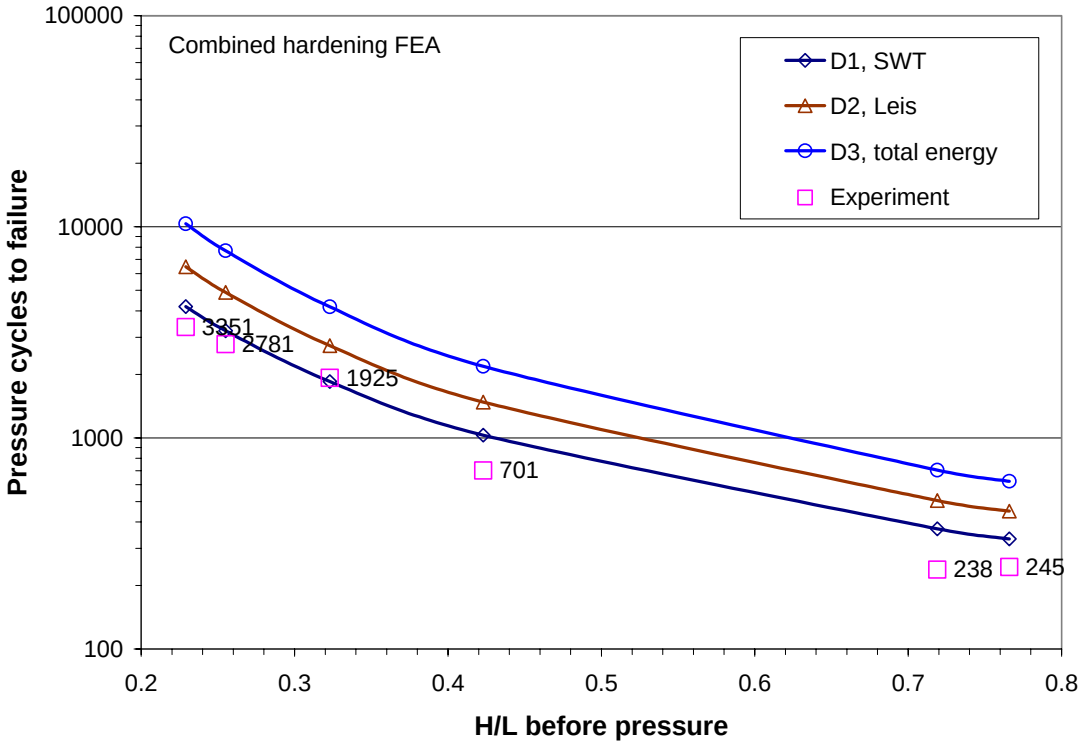

Figure 66. Comparison of experimental and predicted life

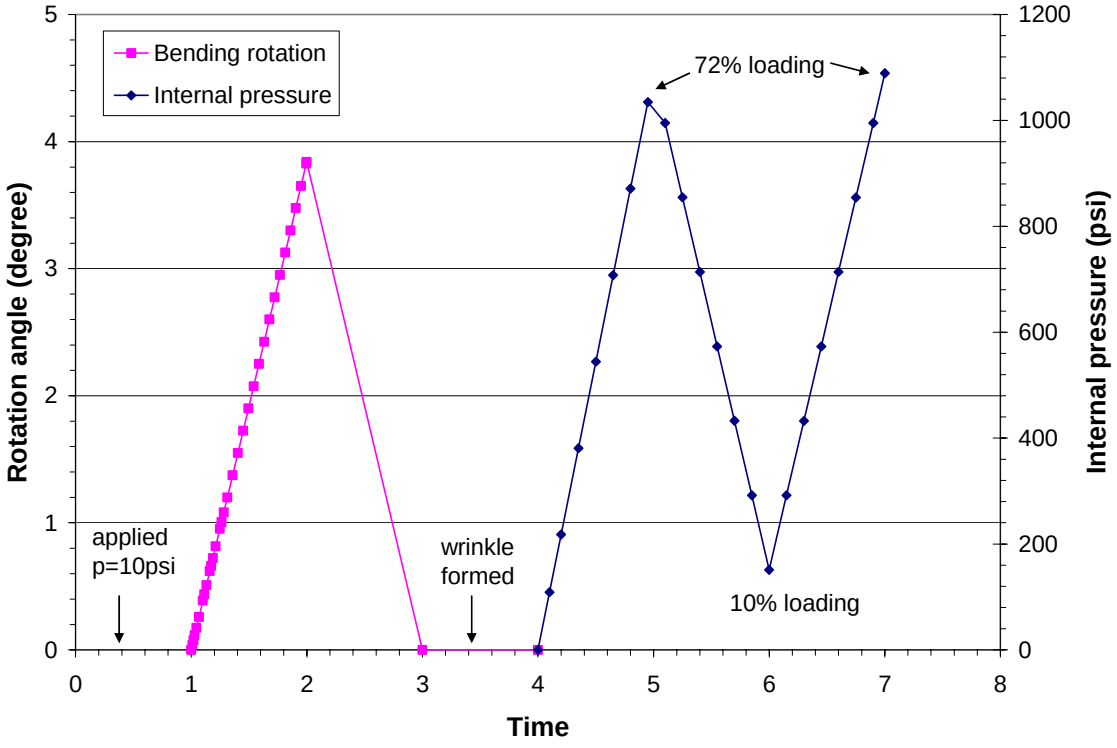

Figure 67. Rotation during wrinkle formation and cyclic pressure during loading

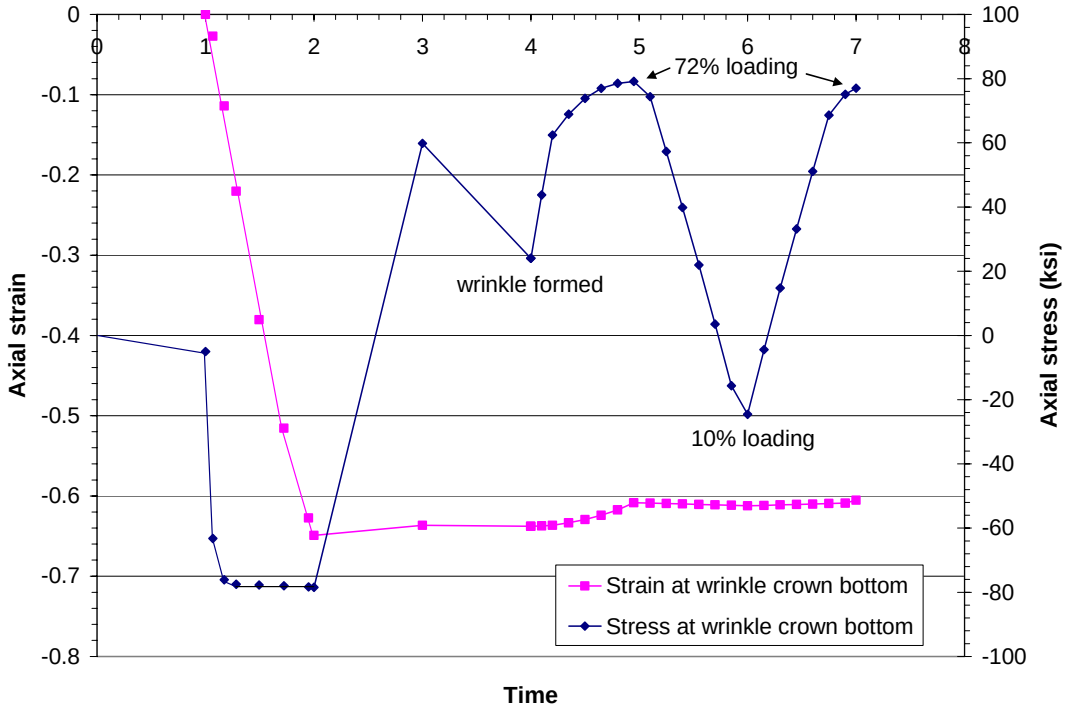

Figure 68. Cyclic stress and strain during wrinkle formation and loading

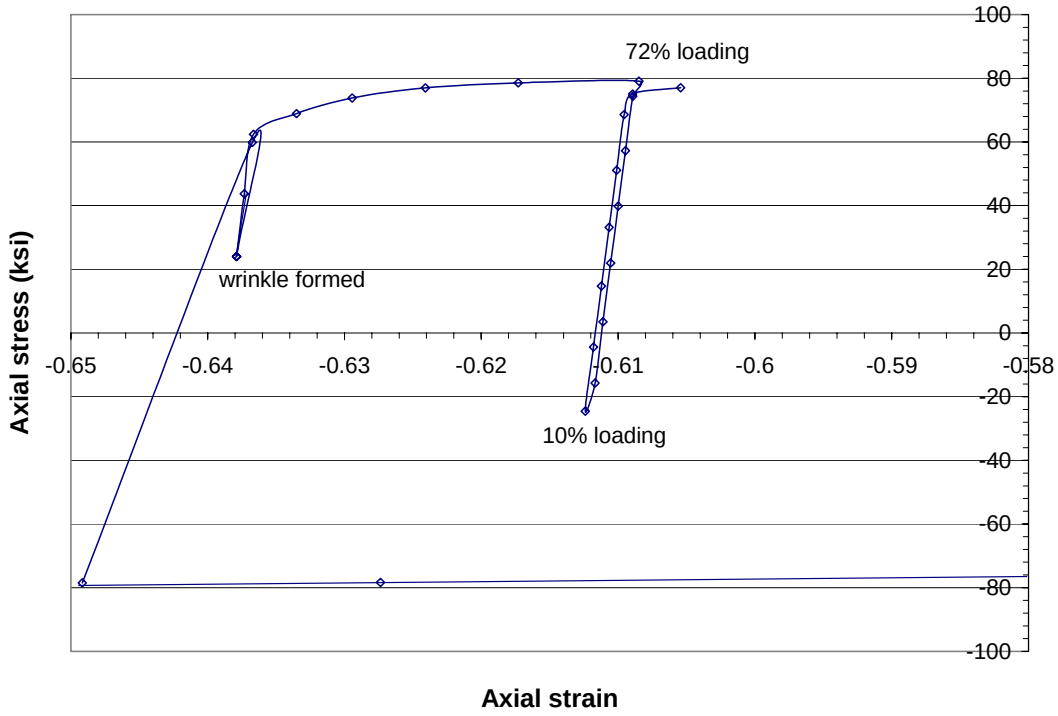

Figure 69. Cyclic axial stress – axial strain during cyclic pressure

References

1. Smith, K.N., Watson, P. and Topper, T.H., 1970, "A Stress-Strain Function for the Fatigue of Metal," Journal of Materials, 5, pp. 767-778.
2. Leis, B.N., 1977, "An energy-based fatigue and creep-fatigue damage parameter," Journal of Pressure Vessel Technology, **99**, pp.524-533.
3. Glinka TG., Plumtree, A., and Shen, G., 1995, "A multiaxial fatigue strain energy parameter related to the critical plane," Fatigue and Fracture of Engineering Materials and Strcutures, 18, pp.37-46.
4. Dowling, N.E., 1999, "Mechanical Behavior of Materials: Engineering Methods for Deformation, Fracture and Fatigue," Second edition, Prentice Hall, Upper Saddle River, New Jersey.
5. Leis, B. N., Zhu, X.-K., and Clark, E. B., "Criteria to Assess Wrinklebend Severity for Use in Pipeline Integrity Management," Project Report PR-003-03112, PRCI Catalog L52190, August 2004.